UNIVERSITA' DEGLI STUDI DI GENOVA
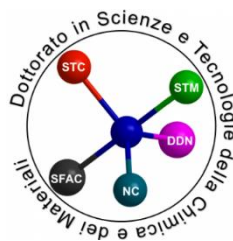
DOCTORATE SCHOOL IN SCIENCES AND TECHNOLOGIES OF CHEMISTRY AND MATERIALS

Curriculum in pharmaceutical, food and cosmetic sciences

XXXII cycle

PhD Thesis

Synthesis and biological evaluation of nitrogen heterocycle systems as potential antiviral agents

Valeria Francesconi

Advisor: Prof. Michele Tonelli

Defense date: 20/03/2020

Table of Contents

LIST OF ABBREVIATIONS

aa	Aminoacid
ADL	Average dynamic length
APPV	Atypical porcine pestivirus
ARI	Acute respiratory infections
ATP	Adenosine triphosphate
BAM	Baloxavir marboxil
BDV	Border disease virus
BHK-21	Hamster normal kidney fibroblast
bnmAbs	Broadly-neutralizing monoclonal antibodies
BPdC	1-benzyl-1H-pyrazole-3,5-dicarboxylate
BVDV	Bovine viral diarrhea virus
CC_{50}	Cytotoxic concentration 50
CNS	Central nervous system
COPD	Chronic obstructive pulmonary disease
CoV	Coronavirus
cp	Cytopathic
CPE	Cytopathic effect
CPM	Cyclopamine
cRNA	Complementary RNA
CSFV	Classical swine fever virus
CVB-4	Coxsackie B virus
DCM	Dichloromethane
DENV	Dengue virus
DHFR	Dihydrofolate reductase
DHFR-TS	Dihydrofolate reductase-thymidylate synthetase
DIPEA	Diisopropylamine
DNA	Deoxyribonucleic Acid
ds	Double stranded
EC_{50}	Effective concentration 50
EDC	Ethyldimethylaminopropyl carbodiimide
ER	Endoplasmic reticulum
FDA	Food and Drug administration
FGFR	Fibroblast growth factor receptor
FIPV	Feline infectious peritonitis virus
FIRSV	Formalin-inactivated RSV vaccine
FHV	Feline herpesvirus
FP	Favipiravir
FRTP	Favipiravir ribofuranosyl-5′-triphosphate

GTP	Guanosine-5'-triphosphate
HA	Hemagglutinin
hAdV	Human Adenovirus
HB	Hydrogen bond
HBV	Hepatitis B virus
HCoV	Human coronavirus
HCV	Hepatitis C virus
hDHFR	Human dihydrofolate reductase
HEF	Hemagglutinin-esterase-fusion
Hep-2	Human epithelial type 2 cells
HIV	Human immunodeficiency virus
hMPV	Human metapneumovirus
HOBT	Hydroxybenzotriazole
HPIV	Human parainfluenza virus
HSV	Herpes simplex virus
HTA	Host-Targeting antiviral
IAV	Influenza A virus
IBV	Influenza B virus
IC_{50}	Half maximal inhibitory concentration
ICTV	International Committee on Taxonomy of Viruses
ICV	Influenza C virus
IDV	Influenza D virus
IFN	Interferon
IgG	Immunoglobulin G
IMPDH	Inosine-5'-monophosphate dehydrogenase
IP3	Inositol trisphosphate
IRES	Internal Ribosome Entry Site
IRF-3	Interferon regulatory factor 3
ITC	Isothermal titration calorimetry
IV	Influenza Virus
IVIG	Intravenous immunoglobulins
JEV	Japanese encephalitis
LDL	Low Density Lipoproteins
LRI	Lower respiratory tract infections
mAb	Monoclonal antibodies
MD	Mucosal Disease
MDCK	Madin-Darby Canine Kidney
MLV	Modified-live viral vaccines
MPV	Metapneumovirus

MTX	Methotrexate
MVA	Modified Vaccinia Ankara
NA	Neuraminidase
NAI	Neuraminidase inhibitor
NANA	N-acetyl-9-O-acetylneuraminic acid
ncp	Non-cytopathic
NE	Nanoemulsion
NEP	Nuclear export protein
NES	Nuclear export signal
NI	Nucleoside inhibitor
NLS	Nuclear Localization Signal
NNI	Non-nucleoside inhibitor
NP	Nuclear protein
NPC	Nuclear pore complexes
NS1	Non-structural protein-1
NS2	Non-structural protein-2
NTP	Nucleoside triphosphate
NTZ	Nitazoxanide
ORF	Open reading frame
P3	Polymerase 3
PA	Polymerase acidic protein
PB1	Polymerase basic 1 protein
PB2	Polymerase basic 2 protein
PI	Persistent infected
PI3K	Phosphatidylinositol-3-kinase
PIV	Parainfluenza virus
PKC	Protein kinase C
RdRp	RNA-dependent RNA-polymerase
Reo-1	Reovirus-1
RhV	Rhinovirus
RNA	Ribonucleic Acid
RNP	Endoplasmic reticulum
RRM	RNA Recognizing Motif
RSV	Respiratory syncytial virus
r.t.	Room temperature
RT	Reverse transcription
SAR	Structure-activity relationships
SEM	Standard error of the mean
SI	Selectivity Index

SN	Serum neutralization
ss	Single stranded
TBHQ	Tert-butyl hydroquinone
TFA	Trifluoroacetic acid
THF	Tetrahydrofuran
TM	Transmembrane
UDA	Urtica dioica agglutinin
URI	Upper respiratory tract infections
UTR	Untranslated region
VHH	Heavy chain variable domains
vRNA	Viral ribonucleic Acid
vRNP	Viral ribonucleoprotein
VSV	Vesicular stomatitis virus
VV	Vaccinia Virus
WNV	West Nile virus
YFV	Yellow Fever Virus

SUMMARY

Viruses, being obligate intracellular parasites, depend on host cell factors to complete their replicative cycle. They are made up of genetic material, either double- or single-stranded DNA or RNA, surrounded by a protein coat called capsid. They may also contain some pre-synthesized viral proteins, otherwise all the viral factors and enzymes needed for completing their reproduction are encoded by the viral genome and synthesized inside the host cell by hijacking its metabolic machinery. Some viruses also possess an external lipid envelope derived from the host cell membrane that exhibits antigenic proteins and glycoproteins[1].

In the fight to infectious disease, traditional therapeutic approaches have mostly focused on targeting specific viral components or enzymes. This pathogen-directed strategy, while successful in numerous cases, in many others results ineffective due to the emergence of drug-resistance; this event derives from the high mutation rate of viral genome, which may lead to the selection of resistant strains.

A different approach, addressed to target host-factors essential for viral replication, has recently draw an increasing attention; viruses, as obligated parasites, usurp the metabolic machinery of host cells to synthesize some crucial factors and to complete replication. Thus, blocking one or more host factors could be effective against the pathogen growth, allowing the escape of drug-resistance and could also provide broad-spectrum antivirals capable of hitting common targets shared by different viruses[2].

My PhD project was aimed at synthesizing new nitrogen heterocycle systems, designed especially against RNA viruses, such as those belonging to *Flaviviridae*, *Orthomyxoviridae* and *Paramyxoviridae* families. Among them there are, respectively, pathogens responsible for diseases with a high epidemiological impact, as BVDV in cattle and HCV in humans, influenza A and B viruses and respiratory syncytial virus (RSV).

The Bovine Viral Diarrhea - Mucosal Disease (BVD-MD) is a highly contagious infectious disease that affects cattle. The causative agent is the Bovine Viral Diarrhea Virus (BVDV), which causes a wide range of symptoms including abortion, teratogenesis, respiratory problems, chronic wasting disease, immune system dysfunction and predisposition to secondary viral and bacterial infections, thus determining significant economic losses to livestock industry[3]. Besides vaccination, currently there is no completely efficacy pharmaceutical options for controlling

BVDV infection, thus there is an urgent need to develop novel antiviral drugs in order to limit the pathogen diffusion and prevent birth of persistent infected calves. The interest towards BVDV is also associated to its similarity with the human pathogen HCV. In this case also, the access to the currently available therapy is limited due to the limited efficacy and marked side effect of the traditional drugs or by the high cost of the therapy with the recently approved drugs (e.g. Sofosbuvir)[4]. Additionally, as *Hepaciviruses* can hardly be used in routine cell-based assays, antiviral activity against HCV was evaluated against BVDV because of similar genome organization (sequence homology > 30%) and replication mechanisms. Both BVDV and HCV possess an RNA-dependent RNA-polymerase (RdRp) which is the central enzyme in the replication of genome, thus it represents an ideal target for small molecule drugs.

The research group where I develop my Ph.D. research work has previously discovered the specific anti-BVDV activity of a series of N-substituted derivatives of 9-amino-6-chloro-2-methoxyacridine against BVDV[5]. These results represented the starting point of my Ph.D. research work: throughout my first year I synthesized a new small library of acridine-based molecules, starting from three prototypes selected among the previous series and exploring the variation of the 9-amino side chain, including differently functionalized aromatic or heteroaromatic rings, with the aim of achieving more effective and safe BVDV inhibitors. The most potent compounds demonstrate to effectively inhibit BVDV replication, (EC_{50} values in the range 0.8-11.5 μM) and also exhibited a low cytotoxicity and a high safety profile in *in vitro* cellular assays. In addition, *in vitro* enzymatic inhibition assays against the BVDV RdRp and ITC measurements of the binding process and molecular modeling studies confirmed the BVDV RNA-dependent RNA-polymerase as the molecular target of these compounds[6].

The second part of my PhD project was focused on the research of novel anti-influenza agents either acting on viral proteins or host factors involved in the viral replication processes.

Respiratory tract infections represent a serious burden with significant morbidity and mortality especially occurring in children, elderly and immunocompromised people. The vast majority of ARIs have a viral aetiology and may be the result of the infection of different respiratory viruses, in particular RNA viruses, such as respiratory syncytial virus (RSV), influenza virus (IV), parainfluenza virus (PIV), metapneumovirus (MPV), rhinovirus (RhV), and coronavirus (CoV)[7].

Respiratory syncytial virus (RSV) is the etiological agent of many respiratory tract infections that represent the major cause of hospitalization of infants and children. The virus is highly contagious and re-infection occurs. To date, therapy is restricted to Ribavirin, whose effectiveness, however, is highly questionable while humanized monoclonal antibody Palivizumab (Synagis®) is used for the prevention in high-risk infants, but with only partially efficacy[8]. RSV has an RNA genome that encodes 11 viral proteins: the F (fusion) and G (attachment) surface glycoproteins are the main antigenic determinants and play an important role in viral entry into host cells, thus they represent interesting targets for designing small molecule inhibitors.

Influenza also causes respiratory tract infections that seasonally occur in epidemic form, and sometimes evolves with pandemic proportions. Influenza viruses are members of the *Orthomyxoviridae* family and can be divided into four types A, B, C and D. Among them the virus types A and B are the most common human pathogens. The influenza viruses are capable of reassorting their genetic material between different human and animal strains (*antigenic shift*) and to continuously evolve to evade the host immune system through the mutation of the genes encoding for surface glycoproteins (*antigenic drift*). The current therapy is limited to two classes of drugs: neuraminidase (NA) inhibitors and the M2 proton channel blockers. Recently research efforts are oriented to the identification of new potential target to be inhibited in order to obtain a therapeutic effect, such as the viral factors RNA polymerase or hemagglutinin HA inhibitors. Recently, also novel anti-influenza compounds directed against host-factors essential for viral replication have been developed since they could potentially represent a new strategy to pursue in order to resolve the problem of the emergence of mutant resistant viruses and parallelly obtain a broad-spectrum antiviral effect[9].

During my PhD I synthesized several molecular series that demonstrated to be active against different RNA respiratory viruses.

The research group of Prof. Tonelli has previously identified a series of dihydrotriazines, structurally related to the antimalarial drug cycloguanil, which acted as potent inhibitors of influenza B replication *in vitro*[10]. These derivatives have been demonstrated to achieve the antiviral effect by blocking the host-factor *h*DHFR. Thus, during my PhD I synthesized two novel series of dihydrotriazine-inspired compounds: a set of 4-azaspiro-1,2-dihydrotriazines[11] and a second smaller series of 2-amino-3,4-dihydrotriazino[1,2-a]benzimidazoles, in order to further explore the effect of different derivatizations of this chemical scaffold. Only few compounds

belonging to the first series demonstrated efficacy towards influenza A H1N1, or influenza B, or RSV with a lower antiviral potency if compared to the previous series prototypes. Despite the general lower activity trend, the enzymatic inhibition assays and the molecular modeling calculations allow to better understand the structural requirements to optimize the enzyme-ligand interactions in order to guide the design of a future series of compounds.

During the second year and the third year of my PhD I joined Professor S. Vázquez' research group at the University of Barcelona for a six months period. During my stay I continued my research in the field of anti-influenza agents by working on the synthesis of three series of compounds including a series of anilino-derivatives, and a series of benzenesulfonamides, both structurally related to the HA inhibitor CL-61917[12]. Unfortunately, only few of these compounds showed only a marginal activity against human coronavirus HCoV 229E, while no visible effect has been recorded towards influenza viruses. The third set of compounds will not be reported in this thesis since some of the derivatives within this series proved nanomolar activity towards the influenza A subtype used in the in vitro assays, thus they will be subject of a future patent application.

Finally, during my third year of PhD I completed the synthesis of a series of benzimidazole analogues, derivatized with (thio)semicarbazone and hydrazone moieties. The novel compounds have been designed taking inspiration from a previous series of benzyl- and benzotriazol-1/2-yl- benzimidazoles which proved sub-micromolar potency against RSV and also other RNA viruses[13]. The newly synthesized derivatives, although not being endowed with the same potency of the previously studied analogues, showed occasional activity against influenza A and RSV. Additionally, five compounds exhibited the capability to inhibit the HCoV 229E, being the first benzimidazole-derivatives manifesting an activity towards this virus.

CHAPTER 1. Introduction

1.1 The Origin of Viruses

Viruses are obligate intracellular parasites; they are able to complete their life cycle and replicate only inside a host organism. They can be defined as sub-microscopic molecular complex constituted of nucleic acids and protein shells surrounding the genetic material. Viruses are capable of infecting a wide range of living organisms and exploit bacteria, fungi, amoeba, plants and animals to complete their replicative cycle[1].

Traditionally, three different hypotheses have been formulated regarding the origins of viruses; according to the first one, the *"virus early-hypothesis"*, viruses are supposed to directly descent from the first replicons, DNA or RNA molecules capable of replicating from a single origin of replication, existing in the precellular stage of the life evolution. As stated by the second theory, the *"regression hypothesis"* viruses might derive from the degeneration of ancestral cells that lost their autonomy and became unable to live and replicate without the help of a host organism, turning, in effect, into an obligate intracellular parasite. In the last scenario, depicted by the *"escaped gene hypothesis",* viruses are the product of cellular host genes' acquisition of the ability to infect and replicate in a semi-autonomous way, escaping from the parent cells and given rise to the different bacterial, archaeal and eukaryotic viruses.

These three theories are equally valid but each one if singly considered exhibits some inconsistency and cannot satisfy the whole aspects underlying the development of all circulating virus strains. The wide differences among viruses, exploiting all possible strategies of genome replication and expression, and carrying different nucleic acid, has allowed to emerge a recent theory where different groups of viruses could be potentially evolved following different routes.

Recently a new *"chimeric hypothesis"* have been formulated stating that the structural protein and the proteins required for genome replication, both encoded by the viral genome, might derive from different ancestors. This theory involves a two-stage process in which pre-cellular replicons emerge before the first cellular life forms and then capture capsid protein genes from cellular organisms, which enables them to form virions. This theory is supported by the fact that many viral enzymes involved into the genome replication does not have a cellular counterpart, while the structural proteins, whose cellular homologues have been identified, may have evolved from ancestral cellular proteins[14].

1.2 Classification of Viruses

Traditionally viruses have been classified by their phenotypic features, such as morphology, nucleic acid types, mode of replication, host organisms, and the kind of disease they can cause.

1.2.1 Baltimore Classification

The Baltimore Classification, developed by David Baltimore (1971), classifies animal viruses on the base of their genome type (RNA, DNA, single or double stranded) and method of replication[15]. Viruses are called "RNA viruses" or "DNA viruses" depending on their nucleic acids; viruses that replicate via reverse transcription are grouped in a separate category as "reverse transcribing (RT) viruses," regardless of whether the genome is RNA or DNA. The viral genome could also be a single molecule of DNA or RNA or it could be segmented in different parts, each one encoding for different proteins.

This classification divides animal viruses in seven groups, considering the nucleic acids species (DNA or RNA), if the genome is a positive-strand or negative-strand and whether it is a single-strand or double-strand (Figure 1). The different nature of the nucleic acid affects also the mechanism of genome replication and expression, and the transcription into mRNA necessary to protein biosynthesis.

- *Group I* — (+/-) dsDNA, double-strand DNA genome, it serves as a template to transcript the mRNA.
- *Group II* — (+) ssDNA, positive polarity single-strand DNA genome, these viruses first convert their ssDNA genome to dsDNA, then used as a template for mRNA transcription.
- *Group III* — (+/-) dsRNA, double-strand RNA genome, it also serves as a template to transcript the mRNA.
- *Group IV* — (+) ssRNA, positive polarity single-strand RNA genome, in this case the genomic RNA is directly by host's ribosomes as mRNA.

- *Group V —* (-) ssRNA, negative polarity single-strand RNA genome, it can't be directly read by ribosomes so it serves as a template for the synthesis of the positive strand reciprocal mRNA by the viral polymerases.
- *Group VI —* (+) ssRNA-RT, positive polarity single-strand RNA genome, *retroviruses* are part of this groups, differently from Group IV the RNA genome is not directly read by the ribosome but is converted into DNA by a reverse transcriptase enzyme. Thereafter, the new DNA is integrated into the host's genome by means of an integrase enzyme. Then it serves as template for the hosts polymerases for the synthesis of mRNA.
- *Group VII —* (+/-) dsDNA-RT, double-strand DNA genome, the viral DNA serves as template for RNA that acts as mRNA for the protein synthesis but it also serves for viral replication. Indeed, the viral reverse transcriptase synthesizes the new DNA by retro-transcription from the RNA template.
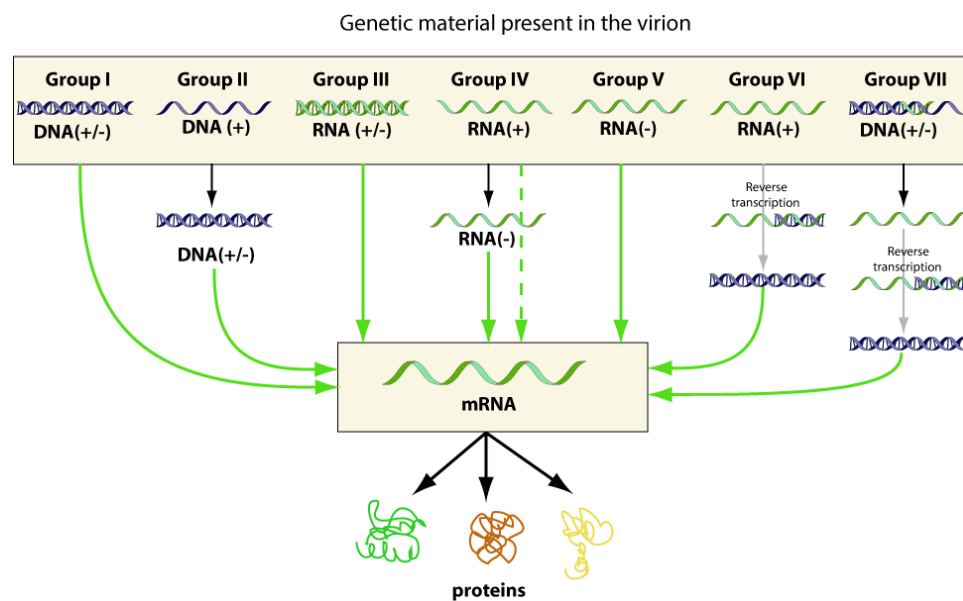
Figure 1. Baltimore classification of viruses, divided in DNA viruses (Group I and II), RNA viruses (Group III, IV, and V), and RT viruses (Group VI and VII). The figure shows the differences of viral genome structure in each group (DNA or RNA), the strandness (ss: single-strand or ds: double-strand), and the polarity (+/-). The relationship of the genome to mRNA is indicated by solid line (transcription) or dotted line (no transcription)[1]. RT: reverse transcription

1.2.2 ICTV classification

The International Committee on Taxonomy of Viruses (ICTV) is responsible of establishing guidelines for taxonomic classification of viruses and of naming and classifying the viral species[16]. The ICTV recognizes five hierarchical ranks that are used to define the universal viral taxonomy, starting with *orders* (suffix *-virales*), which are divided into *families* (suffix *-viridae*), *subfamilies* (suffix *-virinae*), *genera* (suffix *-virus*) and then *species*. Species can be further subdivided into *genotypes* or *subtypes*.

Viruses are classified on the base of their shared characteristics with the other members of the groups, sequence similarity and phylogenetic relationships are primarily considered in order to assign one virus to a group or another. Hereafter viruses with similar properties are grouped together. The characteristics displayed by the members of a higher-level class are shared with all the lower-level classes that belong to higher level class[17].

1.3 Viral Structure

Viruses are sub-microscopic particles since most viruses vary in diameter from 20 nm to 250–400 nm. The virus particle, called *virion*, is composed of a nucleic acid surrounded by a protective protein coat called *capsid*, that is formed by structural proteins arranged together, called *capsomeres,* which are encoded by the viral genome*. Nucleocapsid* is the term referring to a viral capsid associated with the viral genome. Some viruses might also have a lipid bilayer surrounding the capsid, called *envelop,* that derives from the host cell membrane that previously supported virions replication; the viral envelop is studded with viral proteins and glycoproteins. Viral proteins can be divided in "structural proteins", as the capsid proteins and all the proteins that constitute the virus particle, and "non-structural proteins", all the proteins that are absent in the virion structure (i.e. many virus-coded enzymes such DNA/RNA polymerase and proteases) and that are synthesized only in the replicative phase by exploiting the host' cell machinery.
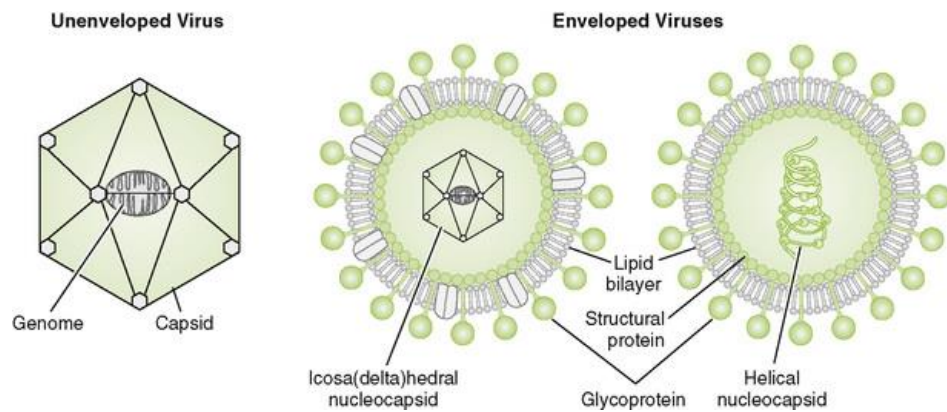
Figure 2. Different shapes of virion structures: nonenveloped (naked) virus with an icosahedral capsid, the most common type in naked viruses. Enveloped viruses have a membrane that surrounds the nucleocapsid, which can have an icosahedral, icosa(delta)hedral, or helical shape. Source: https://clinicalgate.com/viral-structure-classification-and-replication/

Different classes of viruses have distinctive shapes depending on the capsid arrangement (Figure 2): in animal viruses, two kinds of capsid structures are the most common, such as the spherical capsid and the helical capsid. Structural proteins assembly into subunits that serve as building blocks for the build of viral capsid; they are organised in a symmetric manner, which can acquire either icosahedral or helical symmetry. Spherical shaped viruses possess an icosahedral structure geometry, while helical capsids possess an elongated capsid structure[1] (Figure 3).
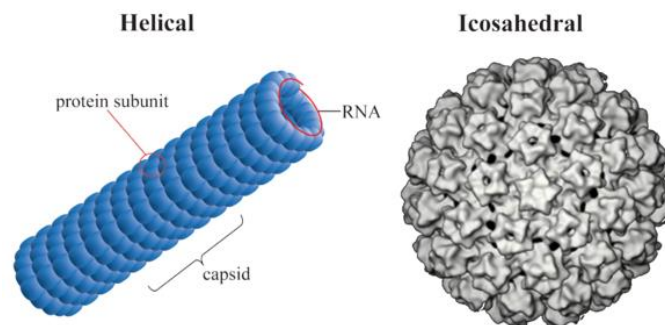
Figure 3. Different organization of the viral capsomers into helical and icosahedral geometries. Source: https://www.ck12.org/book/CK-12-Biology/section/13.2/

1.4 Virus Life Cycle in Animal Hosts

Viruses, as intracellular obligate parasites, are forced to usurp the metabolic machinery of their hosts to complete their life cycle. The virus life cycle can be divided into three main stages: entry, genome replication, and exit.

1.4.1 Virus Entry Phase

This phase can be further sub-divided in four different steps: attachment, penetration, cytoplasmic trafficking, and uncoating.

- In the *attachment phase* the virus particle needs to recognise some attachment factors (i.e. glycosaminoglycans) on the host cell surface; these factors help the virus to interact with some specific membrane receptors which recognise and bind the viral structural proteins. These viral receptors may have different molecular composition (i.e. protein, glycoproteins phospholipids) and function; indeed, that the virus exploit them as receptors for entry process. For instance, the physiological function of LDL receptor is to uptake LDL particles into cells, but is also serves as entry receptor for *Rhinovirus*[18].

- To entry the host cell the virus needs to permeate the phospholipidic membrane. Enveloped viruses enter into the cell by using two mechanisms: *direct fusion* of the viral envelop with the cell membrane followed by the release of the nucleocapsid in the cytoplasm or *receptor-mediated endocytosis* where the virus enters the cell inside an endosome. Non-enveloped viruses use only the *receptor-mediated endocytosis* mechanism.

- Inside the cell the virion needs to get to an appropriate site for genome replication that could be located either in cytoplasm or in the nucleus. Regardless the site of replication, the viral particle makes use of the host's *microtubule-mediated transport* to reach the replication site[19]. If viruses have to reach the nucleus for replicating, they often employ nuclear pore complexes (NPCs) — large protein complexes that act as passageways for the transport of molecules into and out of the nucleus[20].

- The uncoating phase allows the viral genome to be exposed to cellular machinery for viral gene expression. This process may occur in different sites depending on the virus type. For viruses that replicate in the nucleus, the uncoating may occur in the cytosol or inside the nucleus, depending on the size of the viral genome: in the case of human immunodeficiency virus 1 (HIV-1) and influenza A virus the capsid goes toward dismantling before accessing the nucleus and only their genome passes through the NPCs, while other viral capsids, such as those of hepatitis B virus (HBV) are small enough to cross the NPC and genome release occurs when inside the nucleus[20].

1.4.2 Genome Replication Phase

This phase varies among the different virus families, since viruses are endowed with different replication mechanisms, even though they are in common with the members of the same family. Moreover, the dependency on host machinery to complete the replication process varies among the different families, ranging from viruses that entirely depends on host machinery for replication to ones that rely more on self-enzymes[1].

1.4.3 Virus Exit Phase

In this final phase the new assembled virion is released from the host cell membrane. The exit stage can be divided into three steps: capsid assembly, release, and maturation (Figure 4).

- The capsid assembly is composed of two stages: capsid assembly and genome packaging. These two processes can occur sequentially or simultaneously depending on the virus type. In the case of picornavirus, for instance, an empty capsid is first assembled without the RNA, that is next inserted passing through a pore formed in the procapsid structure[21]. In other viruses the capsid assembly at the same moment of the genome packaging. The virus is able to selectively package its genome since the viral capsid proteins contain a binding site that recognizes a specific sequence of the genome[22].

- The release of the assembled virions follows different ways on the base of virus strain. Naked viruses exit via cell lysis, the host membrane is disrupted and the virions are released from the host cell. In the case of enveloped viruses, the envelopment of the capsid is required to occur before the release. The envelopment may take place after the capsid assembly by interaction of the viral capsids with viral envelope glycoprotein (i.e. HBV)[23], or in parallel to the capsid assembly (i.e. retroviruses). Besides, the envelopment site changes among different viruses. The plasma membrane is the site of envelopment for some viruses, such as retrovirus and influenza virus, whereas endoplasmic reticulum (ER) and Golgi bodies are the sites of envelopment for others, such as herpesvirus and HBV. In any case, enveloped viruses are usually released extracellularly via exocytosis; this process is called *"budding"*[1].

- The maturation step does not occur in all viruses but for some of them is essential to acquire infectious potential. Maturation induces structural and physical changes in the viral particle that may restart the cycle in a new host cell. In the case of HIV, the virion particles released in the extracellular space contain the GagPol polyprotein, which comprises three enzymes critical for the infectious cycle: integrase, reverse transcriptase, and protease. During the maturation phase the viral protease cleaves GagPol into the individual polypeptides, triggering a conformational change and producing the mature virion[24].
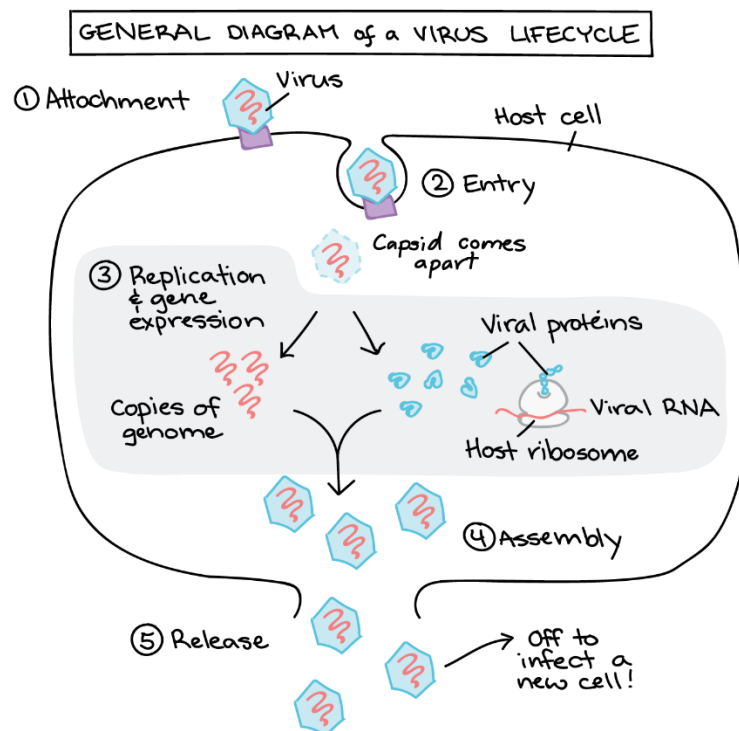
Figure 4. General representation of a virus life cycle. Source: https://www.khanacademy.org by Anderson Brito, CC BY-SA 3.0.4.

The present PhD thesis has been then organised in three main issues related to three virus strains which have represented the main targets of the compound series here developed as potential antiviral agents.

CHAPTER 2. *Flaviviridae* Family Viruses

Flaviviridae is a family of small enveloped viruses with positive stranded, non-segmented RNA genomes of 9.000–13.000 bases. This family includes several viruses capable of infecting mammals and birds such as yellow fever virus YFV, Japanese encephalitis JEV, Dengue virus DENV, West Nile virus WNV, Zika virus, human hepatitis C virus HCV and bovine viral diarrhea virus BVDV, and can cause many diseases, such as hepatitis and fatal mucosal disease. At present, more than 100 species have been identified in this family and they can be divided among four genera, genus *Flavivirus*, genus *Hepacivirus*, genus *Pegivirus*, as well as genus *Pestivirus*[25] (Figure 5).
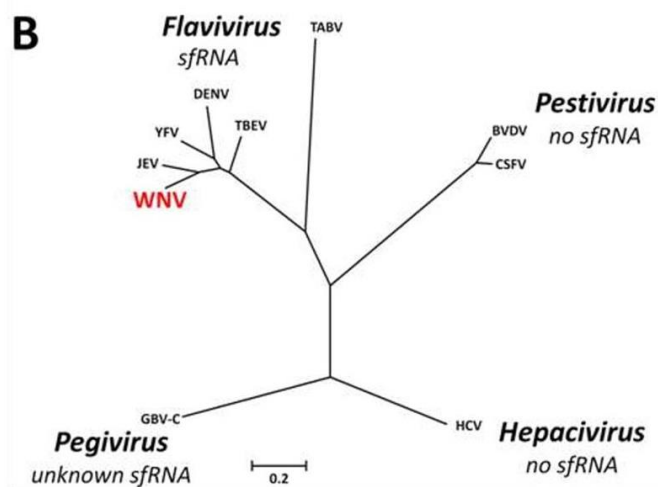
Figure 5. Phylogenetic Relationships within The Family Flaviviridae. (Roby J.A, et al, 2014)

2.1 *Pestiviruses*

Viruses in the genus Pestivirus infect pigs and ruminants, including cattle, sheep, goats, and wild ruminants. Pestivirus genus comprises three species, Bovine viral diarrhea virus (BVDV), Border disease virus (BDV) and Classical swine fever virus (CSFV)[26]. Along these, in the past decades, new members of pestiviruses have been found infecting animal either causing clinical manifestations or asymptomatic infections. These currently unclassified pestiviruses have been isolated in the past decade from giraffes (Giraffe-1 pestivirus), cattle (Atypical ruminant pestiviruses or Hobi-like viruses), antelopes (Pronghorn antelope pestivirus), piglets (Bungowannah virus; Atypical porcine pestivirus, APPV; Lateral-shaking Inducing Neurodegenerative

Agent (Linda) virus), small ruminants (Aydin-like pestivirus, Tunisian sheep pestiviruses), rats (Norway-rat pestivirus) and bats (bat pestivirus)[27,28] (Figure 6).

Figure 6. Phylogenetic classification of pestiviruses. Roby J.A, et al. (2014). "Noncoding sub-genomic flavivirus RNA: multiple functions in West Nile virus pathogenesis and modulation of host responses." *Viruses.* 6(2), 404-27.

Differentiation based on comparison of conserved genomic sequences has led to the division of BVDV, CSFV and BDV into different genotypes (Figure 7). The most conserved portion of the pestivirus genome is located in the untranslated sequences that proceed the open reading frame (5'-untranslated region or 5'-UTR). This sequence has been compared among the different viruses within each species in order to define distinct genotypes, thus it has been observed that these 5'-UTR sequences are conserved among viruses within the same pestiviral genotype[26,29].

Figure 7. Phylogenetic analysis of some pestiviruses based on comparison of the 5′ untranslated region showing the similarity percentage among different genotypes[30].

Pestiviruses are capable of causing zoonotic infections that may be subclinical or cause enteric, haemorrhagic or wasting diseases, such as the Bovine Viral Diarrhoea, related to important economic losses for livestock industry worldwide[31].

2.2 Bovine Viral Diarrhea Virus (BVDV)

Bovine viral diarrhea viruses (BVDVs) are a heterogeneous group of viruses with global distribution that vary in antigenicity, cytopathology and virulence. BVDV has a positive sense, single stranded RNA genome that is prone to mutation. The high mutation rate of its genome helps BVDVs to adapt and to bypass the host immune system, thus complicating the development of efficient therapeutic options to fight it and also make difficult the proper classification for these viruses[30]. Traditionally, pestiviruses are named after the affected host species and/or the diseases they cause. BVDVs are able to cross species barriers to infect a wide range of hosts, thus BVDV's infections have been detected in diverse domestic, and wildlife animal species, including cattle, sheep, goat, pig, deer, buffalo, bison, and alpaca[26,32].

Among these species may be distinguished two different genotypes BVDV-1 and BVDV-2, which can cause infections characterized by mild or subclinical symptoms in adult animals.

The viruses isolated from either genotype can be distinguished in two biotypes, cytopathic (cp) and non-cytopathic (ncp), based on their activity in cell cultures: cp biotypes, unlike ncp, induce apoptosis in cultured cells. The non-cytopathic biotype predominates in nature and possess the ability to establish persistent infections

15

(PIs)[30]. These persistent infected animals are the result of the fetus' infection by the ncp BVDV strains in the early stage of gestation, and they represent the main source of viral spread and the perpetuation of BVDV within herds[33,34].

Further characterization of the BVDV-1 genotype has revealed two distinct sub-genotypes (BVDV-1a and BVDV-1b). Studies on South American BVDV2 disclosed the existence of two diverse BVDV-2 sub-genotypes (BVDV-2a and BVDV-2b)[35]. More recent studies identified at least 11 BVDV-1 sub-genotypes and 3 BVDV-2 sub-genotypes indicating considerable genetic diversity within this species[36].

Polyclonal sera and monoclonal antibodies distinguish between BVDV genotypes, that can be translated into clear antigenic differences between BVDV-1 and BVDV-2 strains (Figure 8). Many studies suggest the clear antigenic diversity among BVDV sub-genotypes, since have been observed that calves vaccinated with killed or modified live vaccines derived from BVDV-1a strains showed clear differences in serum neutralization (SN) titres to a panel of BVDVs, besides consistently lower SN titres were observed against viruses from the BVDV-1b sub-genotype[30].
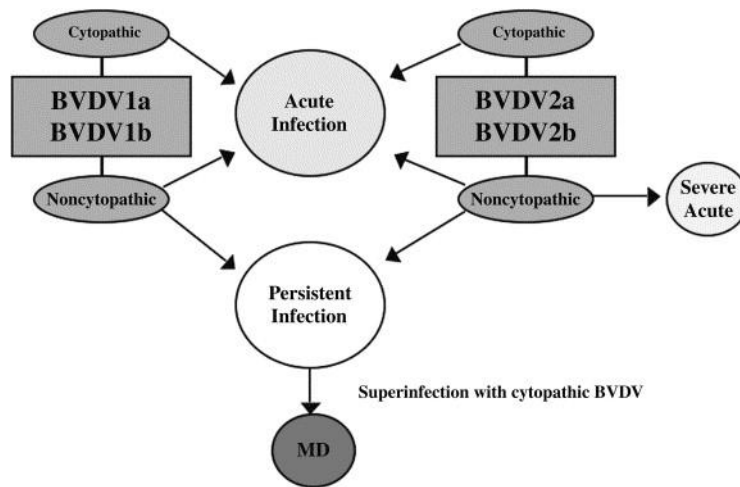
Figure. 8. Differences and similarities among BVDV1 and BVDV2. MD = mucosal disease[30].

The interest for this virus is strongly encouraged by its similarity with the human pathogen hepatitis C virus (HCV). Due to the difficulties in preparing *in vitro* HCV cultures, BVDV has been largely used as HCV surrogate model for the identification and development of anti-HCV agents[37].

2.2.1 BVDV Virion Structure and Genome organization

The intact BVDV virion has a diameter of about 40-60 nm and it is composed of a nucleocapsid carrying the genomic RNA coated with the capsid proteins. It is an enveloped virus, that is surrounded by a lipid bilayer supporting virus-encoded glycoproteins (Figure 9).

The genome of BVDV is a single-stranded, positive-sense RNA molecule of approximately 12,300 bases in length in non-cytopathic strains, though the genome length is variable, strain-dependent and may vary between cp and ncp biotypes.
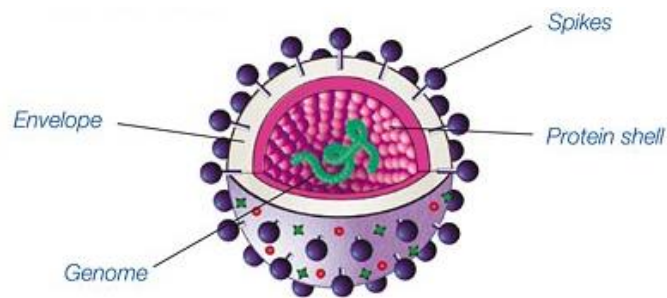
Figure 9. Structure of BVDV. Source: https://www.bode-science-center.com/center/glossary/bvd-virus.html.

BVDV's genome is not polyadenylated at the 3' end and is organized in a large open reading frame (ORF) region that encodes all viral proteins (N^{pro}, Cap, E^{rns}. E1, E2, p7, NS2, NS3, NS4a, NS4b, NS5a, NS5b). The two nucleotide tracts at both the 5' and 3' ends are the 3'/5'-untranslated regions (UTR), thus they do not encode for proteins. However, these two regions possess an important function since they can fold to form secondary structures capable of interacting with both viral and cellular proteins and the RNA itself to regulate replication/transcription as well as translation of ORF polyprotein. The 5'-UTR plays also a fundamental role in the ribosome binding to the IRES region and protein translation processes of the ORF sequence into a large polyprotein, subsequentially cleaved into the single viral proteins[38] (Figure 10).
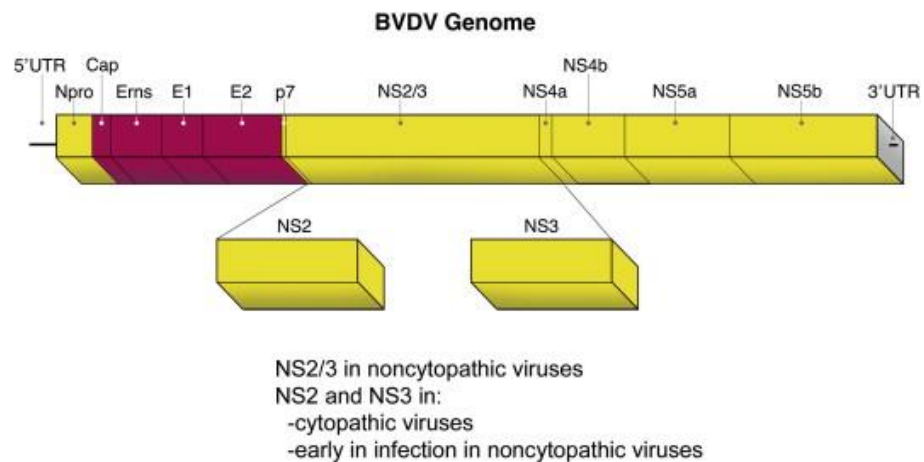
Figure 10. BVDV genome organization and differences between cytopathic and non-cytopathic biotypes[39].

2.2.1.1 BVDV Structural Proteins

The encoded proteins Cap, E^{rns}. E1, E2 are all viral structural protein; the Cap region encodes for the capsid or core proteins while E^{rns}, E1 and E2 are three envelope glycoproteins.

E^{rns} is a glycosylated protein, organized in homodimers, that is linked with weak interactions of its C-terminus to the virion's surface in order to be able to dissociate from the virus particle and be secreted in soluble form from the infected cells. E^{rns} protein is also endowed with RNase activity, degrading both single-stranded and double-stranded RNAs. This function is thought to be important in limiting the host interferon (IFN) mediated innate immune response to the viral ssRNA[40].

On the other hand, E1 and E2 are integral membrane proteins that can be organized in homodimers of E2 and heterodimers of E1/E2[41]. The heterodimers of E1 and E2 are necessary for infectivity of the virus particle: the E2 glycoprotein contains the major antigenic determinants and possess a receptor binding function as well as membrane fusion domain, playing a pivotal role into the virus attachment and entry phases; the E1 protein is believed to possess a regulation function in preventing the premature activation of the membrane fusion domain of E2[39].

2.2.1.2 BVDV Non-structural Proteins

The genomic RNA encodes for non-structural proteins that are necessary for the viral replication and infectivity processes.

The autoprotease N[pro] is a protein only expressed within the Pestivirus genus; it is endowed with protease activity and cleaves itself from the BVDV polyprotein. It is also involved into the proteasomal degradation of the host factor IRF-3, an important inducer of interferon production in virus infected cells[42].

The p7 protein is cleaved from the polyprotein by the activity of a cellular peptidase and it exists in infected cells as free p7 or as E2-p7 dimers. It is thought to play a similar role to that of HCV p7 protein by inducing the formation of ion channels in the host cell's membrane in order to facilitate the cell-to-cell movement of the virus.

The NS2 and NS3 proteins are the key enzymes involved in viral RNA replication. These proteins are mainly present in unprocessed form NS2/3 in cells infected by ncp biotypes, while in cell infected by cp biotypes, they are primarily cleaved in the two separate enzymes. The cleavage of NS2/3 is mediated by the autoprotease activity of the NS2 protein and is fundamental for replication; Lackner, T. et al. demonstrated that there is a temporal modulation in ncp viruses, thus the NS2/3 cleavage is performed only in the early stages of infection and drastically drops off later in the infection process, resulting in mainly unprocessed NS2/3 present in the ncp virus infected cells. This is thought to be related to the incapability of the cp BVDV biotypes of establishing persistent infections, while the temporal modulation may help the ncp viral strains to adapt to its animal hosts causing persistent infections[43].

The NS2 protein is endowed with a protease activity and is involved into NS2/3 cleavage, it also contains two internal signal peptides that are necessary for protein translocation to the endoplasmic reticulum.

The NS3 protein possesses different enzymatic activities. The N-terminus portion contains a serine protease domain responsible for many cleavages in the viral polyprotein i.e., NS3/NS4A, NS4A/NS4B, NS4B/NS5A, and NS5A/NS5B. The C-terminus of the protein contains an RNA helicase domain that unwinds the secondary structure of the viral genome in order to start the translation process, associated with nucleoside triphosphatase (NTPase) domain, both fundamental for RNA replication[44].

The NS4a is a 63 aa protein and functions as cofactor for the NS3 serine protease activity. The hydrophobic protein NS4b is a membrane associated protein placed on the Golgi compartment membrane that interacts with the viral RNA replication complex by anchoring it to the cellular membrane.

The NS5A protein is part of the replicase complex; it is a large hydrophilic phosphoprotein similar to the hepaciviruses NS5A, whose functions are not completely clear yet. The NS5b protein is the RNA-dependent RNA-polymerase and is the major protein in replication of the genomic RNA taking place in the host cell cytoplasm. This protein contains the GDD amino acid motif (Gly-Asp-Asp) present in all positive-strand viral RNA polymerases and NTPase domains[39,45].

2.2.1.2.1 BVDV RNA dependent RNA polymerase

The RNA dependent RNA polymerase is the key enzyme involved in RNA viruses' genome replication. Polymerase enzymes of different viral strains have common features along with peculiar tracts and structural features shared by the members of the same family or genus.

The core RdRp domain is composed by the thumb, palm and the fingers subdomains. These regions are fundamental for template binding, polymerization and nucleoside triphosphate (NTP) entry. A comparative analysis of the RNA polymerases of different RNA viruses highlighted eight conserved sequence motifs, I-VIII. Five of these motifs are in the palm domain, including the GDD motif (VI).

BVDV polymerase is a protein of 688 aminoacids and presents all the typical RdRp domains. In the core region, the fingers domain presents also a three stranded fingertip subdomain directly associated with the thumb domain (Figure 11). The palm domain, placed at the junction of the fingers and the thumb domains, comprehends the RNA Recognizing Motif (RRM) which selects NTPs over dNTPs and catalyses the phosphoryl transfer reaction by coordinating two metal ions. The thumb domain contains the GTP-binding site that is specifically required for the initiation of RNA synthesis in BVDV, regardless of the nucleotide at the 3' end of the RNA template. Finally, the finger domain is responsible for the translocation of the template or the products during replication.

BVDV polymerase has high structural similarity to HCV polymerase even if it presents some differences in the fingertip region, which is three stranded in the BVDV polymerase, whereas has 4 strands in the HCV RdRp. In addition, the BVDV polymerase is about 130 amino acids longer at the N-terminus than HCV polymerase.

Flaviviridae RNA replication process uses a primer-independent (*de novo*) mechanism, in which the polymerization directly starts at the 3' end by direct addition of NTPs to the new RNA chain without primer intervention[46].

Figure 11. 2.6 Å X-ray crystal structure of BVDV polymerase. The N-terminal, fingers, palm, and the thumb domains are coloured yellow, blue, green, and red, respectively[47].

2.2.2 Bovine Viral Diarrhea: Pathogenesis

BVDV-1 and BVDV-2 genotypes are capable of causing both acute and persistent infections related to a wide range of symptoms and different clinical manifestations. Cattle represent the BVDV natural hosts, nevertheless infection by BVDV has been demonstrated in numerous other species[27].

Type 1 is the most prevalent genotype, whilst type-2 genotype is less common but it is more virulent, provoking severe diseases including thrombocytopenia[48].

Acute infection in cattle result in transient clinical manifestations that begin on day 3 post-infection and last 10-14 days. The infection usually occur by contact with persistently infected cattle since the virus can be transmitted through a wide range of body fluids. The acute infection can be associated with several clinical manifestations such as leukopenia, lymphopenia, thrombocytopenia, immunosuppression, pyrexia and diarrhea, in addition the resultant immunosuppression can ease the emergence of co-infections[34]. Highly virulent strains of BVDV may also cause severe ulceration of the oropharynx, larynx, and oesophagus and haemorrhagic enteritis[48].

Fetal infection in the first trimester with ncp BVDV will cause the born of new persistent infected PI calves. After birth, these PI animals will shed large amounts of virus in all excretions and secretions including milk, semen, saliva, nasal secretions,

urine, blood and aerosols, contributing to the spread of infection. These animals may be clinically healthy but often they appear smaller and weaker compared to the other calves and are also more susceptible to secondary infections. Moreover, if PI animals are subsequently infected during their life with a cp strain of a closely related or homologous virus, may develop severe disease with widespread lesions of the mucosal surfaces and lymphoid tissues, referred to as mucosal disease (MD): the mucosal ulceration and fluid leakage in the gastrointestinal tract provoke diarrhea and dehydration; the damaged tissue become sensitive to bacterial infection and inflammation leading to fatal outcome[34,48].

2.2.3 BVDV Infections: Therapeutic approaches

Two main strategies are pursued in order to limit the virus transmission within herds: eradication of the pathogen's reservoirs, mainly represented by the PI animals and to limit the transmission from the infected cattle to susceptible animals. However, the first strategy can be costly and difficult to pursue, considering the expense of diagnostic testing and taking into account that only less than 1% of the cattle population are PI. In order to limit the transmission of the pathogen among cattle, vaccination represent an essential tool to control the disease' spread; even if currently available vaccines are not completely effective against all the viral genotypes and sub-genotypes they indeed represent a valuable weapon in order to limit the pathogen diffusion and prevent birth of PI calves.

2.2.3.1 Vaccination

The vaccines available can be distinguished among inactivated and modified-live viral (MLV) vaccines. Inactivated vaccines are safer, since they contain viral antigen incapable of replication, on the other hand they need to be administered multiple times to achieve protective antibody levels in the animal. The onset of immunity is delayed of about six weeks, with the possibility of vaccine program failure. Differently, MLV vaccines stimulate immune system and trigger the production of higher levels of antibodies achieving a rapid onset of immunity in the treated animals[49].

Due to the existence of two genotypes and several sub-genotypes of BVDV as well as the two distinct biotypes, cytopathic and non-cytopathic, thus the ability of BVDV

vaccines to cross-protect against the different genotypes and sub-genotypes is fundamental. Historically, BVDV vaccines were developed as monovalent vaccines containing only BVDV-1a as the viral antigen, even though the most diffuse sub-genotype is BVDV-1b; R.W. Fulton et al. demonstrated that MLV vaccination with BVDV-1a vaccines also induce antibody production against BVDV-1b even if in lower titres, that might be translated in a diminished protection against BVDV-1b exposure[50]. Consequently, the development of multivalent vaccines, containing antigens from different viral genotypes and sub-genotypes is recommended to prevent infection by different strains of BVDV[49].

2.2.3.2 Antiviral Drugs

Currently there is no approved antiviral therapy available besides vaccination, thus there is an urgent need to develop new small-molecules to control BVDV infections. The research of new anti-pestivirus agents is complicated by the high mutation rate of the genomic RNA due to the absence of proof-reading activity of its RNA-dependent RNA-polymerase. Therefore, the research of BVDV inhibitors is moving forward and currently many compounds have been discovered endowed with antiviral activity by interfering with different potential targets.

The RNA-dependent RNA polymerase (RdRp), the key-enzyme involved in genome replication, is the most frequent target for the design of antiviral compounds, with many efficient inhibitors reported in literature, divided in nucleoside NI and non-nucleoside NNI inhibitors. While NIs have generally a broad-spectrum activity, NNIs are usually specific toward a single genus and in few cases they could also be active against different genera within the same family[51].

Among the NIs, the inhibitory effect against the viral RdRp of the two highly hindered adenine derivatives FEVB28 and FEG118 and their analogues have been described[52].

In addition, several RdRp non-nucleoside inhibitors NNIs belonging to diverse chemical classes have been identified. Among the non-nucleosidic compounds the nitrogen heterocyclic drugs represent the largest subgroup[51].

2.2.3.2.1 RdRp non-nucleosidic inhibitors NNIs: Nitrogen Heterocycles.

The nitrogen heterocyclic compounds represent a subgroup of anti-BVDV molecules acting as RdRp inhibitors (Figure 12). These compounds have been tested

in vitro against BVDV infected cell lines and revealed an interesting antiviral activity. Currently, due to the paucity of in vivo data, the application in therapy of these compounds have been hindered[51].

Baginski, S. G. et al. identified a triazinoindole based molecule, VP32947, that showed in vitro antiviral activity against virus isolates from pestivirus species, including cytopathic and noncytopathic isolates of BVDV-1 (NADL, NY1 sub-genotypes), BVDV-2 (125C, 125NC sub-genotypes), BDV and CSFV. In particular, regarding its anti-BVDV activity its molecular target have been identified in the viral RdRp. By testing the compound in drug-resistant virus variants, the site of action have been confirmed to be located in a turn region between two α-helix domains in the finger portion of the enzyme involving a key contact with the F224[53].

Paeshuyse, J. et described the anti-BVDV activity of the 5-[(4-bromophenyl)methyl]-2-phenyl-5H-imidazo[4,5-c]pyridine (BPIP) and this discovery has been followed by further studies on different series of imidazo[4,5-c]pyridines[54,55,56]. These compound class proved to be effective in blocking the RdRp of BVDV by binding the same portion of the finger region involved into the VP32947 interaction. Molecular docking studies highlighted the key contacts within the site of action, such as the establishment of three hydrophobic contacts of the inhibitor with A221, A222, and F224, and of an hydrogen bond between N3 of the imidazole ring with the backbone oxygen of residue F224[54]. Interestingly, some of the imidazo[4,5-c]pyridines demonstrated to be also endowed with an anti-HCV activity[56].

Paeshuyse, J. et al discovered also the anti-BVDV activity of a series of imidazo[1,2-a]pyrrolo[2,3-c]pyridine[57,58]. Among them, compound AG110 demonstrated the ability to interfere with the functioning of the replication complex of the virus by binding to the finger domain of the RdRp, besides it showed no activity against RdRp E291G and F224S mutants suggesting the possible establishment of key contacts with those residues in the active site[57].

More recently, compound LZ37, a pyrazolo[4,3-e][1,2,4]triazolo[1,5-c]pyrimidine formerly known as an A_{2A} adenosine receptor antagonist, was identified as a selective inhibitor of in vitro BVDV-1 (NADL strain) replication by interfering with the formation of the replication complex and the RNA synthesis processes. The viral strains carrying the F224Y mutation revealed to be significantly less sensitive to LZ37, confirming the hypothesized binding site as the tip of the finger domain[59].

The capability of inhibiting the BVDV RNA synthesis has been described for some γ-Carboline derivatives[60] and quinoline derivatives[61]. The anti-BVDV activity of the acridine nucleus, by blocking the viral RNA synthesis, have been also reported[5,62].

The benzimidazole derivative 227G has been reported as the first benzimidazole derivative endowed with potent and selective activity against both BVDV and HCV. Enzymatic assays along with docking calculations disclosed the mechanism of action of this compound as a RdRp inhibitor by binding the BVDV polymerase finger domain establishing key interactions with residues I261, N264 and A392[63].

Finally, in a recent paper, the antiviral activity of a series of imidazole derivatives have been evaluated in vitro against a panel of viruses, revealing some potent anti-BVDV compounds capable of inhibiting viral replication with a better potency than the reference drug ribavirin (i.e. compound 8a)[64].
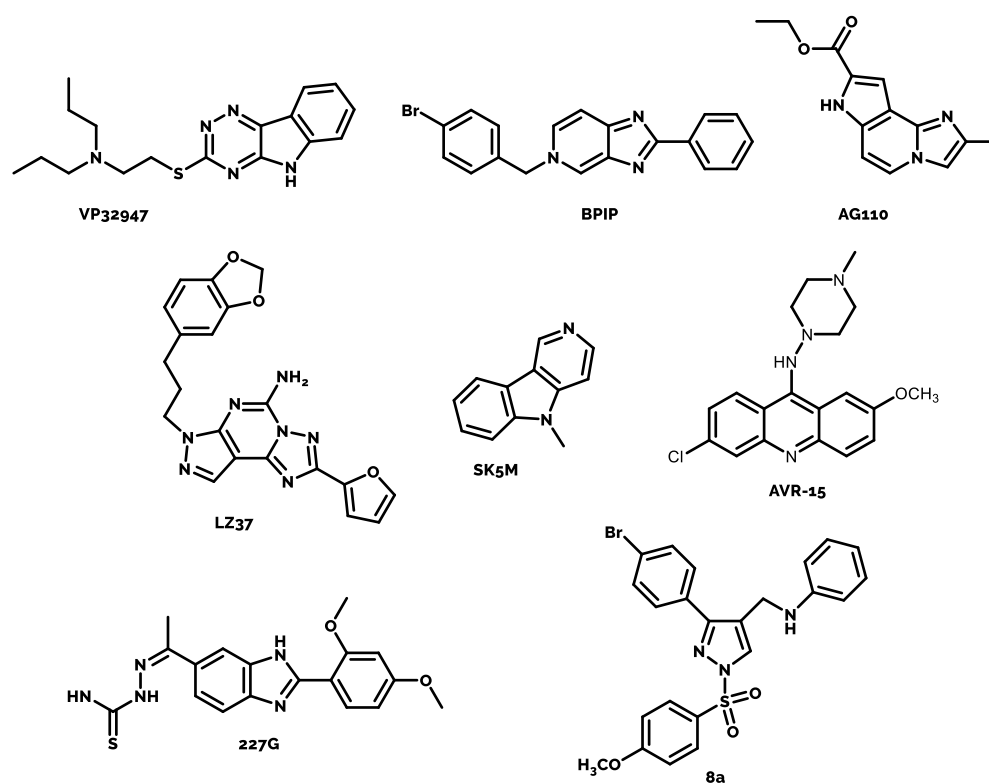
Figure 12. Chemical structure of some nitrogen heterocyclic compounds that demonstrated anti- BVDV activity in vitro.

2.2.3.3 Interferons

Interferons (IFNs) are multifunctional proteins released from host cells in response to the presence of viruses. Interferons have been studied as nonspecific anti-BVDV

agents both *in vitro* and *in vivo*. Both cytopathic and non-cytopathic biotypes of BVDV revealed to be susceptible *in vitro* to the treatment with recombinant human interferons. However, the *in vivo* administration of IFN to treat the infection has been difficult to demonstrate, since, in many cases, interferon treatment revealed poor *in vivo* efficacy[65].

CHAPTER 3. Respiratory Viruses RVs

Acute respiratory infections (ARIs) represent a major health problem with significant morbidity and mortality, especially in children, elderly and immunocompromised people. ARIs manifest as Upper (URI) or Lower (LRI) respiratory tract infections and may move between the two compartments. These infections are associated with a wide range of diseases and symptoms, varying from mild and self-limiting to severe clinical manifestations[7,66]. Respiratory tract infections represent a serious burden with significant morbidity and mortality especially occurring in children, elderly and immunocompromised people. The severity of this infections, especially in children under five, is worse in low-income countries due to poor hygiene conditions, malnutrition and lack of adequate diagnosis and treatment facilities, resulting in a higher case-fatality rate. The vast majority of ARIs have a viral aetiology and may be the result of the infection of different respiratory viruses, in particular RNA viruses, such as respiratory syncytial virus (RSV), influenza virus (IV), parainfluenza virus (PIV), metapneumovirus (MPV), rhinovirus (RhV), and coronavirus (CoV)[7] (Table 1).

VIRUS	FAMILY	SIZE (nm)	RNA GENOME	ENVELOPE	GENETIC OR ANTIGENIC TYPES
RSV *Respiratory Syncytial Virus*	*Paramyxoviridae*	120–200	Linear ss(-)	Yes	Antigenic subgroups A and B with 10 A genotypes and 13 B genotypes
IV *Influenza Virus*	*Orthomyxoviridae*	80–120	Segmented ss(-)	Yes	3 antigenic types (A, B, C)
PIV *Parainfluenza Virus*	*Paramyxoviridae*	120-180	Linear ss(-)	Yes	4 serotypes (1, 2, 3, 4); subtypes 4a and 4b
MPV *Meta- -pneumovirus*	*Paramyxoviridae*	120-180	Linear ss(-)	Yes	Subtypes A and B; subgroups A1/A2 and B1/B2, respectively
RhV *Rhinovirus*	*Picornaviridae*	20–27	Linear ss(+)	No	>100 antigenic types
CoV *Coronavirus*	*Coronaviridae*	80–160	Linear ss(+)	Yes	6 genotypes (229E, OC43, NL63, HKU1, SARS-CoV, MERS-CoV)

Table 1. Taxonomy and virologic properties of the major human respiratory RNA viruses[7].

ss(-), single-stranded negative-sense RNA; ss(+), single-stranded positive-sense RNA; SARS-CoV, severe acute respiratory syndrome-coronavirus; MERS-CoV, Middle East respiratory syndrome-coronavirus.

3.1 Upper Respiratory Tract Infections URIs

Upper respiratory tract infections involve the nose, sinuses, pharynx, larynx, and the large airways. Approximately 90% of these infections are caused by respiratory viruses while only the 10% has bacterial aetiology; the most common aetiological cause is the rhinovirus (RhV) infection, but acute upper respiratory tract infections can also be caused by influenza virus, adenovirus, enterovirus, and RSV[67].

These infections are often associated with clinical manifestations as rhinitis, pharyngitis, tonsillitis, and laryngitis with self-limiting symptoms that commonly include: cough, sore throat, nasal congestion, headache, low-grade fever and myalgias. The onset of symptoms usually begins one to three days after exposure and lasts approximately 7–10 days[68]. URIs are accountable for generating a large economic burden in terms of missed days of work[69]. Even if these infections are usually mild and self-limiting in adults in some cases if neglected, they can extend to the lower respiratory tract, predispose to secondary bacterial infections and cause the exacerbation of pre-existing medical conditions, such as asthma and chronic obstructive pulmonary disease (COPD). Among these possible complications pneumonia and bronchitis contributes significantly to morbidity and mortality, especially among children and high-risk population[68,70].

3.2 Lower Respiratory Tract Infections LRIs

Lower respiratory tract infections differ from upper respiratory tract infections by the area of the respiratory tract they affect, thus they involve the airways below the larynx. Lower respiratory tract infections include: bronchitis, pneumonia and bronchiolitis. The main aetiological causes of LRIs are bacterial infections of *Streptococcus pneumoniae* or *Haemophilus influenza* along with viral infections, in particular of influenza virus, rhinovirus (RhV), human adenovirus (HAdV), respiratory syncytial virus (RSV), and human metapneumovirus (hMPV)[71,72].

Symptoms of lower respiratory tract infections vary and depend on the severity of the infection, ranging from symptoms similar to the common cold, to more severe clinical manifestations including, severe cough, fever, difficulty breathing and chest pain. When neglected, complications may occur including congestive heart failure, respiratory failure, respiratory arrest, sepsis and lung abscesses, often with fatal outcome[73].

The risk of complication is major for children, adults over 65 years of age, immunocompromised people, and also for patient with underlying medical conditions, such as asthma and COPD[74].

Nearly 2.38 million deaths resulted from lower respiratory infections in 2016, making LRIs the sixth leading cause of mortality for all ages and the leading cause of death among children younger than 5 years and adults over 65 years old[71].

3.3 Respiratory Syncytial Virus, RSV

Human respiratory syncytial virus (RSV) is one of the most common causes of respiratory infections in children, and may manifests as upper respiratory infection or as bronchiolitis, a lower respiratory tract illness with small airway obstruction that can rarely progress to pneumonia.

Human RSV belongs to the *Pneumoviride* family, and is in the genus *Orthopneumovirus*. The former *Pneumovirinae* subfamily have been recently promoted to family, before that the RSV belonged to the *Paramyxoviridae* family, *Pneumovirinae* subfamily, *Pneumovirus* genus[75].

It is an enveloped virus *with a* single-stranded negative-sense RNA genome. *Paramyxoviridae* family includes several highly contagious viruses including the human pathogens measles, mumps, as well as the zoonotic viruses Hendra and Nipah[76].

RSV is a medium diameter virus (120-300 nm) and its virion particle consists of a helical nucleocapsid containing the negative-sense single-stranded RNA, tightly bound to the nucleoprotein (N) (Figure 13). The capsid is surrounded by a lipidic membrane containing the integral glycoproteins G (receptor binding), F (membrane fusion), and the short hydrophobic protein SH. The M (matrix) protein at the inner surface of the envelope is important in viral morphogenesis. The virions also contain an RNA-dependent RNA polymerase (L), a phosphoprotein (P), and the matrix protein M2-1. The RdRp (L) along with the N, P and M2-1 proteins compose the ribonucleoprotein complex (RNP). In addition, three non-structural proteins (NS1, NS2, and M2-2) are produced in infected cells[77,78].

Human RSV can be divided into two antigenic groups A and B, originally distinguished based on the antigenic differences in the attachment glycoprotein G. Later, further studies of the viral genome allowed the subdivision of the two groups

into at least 13 A genotypes and 20 B genotypes. Differently, the F glycoprotein is highly conserved between strains and is one of the antibodies targets; it is therefore a potential candidate as an RSV vaccine antigen[78].
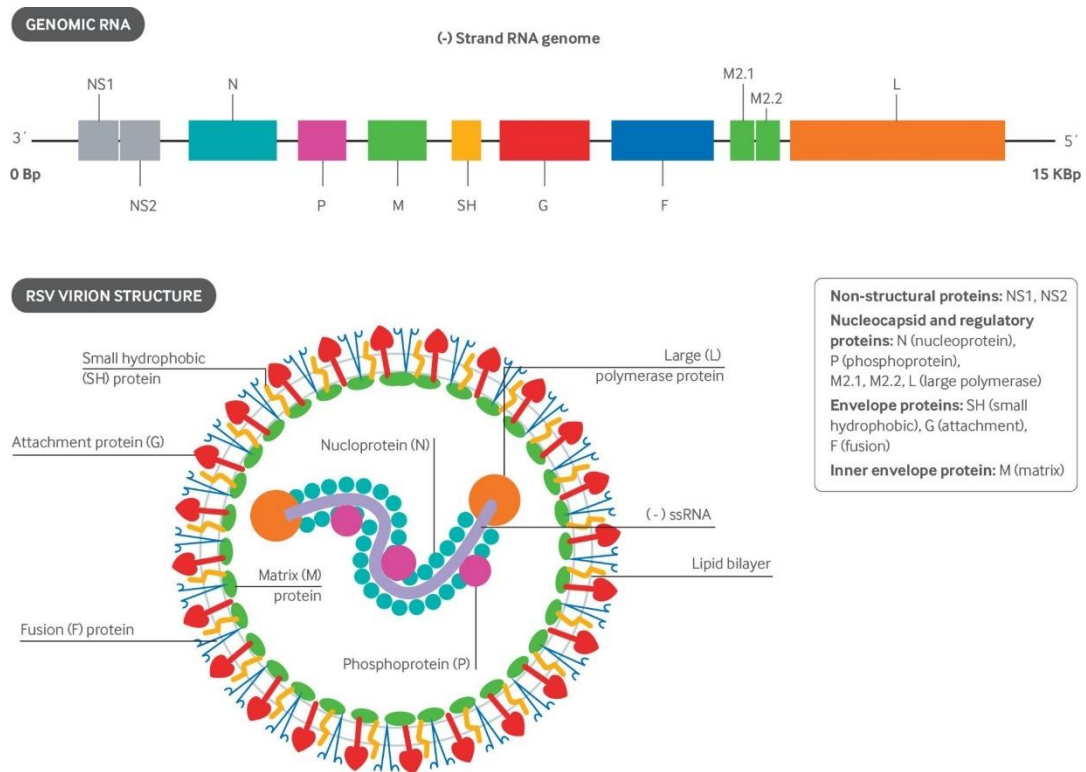
Figure 13. Structure of the human respiratory syncytial virus RSV and its genome organization[78].

3.3.1 RSV: virion structure and replicative cycle

RSV binds the cellular membrane thanks to the G glycoprotein which mediates virus attachment by binding the surface glycosaminoglycans of the ciliated cells of the airways. However, the fusion process requires the participation of all the three surface glycoproteins jointly. These surface glycoproteins represent also the main antigenic determinants for host protective antibodies and may also represent a potential target for therapeutic agents. Following the G binding, the F protein undergo a conformational change that allows viral penetration by fusing the cellular and viral membranes, switching from one metastable structure called pre-fusion (pre-F), to another stable post-fusion (post-F) structure[79]. In the infected cells, F protein is expressed on the cellular membranes and promotes the fusion of the infected cell membrane to the uninfected cells triggering the formation of the characteristic RSV syncytia[77,80]. The SH protein is another envelop protein that forms pentameric pore-like structures that confer cation-selective channel-like activity,

thus the SH protein appears to be a viroporin, a class of small viral proteins that can modify membrane permeability and can affect budding and apoptosis, although its particular function in RSV life cycle is not completely clear[81].

Once inside the host cell the (-)ssRNA is transcribed by the viral RNA dependent RNA polymerase (L), with participation of the nucleoprotein (N), the phosphoprotein (P) and the M2-1 protein. The M2-1 protein functions as a transcription anti-termination factor allowing the synthesis of complete RNA, it is also responsible of the binding of the ribonucleoprotein complex RNP with the M protein which initiates assembly and budding processess[82,83].

The nucleoprotein N tightly binds the RNA genome forming a left-handed helical N-RNA ribonucleoprotein complex (RNP). The RSV genome replication takes place in the host cell cytoplasm where the viral RdRp (L) interacts with the multifunctional phosphoprotein (P). The P protein mediates the interaction between the L protein and the nucleoprotein (N) allowing the specific recognition of the RNP template by the RdRp and subsequent RNA polymerization. The N protein consists of a N- and C-terminal domain linked with a hinge region; N forms the helical RNP complex due to the establishment of intermolecular interactions between different N proteins and the viral genome. The P protein is multimeric and establish a contact with the RNP complex with its C-terminal domains by a hydrophobic interaction within a binding pocket located in the N protein N-terminal[84].

The RdRp (L) is a large protein that mediates transcription and replication of RSV genome and also intervene in capping and methylation of mRNA. The active form of L is a heterodimer of the L and P proteins[83]. During the transcription phase the viral genome is transcribed in a set of in 10 capped, methylated and polyadenylated mRNAs, which then direct the synthesis of viral proteins by hijacking the cellular ribosome machinery. Glycoproteins are subsequentially translated and traffic through the secretory pathway to the apical surface, while internal virion proteins remain in the cytoplasm[85].
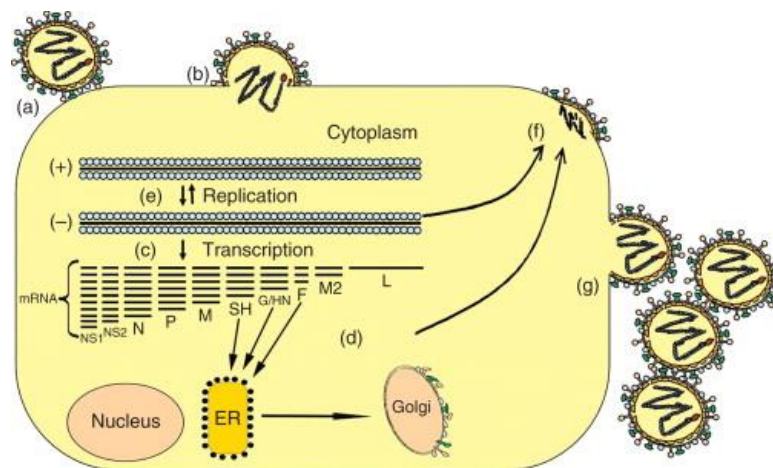
Figure 14. Replicative cycle of Respiratory Syncytial Virus inside the host cell[77].

RSV genome replication requires the production of a complete positive sense anti-genome as intermediate. The non-structural protein M2-2 is involved into the switching of the replication complex from gene transcription to replication.

After replication, the newly synthesised viral genomes are associated with the N protein and wrapped around a nucleocapsid core containing L and P proteins forming the ribonucleoprotein complex (RNPs), that associate with the M protein. These cytoplasmatic inclusions then then traffic to the apical cell surface where the glycoproteins are present already. The translocation of the cytoplasmatic inclusions from the cytosol to the apical membrane requires the cytoskeleton intervention, which is also involved into the filamentous virions formation and budding processess[85].

At the apical membrane the interaction of the cytoplasmatic inclusions with the membrane glycoprotein complex takes place, and the M protein helps determine the shape of virus particles in order to complete viral assembly and initiate budding hijacking cellular apical recycling endosomes to release the new viral particles[81].

The NS1 and NS2 non-structural proteins are not included into the virion particle and are synthesized only inside the host cell, they both interfere with innate immune responses including interferon induction and signalling and also inhibit apoptosis, prolonging the life of the cell, thus increasing viral yield[81,83].

3.3.2 RSV Infections: Therapeutic approaches

Despite the huge economic impact and the medical needs associated with severe RSV infection there are only few antiviral drugs approved for the treatment or prevention of serious respiratory tract infections caused by RSV, thus there is a clear need for new therapeutic options to prevent and treat this infection.

3.3.2.1 Antiviral Drugs

The only licensed drug approved for the treatment of RSV infections in selected cases is the non-specific antiviral ribavirin in inhaled formulation (Figure 15). Therefore, due to its side-effects and lack of reproducible data on efficacy its routine use it is no longer recommended in the treatment of RSV bronchiolitis in UK and USA, thus is still used to treat RSV infections only in selected immunocompromised patient[8].
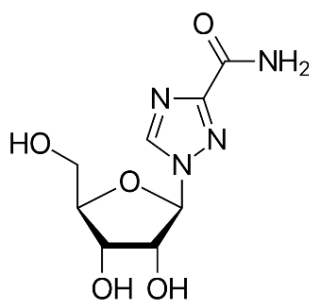
Figure 15. Chemical structure of the unspecific antiviral drug Ribavirin.

Therefore, numerous studies have been made to identify the viral and host factors that contribute to replication of viruses in order to develop new small molecules with the final aim to develop new potential anti-RSV drugs. Several anti-RSV molecules have been discovered and studied, nonetheless none of them have already been approved yet. Many of them are being evaluated in clinical trials, while many others failed to show the expected efficacy either in pre-clinical tests or clinical trials. Most of these new anti-RSV small molecules discovered are directed against the viral F protein, blocking the membrane fusion and viral penetration[9].

3.3.2.1.1 Fusion Inhibitors

GS-5806 (Presatovir®) (Figure 16) is a potent small molecule inhibitor that targets the RSV F protein by inhibiting F protein-mediated cell-to-cell fusion. GS-5806 was found to be active *in vitro* to a wide range of RSV clinical isolates, even if appeared to be involved in the selection of RSV resistant strains carrying mutations L138F and F140L/N571I in the F protein for RSV-A and F488L or F488S for RSV-B. GS-5806 has been evaluated in clinical trials and it showed efficacy in a phase 2a challenge model (attenuated virus in healthy adults) in patients with URIs reducing lower respiratory tract complication progression rate, on the other hand it failed to reach pre-specified efficacy thresholds when infection has already evolved into LRI. However, the phase 2a study showed also the appearance of treatment-emergent GS-5806 resistant RSV variants in which the F140L and T400I mutations were most frequently observed[84]. Thus in order to confirm the beneficial effects of this drug in treating RSV infections, further studies are required[9,86,87].
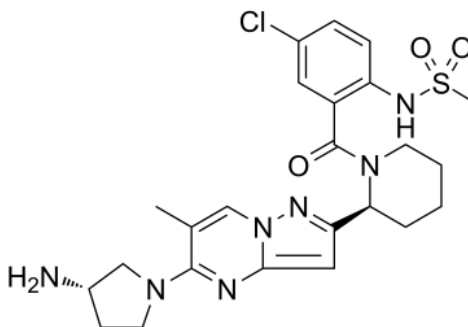
Figure 16. Chemical structure of Presatovir®, GS-5806.

MDT-637 (VP-14637) (Figure 17) is an RSV fusion inhibitor targeting the virus F-protein by binding a hydrophobic pocket. The compound demonstrated a good efficacy in reducing RSV infection in cotton rats, administered by small droplet aerosol. MDT-637 have been reformulated in order to be deliverable to humans, administered by powder inhaler with a quick delivery to the respiratory tract (VP-14637). The results of a phase 1 clinical trial on healthy adults also confirm a good pharmacokinetic profile, that along with MDT-637 in vitro potency on both RSV A and RSV B subtypes, thousand-fold higher than the reference drug ribavirin, suggests the possibility to produce a superior clinical effect compared to ribavirin on natural human RSV infections[9,88].

JNJ-53718678 (Figure 17) is a small-molecule RSV fusion inhibitor interacting with the pre-fusion F protein in a similar manner as MDT-637, despite their structural dissimilarity. It exhibited a high potency against RSV in *in vitro* tests[89]. JNJ-53718678 also demonstrated to be well tolerated and to have a good pharmacokinetic profile in a phase 2a trial on healthy adult volunteers infected with RSV, showing also efficacy in reducing the symptoms and disease severity and duration. Further studies are needed in infants and children to prove the usefulness of the administration of this new anti-RSV agent in future therapies[90,91].

MDT-637 **JNJ-53718678**
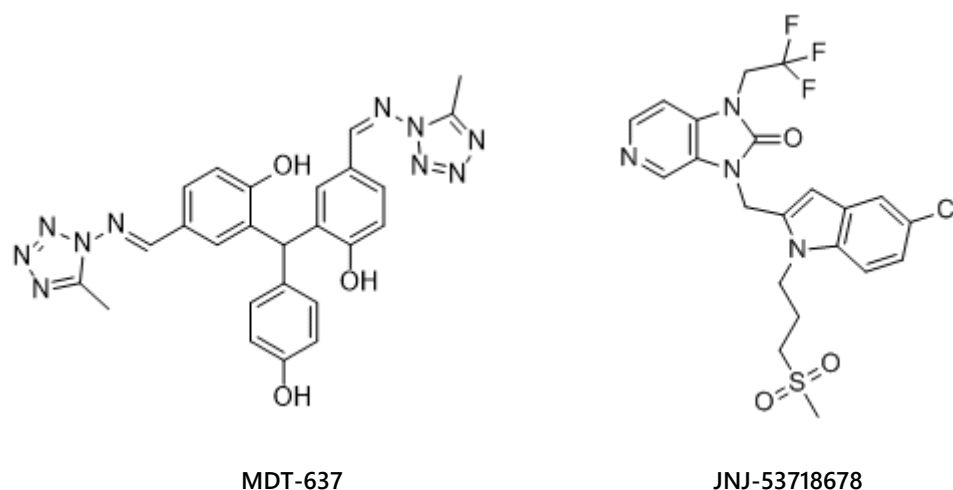
Figure 17. Chemical structures of the small molecules drug candidates as anti-RSV fusion inhibitors MDT-637 (VP-14637) and JNJ-53718678.

Johnson & Johnson also identified benzimidazole-based compound exhibiting extremely potent anti-RSV activity (EC_{50} = 0.16 nM). JNJ-2408068 (Figure 18) also inhibits RSV fusion by binding to a hydrophobic pocket of the protein F core in a similar manner to MDT-637[92]. Despite its high potency against different RSV A and RSV B strains and its anti-inflammatory activity, JNJ-2408068 was later found to be unsuitable for further development because of its long tissue retention in several animal species, such as rats, dogs and monkeys[93].

Thus, further optimization of JNJ-2408068 resulted in identification of the (morpholino)propyl- derivative TMC-353121 (Figure 18), with an improved pharmacokinetic profile, shorter half-life, a high potency *in vitro* blocking both the virus-cell fusion and cell-cell syncytia formation. It also demonstrated the capability of reducing the viral load in in several animal models such as cotton rats, mice, and

primates[94]. TMC353121 could be a drug candidate for treatment of RSV infection; however, safety studies and clinical evaluations are still needed[9].
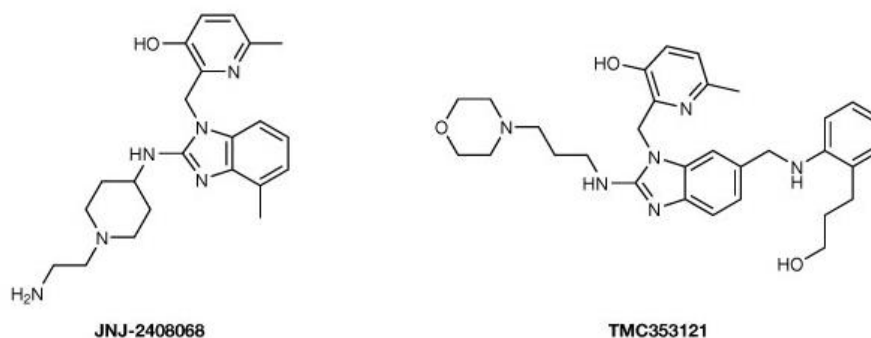
Figure 18. Chemical structures of the benzimidazole derivatives JNJ-2408068 and TMC353121.

AK-0529 Ziresovir® (Figure 19) is a novel compound developed as RSV protein F inhibitor. It has been subject of several clinical trials, which confirmed its safety and good pharmacokinetic profile after oral administration in healthy volunteers (phase 1)[95]. A phase 2 clinical trial (NCT02654171) in hospitalized infants infected with RSV have been recently completed but the results have not yet been published[9].
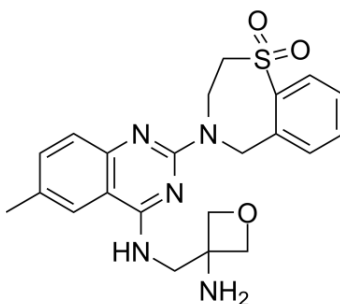
Figure 19. Chemical structure of AK-0529 Ziresovir®.

3.3.2.1.2 L-protein Nis and NNIs Inhibitors

RSV L-protein is an RNA-dependent RNA polymerase with several enzymatic activities, it replicates the viral genome and transcribes mRNAs, it is also a capping enzyme that guanylylates and methylates the 5' end of the viral mRNA transcripts. Moreover, it is also responsible for the polyadenylation at the 3'-ends of the viral mRNAs[96]. The only licensed drug for the treatment of RSV infections is the broad-spectrum antiviral ribavirin, that also inhibits RSV RNA synthesis by interfering in the

viral infection processes at different phases; several mechanism of action have been purposed including inhibition of the cellular enzyme inosine 5-monophosphate dehydrogenase (IMPDH), immunomodulation of antiviral innate and cellular responses, chain termination during viral RNA synthesis, inhibition of viral mRNA capping and accumulation of mutations in viral genomes. This enzyme could also represent a potential new target for the development of new antiviral agents; thus, several nucleoside and non-nucleoside RSV L-protein inhibitors have been developed and are currently under evaluation.

ALS-008176 (Lumicitabine) (Figure 20), a cytidine nucleoside analogue, is a potent and selective inhibitor of RSV RNA-dependent RNA-polymerase activity *via* a classic chain termination mechanism. ALS-008176 showed also a high level of oral bioavailability and a good pharmacokinetic profile in preclinical studies in primates[84]. A clinical trial in healthy adults inoculated with RSV demonstrated a greater reduction of viral load in the groups treated with ALS-008176 than in the placebo group[97]. Following these promising results clinical trials in infants hospitalized with RSV infection are currently ongoing[9,84].
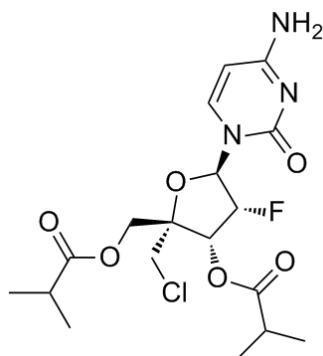
Figure 20. Chemical structure of the nucleoside inhibitor ALS-008176 (Lumicitabine).

BI-D (Figure 21) is a non-nucleoside inhibitor of RSV L-protein that interferes with the viral mRNA guanylylation activity. It demonstrated a sub-micromolar potency *in vitro* against both RSV-A and RSV-B strains and it also proved to reduce the viral load *in vivo* in tested mice[98]. Further studies elucidated the mechanism of action of this compound that but that causes premature abortion of transcription leading to increased amounts of short RNA species (<50 nt) and seems also to interfere in the capping activity of the RSV polymerase. Indeed, *in vitro* selected BI-D resistant mutants carried mutations at positions 1269, 1381 and 1421 of the L-protein, and a

sequence motif around the aa 1269 has been identified as responsible of the formation of a binding pocket essential for the RNA capping activity[84].

AZ-27 (Figure 21) is a non-nucleoside inhibitor of RSV L-protein derived from the structural optimization of the previous developed YM-53403[99]. It interferes in RSV A replication mechanisms, while the *in vitro* activity against RSV B strains is significantly lower. The selected resistant mutants after in vitro inoculation are endowed with the Y1631H mutation that is located in a linker region between the capping domain and the methyltransferase domain that is important for protein flexibility. Thus, AZ-27 probably hinders the structural modification of the polymerase in the form required for the RNA synthesis[84]. Unfortunately, further *in vivo* studies in rats revealed that AZ-27 was not retained to a significant extent in lung tissue after administration of different formulations but was, instead, rapidly absorbed into the systemic circulation. Thus, AZ-27 will be unlikely a suitable candidate for development as future anti-RSV drug[100].
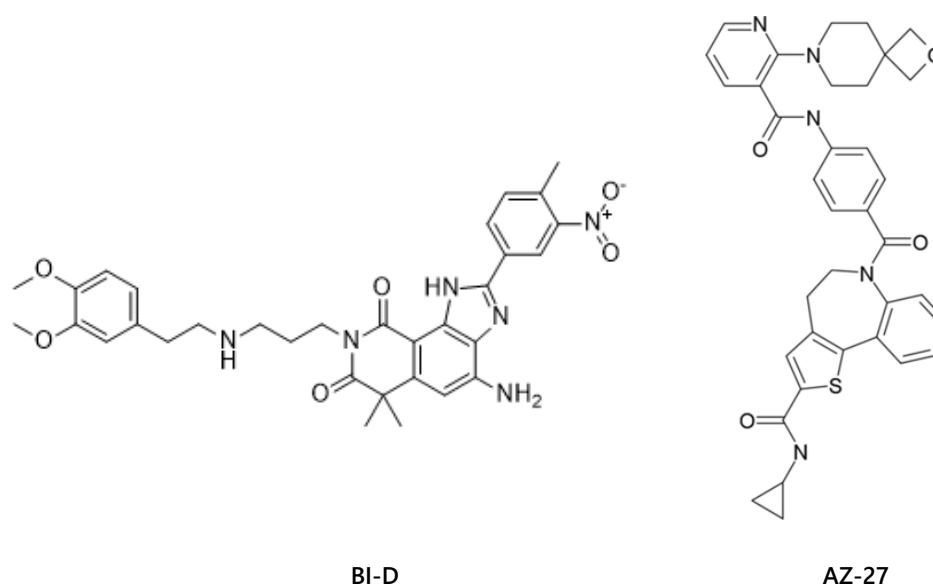
BI-D **AZ-27**

Figure 21. Chemical structures of the non-nucleoside inhibitors BI-D and AZ-27.

3.3.2.1.3 Nucleoprotein (N) inhibitors

RSV nucleoprotein (N) is essential for virus replication and is one of the most conserved genes among RSV A and B subtypes, thus represents an attractive target for antiviral therapy.

RSV-604 (Figure 22) is a small molecule inhibitor of both RSV A and B replication by targeting the nucleoprotein N, thus blocking the RNA synthesis and inhibiting the

infectivity of the released virions. Drug-resistant variants selected *in vitro* carry mutations I129L and L139I in the N-protein sequence. In a Phase I study orally administered RSV604 shown a good safety profile in healthy volunteers. The compound has also been administered in a phase 2a clinical trial hematopoietic stem cell transplant patients with concomitant RSV infection. During the trial most patients had lower RSV604 drug levels than anticipated and no significant difference in viral load with placebo could be observed, in addition, the limited number of patients and their underlying clinical conditions further complicated the trial development. Only the patients whose plasma exposure to the drug reached the 90% effective concentration (EC_{90}) a significative drop in viral load was reached[9,84].
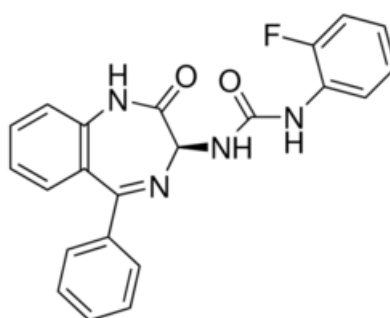
Figure 22. Chemical structure of the nucleoprotein inhibitor RSV-604.

ALN-RSV01 (Asvasiran) is a small interfering RNA (siRNA) of 19 nucleotides that targets a highly conserved sequence of the RSV nucleoprotein gene and inhibits viral replication. Intranasal administration of ALN-RSV01 in healthy adults infected with RSV significantly inhibited the rate of the infection. The siRNA proved to be safe and well-tolerated in a phase 2b clinical trials in lung transplant recipients with a promising risk/benefit profile[9,101].

3.3.2.1.4 N-P, SH and M2-1 inhibitors

In the search of potential new viral factor to be inhibited in order to develop novel anti-RSV compounds the hypothesis to interfere into the N-P proteins interactions have been advanced, also encouraged by the improved knowledge of the key interactions between these two viral components. The x-ray structure of the N protein in complex with C-terminal peptides of P-protein has allowed to gained detailed insight into the N-P interactions that revealed to identify a pocket on the N protein structure that interacts with the P protein N-terminal; this pocket could

represent a potential new target for the development of antiviral compounds. Virtual screening studies has allowed the identification of a chemical series of compounds with a 1-benzyl-1H-pyrazole-3,5-dicarboxylate (BPdC) scaffold that bind this pocket that has also shown promising *in vitro* anti-RSV activities[102,103].

Among the RSV structural proteins, the SH (small hydrophobic protein) is, along with F and G, one of the three envelop proteins. The SH protein is a viroporin which forms hydrophilic pores in the virus infected cells and whose specific function in promoting viral infection is not completely clear yet. The role of SH in RSV pathogenesis is evidenced in strains lacking SH that behave similar to the wild-type in cell culture, but showed severe attenuation upon infection in primates. This could be due to an increased IL-1b mediated immune response to RSV *in vivo* supporting the possibility that the ionic changes sprung by the SH pore structures could counteract the immune system response to infection. Recently a small molecule inhibitor of the SH protein has been identified; the compound, pyronin B (Figure 23), binds the hydrophobic side of the protein in an allosteric binding pocket, causing a conformational change that is reflected in the pore lumen closure. The compound has also shown a good antiviral activity (EC_{50} = 100 nM) in RSV infected cells in *in vitro* assays[84,104].

Finally, a potential new therapeutic target for anti-RSV therapy could be represented by the M2-1 protein. This protein has a pivotal role in RSV RNA synthesis as transcription anti-termination factor thus is essential for the efficient processing of viral RNA. A small molecule compound, cyclopamine (CPM) (Figure 23), has been identified as a potent inhibitor of RSV infection both *in vitro* as *in vivo*. This steroidal alkaloid is reported as anti-tumoral agent as an antagonist of the smoothened protein (Smo) involved in cell differentiation processes. Nonetheless, its anti-RSV activity is not related to this cellular receptor and it depends only on the specific inhibition of the M2-1 protein[83,105].
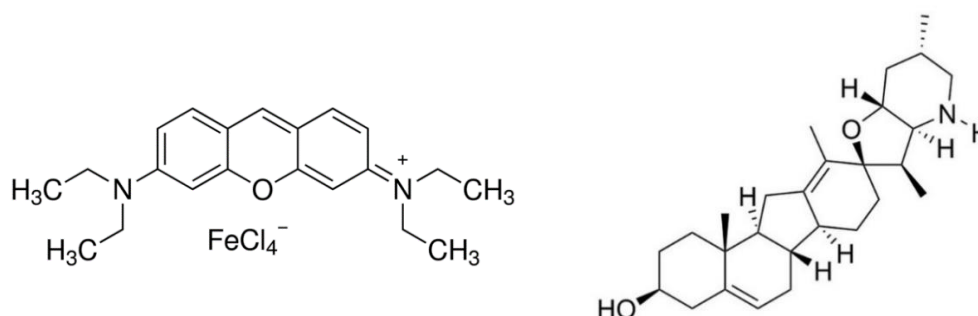
Figure 23. Chemical structures of pyronin B and cyclopamine CPM.

3.3.2.2 Intravenous Immunoglobulins IVIGs and monoclonal antibodies

Intravenous immunoglobulins (IVIG; RespiGam®) have been also administered in order to control RSV infection, although it may be effective at lowering viral titres, they did not appear to correlate with improved clinical outcomes along with the disadvantage of requiring intravenous infusion[106,107]. Ribavirin and immunoglobulins administered in association has also been investigated as a therapeutic option to treat RSV infections in in adult bone marrow transplant recipients, but even in this case with controversial effectiveness[108]. Due to this lack of effectiveness, further studies have been made and have brought to the development of RI-001 and RI-002, which are aqueous intravenous polyclonal human immunoglobulin G (IgG) from pools of source plasma of screened healthy adult donors with high levels of RSV-neutralizing antibodies. Promising data deriving from in vitro tests, preclinical studies and clinical trials demonstrate that RI-001 and RI-002 could be used as new potential therapeutic agents for the treatment of RSV infections in immunocompromised patients[109].

Palivizumab (Synagis®), a humanized mouse monoclonal antibody, even if has not shown appreciable effectiveness when used to treat RSV infections, is currently recommended as a prophylactic agent in high-risk population, with good success rates in preventing the infection[110]. Palivizumab have been designed to identify a shared antigenic epitope between pre-F and post-F, called site II, in order to increase its spectrum of action. The use of Palivizumab as prophylactic agent is limited by the high cost of the treatment, thus is administered only to high-risk premature infants, restricted for adults with immunodeficiency or elderly people, and also by its low neutralizing potency[79].

Motavizumab is a humanized antibody, developed as a higher affinity variant of palivizumab, which demonstrated a 20-fold higher in vitro potency compared to Palivizumab, its activity in vivo have been evaluated in two different clinical trials but, the FDA rejected the license application for motavizumab, due to incapability to demonstrate a greater efficacy than palivizumab as prophylactic agent, in addition to an increased hypersensitivity reactions relative to palivizumab[111].

Suptavumab (REGN2222) is a humanized monoclonal antibody designed to bind specifically the F protein of RSV, that nevertheless failed to meet the endpoint to prevent RSV infections in preterm children in a recent phase III clinical trial, thus it has not been approved for prophylactic use[9,87].

Nb017 and its trimeric derivative ALX-0171, are two nanobodies, therapeutic proteins derived from the heavy chain variable domains (VHH) that are present in heavy chain-only immunoglobulins of the *Camelidae*, that specifically bind the hRSV F antigenic site II, are currently under evaluation as post infection treatment[112,113].

Recently new highly potent antibodies that target specifically antigens of the pre-F protein have been discovered, such as the recombinant mouse 5C4 antibody, targeting the F protein site Ø, that had demonstrated high neutralizing potency decreasing RSV titres by 1000-fold more than Palivizumab in mice, and that is currently being evaluated in different clinical trials as a passive immunisation strategy[114]. Another pre-F specific human antibody, AM14, have been demonstrated to neutralize with higher potency than Palivizumab, all the tested RSV A and B strains, by binding a novel epitope in the pre-F protein, called site V[115]. Recently, another pre-F epitope, designated as site VIII, have been discovered, and its specific antibody mAb hRSV90 neutralized all the tester RSV strains with a potency 1000-fold more than Palivizumab[116]. MEDI8897 is a recombinant human monoclonal antibody that also targets a prefusion conformation of the RSV F protein and neutralizes *in vitro* a diverse panel of RSV A and B strains with >50-fold higher activity than palivizumab[117]. The discovery of these new potent antibodies specifically targeting the pre-F protein could represent an improvement into the control and prevention of RSV infections, on the other hand the discovery of pre-F protein important role into RSV infectivity could prompt to the development of new pre-F protein vaccines[79].

Several studies have also reported broadly-neutralizing monoclonal antibodies (bnmAbs) against RSV protein G, although its protein sequence considerably vary among different viral strains, it presents a highly conserved CCD sequence that could be exploited to develop specific recombinant antibodies. CCD sequence represents a promising target since is fundamental for the viral infectivity and involved into the viral attachment to airway epithelial cells and has a CX3C chemokine motif that binds to the corresponding chemokine cellular receptor CX3CR1[87]. Several monoclonal antibodies have been developed targeting the RSV G protein, such as the mAb 131-2G. The monoclonal antibody 131-2G by binding the CCD sequence, blocks G protein binding to CX3CR1, and decreases several disease manifestations in RSV infected mice. The comparison between 131-2G and a Palivizumab-like mouse anti-F protein mAb, 143-6C demonstrate that treatment with the anti-G protein mAb is more effective in reducing the RSV disease manifestation in preclinic studies, prompting the possibility that anti-G directed mAb might be more effective than anti-F

neutralizing antibodies in treating active RSV infection[118]. In addition, two anti-G protein mAbs 3D3 and 2B11, also react with the CCD sequence and have been shown to neutralize the virus in primary cell-culture systems and also to reduce G-mediated lung inflammation in mice. Thus, these G protein-directed mAbs could be strong candidates for development as anti-RSV therapies combining a high potency in reducing RSV titres and an anti-inflammatory activity[119].

3.3.2.3 Vaccines

To date, there is no approved vaccine to prevent RSV infection. In mid-1960s a clinical trial of a formalin-inactivated RSV vaccine (FIRSV) failed due to the enhancement of the disease following natural RSV infection in vaccinated infants and children, followed by two deaths[120]. Thus, the development of new RSV vaccines has been subsequentially hampered by the need to create robust immune responses avoiding side effects and complications. However, the possibility to establish immunization due to a future RSV directed vaccine is supported by several studies that demonstrated that RSV is relatively stable antigenically and most previously-infected adults are seropositive; in addition, the monoclonal antibody palivizumab is associated with a prophylactic activity in preventing hospitalisation secondary to RSV infection. Nevertheless, re-infections occur repeatedly throughout life, even if the frequency of severe disease decreases in second and subsequent infection. This suggests that immunity from infection is neither sufficient nor long-lasting[121].

However, it's well known that the infection outcomes are more concerning in new-born children, representing a challenge for the implementation of an efficient vaccination program at this stage, considering the immature neonatal immunity, the presence of maternally derived antibodies, and the impact of primary RSV infection. Infants are generally protected against RSV for ~3 months by maternal antibodies. Thus, the peak incidence of RSV in infants has been observed around 2-8 months of age, when maternal antibodies begin to reduce their protective effect[79]. In order to protect infants at this critical age two possible vaccination strategies have been proposed: direct vaccination of infants or vaccination of pregnant mothers prior to transfer maternal antibodies[122].

The most advanced current strategies for RSV vaccine development are live attenuated RSV vaccine strains and recombinant viral vectors expressing RSV antigens. To date, several subunit RSV vaccines have been developed and tested

often derived from the prefusion conformation of the viral F protein; the choose of this specific protein conformation for the development of subunit vaccines is supported by several studies which demonstrated that pre-F-specific antibodies are at least 80-fold more potent than post-F-specific antibodies in terms of virus titres reduction[79].

3.3.2.3.1 Live-attenuated RSV vaccines

Live attenuated RSV vaccines have been studied for several decades, representing attractive candidates for young children because they can be administered intranasally, and are immunogenic even in the presence of maternal antibodies. However, these vaccines development have been hindered by the challenge of obtaining a sufficient attenuation, in terms of safety, and at the same time the capability to determine a protective immune response.

Several candidates are currently undergoing or recently completed clinical trials. Among these live attenuated vaccines, a group of vaccine candidates carries the deletion of a large segment of the M2-2 gene. The M2-2 non-structural protein mediates the transition from transcription to RNA replication.

The strain A2 vaccine candidate RSV rA2cp248/404/1030ΔSH contains attenuating mutations in different genes. In particular, the 404 nucleotide point mutation in the gene-start transcription signal of the gene encoding the M2-1 and M2-2 proteins, the 248 and 1030 aminoacids point mutations in the L protein and the deletion of the SH gene, generated a highly attenuated virus. This vaccine has been evaluated in several clinical trials and appeared to be well tolerated in young children, but evaluation of nasal wash isolates from recipients identified a number of specimens exhibiting a partial loss of the attenuating mutations, primarily the 248 or 1030 mutations[123], Thus, two genetically stabilized versions of this vaccine RSVcps2 and RSVDNSD1313/1314L have been developed and evaluated in a clinical trials confirming an increased genetic stability[121,124]. Furthermore, two other RSV vaccine candidates carrying a M2-2 gene deletion, MEDI/ΔM2-2, and LID/ΔM2-2, have been evaluated in phase 1 studies in 6–24-month old children.

3.3.2.3.2 Inactivated RSV vaccines

The development of inactivated vaccines has been hindered by the failure of FI-RSV vaccine clinical trial, thus only few vaccines of have been developed in this form[123].

However, recently an RSV-L19 inactivated vaccine has been developed in a nanoemulsion (NE) adjuvant formulation and preclinical studies in cotton rats proved to generate a considerable immune response and also cross-protective immunity from a different RSV-A2 strain has been observed[125].

3.3.2.3.3 Particle based vaccines

New vaccine strategies can take advantage of particulate compounds such as microspheres or nanoparticles to target antigen-presenting cells in order to trigger a directed immune response. These particles can carry viral proteins, peptides or protein epitopes.

Novavax Inc. (Gaithersburg, MD, USA) has modified and cloned the RSV F protein (post-F conformation). The recombinant protein glycosylated and cleaved into covalently-linked F2 and F1 polypeptides form homotrimers, that further assemble into nanoparticles. This vaccine demonstrates a strong induction of anti-RSV antibodies in preclinical studies and has also been tested in several clinical trials in different populations including elderly, adults, pregnant and non-pregnant women, and infants. A phase III study to determine the safety and efficacy of the vaccine to protect infants *via* maternal immunization have been recently completed (NCT 02624947).

In addition, GlaxoSmithKline (GSK, Phase 2), GSK (legacy Novartis, Phase 1), and MedImmune (Phase 2) are currently testing RSV F vaccine candidates for use in maternal immunization and for the vaccination in elderly people.

3.3.2.3.4 Subunit-based vaccines

Subunit-based RSV vaccine are produced using the viral envelope glycoproteins as antigens. The development of these vaccines presents some challenges due to the fact that are composed by non-replicating parts of the virus, thus they are often poorly immunogenic[126]. Recently new subunit-based vaccine candidates most commonly use the RSV fusion (F) protein of the virus as the antigen, often in its pre-

fusion conformation, due to its capacity to generate most of the RSV neutralizing antibodies and its high level of conservation among different RSV strains.

GlaxoSmithKline has recently developed a recombinant RSV glycoprotein F vaccine, engineered to preferentially maintain prefusion conformation (RSV-PreF), that have been evaluated in clinical trials in pregnant women in order to assess its safety, reactogenicity, and immunogenicity profiles. The vaccine generated the anticipated immune response that, however, was seen to gradually decline in all study groups on the months after the administration[123,127].

3.3.2.3.5 Gene-based and vectored vaccines

Gene based vaccines include nucleic acid vaccines (naked DNA or RNA) and replication-deficient vectors of nucleotide sequences such as human and primate adenovirus vectors, that are reporter to cause immunization leading to induction of cytotoxic T helper[123].

Janssen Pharmaceutical has developed vectored vaccines consisting of low serovalent adenoviral vectors Ad26 and Ad35, expressing the RSV fusion protein in the pre-F configuration[128]. In addition, Bavarian Nordic also produced a vectored vaccine MVA (Modified Vaccinia Ankara) MVA-BN® engineered to produce immune responses against both RSV A and B subtypes, that expresses 5 RSV proteins such as the F, the G protein from RSV A and B type, the N, and the M2 proteins. MVA-BN® evaluation in a clinical study proved the establishment of a persistent antibody response against multiple RSV targets[122,123].

GSK has also developed its adenovirus for RSV vaccine for children administration, based on a chimpanzee adenovirus subtype 155 vector expressing the RSV F, N, and M2-1 proteins. At date, preclinical data demonstrated a in vivo efficacy in increasing the immune response in several tested animal species, thus clinical trials are currently underway[122].

Vaxart developed an anti-RSV vaccine that contains a nonreplicating E1-, E3-deleted Adenovirus subtype 5 (Ad5) vector encoding the RSV F protein, adjuvanted with double stranded RNA. This vaccine candidate has been recently evaluated in a phase 1 clinical trial to assess its effectiveness and tolerability profile[122].

3.4 Influenza Virus IV

Influenza viruses belong to the *Orthomyxoviridae* family, which was historically divided into five genera: influenza A virus (IAV), influenza B virus, influenza C virus, influenza D virus, isavirus, and thogotovirus. The International Committee on Taxonomy of Viruses (ICTV), has recently revised the classification of the *Orthomyxoviridae* family including eight genera and nine species: genus Alphainfluenzavirus comprising the species influenza A virus, Betainfluenzavirus comprising the species influenza B virus, Gammainfluenzavirus comprising the species influenza C virus, and Delatinfluenzavirus comprising the species influenza D virus, genus Isavirus, genus Quaranjavirus and genus Thogotovirus[129].

Among the influenza viruses, influenza B and C natural hosts are represented by humans even if occasional transmissions to other animal species have been described[130]. Their infection in human hosts causes the respiratory disease, although influenza B is responsible of more severe clinical manifestations compared to influenza C[131].

Influenza D virus (IDV), was first isolated in 2011 from swine and cattle in North America and consequently found also in Europa and Asia. It is also capable of infecting other mammalian species, such has ferrets, pigs and guinea pigs, but it has been never reported infecting humans. It phylogenetically derives from ICV, showing about 50% amino acid homology with influenza C virus[132].

Influenza A viruses originate from birds and swine hosts and subsequently adapted to humans. IVA is associated with a high mutation rate of its genome, thus is capable of acquiring the ability to switch from animal to human hosts and generate pandemics[131]. Over the past 100 years, there have been four flu pandemics associated with several deaths worldwide: 1918 H1N1 Spanish flu, 1957 H2N2 Asian flu, 1968 H3N2 Hong Kong flu, and 2009 H1N1 swine flu[133]. In addition, IVAs are responsible of seasonal epidemics occurring every year; the vast majority of the seasonal influenza virus burden is associated with influenza types A and also type B[134].

Influenza viruses have negative-sense, single-stranded RNA genomes that are divided in either eight or seven segments depending on the genus. Genome sequencing confirmed that IVs share a common genetic ancestry, then they have genetically diverged in the four genera. The exchange of RNA sequences between viruses, genetic reassortment, still occurs within each genus, but not across types[135].

Influenza A can be further classified in different subtypes based on the characteristics of its surface glycoproteins: different combinations of haemagglutinin (HA) and neuraminidase (NA) glycoproteins identify the distinct subtypes. There are currently at least 18 HA subtypes and 11 NA subtypes, but only three combinations are known to have circulated widely in humans: A/H1N1, A/H2N2 and A/H3N2[131]. Differently, influenza B viruses can be antigenically divided in only two lineages, identified in 1970s, named, B/Victoria/2/87 and B/Yamagata/16/88[136],

Influenza A and B could be spherical or filamentous in shape, the spherical forms are on the order of 100 nm in diameter and the filamentous forms could reach up to 300 nm in length. Influenza A and B genome consists of eight segments and encodes 13 proteins: Hemagglutinin (HA), neuraminidase (NA), M1 matrix protein (M1), M2 ion channel protein (M2 or AM2), nuclear protein (NP), non-structural proteins (NS1, NS2), and RNA polymerase complex (PB1, PB2, PA). Each genome segment possesses untranslated regions (UTRs) at both 3′ and 5′ ends which serve as promoters for replication and transcription by the viral polymerase complex and also include the mRNA polyadenylation signal and the packaging signals for virus assembly (Figure 24).

The influenza A virus is surrounded by an envelope that supports glycoprotein spikes of hemagglutinin HA and neuraminidase NA, in a four to one ratio, and a smaller number of matrix (M2) ion channels (M2/HA ratio 1:100). Below the envelop a matrix composed of M1 protein protects the virion core containing the non-structural protein 2 NS2 (also called nuclear export protein NEP) and the ribonucleoprotein (RNP) complex. The RNP complex is composed by the each segment of the viral genome along with the nucleoprotein NP and the RNA dependent RNA polymerase, composed by three subunits forming an heterotrimer: two "polymerase basic" and one "polymerase acidic" subunits (PB1, PB2, and PA)[135].

The organization of the influenza B virion is similar to the influenza A virion organization with few differences; for example, it has four envelop protein, HA, NA and two proteins, NB and BM2 instead of the ion channel M2. The NB protein is encoded by RNA segment 6, which also encodes NA, while BM2 is encoded by segment 7[137]. The NB protein forms a cation-permeable channel, BM2 also forms ion channels and its activity is essential for IBV replication since it triggers the virus uncoating in endosomes in the cell entry process. BM2 also mediates the new virions

assembly process by capturing the M1-ribonucleoproteins complex during virus budding from the host cell[138].
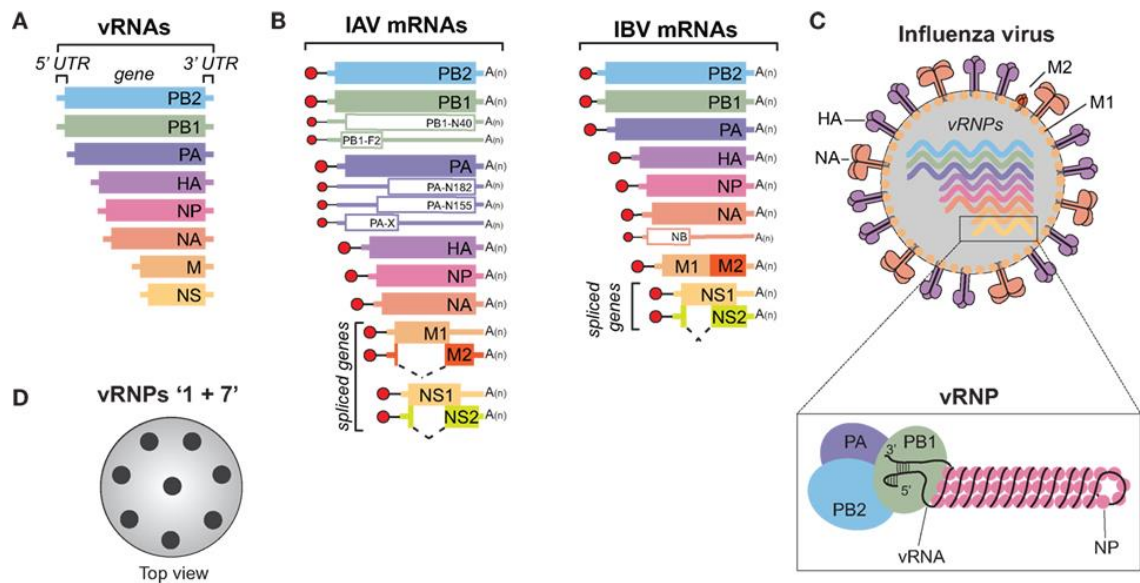
Figure 24. Structure and genome organization of influenza A and B viruses. A) Shows the eight viral RNA segments along with the 5′ and 3′ UTRs, which contain the viral promoters. B) Diagram of the viral mRNAs that are transcribed from the IAV and IBV genomes. C) Structure of an influenza A or B virus with its membrane proteins HA, NA, and M2, the eight viral ribonucleoproteins (vRNPs, represented more in detail below the virion), and the matrix protein M1 that supports the viral envelope. D) Top view of an influenza virus cross-section in which vRNPs are represented with black circles[139].

Influenza C and D viruses are structurally different from A and B viruses; they present a lipid envelope overlying a protein matrix and the RNP complex. The genomes of ICV and IDV consist of 7 gene segments and encode only one envelop glycoprotein (HEF), which combines both the function of HA and NA, along with PB1, PB2, P3, matrix (M1) protein, the ion channel protein (CM2 and DM2, respectively) , and the non-structural proteins NS1 and NS2[140]. Based on the differences into the hemagglutinin-esterase-fusion (HEF) gene, ICV has been divided into six lineages, designated C/Taylor, C/Mississippi, C/Aichi, C/Yamagata, C/Kanagawa, and C/Sao Paulo[141] while ICV can be distinguished in two lineages: the D/swine/Oklahoma/1334/2011 (D/OK) and D/bovine/Oklahoma/660/2013 (D/660)[139].

3.4.1 *Antigenic Shift* and *Antigenic Drift*

Influenza viruses A and B are capable of causing seasonal epidemics and re-infections in humans due to their capability of evade the host immune system by

evolving and mutating their antigenic determinants. In particular, influenza virus A presents a very high mutation rate and its capability to differentiate and generate new viral strains to which the population has limited immunity, could lead to increased transmission and might evolve into a pandemic[142].

The capability of these viruses to evolve and evade the host immune defences by changing its antigenic determinants, represented by the surface glycoproteins the hemagglutinin and neuraminidase, is due to two different processes: *antigenic shift*, which occurs only in influenza A virus and *antigenic drift*, which may occur in both influenza A and B viruses.

Antigenic drift is associated to minor variations into the antigenicity of the envelop glycoproteins compared to *antigenic shift*. Influenza virus RNA-dependent RNA polymerase lack proofreading capability and tend to make errors during replication causing point mutations in the genome. Relevant changes in antigenicity occur only by the accumulation of point mutations of the gene encoding for HA or NA glycoproteins. Single point mutations are not enough to determine a noticeable change in antigenicity, thus aminoacids changes in at least two or more epitopes of the glycoproteins are necessary for a significant antigenic change[143]. This process may occur in both influenza A and influenza B viruses and these antigenic variants are responsible for annual epidemics, due to the accumulation of point mutations that allow viruses to escape neutralization by antibodies directed against previously circulating strains[144].

Antigenic shift only occurs within influenza A viruses, it is less frequent but causes dramatic changes of the antigenic profile and infectivity of the virus. *Antigenic shift* occurs when two different IAV viruses, also from a different host species, co-infects a single host; these two viruses may reassort their genomes within the infected cells creating a completely new virus and generating a new viral strain. The new strain may possess the new ability to infect different hosts and also humans and potentially cause a pandemic, since as no neutralizing antibodies are present in the human population against the new shift variant[145]. For example, the A/H1N1 pandemic in 2009 originated from the generation of a new IAV strain capable of infecting humans due to a triple-reassortment antigenic shift, where HA, NP and NS, NA and M genes derive from swine lineages, PB2 and PA are of avian origin and PB1 gene derives from the human IAV strain H3N2[145].

3.4.2 Influenza Virus Replication

3.4.2.1 Influenza Virus Attachment and Entry processes

Influenza infection starts when the virus specifically binds and recognizes the N-acetylneuraminic acid (sialic acid) on the host cell membrane. Sialic acids are acid monosaccharides deriving from neuraminic acid, an acidic sugar with a nine-carbon backbone; they can be found as components of oligosaccharide chains of mucins, glycoproteins and glycolipids occupying terminal positions of complex carbohydrates that may be exposed on both external and internal membrane areas of many animal species. The N-acetylneuraminic acid is capable of forming carbon-carbon bonds between the carbon-2 of the terminal sialic acid and the carbon-3 or carbon-6 of galactose forming α-2,3 or α-2,6 linkages. These different bonds confer a specific steric configuration to the terminal sialic acid, that is specifically recognised by the viral HA. Different viral strains may recognise specifically only one of the two types of linkages, i.e. the human IAV and IAB strains specifically bind the α-2,6-linkages which are the most common terminal sialic acids in humans. However, human cells may also express α-2,3-linkages in minor quantity, thus also avian viruses whose HA specifically binds the α-2,3-bonded sialic acids possess the capability to infect also human hosts, even if with less efficiency compared to IV human strains[135].

3.4.2.1.1 IAV and IBV Hemagglutinin HA

The influenza virus interacts with the sialic acid by mean of the hemagglutinin glycoprotein HA (in the case of influenza A and B strains), or *via* the hemagglutinin-esterase-fusion HEF protein (in the case of influenza C and D strains)[138]. The HA is polypeptide of 550 aminoacids organized in homotrimers, positioned on the virus envelop. The homotrimer presents two structurally distinct regions, a stem, a region rich of α–helices, and a globular head of antiparallel β–sheet, that also contains the sialic acid receptor binding site. The hemagglutinin glycoproteins present the main antigenic determinants of IV which are designated by different letters in diverse HA subtypes, i.e. in H3 subtype these sites are identified as A, B, C, and D, in the H1 subtype these are named Sa, Sb, Ca1, Ca2, and Cb. Antibodies specifically recognises the HA antigenic sites, neutralizing IV infectivity, thus HA is primarily involved into the antigenic drift process, where accumulated pointed mutations may generate a new

strain allowing the virus to evade the host immune response. However, the stem-head configuration of the HA molecule remains conserved among the different strains and subtypes[135].

In IAV and IBV the hemagglutinin is synthesized by the ribosome machinery of the infected cell in the form HA_0, once transported to cell membrane, is subsequently cleaved by host serine proteases into two segments, HA_1 and HA_2 linked by a disulphide bridge, then incorporated into the newly formed virus particle envelop due to a membrane-anchor sequence near its C terminus. The HA_1 portion contains the receptor binding and antigenic sites while the HA_2 is involved in the fusion process with the cell membrane[146]. The pre-fusion HA_1–HA_2 recognises and binds the sialic acid on the cell membrane due to the HA_1 binding site. Then, the virion undergoes endocytosis due to the physiological plasma membrane recycle. The low pH inside the endosome triggers a conformational change in which HA_2 loses contact with HA_1, except for the disulphide bridge, then refolds and undergoes a loop-to-helix transition in its sequence exposing the N-terminal portion (fusion peptide) and translocating it towards the host membrane, generating an "extended intermediate". The fusion peptide forms an amphipathic helix that is responsible for the interaction with the cell lipidic bilayer. The extended intermediate collapses to generate the post-fusion conformation, in which the HA folding leads to the two membranes (viral and cellular) fusion, followed by the virus release in the cytoplasm. This transition results in a stable trimeric coiled-coil conformation[147] (Figure 25).
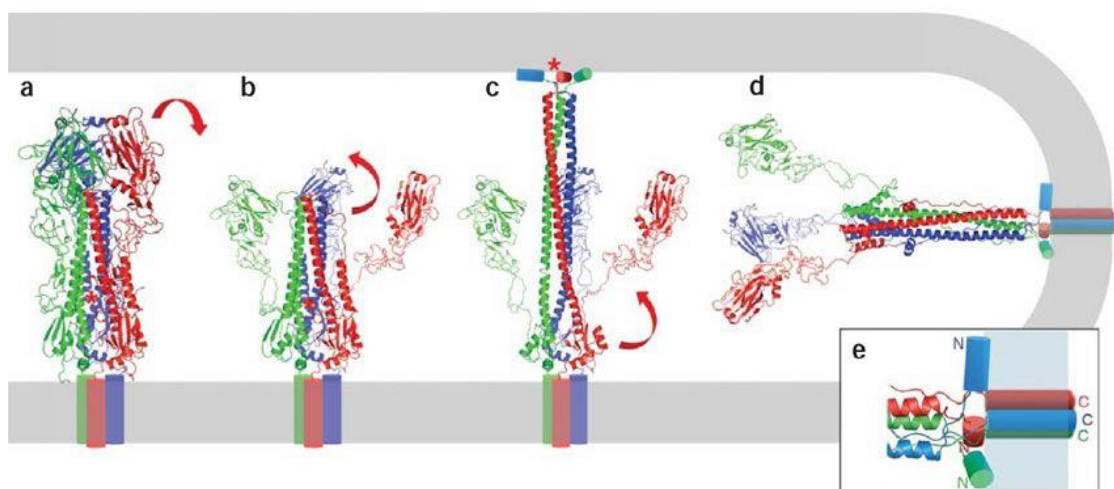
Figure 25. IV hemagglutinin fusion process and conformational changes. a) pre-fusion conformation; b) conformational change from the pre-fusion form to the extended intermediate; c) extended intermediate; d) post-fusion conformation[147].

3.4.2.1.2 Hemagglutinin-esterase-fusion HEF protein

In IVC and IVD the hemagglutinin-esterase-fusion (HEF) protein combines the functions of both HA and NA. The HEF protein, like HA, recognises the sialic acid on the host cell membrane and specifically binds it. It also mediates the membrane fusion process inside the endosome following a mechanism similar to HA's. In addition, HEF also fulfils the NA enzymatic function, that consists in an esterase activity removing the 9-acetyl group of the N-acetyl-9-O-acetylneuraminic acid. This process is fundamental in the virus exit phase since it results in the release of the newly synthesized virus particles from the infected cell[148].
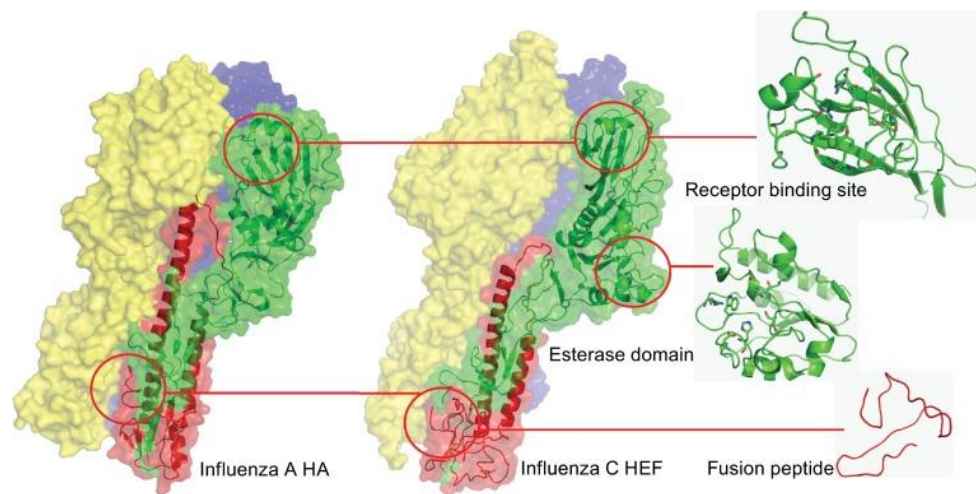
Figure 26. Comparison of the crystal structure of ICV HEF protein and IAV hemagglutinin highlighting the catalytic esterase domain of HEF which is absent in HA, the fusion peptides and the receptor binding sites[148].

3.4.2.2 Ribonucleoprotein RNP pH-induced release

The acidic environment inside the endosome is not only important for inducing the HA or HEF conformational change, but also activates the envelop ion channel proteins: influenza A M2 proton channel, the NB and BM2 ionic channels of IBV, the CM2 and DM2 channels of influenza C and D respectively.

3.4.2.2.1 A/M2 ionic channel

Influenza A M2 protein is a 97 aminoacids glycoprotein that passes through the viral envelop in a single-pass ($N_{in}C_{out}$) encoded by a spliced mRNA derived from the RNA segment 7 of IAV[149]. It's a type III membrane protein organised in a 23-aminoacid N-

terminal ectodomain, a transmembrane TM segment (residues 24-46) and a C-terminal cytoplasmatic domain (from 46 to 97), which is involved into the virus assembly process. These proteins are organised in a homo-tetramer forming the ionic channel, in which two dimers are covalently linked by mean of disulphide bridges. The A/M2 channel is highly selective for protons and preferentially conducts protons from the viral exterior (N-terminus) to the interior (C-terminus). Thus, it is responsible for the generation of the low pH environment inside the virus particle that triggers the RNP release and the HA conformational change. The acidification inside the virus particle causes the matrix M1 protein to lose interaction with the RNP complexes, thus after HA-induced membrane fusion the uncoated RNPs are released into the cytoplasm and trafficked to the nucleus[150,151]. In addition, the M2 channel also regulates the pH in the host Golgi lumen during virus assembly processes in order to keep the neo-synthesized HA in its pre-fusion form, avoiding low pH-induced premature activation[151].

The TM segment are organised into a four-helix bundle with a left-handed twist angle of ~ 23° shaping the channel pore that may switch from a close conformation to an open conformation due to the key residues His37, that acts as a pH sensor and the Trp41 that works as channel gate[152].

The channel entrance at N-terminus is narrow (3.1 Å) due to the presence of a ring of methyl groups from Val27, not allowing water molecules to enter the channel. However, water molecules are required inside the channel pore to support proton conduction, thus small motions of the protein are required for water to enter the channel. In the inner part of the channel the pore further narrows towards the C-terminus due to the presence of the His37 and Trp41 that restrict the diameter to 1.7 and 1.4 Å respectively. The Trp41 is believed to interact with the Asp44 establishing inter-subunit hydrogen bonds that lock the channel gate in the closed conformation. The closed state of the channel is structurally rigid, however when the low pH environment triggers the channel opening, the tetramer evolves to a dynamic open state, with a loose quaternary structure.

At low pH (5 to 6), the His37 imidazole switches to the protonated form resulting in electrostatic repulsion of the charged residues and in losing the H-bond interaction between Asp44 and Trp41. That consequentially loosens the rigid protein packing in the TM domain, opening the channel pore in the conductive state to admit water molecules and allowing the proton flux (Figure 27). The inner channel relies to a

series of polar residues that facilitate the proton flux and the channel hydration; A/M2 channel has four polar residues within the TM, Ser31, His37, Asp44, and Arg45 which are involved in this function[151].
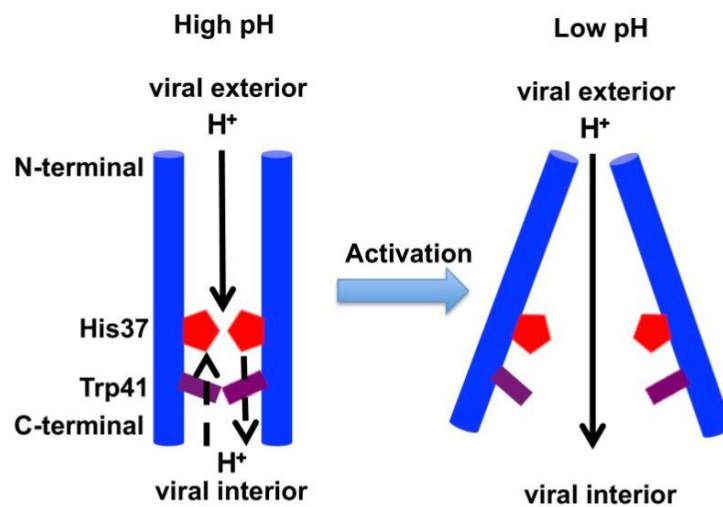
Figure 27. pH dependent conformations of the influenza A M2 proton channel.

3.4.2.2.2 IBV, BM2 ionic channel

The RNA segment 7 of IBV encodes for both M1 and BM2 protein. The unspliced mRNA is traduced into a polyprotein that is subsequentially cleaved into the two virus structural proteins. BM2 protein is similar to A/M2, forms homotetramers in the envelop membrane and selectively conducts protons inside the virion particle, nonetheless they present only few similarities in the aminoacidic sequence, in particular in the TM domain. BM2 is essential for virus uncoating in the endosome and for pH equilibration between Golgi lumen and cytoplasm during virus protein transport and virion assembly. Unlike M2, the TM domain of BM2 channel presents a characteristic coiled-coil assembly with heptad repeats. The tetramer presents a hydrophilic pore that is occluded by Phe5 and Trp23 at the N-, and C-terminal sides respectively. Despite the low sequence similarity, the TM domain also presents the characteristic M2 motif HXXXW, thus His19 and Trp23 are responsible in BM2 of proton selectivity and gating, allowing the channel to switch between the two conformations depending on the external pH[150,153].

3.4.2.2.3 ICV, CM2 ionic channel and IDV, DM2 ionic channel

Influenza C and D ionic channels CM2 and DM2 share many similarities in their aminoacidic sequence and functionality. They are type III membrane proteins forming disulphide linked homodimers which are further organised in tetramers, presenting a N-terminal ectodomain, a TM domain and a C-terminal domain in the internal part of the membrane[153].

CM2 protein is encode by ICV, RNA segment 6 which produces a p42 polyprotein, subsequentially cleaved in two segments generating CM2 composed of the C-terminal 115 amino acids, and the CM1 protein composed of the N-terminal 259 amino acids. The protein is post-translationally modified by N-glycosylation (Asn11), palmitoylation (Cys65), and phosphorylation[154].

Both CM2 and DM2 The CM2-associated ion channel activity is preferentially permeable to Cl⁻ but not to cations (Na⁺ or K⁺), and also presents a small proton channel activity[149]. However, they are capable of altering the pH within the Golgi network, avoiding HEF activation and to trigger the pH modification inside the virus particle in the endosome to activate HEF and initiate the RNP uncoating. Nevertheless, the mechanism of activation and the proton and chloride permeabilities roles require further investigations. Finally, neither CM2 nor DM2 contain the characteristic HXXXW motif of A/M2 and BM2, but probably a YXXXK motif in their TM domain fulfils the same role in sensing pH and gating the channel pore[153].

IAV and IBV genomes also encode for other viroporins, PB1-F2 and NB, respectively, forming ion channels. PB1-F2 forms nonselective ion channels in lipid bilayers and is known to localize to the mitochondria of infected cells. NB protein form ion channels in lipid bilayers however NB seems to not be fundamental for viral replication[138].

3.4.2.3 Entry of influenza virus RNPs into the nucleus

Influenza virus ribonucleoproteins RNPs are released into the cytosol, then thy need to be translated into the nucleus where the transcription and replication processes take place. Each viral RNP is composed by an (-) ssRNA segment complexed with the NP, PB1, PB2 and PA (in IAV and IBV) or P3 proteins (in ICV and IDV). To enter the nucleus proteins and protein-RNA complexes have to be recognised by the nuclear pore complex (NPC) by presenting specific aminoacidic signals. For nuclear import a

protein needs to expose a Nuclear Localization Signal (NLS) and for export a protein needs to have a Nuclear Export Signal (NES). Nuclear pores are very large molecular complexes), structurally composed by nucleoporins. These nucleoproteins presents some aminoacidic sequences that specifically binds the proteins of the importin β family or from the exportin family in order to allow the molecules inside the nucleus[155]. All individual protein components of the RNP presents different NES sequences that can be recognised by importin α. Upon binding to the vRNP, importin-α is recognized by the importin-β receptor, which then interacts with the nuclear pore complex to enter the nucleus[156,157].

3.4.2.4 Transcription and replication of the IV RNAs

The transcription and replication processes of vRNAs occur in the host cell nucleus where the viral RNA-dependent RNA-polymerase, part of the RNP complexes, mediates the two processes. The influenza viruses RNP complexes are composed by an antiparallel double helix of NP-coated vRNA that contains a polymerase at one end and an NP loop at the other end. The influenza virus RdRp consists of three subunits: polymerase basic 1 (PB1) and polymerase basic 2 (PB2) are present in all influenza viruses, whereas the third subunit is polymerase acidic (PA) in influenza A and influenza B viruses, and polymerase 3 (P3) is characteristic of influenza C viruses[158].

3.4.2.4.1 Transcription of the vRNAs

Influenza viruses' genomes are negative-sense single stranded RNAs and they cannot be directly recognised by the cellular ribosomes, thus the RdRp synthesised the positive-sense mRNAs for the viral proteins' synthesis. The viral mRNAs are capped at the 5' end and polyadenylated at the 3' end. Transcription is a primer-dependent process, nonetheless the viral RdRp does not possess intrinsic capping activity, thus the polymerase obtains the 5'-caps, that act as primers, from the host cell's capped mRNAs in a process called *cap-snatching*. This process is aided by the association of the viral polymerase with the C-terminal domain of the host RNA polymerase II, and occurs when the conserved 5'-end of the template vRNA interacts with the polymerase complex activating the cap-binding function of PB2. The PB2 binds the 5' end of host capped mRNAs and cleaves 10-13 nucleotides downstream of the 5' cap, that the polymerase uses as a primer to start the transcription of the

viral mRNA[138]. The mature viral mRNA needs to be polyadenylated at the 3' end; the poly(A) tail of influenza virus mRNA is encoded in the negative-sense vRNAs as a sequence of 6-7 uracil residues, which are recognised by the viral polymerase and translated into a string of adenosines. Once polyadenylated and capped, the viral mRNA needs to reach the host ER membrane in order to star viral proteins' synthesis[135]. The M1 protein mediates this process by binding the (+) viral mRNAs and the NP proteins promoting NP-RNA core formation. At this stage, the viral NS2 protein also binds M1 and recognises a NEP sequence on the nucleoporins of a nuclear pore complex, promoting the export of the viral mRNA[155].

3.4.2.4.2 Replication of the vRNAs

The nucleus is also the location of the synthesis of the vRNA segments that form the genomes of progeny viruses. The viral RNA-dependent RNA polymerase synthesises complementary RNA (cRNA) intermediates that serve as templates for the synthesis of more copies of negative-sense, genomic vRNA. Likewise, nuclear export of the viral genome vRNPs is mediated by the viral proteins M1 and NEP/NS2[158].

3.4.2.4.3 IVs RNA-dependent RNA-polymerase

Influenza viruses RdRps structures has been studied thoroughly due to the availability thoroughly of X-ray crystallography structures of the heterotrimers of the polymerases of influenza A virus and human influenza B and influenza C viruses.

The influenza virus polymerase is a complex composed by a core, consisting of PB1, the C-terminal domain of PA (or P3) and the N-terminal region of PB2, and flexible peripheral appendices formed by the PA (or P3) endonuclease domain and the PB2 cap-binding, mid, linker, 627- and NLS domains.

The core of the polymerase is represented by the PB1 subunit which contains characteristic motifs such as the pre-A motif, and motifs A-E, that are a common feature of the RNA-dependent RNA polymerases. PB1 possess the typical right-hand-like fold, in which the fingers and fingertips, palm and thumb domains. In addition, the N-terminal and C-terminal extensions play a fundamental role, interacting with the PA or (P3) and PB2 subunits respectively. The PB2 subunit

consists of several flexible domains, whose are arranged differently in influenza A and B polymerases compare to C and D polymerases. PB2 domains include the mid domain, the cap-binding domain, the cap-627 linker, the 627-domain, the C-terminal nuclear-localization signal (NLS) domain and the N-terminal, which includes the lid subdomain, that interacts with the PB1 C-terminal and thumb domain (Figure 28).
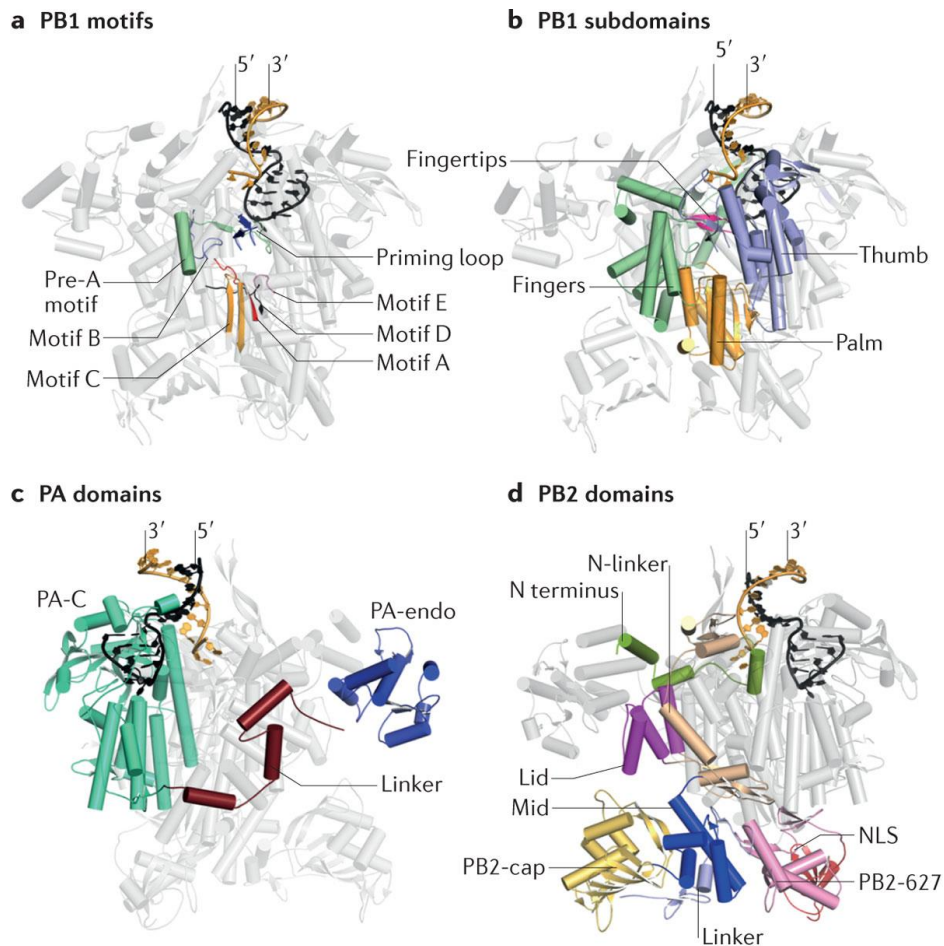
Figure 28. Structure of the influenza A virus polymerase (PDB = 4WSB) bound to genomic vRNA[158].

3.4.2.5 Viral proteins synthesis

The viral mRNAs of influenza viruses are traduced into the many viral encoded proteins exploiting the host cell translation machinery. Part of the viral proteins are synthesized by cytosolic ribosomes (proteins PB1, PB2, PA or P3, NP, NS1, NS2 and M1), while the membrane proteins HA, NA (or HEF) and M2 are formed by the endoplasmic reticulum (ER)-associated ribosomes. The envelop proteins synthesized in the ER are folded and trafficked to the Golgi apparatus where they are

subject of post-translational modification, then specific signal residues on the proteins direct them to the cell membrane where the virus assembly process takes place. The RNA-binding protein NS1 is synthesized in the cytosol, then imported into the nucleus where act as an inhibitor of interferon signalling. In addition, also the NS2 and M1 proteins are directly imported in the nucleus right after their synthesis[157].

3.4.2.6 Virion assembly and budding

The M1 protein inside the nucleus binds the viral RNAs and the NP proteins promoting NP-RNA core formation. After being exported in the cytoplasm, the RNP complex is transported to the budding site where the M1 proteins interacts with specific binding sites on the HA and NA proteins for packaging at the host cell membrane. To obtain an infective virus particle incorporation of all eight or seven vRNA segments is required, thus after budding only the virion possessing the complete genomic inheritance are capable of infecting new cells[135].

Several viral and host components are involved into the budding process, and may be involved in one or more different stages of bud initiation, bud growth or bud release. Viral budding is probably triggered by an accumulation of M1 protein at the cytoplasmatic side of the host membrane. The M1 protein's role is crucial for the virions budding since it is involved both in the bud initiation and bud release processes. It provokes budding initiation by interacting with the lipidic bilayer causing a membrane bending that facilitates the bud formation. M1 is also crucial in the final stage, the bud release, mediating bud closing and virion release[159].

The surface glycoproteins are directly involved not only in the assembly process (HA, NA or HEF, M2), but also in the budding process, in particular the viral NA neuraminidase of IAV and IBV is necessary in the final stage of virion release since, after budding the HA envelop glycoprotein remain bonded to the cell membrane sialic acid. Thus, the NA possess a sialidase activity that is necessary to cleave the terminal sialic acid residues on the host cell membrane and release virus particles[160]. NA also removes sialic acid residues from the virus envelope, preventing aggregation of the viral particles. The sialidase activity of NA proved also to be crucial in the entry phase of the virus, by easing the virus' access at the host cell membrane; the NA cleaves the sialic acid of the mucins, highly sialylated secretions composing the protective mucus that covers the host cells of the respiratory epithelia[161].

3.4.2.6.1 Neuraminidase NA

The NA is a tetrameric IVs envelop glycoprotein, composed by 4 identical subunits, of approximately 470 aminoacids each. In the monomers, three structural domains can be found: the cytoplasmic tail, the transmembrane region, the stalk, and the catalytic head (Figure 29). The cytoplasmatic tail is thought to be involved in NA interaction with M1 protein in the assembly process, while the transmembrane region at the N-terminal anchors the protein to the viral envelop. The TM domain, which is organized as an α-helix, also possess signals for translocation from the ER to the apical surface. The stalk domain aids tetramer stabilization thanks to the disulphide bonds formed between the cysteine residues of each monomer. The length of this region may vary in the different subtypes affecting the virus infectivity; a short NA stalk domain could hinder the contact of its catalytic site with the sialic acids of host cell membrane receptors. The head of the NA hosts the catalytic site which possesses the sialidase enzymatic activity. The active site e is highly conserved in both spatial orientation and sequence properties and includes eight highly conserved aminoacids that are involved into the NA-sialic acid interaction: Arg118, Asp151, Arg152, Arg224, Glu276, Arg292, Arg371, and Tyr406. In particular the three arginine residues Arg118, 292 and 371 are involved in a stabilizing interaction with the carboxylic acid of the substrate[160].
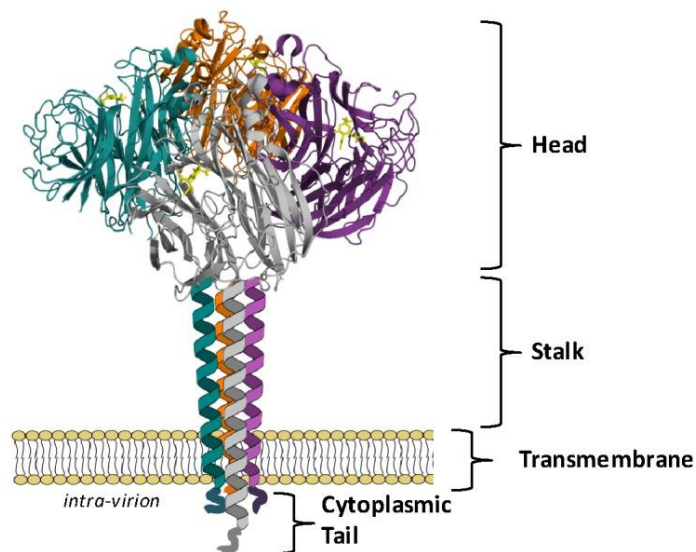
Figure 29. Structure and organization of the influenza A neuraminidase NA[160]

3.4.3 Influenza Virus Infections: Therapeutic approaches.

Nowadays, influenza therapy is restricted to two classes of virus-directed drugs: M2 ion channel blockers and neuraminidase inhibitors. However, the first class, including drugs like amantadine and rimantadine, is associated with virus resistance phenomena and neurological side effects, while the licensed NA inhibitors can also induce resistance and only provides rather modest clinical outcomes[162].

Besides antiviral drugs, seasonal vaccination represent the most efficacious way to reduce the influenza impact, even if the development of effective vaccines is complicated by the genetic variation, since influenza viruses vary continuously through antigenic drifts and antigenic shifts, acquiring the ability to evade the host pre-existing immunity. Therefore, continuous reformulation of vaccine compositions and annual immunization are needed. In addition, the immune responses induced by the influenza vaccines could be suboptimal in many treated people, especially in younger children and the elderly, who are at risk of severe influenza[84].

Thus, there is an urgent need to develop new antiviral strategies with entirely novel action principles and reduced risk for drug resistance. Currently, the search of novel anti-influenza small molecules could be directed towards different potential viral and host targets; novel antiviral agents are in different stages of development, fulfilling their antiviral activity either by targeting viral proteins or the viral genome, or by inhibiting host factors which are directly exploited by the virus in order to complete its life cycle[163].

3.4.3.1 Licensed Anti-influenza Virus Drugs

3.4.3.1.1 Proton channel M2 inhibitors: adamantanes

Among the traditional anti-influenza licensed drugs, amantadine and rimantadine are adamantane derivatives (Figure 30), that inhibit viral replication by blocking the M2 proton channel, thus inhibiting the release of the RNP complex in the host cell cytoplasm. Along with the problem of the increased viral resistance to these drugs, the therapeutic application of these compounds is also limited by their specificity for influenza A viruses M2 channels, thus they are not useful in IBV infections. For these reasons, and also for the sporadic occurrence of CNS side effects, the use of adamantanes as antiviral therapeutics is no longer recommended[9,164].

Amantadine   Rimantadine
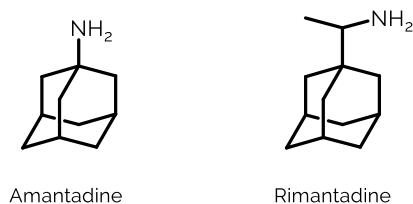
Figure 30. Structure of the adamantane drugs, amantadine and rimantadine.

3.4.3.1.2 NAI neuraminidase inhibitors

Another class of licensed anti-influenza drugs are the viral neuraminidase inhibitors (NAIs). These compounds are structural analogues of the sialic acid, which is physiologically present on the host cells' surface[9]. Sialic acid is most commonly present in the form of N-acetyl-9-O-acetylneuraminic acid (NANA). Since the viral neuraminidase possess a sialidase enzymatic activity, it facilitates the virus entry process by removing the NANA from the host cells surface and is also involved in the release of the newly synthesized virus particles from the infected cell[148].

Currently, four NAI are used in clinical practice: zanamivir, oseltamivir, laninamivir and peramivir (Figure 31). Oseltamivir is an orally available pro-drug, which is well absorbed and rapidly cleaved in the gastrointestinal tract releasing its active metabolite oseltamivir carboxylate. Due to their poor oral bioavailability, zanamivir is approved for inhalation delivery while peramivir has been approved for intravenous administration only. To date, Laninamivir is only approved for use in Japan to treat and prevent influenza A and B infection and is administered by inhalation as laninamivir octanoate prodrug, subsequentially converted by endogenous esterases in the airway to obtain laninamivir[165].

The therapeutic use of NAI has been limited by the emergence of viral resistance, especially to the orally bioavailable oseltamivir. These NAI-resistant variants of influenza A viruses of N1 NA subtype most frequently carry H274Y and N294S NA amino acid mutations, while viruses of N2 NA subtype carry E119V and R292K NA mutations, and NAI-resistant variants of influenza B viruses carry R152K and D198N NA mutations. However, generally cross resistance among oseltamivir and other NAIs has not been observed, thus oseltamivir-resistant infections could be successfully treated with other NAI[163].

In addition, the efficacy of these NAI is reported to be time-dependent, since therapeutic effect of these drugs can be observed mainly in subjects who receive the treatment within the first 48 h of symptom onset[166].

Oseltamivir   Zanamivir

Peramivir   Laninamivir
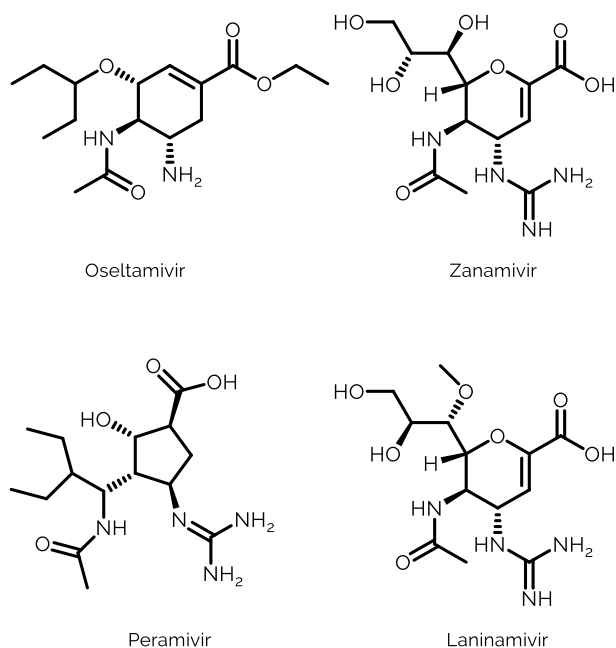
Figure 31. Structure of the NAI inhibitors currently approved for therapeutic use.

3.4.3.1.3 IV polymerase inhibitors

More recently, two novel anti-influenza drugs directed against different viral targets have been approved for therapeutic use. In particular, the influenza virus RdRp complex is the molecular target of baloxavir marboxil (BAM) and favipiravir (FP) two recently approved drugs that have reached the market (the first in Japan and the USA and the second only in Japan)[166].

Baloxavir marboxil (Xofluza®) (Figure 32) is a pro-drug that is hydrolysed in vivo to its active form which acts by inhibiting the cap-dependent endonuclease activity of the influenza A and B virus PA protein, which is part of the polymerase complex. It is licensed only in Japan and the USA for the treatment of uncomplicated influenza in subjects aged ≥ 12 years with influenza clinical manifestations for ≤48 h. Baloxavir is administered orally as a single dose, and is also reported to be effective against viruses resistant to NAIs. On the other hand, the high cost of the treatment and the

observed rapid and substantial emergence of resistant strains need to be monitored and could limit the use of this drugs in the future[9,166].
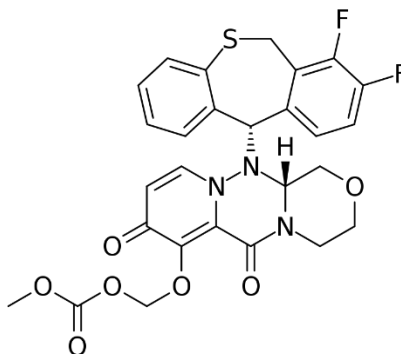
Figure 32. Structure of baloxavir marboxil (Xofluza®).

Favipiravir (FP) (Figure 33) is a nucleoside analogue administered orally and transformed *in vivo* in its active form, FP ribofuranosyl-5′-triphosphate (FRTP). FP directly inhibits the RNA-dependent RNA polymerase (RdRp) of RNA viruses by interacting with a highly conserved region among the different viral polymerases. Thus, it its activity is extended to several RNA viruses including all of the influenza virus subtypes. Favipiravir is also reported to have a good safety profile and only rarely influenza virus mutations have been observed.   However, favipiravir has reported to potentially cause teratogenicity and embryotoxicity, thus it is only approved in Japan with several limitations[167].
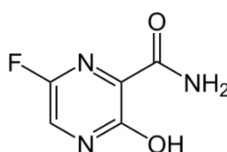
Figure 33. Structure of the polymerase inhibitor favipiravir.

Umifenovir (Arbidol) (Figure 34) is the only small-molecule influenza virus fusion inhibitor that is commercially available in Russia and China. It is a broad-spectrum antiviral agent which is reported to cause a general membrane perturbing effect; thus, its activity is not restricted only to influenza viruses but it also inhibits several other viruses. Its activity against influenza A virus is due to the inhibition of the viral HA, that interacts with Arbidol by mean of its stem region.
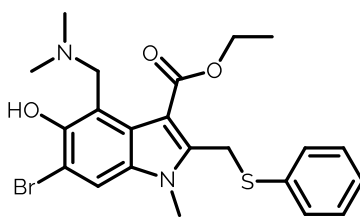
Figure 34. Structure of the broad spectrum antiviral Umifenovir (Arbidol).

3.4.3.2 Anti-influenza Virus preparations in phase of development.

Along the traditional licensed drugs, diverse new approaches have been attempted in order to control and prevent influenza. New small molecules designed to target different stages of the influenza virus life cycle, along with monoclonal antibodies directed against the highly conserved stem region of the viral haemagglutinin (HA) are currently under evaluation at different stages of development.

3.4.3.2.1 Monoclonal antibodies

The viral hemagglutinin is the principal target of vaccine-induced neutralizing antibodies which provide protective immunity against influenza. Thus, several monoclonal antibodies directed against this target have been developed and are currently at different stages of clinical evaluation[168].

Within the HA protein sequence, a highly conserved domain, corresponding to the N-linked glycosylation site in the stem region have been identified and monoclonal antibodies directed against these sites proved to be effective against a large number of influenza viruses.

CR6261 is a human monoclonal antibody which is directed against a highly conserved helical region in the membrane-proximal domain of hemagglutinin. It demonstrated neutralization activity against several influenza A subtypes *in vitro*, including the "Spanish flu" strain H5N1[169]. This mAb has recently been evaluated in a clinical trial phase 2 (NCT02371668) but results are still not available.

The preparation labelled CT-P27 is composed of two mAbs which have shown to neutralize several influenza subtypes. The product is currently undergoing phase 2 clinical trials in order to evaluate its efficacy and safety in subjects with acute uncomplicated influenza A infections[9].

The mAbs MHAA4549A, MEDI8852 and VIS-410 also target the highly conserved HA stalk region showing effective inhibition of all influenza A HA subtypes, and are currently being recruited in phase 2 clinical trials in monotherapy or in combination with oseltamivir[166].

TCN032 is a mAb which differs from those previously discussed as it targets an epitope at the N- terminus of the matrix 2 M2 protein which is a conserved epitope in influenza A viruses. It appeared to be well tolerated in a phase 2 human challenge study (NCT01719874) and also showed to inhibit almost all influenza virus types[170].

3.4.3.2.2 Other anti-influenza agents: small molecules

Pimodivir (Figure 35) is an orally available, non-nucleoside polymerase inhibitor currently under evaluation in a phase 3 clinical trial (NCT03381196) aimed to evaluate the efficacy and safety of pimodivir in combination with oseltamivir. The target of this molecule is the PB2 protein, which is part of the RNP ribonucleoprotein complex, thus is capable of inhibiting the viral RNA synthesis. It is active against a diverse group of influenza A viruses including the H1N1, H5N1, and H7N9[9].
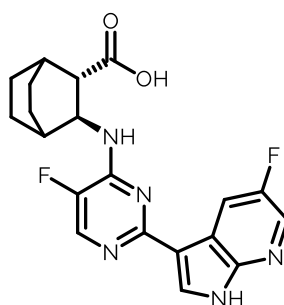
Figure 35. Structure of the polymerase inhibitor pimodivir.

Influenza virus hemagglutinin HA is also studied as a potential target of small molecule inhibitors. A compound named tert-butyl hydroquinone (TBHQ) (Figure 36) had been shown to bind and inhibit several HA subtypes *in vitro* (with K_d of 5 to 50 µM). It selectively binds a hydrophobic pocket near the highly conserved stem region, blocking the influenza virus fusion process.
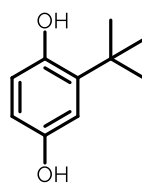
Figure 36. Structure of tert-butyl hydroquinone (TBHQ).

Due to the recent availability of crystallographic data of the different HA subtypes and to the discovery of the highly conserved stem region of the protein, influenza hemagglutinin is currently an attractive target for the development of novel antiviral agents: several other molecules have been designed and evaluated *in vitro* against this target such as BMY-27709, CL-385319 and RO5464466 (Figure 37) which inhibit the conformational change of H1 and H2 subtypes, but have no activity against H3 viruses[171].
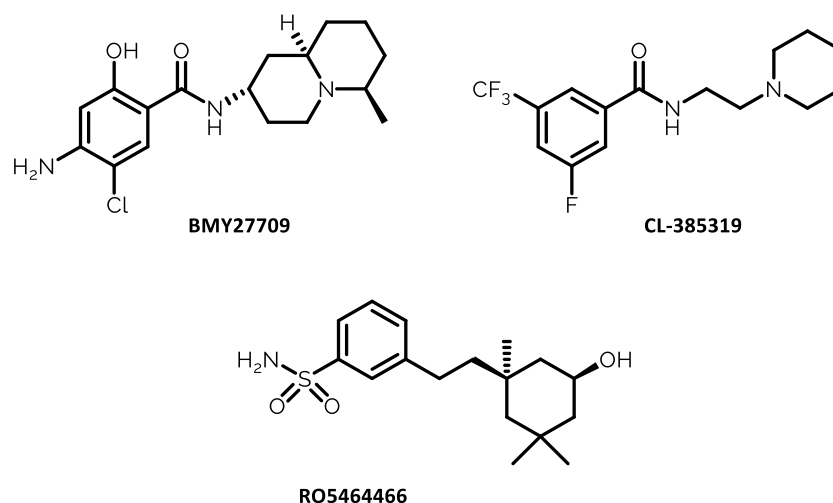
Figure 37. Structure of hemagglutinin inhibitors BMY-27709, CL-385319 and RO5464466.

3.4.3.2.3 Host-Targeting antivirals HTAs

The host factor-directed antiviral therapy is an emerging strategy that may help preventing the emergence of viral resistance and obtaining broad-spectrum antiviral agents. Host factors with a critical role in virus replication might become potential drug targets for new antiviral molecules, and today, different classes of anti-influenza agents are under development to target cellular proteins/processes[171].

Different studies using genome-wide RNA interference screening and a pseudo-typed particle entry assay allowed to identify several host cell' factors necessary for influenza virus replication (e.g. the IP3-protein kinase C (PKC), phosphatidylinositol-

3-kinase (PI3K)-Akt signalling pathways, vacuolar ATPases, fibroblast growth factor receptors FGFRs) and the dihydrofolate reductase DHFR enzyme[10,171].

DAS181 (Fludase) is a host-targeted recombinant sialidase fusion protein designed to remove sialic acid receptors on the respiratory epithelium, thereby restricting the ability of influenza viruses to bind and enter the host cell. It presents a heparin binding sequence which is responsible to bind the respiratory epithelium and a sialidase catalytic domain derived from *Actinomyces viscous,* which cleaves both α(2,6)- linked and α(2,3)- linked sialic acid receptors. DAS181 is formulated as a dry inhalation powder with microparticles (5-10 µm). It has been shown activity against several influenza viruses (H1N1, H3N2, H7N9, H5N1 and influenza B) in *in vitro* and *in vivo* tests and is currently under evaluation in different clinical trials. Regrettably, DAS181 seems to induce the selection of several mutations in the HA (G137R, S136T, S186I) and NA (W438L, L38P), thus the therapeutic use of this preparation could be limited due to emergence of viral strains with an increased receptor binding[166]

Nitazoxanide (NTZ) (Figure 38) is a pro-drug originally developed and licensed as an antiprotozoal drug for the treatment of *Cryptosporidium parvum* and *Giardia lamblia* infections. After oral administration it is rapidly deacetylated in the blood to the active metabolic form tizoxanide. In addition to its antiparasitic activity, NTZ has shown activity against a broad range of viruses including influenza. Its mechanism of action against influenza viruses is achieved by blocking HA maturation, due to the inhibition of the trafficking of the viral HA from the endoplasmic reticulum to the Golgi apparatus and by blocking HA terminal glycosylation. A phase 3 study (NCT03336619) to evaluate the efficacy and safety of nitazoxanide in the treatment of uncomplicated influenza has been recently concluded, but results have not been posted yet[9].
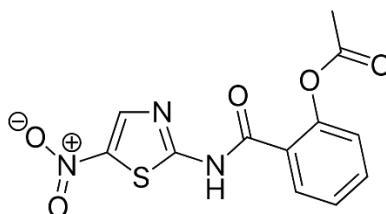
Figure 38. Structure of the broad spectrum HTA nitazoxanide.

CHAPTER 5. Discussion. Synthesis of 9-Aminoacridine-based molecules as novel bovine viral diarrhea virus (BVDV) inhibitors

5.1 Background

In the last years, the research group of Professor Tonelli has identified several molecules, belonging to different chemotypes endowed with and antiviral activity against BVDV, inhibiting its genome replication by interfering with the viral enzyme RNA-dependent RNA polymerase (RdRp) functioning. In particular, the anti-BVDV activity of arylazoenamines[172,173], 4-[(tert-aminoalkyl)amino]arylazo compounds[174] and 2-phenylbenzimidazole derivatives[175,176], have been described in scientific papers. The antiviral activity of acriflavine and other acridine derivatives have been first-time discovered as anti-*Flaviviruses* agents by Malina, A. et al., who demonstrated their capability of interfering with the HCV-IRES mediated protein synthesis[177]. Tabarrini, O. et al. identified a series of 9-acridone-based compounds endowed with micromolar activities against the bovine viral diarrhea virus, proposed as RdRp inhibitors acting as intercalant agents of the viral RNA, during genome replication[62]. More recently Tonelli et al. synthesized a series of 9-amino-6-chloro-2-methoxyacridine derivatives structurally related to quinacrine and acranil, which have been screened *in vitro* against a panel of RNA and DNA viruses in order to evaluate cytotoxicity and antiviral activity. These studies permitted to discover that the majority of these acridine-based compounds were endowed with an anti-BVDV activity, showing EC_{50} values in the range 0.1-31 µM associated also with good selectivity indexes (Figure 39)[5].
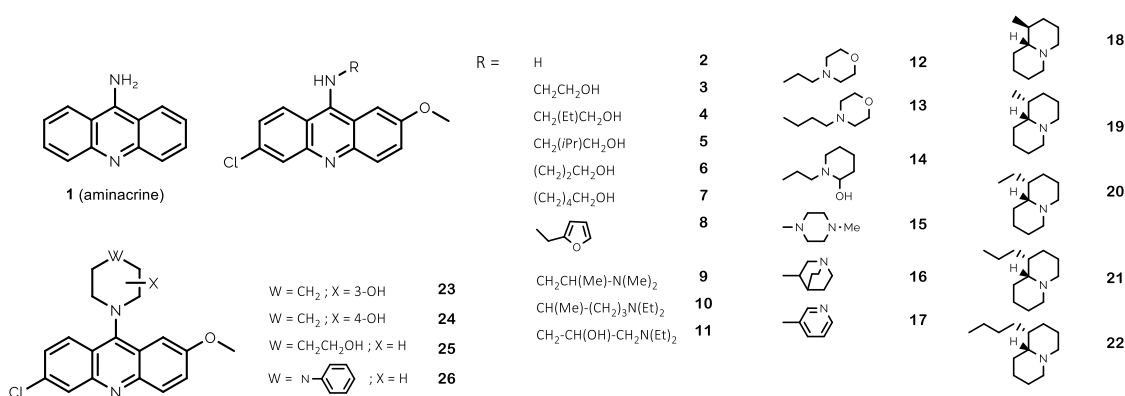
Figure 39. 9-Aminoacridine derivatives previously studied as anti-BVDV agents[5].

5.2 Project

During my PhD, I worked on the synthesis of new 2-methoxy-6-aminoacridine analogues in order to further explore the SAR of this chemical class against BVDV and also trying to find new more potent antiviral compounds, parallelly improving their safety profiles. Thus, three of the most promising compounds of the previous series (compounds **AVR15**, **AVR17** and **AVR26**)[5] have been selected as prototypes for the synthesis of the new analogues (Figure 40).
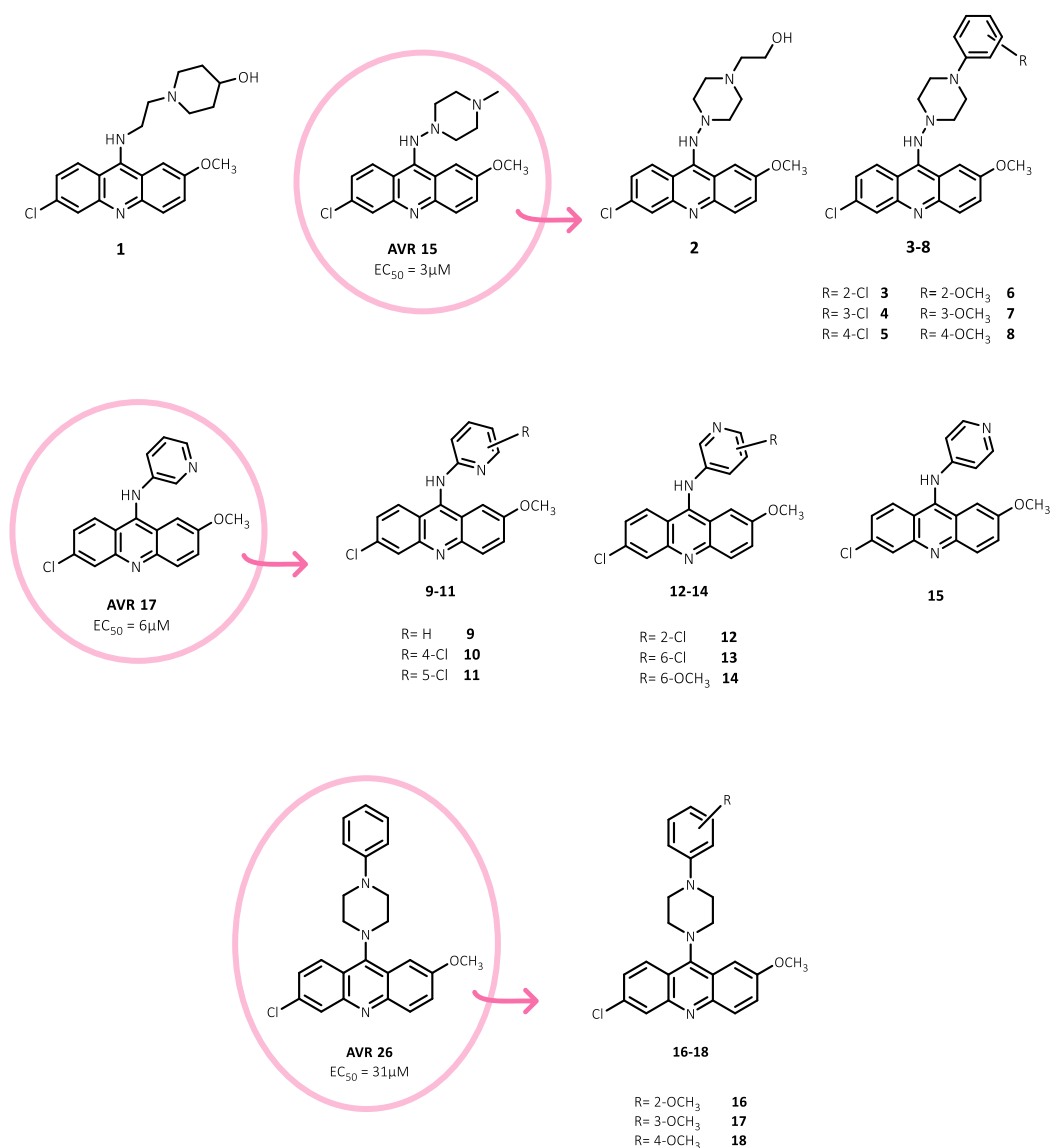
Figure 40. Chemical structure of the three prototypes of the previous series and of the newly synthesized analogues.

71

5.2.1 Chemistry

The novel compounds (**1-14** and **16-18**) were obtained by reacting the 6,9-dichloro-2-methoxyacridine, previously dissolved in phenol or DMF, with the proper amine in a molar ratio 1:1 or 1:2 for primary or secondary amines, respectively (Scheme 1). Compound **15**, 6-chloro-2-methoxy-9-[(pyridin-4'-yl)]aminoacridine, has been already synthesized and characterized by Luan, X. et al., thus it was synthesized according to the procedure reported in literature[178].

Scheme 1. Reagents and conditions: (a) ratio 1:1 in phenol, 90°C, 5h; (b) ratio 1:2 in DMF, 140°C, 3h.

The 1-aminopiperazines (**f-k**) needed for the synthesis of compounds **3**-**8** were obtained by nitrosating the proper 1-substituted piperazines with sodium nitrite and hydrochloric acid, and then reducing the corresponding N-nitrosopiperazine with zinc dust in acetic acid (Scheme 2).

a-e	**f-i; k**
a, R = o-Cl	**f**, R_1 = o-Cl
b, R = m-Cl	**g**, R_1 = m-Cl
c, R = p-Cl	**h**, R_1 = p-Cl
d, R = o-OCH$_3$	**i**, R_1 = o-OCH$_3$
e, R = p-OCH$_3$	**k**, R_1 = p-OCH$_3$

Scheme 2. Reagents and conditions: (a) NaNO$_2$, 1N HCl (pH=5-6), 70°C, 1h; b) Zinc dust, AcOH/H$_2$O ratio 1:1, 50°C, 3h.

Starting from the 1-(3-methoxyphenyl)piperazine the nitrosating reaction moved far from the expected product towards decomposition; thus, 1-amino-4-(3-methoxyphenyl)piperazine (**j**) was prepared by direct amination of 1-(3-

methoxyphenyl)piperazine with hydroxylamine-O-sulfonic acid in basic medium (Scheme 3).
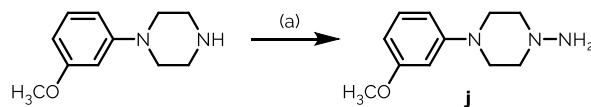
Scheme 3. Reagents and conditions: (a) hydroxylamine-O-sulfonic acid, NaOH pellets, H_2O, 60°C, 15 minutes; then r.t., 24h.

5.2.2. In vitro studies: anti-BVDV activity

The novel acridine derivatives have been tested for antiviral activity against a panel of DNA and RNA viruses by the research group of Prof. R. Loddo at the University of Cagliari. Eight of the novel compounds proved to selectively inhibit BVDV replication with EC_{50} values ranging between 0.8 and 11.9 µM, leaving unaffected the remaining viruses at concentrations up to their corresponding CC_{50} values on host cells or up to the highest concentration used (100 µM). Among the other virus strains only CVB-5 virus is occasionally susceptible to two compounds (**11** and **12**) (Table 2).

Table 2. Antiviral activity against BVDV and cytotoxicity of the three prototypes (AVR) and of new 9-aminocridine derivatives **1**-**18**[a].

COMPOUND	BVDV EC$_{50}$ (µM) [b]	MDCK CC$_{50}$ (µM) [c]	SI [d] CC$_{50}$/EC$_{50}$	BHK-21 CC$_{50}$ (µM) [e]	VERO76 CC$_{50}$ (µM) [f]	MEAN CC$_{50}$ FOR HOST CELLS
AVR15	3.0	>100	>33.3	32	10	>47.3
1	11.5	>100	>8.7	>100	>100	>100
2	0.80	9.2	11.5	19.7	20.6	16.5
3	7.5	>100	>13.3	>100	>100	>100
4	>100	>100	-	>100	>100	>100
5	68	68	1	30	33	43.7
6	2.9	46	15.9	42.5	49.8	46.1
7	35	54	1.5	70	66	63.3
8	11.9	43	3.6	38	32	37.7
AVR17	6	>100	>16.7	>100	>100	>100
9	34	34	1	45	42	40.3
10	38	>100	>2.6	>100	96	>98.7
11[g]	10.3	100	9.7	>100	>100	>100

12[g]	>100	>100	-	>100	>100	>100
13	8	80	10	95	>100	>91.7
14	**1.2**	40	33.3	>100	88	>76
15	63	>100	1.6	>100	>100	>100
AVR26	31	>100	>3.2	>100	>100	>100
16	20.2	>100	>5.0	>100	>100	>100
17	59	>100	1.7	>100	>100	>100
18	75	75	1	>100	89	>88
2'-C methyl guanosine	1.7	>100	>58.8	>100	>100	>100
Ribavirin	8.0	>100	>12.5	>100	>100	>100

[a]None of the compounds **1**-**18** proved active against any of the other investigated viruses (EC_{50}> 100 µM or > CC_{50}; data not shown). [b]Compound concentration (µM) required to achieve 50% protection of MDBK cells from the BVDV-induced cytopathogenicity, as determined by the MTT method. [c]Compound concentration (µM) required to reduce the viability of mock-infected MDBK cells by 50%, as determined by the MTT method. [d]SI= selectivity index. [e]Compound concentration (µM) required to reduce the viability of mock-infected BHK (Hamster normal kidney fibroblast) monolayers by 50%, as determined by the MTT method. [f]Compound concentration (µM) required to reduce the viability of mock-infected VERO 76 (Monkey normal kidney) monolayers by 50%. [g]Active against CVB-5: **11**, EC_{50}= 39 µM; **12**, EC_{50}= 23 µM (reference cpd. pleconaril: EC_{50}= 0.005 µM). Values shown are the mean of two different determinations, each performed in duplicate; SD <10%.

The most active compounds exhibited a potency profile against BVDV comparable (**1**, **3**, **11**, **13**) or superior (**2**, **6**, **14**) to the reference drug ribavirin. The 4-(2'-hydoxyethyl)piperazinyl (**2**) and (6'-methoxy)pyridin-3-yl moieties (**14**) represent the most efficient substitution of the 9 position of the 9-aminoacridine nucleus in order to achieve an anti-BVDV effect. The active compounds also exhibit a general low cytotoxicity (mean CC_{50} > 76 µM) against three different host cell lines.

5.2.3 *In vitro* studies: BVDV RdRp inhibition assays

The RNA-dependent RNA-polymerase plays a critical role in viral replication representing one of the most promising drug targets for the development of new anti-BVDV agents. Thus, in order to confirm the hypothesis of the RdRp as the molecular target of these compounds, the three prototypes (**AVR15**, **AVR17**, **AVR26**) from the previous series and the three most promising compounds (**2**, **6**, **14**) of the new series have been tested *in vitro* against the BVDV RdRp by the research group of Prof. S. Pricl at the Molecular Simulation Engineering (MOSE) Laboratory of the University of Trieste (Table 3; Figure 41).

Five of the six tested compounds clearly inhibit the viral enzyme in a dose dependent manner resulting with IC_{50} values in the range 0.62 μM (**2**)-4.3 μM (**AVR17**), supporting the hypothesis of the enzyme RNA-dependent RNA-polymerase as the specific molecular target.

Table 3. *In vitro* BVDV RdRp inhibition by the test set of 6 new 9-aminoacridine derivatives.

CPD.	IC_{50} (μM)	CPD.	IC_{50} (μM)
AVR15	1.2	**AVR17**	4.3
2	0.62	**14**	0.81
6	0.88	**AVR26**	38
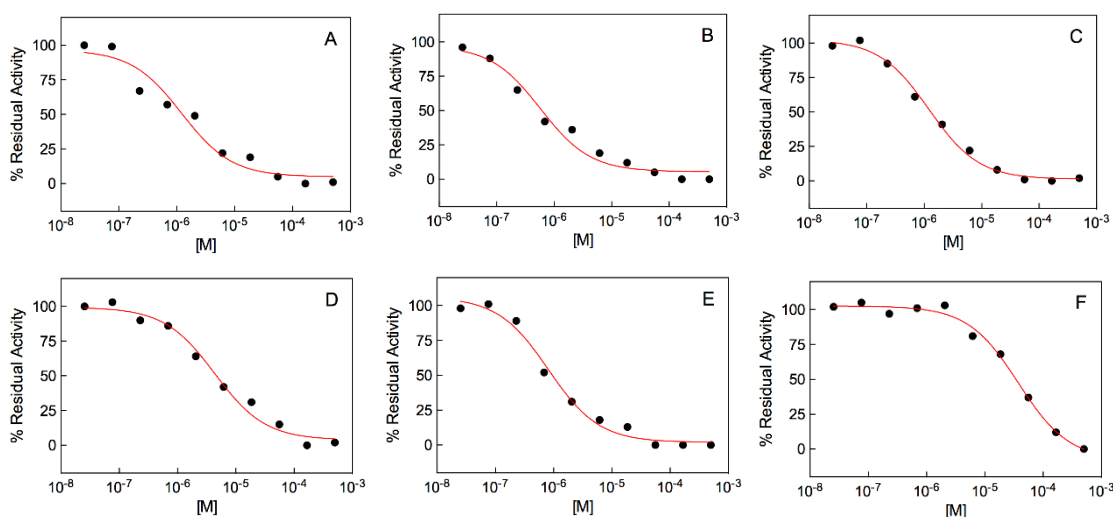
Figure 41. Dose-response curves for the test set of 6 new 9-aminoacridine derivatives **AVR15** (A), **2** (B), **6** (C), **AVR17** (D), **14** (E), and **AVR26** (F) as obtained from *in vitro* enzyme assay with the BVDV RNA-dependent RNA-polymerase.

5.2.4 Binding thermodynamics of compounds to the BVDV RdRp by Isothermal Titration Calorimetry (ITC)

In addition, binding affinities of the entire molecular series for the viral polymerase have been directly determined by Isothermal Titration Calorimetry (ITC) measurements by the research group of Prof. S. Pricl at University of Trieste. The averaged dissociation constant (K_d), binding free energy (ΔG_b), enthalpy (ΔH_b) and entropy terms ($-T\Delta S_b$) resulting from three independent ITC measurements on each compound are listed in Table 4.

Table 4. ITC determined thermodynamic data of the 9-aminoacridines binding the BVDV RdRp.

CPD	K_d (μM)	ΔG_b (kcal/mol)	ΔH_b (kcal/mol)	$-T\Delta S_b$ (kcal/mol)	n (-)
AVR15	0.91	-8.24	-11.26	3.02	0.92
1	9.1	-6.88	-13.84	6.96	1.10
2	0.57	-8.52	-14.07	5.55	1.03
3	4.8	-7.26	-12.46	5.20	0.98
4	38	-6.03	-10.43	4.40	1.00
5	41	-5.99	-10.37	4.38	1.04
6	0.95	-8.22	-13.52	5.30	0.95
7	23	-6.33	-11.96	5.63	0.99
8	8.6	-6.91	-13.15	6.24	0.93
AVR17	0.98	-8.20	-11.94	3.74	1.03
9	15	-6.58	-10.21	3.63	1.01
10	21	-6.38	-10.15	3.77	0.98
11	18	-6.48	-10.09	3.61	0.96
12	44	-5.45	-8.87	3.42	0.90
13	1.8	-7.84	-11.53	3.69	0.92
14	0.72	-8.38	-12.39	4.01	1.05
15	31	-6.15	-9.87	3.72	0.89
AVR26	28	-6.21	-11.42	5.21	1.08
16	22	-6.36	-11.76	5.40	1.11
17	39	-6.02	-11.00	4.98	0.99
18	48	-5.89	-10.78	4.89	0.91

$\Delta G_b = \Delta H_b - T\Delta S_b$. $\Delta G_b = RT \ln K_d$. n = number of binding sites. All experiments were run in triplicate. Errors on ΔH_b are within 5%.

The compounds interact with the viral protein in an exothermic ligand-binding event, with K_d values in the range 0.57 - 48 μM. The RdRp-ligand binding is supported by stabilizing hydrogen bonds and cationic/interactions ($\Delta H_b < 0$), while entropy disfavors complex formation ($-T\Delta S_b > 0$). The stoichiometry of the binding process, n, is always close to 1, confirming the 1:1 character of each binding event.

Of note, the K_d values for the six compounds (**AVR15**, **2**, **6**, **AVR17**, **14**, and **AVR26**) are in agreement with the IC_{50} values obtained by the *in vitro* enzymatic inhibition assays, showing that the most potent inhibitors result also the compounds presenting higher affinity to the viral polymerase in ITC binding assays, further supporting the notion that the viral polymerase is the target protein for this series of compounds (Figure 42).
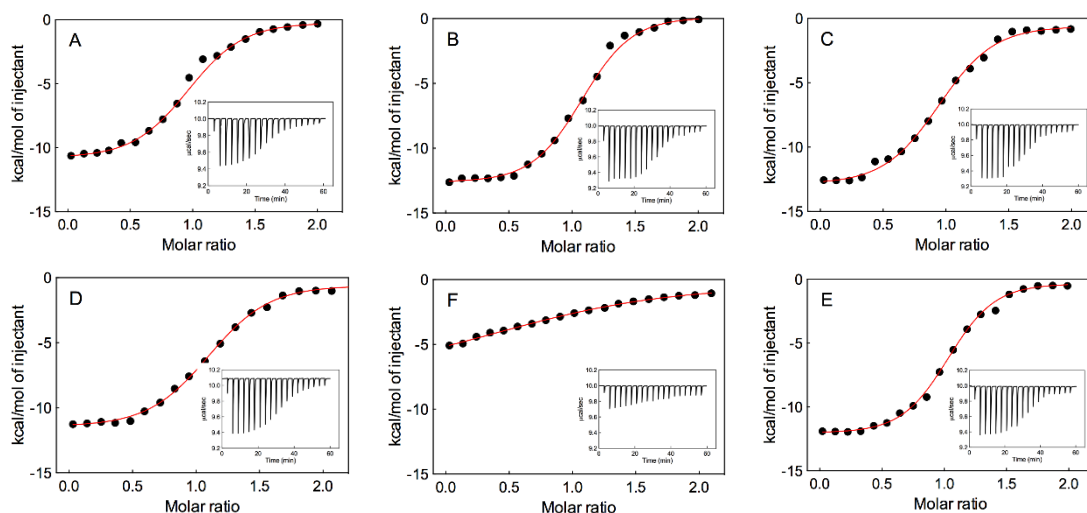
Figure 42. Representative ITC binding isotherms for **AVR15** (A), **2** (B), **6** (C), **AVR17** (D), **14** (E), and **AVR26** (F) titrations into BVDV RdRp solutions. Inserts: ITC raw data.

In addition, the K_d values derived by the ITC experiments and the EC_{50} values determined in the cell-based assays also shows a highly positive correlation (R^2 = 0.90) in the corresponding EC_{50} vs. K_d plot, demonstrating a strong correspondence between the binding of the new 9-aminoacridine derivatives to their target protein and their potency against BVDV (Figure 43).
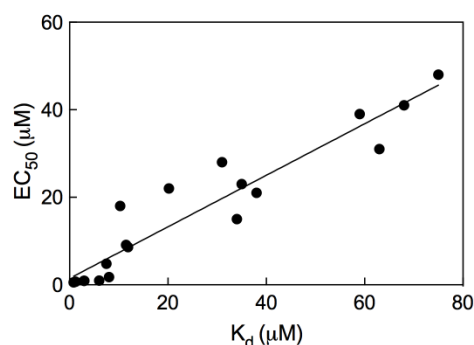
Figure 43. Correlation between BVDV RdRp binding activity (K_d, Table 2) and antiviral activity (EC_{50}, Table 1) of all new 9-aminoacridine derivatives (R^2 = 0.90).

5.2.5 Molecular modeling

Prof. S. Pricl's research group also performed Molecular modeling studies of the novel compounds in complex with the BVDV RdRp, in order to identify the key contacts established in the protein/ligand binding mode. Docking followed by free energy of binding scoring in the framework of the MM/PBSA methodologies resulted in calculated $\Delta G_{b,comp}$ values in excellent agreement (R^2 = 0.85) with the corresponding ITC-derived experimental data (ΔG_b). Analogous results were found for the enthalpic component ($\Delta H_{b,comp}$ and ΔH_b, R^2 = 0.89), and also for the entropic term (R^2 = 0.54) (Figure 44).
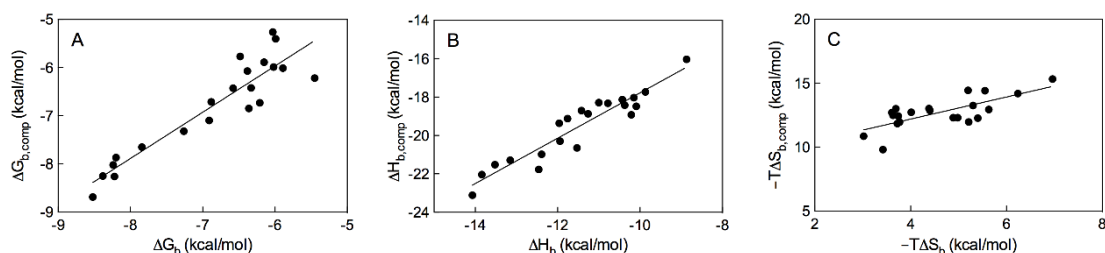
Figure 44. Correlation between computational and ITC-derived free energy of binding (A, R2 = 0.85), enthalpy (B, R2 = 0.89) and entropy (C, R2 = 0.54) for all new 9-aminoacridine derivatives in complex with the BVDV RdRp.

Molecular dynamics (MD) calculations have been made with the most potent compounds of the novel series in complex with the RdRp binding site; compound **2** revealed to be engaged in a bifurcated hydrogen bond (HB) between the –NH group bridging the tricyclic scaffold and the piperazine moiety and the side chains of E265 (average dynamic length (ADL) = 2.03 ± 0.04 Å) and R285 (ADL = 1.93 ± 0.02 Å). It also establishes a permanent HB between the methoxy substituent on the acridine nucleus and the ammonium group of K263 (ADL = 1.95 ± 0.01 Å) and a third HB between the hydroxyethyl group of **2** and the positively charged side chain of K525 (ADL = 2.10 ± 0.04 Å) (Figure 45; Figure 46).

The previous series compound **AVR15**, which presents a freely rotating methyl group in place of the hydroxyethyl substituent of compound **2**, has been also involved in MD calculations and shows to preserve the first two HBs performed by **2** (ADL = 1.91 ± 0.01 Å and 1.90 ± 0.02 Å, respectively).
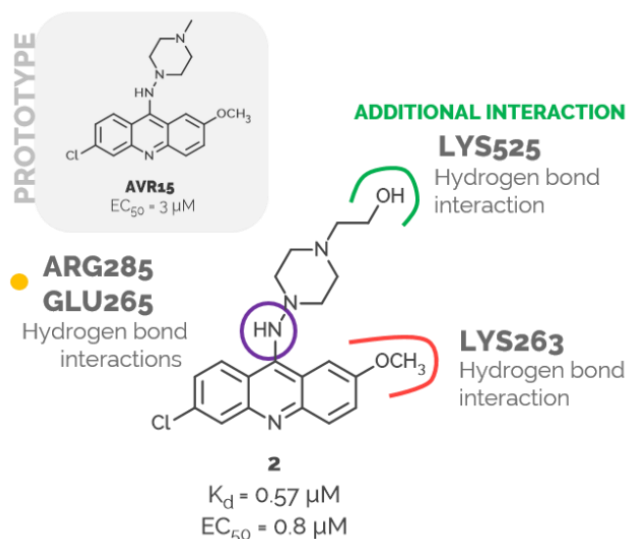
Figure 45. Chemical structure of compound 2 highlighting the key interaction involved in the ligand/protein interaction.

The compounds **3**, **4** and **5**, differ from **AVR15** by substitution of the methyl group on the piperazine ring with a phenyl moiety with different positions of the Cl atom on the phenyl ring, Indeed, **4** and **5** establish the same interactions described for **AVR15** with the protein, even less optimized, resulting in considerably lower protein affinity. On the contrary, compound **3**, besides the same two stabilizing HBs, is engaged in an additional favorable π-cation interaction between the ortho-chlorine substituted phenyl ring and the positively charged side chain of R529, resulting in a lower K_d value and higher affinity compared with compounds **4** and **5**. The different position of the chlorine atom on the phenyl substituent affects the molecule orientation within the binding pocket, resulting in an effective interaction only when the substituent occupies the ortho position. In the small subset of analogues **6**, **7** and **8**, only compound **6** maintain the same interactions described for compound **3**, resulting in an even higher binding affinity compared to compound **3**. Compound **8**, featuring the $-OCH_3$ group at the para position of the phenyl ring, although not able to perform the π-cation interaction described for **3**, is involved in an additional HB interaction between its OCH_3 substituent and the same residue R529 (ADL = 2.32 ± 0.06 Å). Finally, compound **7**, carrying the $-OCH_3$ group in meta position, results incapable of engaging the same stabilizing interactions of compounds **6** and **8**, leading to a lower binding affinity (Figure 46).
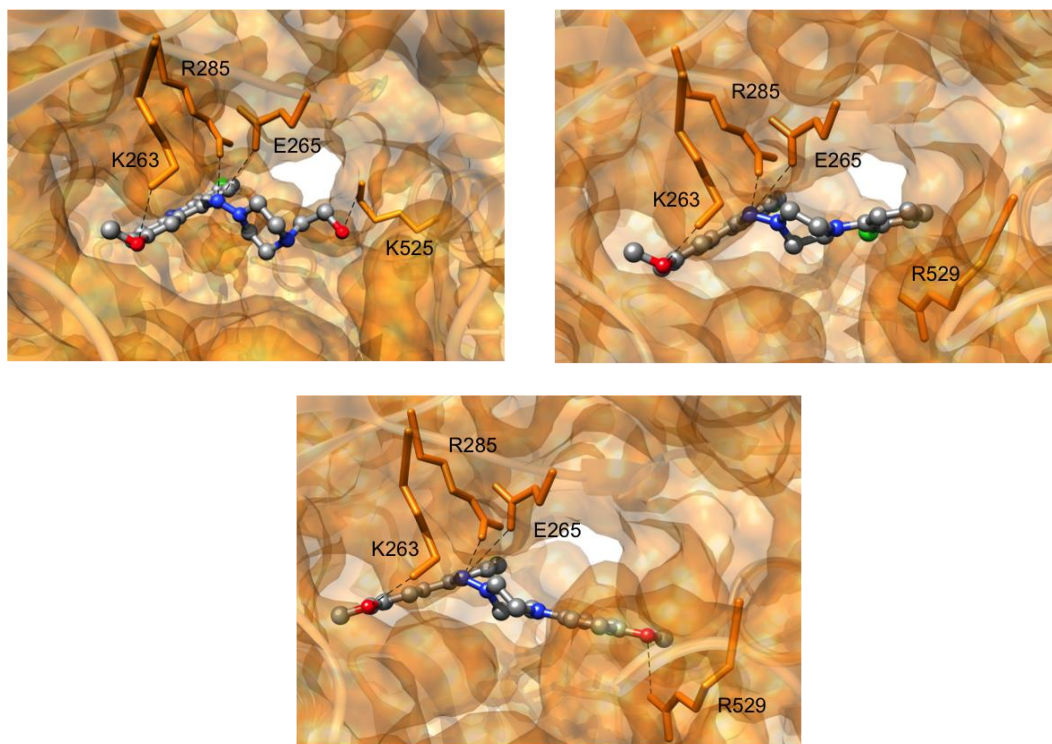
Figure 46. Equilibrated snapshots of compounds **2** (top left), **3** (top right), and **8** (bottom), in complex with the BVDV RdRp. The protein is portrayed as a transparent orange ribbon. Compounds are shown as atom-colored sticks-and-balls (C, gray; N, blue; O, red; Cl, green). Hydrogen atoms, water molecules, ions and counterions are omitted.

The binding mode of the **AVR17** prototype within the BVDV RdRp active site shows the same HB described for compound **2**, though **AVR17** establishes the third HB between the pyridine nitrogen and the side chain of R267 (ADL = 2.02 ± 0.01 Å). The pyridine derivatives **9** and **15**, presenting the pyridine moiety linked to the acridine nucleus in different positions, with the -N atom in ortho and para, respectively, show a consistently lower binding affinity, due to the absence of the HB with R267. Also compounds **11**, **12** and **13**, carrying a chlorine atom in different positions on the pyridine ring resulted in a reduced affinity for the binding site, due to the steric hindrance of the Cl atom. Thus, in the case of compound **14** the combination of the favorable meta position of the pyridine –N and the substitution with a para OCH_3 group leads to an improvement in the binding affinity with the viral enzyme, due to the establishment of the same HB network previously described for **AVR17** with an

additional HB interaction between the -OCH3 and the backbone –NH group between E265 and K266 (ADL = 2.43 ± 0.05 Å).

Finally, the last **AVR26**-derived small subset of compounds, whose lacks of the –NH group bridging the acridine scaffold and the piperazine/pyridine moieties, resulted in substantially lower RdRp binding affinities, resulting by the absence of the bifurcated HB described for the two previous series. In particular, AVR26 only establishes two HB with the RdRp binding site, the former between the –OCH$_3$ group and K263 and the second one between one of the piperazine nitrogen and the side chain of R285.

5.2.6 Conclusions

In this work, starting from the encouraging results of a previous study we selected the three most promising molecules of the previously studied series (**AVR15**, **AVR17**, and **AVR26**), in order to synthesize new structurally related derivatives. During my PhD, I've been able to synthesize a novel series of 9-aminoacridine derivatives, that demonstrate to selectively inhibit BVDV replication in *in vitro* assays. The most potent compounds demonstrate to inhibit BDVD replication, exhibiting EC$_{50}$ values in the range 0.8-11.5 µM. In addition, most of the active compounds provided high CC$_{50}$ values against three animal host cells, denotative of a high safety profile for these novel 9-aminoacridine derivatives. *In vitro* enzymatic inhibition assays against the BVDV RNA-dependent RNA-polymerase have been performed in order to prove the mechanism of action hypothesized for this series; the most promising compounds demonstrated to inhibit the target enzyme with sub-micromolar or low micromolar potencies. In addition, binding affinities of the entire molecular series for the viral polymerase were determined by ITC measurements yielding K$_d$ values in the range 0.57 - 48 µM and a positive correlation between the binding affinity and the antiviral potency/enzyme inhibition scores, calculated from the previous tests. Thus, the BVDV RNA-dependent RNA-polymerase have been confirmed. Finally, molecular modeling, and in particular MD calculation of the novel compounds in complex with the viral RdRp disclosed the most probable binding mode of this class of antiviral compounds on the viral polymerase.

CHAPTER 6. Discussion. Design, synthesis and biological evaluation of novel host-targeting antiviral (HTA) compounds active towards respiratory viruses (RVs).

6.1 Host-directed antivirals: synthesis of a set of azaspiro-dihydrotriazines as new potential anti-influenza and anti-RSV dual-acting antivirals, targeting the host *h*DHFR.

6.1.1 Background

In a recent paper Tonelli et al. have identified the interesting antiviral profile of a series of 1-aryl-4,6-diamino-1,2-dihydrotriazines structurally related to the former antimalarial drug cycloguanil, acting as host-directed antivirals targeting the human dihydrofolate reductase (*h*DHFR)[10]. Cycloguanil is the active metabolite of the antimalarial drug proguanil (Paludrine® or Malarone®), approved for prophylaxis and treatment of infections by *Plasmodium vivax* or *falciparum* whose activity against the parasite has traditionally been attributed by a selective action directed toward the plasmodium bifunctional dihydrofolate reductase-thymidylate synthetase (DHFR-TS). Indeed, cycloguanil and other dihydrofolate reductase (DHFR) inhibitors (such as methotrexate MTX), are known to be effective antineoplastic, anti-bacterial, and anti-protozoal agents because of the central role played by DHFR in the *de novo* synthesis of nucleic acid precursors. Even though the antimalarial cycloguanil presents a higher binding affinity to the plasmodium DHFR rather than the human isoform of the enzyme, its capability of also inhibiting the mammalian isoform *h*DHFR have been described, exhibiting a K_i value toward the human enzyme of 0.41 μM[179].

Thus, the cycloguanil-derived 1-aryl-4,6-diamino-1,2-dihydrotriazines displayed a dual activity against influenza (A and B) and respiratory syncytial virus (RSV) targeting the host cell DHFR enzyme which is involved in the replication processes of both viruses. In order to assess that the observed antiviral activity was influenced by the inhibition of the host enzyme, some selected compounds have been tested against *h*DHFR, resulting in the K_i values ranging between 0.07 and 0.13 μM for the best antiviral compounds. The docking studies on some selected compounds also permitted to identify the pivotal role of the two H-bonds with the protein residues I7 and E30, by means of the two NH_2 groups of 1,2-dihydrotriazine scaffold, for the stabilization of the inhibitor within the hDHFR binding site[10].
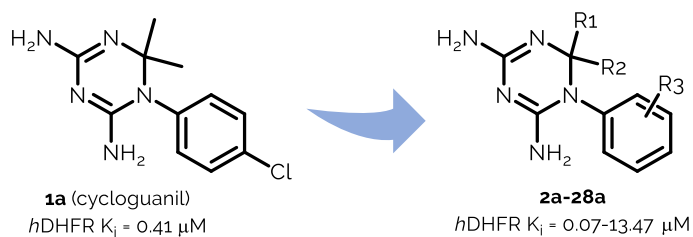
Figure 47. Structure of cycloguanil and general structure of the first series of dihydrotriazines analogues discovered as host-directed antivirals[10].

6.1.2 Project

During the first and second year of my PhD, I synthesized a new set of 23 azaspiro dihydrotriazines, with the aim to improve the antiviral activity exploiting enhanced interactions at the active site of the host (human) DHFR. Thus, two novel azaspiro-2,4-diamino-1,6-dihydrotriazine scaffolds have been explored utilizing the 4-piperidone or 3-piperidone as versatile building blocks in order to introduce an additional center for chemical derivatization, represented by the spiro-piperidine nitrogen. The position 1 of the dihydrotriazine core have been functionalized with differently substituted aromatic rings or aliphatic chains (Figure 48-49).
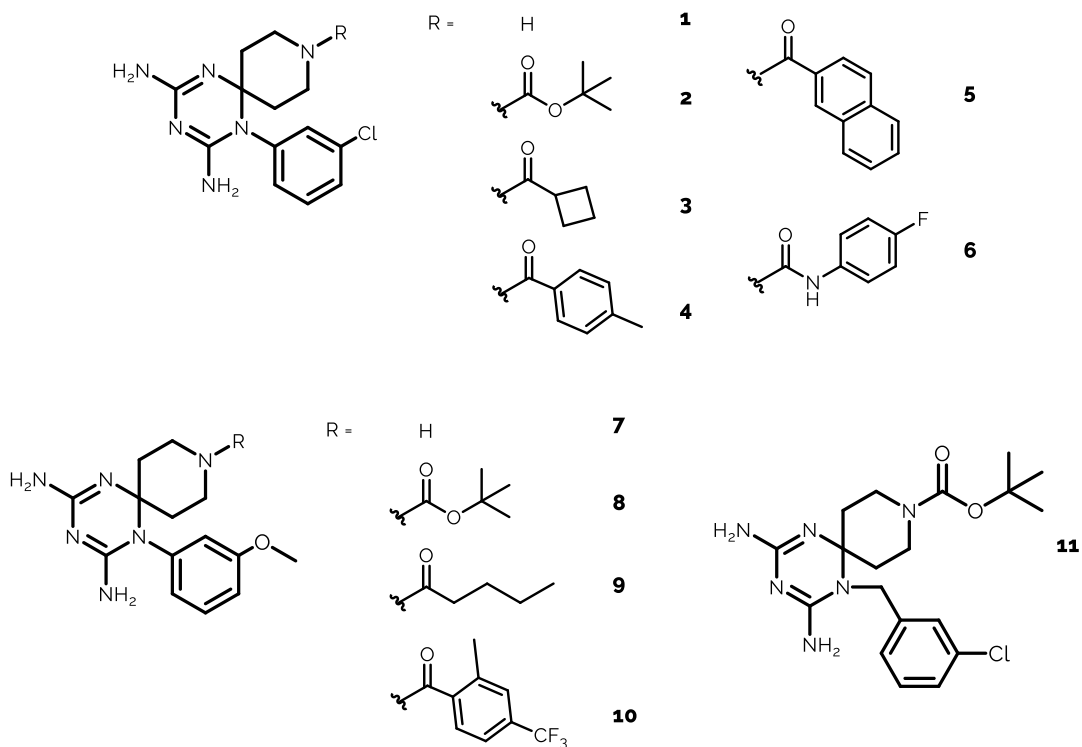
Figure 48. Structure of the investigated azaspiro-2,4-diamino-1,6-dihydrotriazine derivatives **1-11**.
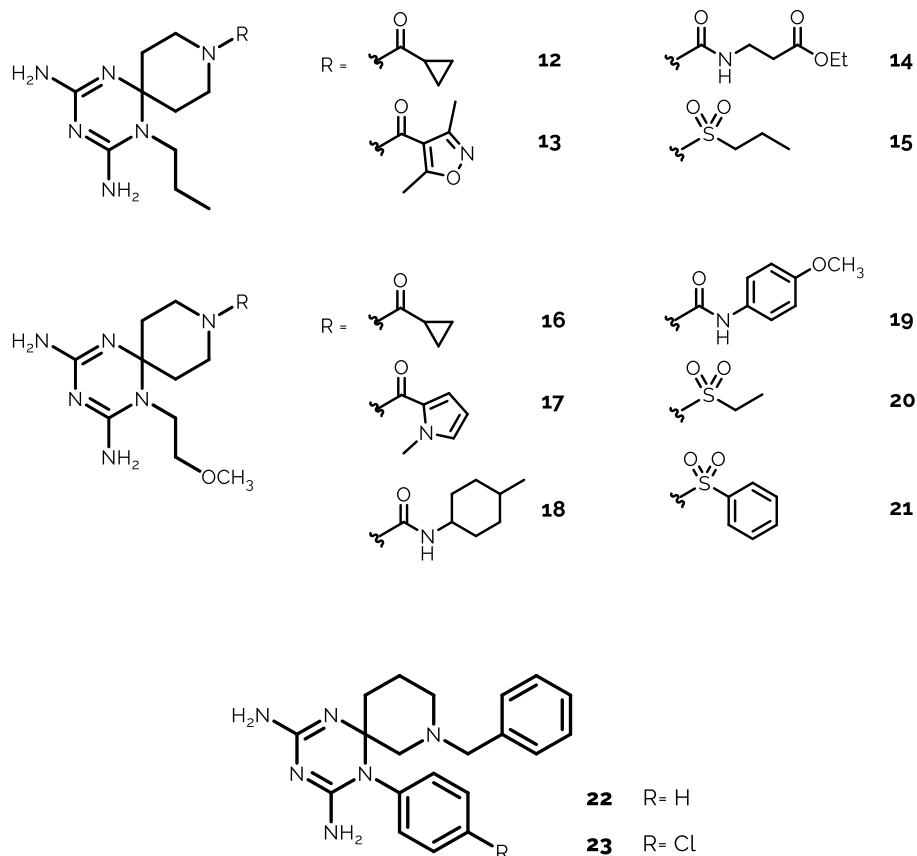
Figure 49. Structure of the investigated azaspiro-2,4-diamino-1,6-dihydrotriazine derivatives **12**-**23**.

6.1.2.1 Chemistry

Compounds **1**-**21** have been prepared by means of a three-step synthetic route. In the first step the proper amine, cyanoguanidine and 1-Boc-4-piperidone have been refluxed in acid catalyzed conditions, then the protective group has been removed with trifluoroacetic acid (20%) (Scheme 4).

Scheme 4. First two steps: cyclization and removal of the protective group. Reagents and conditions: a) 1 equiv. amine, HCl conc., EtOH, 90°C, 17 h. b) DCM/TFA 20%, r.t. 6-7 h.

In the last step the piperidine nitrogen has been reacted with acyl chlorides, isocyanates, sulphonyl chlorides and carboxylic acids to obtain the corresponding carbamate, amide, sulphonamide and ureido functions (Schemes 5-7).

Scheme 5. Reagents and conditions: a) THF o DCM / Et$_3$N, r.t. 12 h; b) DMF, HOBT/EDC, DIPEA, r.t. 12 h.
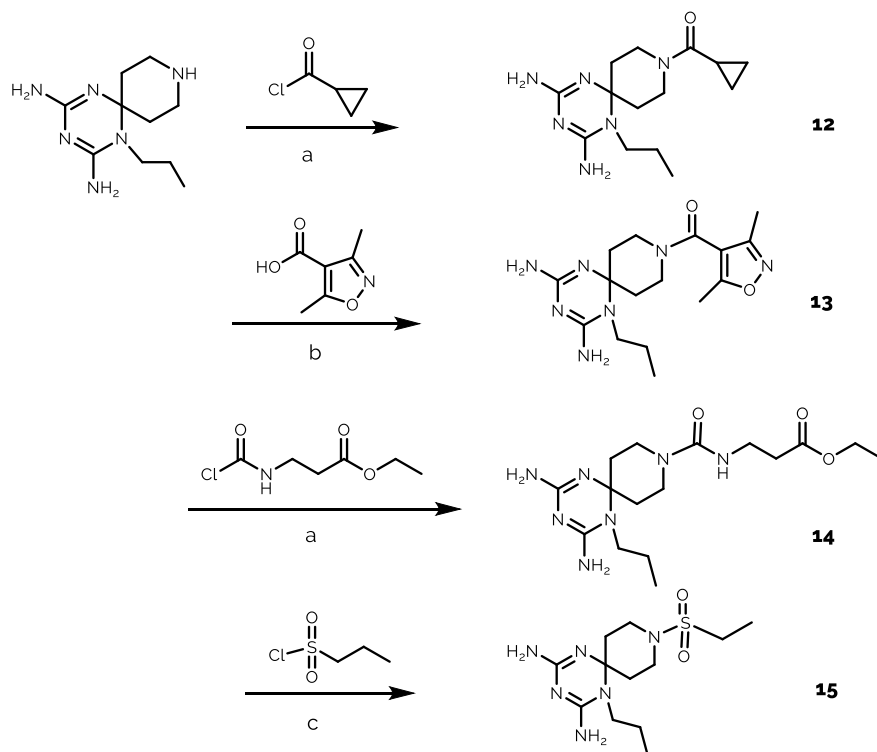
Scheme 6. Reagents and conditions: a) THF o DCM / Et$_3$N, r.t. 12 h; b) DMF, HOBT/EDC, DIPEA, r.t. 12 h; c) DCM, DIPEA, r.t. 12 h.
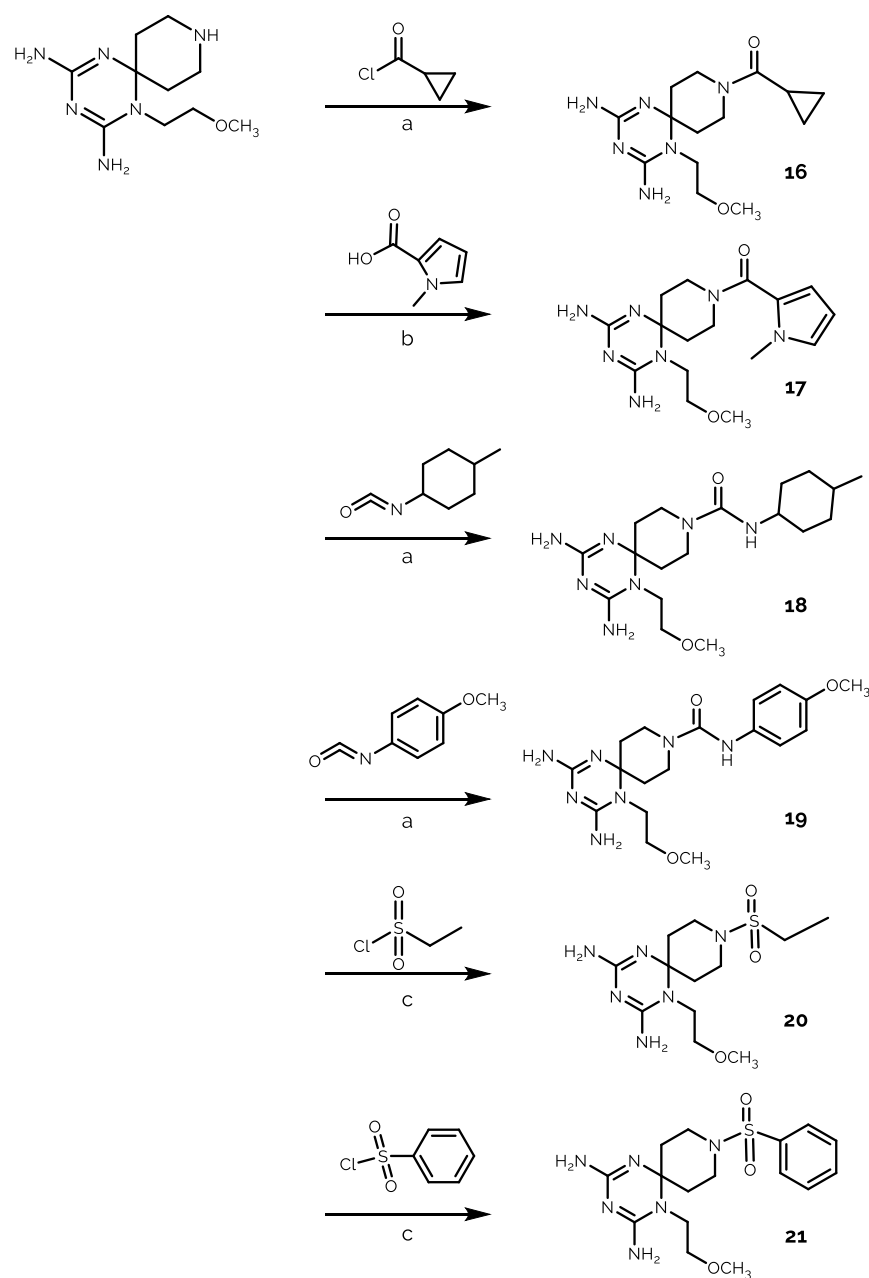
Scheme 7. Reagents and conditions: a) THF o DCM / Et$_3$N, r.t. 12 h; b) DMF, HOBT/EDC, DIPEA, r.t. 12 h; c) DCM, DIPEA, r.t. 12 h.

A "one pot" reaction of the proper aniline derivative, 1-benzylpiperidin-3-one, previously converted into hydrochloride salt, and dicyandiamide at reflux for 8 h afforded compounds 22 and 23 (Scheme 8). These compounds crystallized directly from the reaction mixture as pure hydrochlorides.
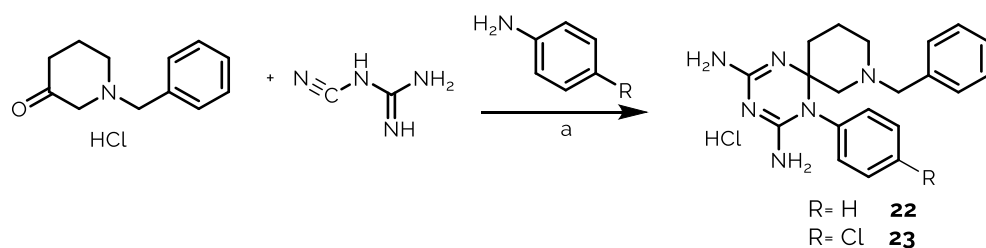
Scheme 8. Reagents and conditions: a) EtOH, HCl, 130°C, 8 h.

6.1.2.2 *In vitro* studies: antiviral activity

The entire compound series have been evaluated in cellular assays against influenza A, subtypes H1N1 (A/PR/8/34 and A/Virginia/ATCC3/2009) and H3N2 (A/HK/7/87), and influenza B (B/Ned/537/05) viruses. In addition, the target compounds have been tested against a diverse panel of other viruses, including RSV, which was susceptible which was highly susceptible to the previously synthesized series of dihydrotriazines. Biological assays have been performed by Prof. Lieve Naesens at the University of Leuven, Belgium.

Table 5. Antiviral activity of compounds **1**-**23** against influenza A and B viruses and RSV in MDCK[a] and HeLa cells, respectively.

CPD	INFLUENZA[b] ASSAY IN MDCK CELLS				RSV ASSAY IN HELA CELLS	
	EC$_{50}$[c] (µM)		CYTOTOXICITY (µM)		EC$_{50}$[d] (µM)	CYTOTOXICITY
	INFLUENZA-A	INFLUENZA-B	MCC[e]	CC$_{50}$[f]		MCC[e] (µM)
1	>100	>100	>100	>100	>100	>100
2	11	24	≥20	>100	>100	>100
3	35	7.7	≥20	>100	>100	>100
4	>100	0.29	≥0.8	18	0.40	≥100
5	28	4.0	≥4	>100	>100	≥100
6	>100	0.2	≥0.16	51	1.8	≥100
7	>100	>100	>100	>100	>100	>100
8	87	39	≥100	>100	>100	>100
9	>100	28	≥100	>100	>100	>100
10	>100	>100	>100	>100	>100	>100
11	>100	>100	>100	>100	>100	>100

12	>100	>100	>100	>100	>100	>100
13	>100	>100	>100	>100	>100	>100
14	>100	>100	>100	>100	>100	>100
15	>100	>100	>100	>100	>100	>100
16	>100	>100	>100	>100	>100	>100
17	>100	>100	>100	>100	>100	>100
18	>100	>100	>100	>100	>100	>100
19	>100	>100	>100	>100	>100	>100
20	>100	3.0	>100	>100	>100	>100
21	>100	>100	>100	>100	>100	>100
22	>100	>100	>100	>100	>100	>100
23	>100	>100	100	45	>100	100
Zanamivir	1.33	0.14	>100	>100	-	-
Amantadine	26	>500	>500	>500	-	-
Rimantadine	28	>500	≥500	>500	-	-
Ribavirin	11	3.2	≥20	>100	5.8	>250
DS-10,000[g]	-	-	-	-	0.8	>100

[a]MDCK: Madin-Darby canine kidney cells. [b]Influenza virus strains: A/PR/8/34 (A/H1N1) and B/Ned/537/05. [c]EC_{50}: 50% effective concentration producing 50% inhibition of virus-induced cytopathic effect (CPE), as determined by colorimetric formazan-based MTS cell viability assay. [d]EC_{50}: 50% effective concentration producing 50% inhibition of virus-induced cytopathic effect (CPE), as determined by microscopy. [e]MCC: minimum compound concentration producing a microscopically detectable alteration in normal cell morphology. [f]CC_{50}: 50% cytotoxic concentration, as determined by measuring the cell viability with the MTS assay. [g]For DS-10,000 (dextran sulphate of MW 10,000) concentrations are in µg/mL. Values shown are the mean of three determinations.

The compounds showed in general lower potency against the different viral targets compared to the previous series, hinting that a bulkier chemical scaffold is less tolerated in order to bind the target active site. Only few compounds (**2**, **3**, **5**, **8**) demonstrated a weak activity against influenza A virus with EC_{50} values in the range 11-87 µM. Five compounds (**3**-**6** and **20**) proved to inhibit influenza B replication with EC_{50} values in the range of 0.29-7.7 µM, while a lower anti-IBV activity have been reported for three compounds (compounds **2**, **8**, **9** showing EC_{50} values of 24 µM, 39

μM and 28 μM, respectively). Finally, two compounds were also active against RSV (**4** and **6**, EC_{50} 0.40 and 1.8 μM, respectively).

Although the test compounds were directed towards a host cell enzyme, they produced no or marginal cytotoxicity at 100 μM in human cervix carcinoma HeLa or African green monkey Vero (results not reported) cell cultures. A higher cytotoxicity was observed in the MDCK cells: the two most potent compounds **4** and **6**, resulted active against both IBV and RSV, showed CC_{50} values of 18 and 51 μM, respectively.

The most promising compounds in terms of antiviral activity against influenza B virus, are functionalized at the piperidine nitrogen with a *p*-tolylcarbonyl (**4**) or (4-fluorophenyl)carbamoyl moieties (**6**).

Compound **4** exhibited similar activity for influenza B and RSV (EC_{50} values of 0.29 and 0.40 μM, respectively with an anti-influenza potency comparable to that of the approved drugs zanamivir (EC_{50} = 0.14 μM) and higher than that of ribavirin (EC_{50} = 3.2 μM against influenza B and EC_{50} = 5.8 μM versus RSV). Despite the compound showed a marginal cytotoxicity in MDCK cell assays, it exhibits a favourable selectivity index (CC_{50}/EC_{50}), SI = 62. Compound **6** showed an even higher activity against influenza B virus (EC_{50} = 0.19 μM) and an improved safety profile (SI = 268). Likewise compound **4**, it also proved to be active against RSV (EC_{50} = 1.8 μM).

The Cl or OCH_3 substituents on the phenyl ring at N(1) position have been chosen basing on the results obtained for the previous series of cycloguanil analogs. The data confirmed that the chlorine atom in meta position (**2**-**6**) enhances the antiviral potency for influenza B, whereas the 3–OCH_3 group results less effective (**8**, **9**). Additionally, it's noticeable that the replacement of the aromatic substituents on N(1) with a n-propyl or methoxyethyl chain abolishes the activity against influenza viruses and RSV; among this second sub-group of compounds, only compound **20** results capable to inhibit influenza B virus in vitro, with an EC_{50} = 3.0 μM combining an ethyl sulfonic moiety on the spiropiperidine nitrogen and a methoxyethyl chain on N(1) of the dihydrotriazine core.

None of the compounds displayed activity against enveloped DNA viruses (i.e., herpes simplex virus or vaccinia virus), enveloped RNA viruses (i.e., feline coronavirus, parainfluenza-3 virus, vesicular stomatitis virus, sindbis virus or Punta Toro virus) or non-enveloped RNA viruses (i.e., Coxsackievirus B4 and Reovirus-1) (data not reported).

6.1.2.3 Molecular modeling

Prof. E. Cichero performed molecular modeling studies of the novel compounds in complex with the human enzyme hDHFR, The X-ray data chosen included the host enzyme in complex with a pyridopyrimidine-based inhibitor (**I**) (pdb code = 4QHV; resolution = 1.61 Å)[180] (Figure 48).

Co-crystallized inhibitor **I**
in complex with hDHFR
(pdb code = 4QHV)
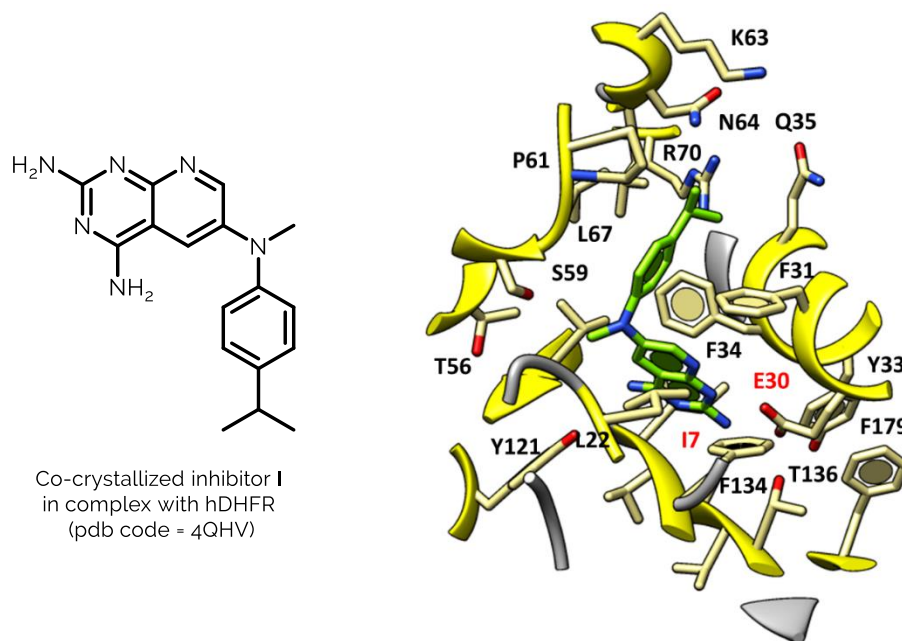
Figure 48. X-ray crystallographic complex *h*DHFR - inhibitor **I** (*C* atom; green).

Molecular docking studies on the most promising derivatives of the first series of dihydrotriazines highlighted some important interactions responsible for the protein-ligand complex stabilization. All of the most potent compounds established two H-bonds with I7 and E30, thanks to the two NH_2 groups onto the dihydrotriazine scaffold; in particular, the dimethyl substitution on the dihydrotriazine core together with lipophilic substituents at the meta position of the phenyl ring proved to be particularly effective in terms of potency.

Thus, docking studies on the new series permitted to better understand the relevance of steric properties for dihydrotriazines targeting *h*DHFR, by replacing the dimethyl substitution at C(6) of dihydrotriazine with an azaspiro-containing substituent, along with the introduction in position 1 of differently substituted phenyl- and benzyl- rings or alkyl chains.

Regarding the new compound series, docking results suggest a beneficial role played by the azaspiro group bearing an aromatic substituent, since it appears superposed on the aniline moiety of the reference inhibitor **I**, and could be responsible of the establishment of additional hydrophobic interactions within the enzyme cavity. On the other hand, the key H-bonds with the I7 and E30 residues, identified in the previous series, appeared to be absent in the docking poses of the novel compound in the enzyme cavity, accounting for the trend towards a generally lower antiviral potency. Nevertheless, among the compounds bearing a phenyl ring on the N(1) of the dihydrotriazine core, the presence of lipophilic and electron-withdrawing groups at the *meta* position of the aromatic substituent sometimes allows the inhibitor to maintain the key H-bond interaction with I7.

In particular, docking poses of the most promising compounds **4** and **6** in complex with the *h*DHFR displayed additional stacking interactions between the phenyl ring on N(1) and the Y121 residue, and also one H-bond between their carbonyl oxygen atom and the S59 side-chain (Figure 49).
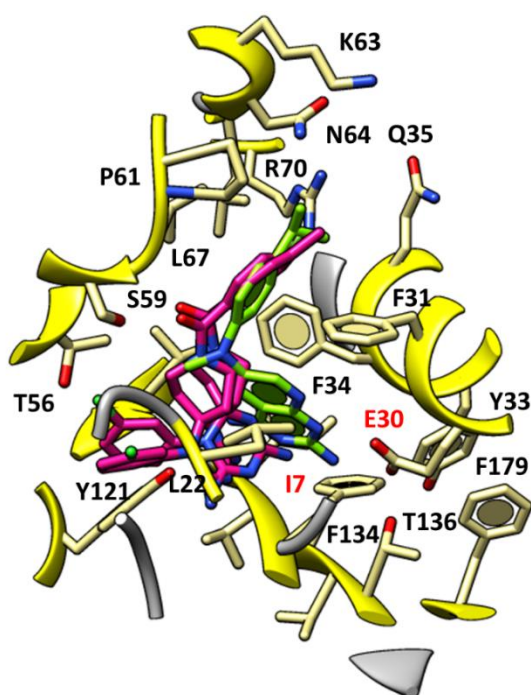
Figure 49. Docking pose of compound **4** and **6** (C atom; magenta) within the X-ray crystallographic structure of the human DHFR in complex with the inhibitor I (C atom; green).

Among the sub-set of derivatives bearing an alkyl chain at N(1) of dihydrotriazine (compounds **12**-**21**), only compound **20** (IBV, EC_{50} = 3.0 μM) exhibited an effective docking mode within the enzyme cavity. Its flexible alkyl side chain permitted to the dihydrotriazine portion of the ligand to fill the binding cavity better than reference compound **I** and the previously described analogues, which were decorated with conformationally rigid aromatic rings at N(1) of dihydrotriazine (Figure 50).
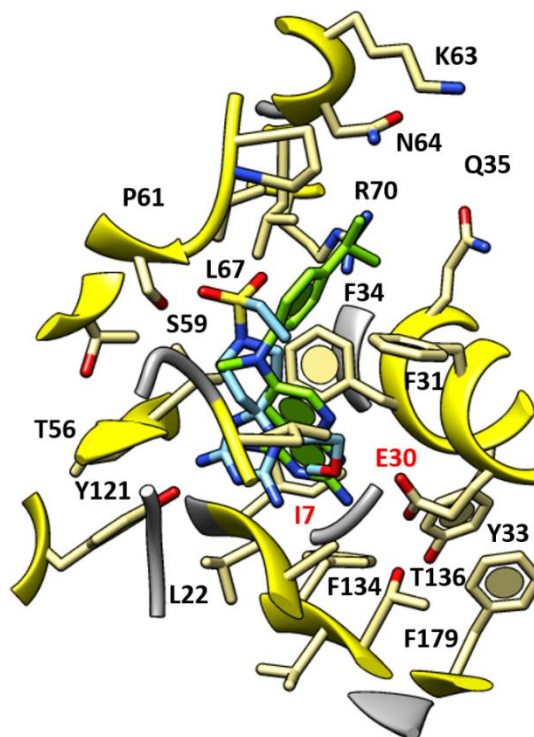
Figure 50. Docking pose of 20 (C atom; cyan) at the X-ray crystallographic complex *h*DHFR - inhibitor **I** (C atom; green).

In particular, compound **20** has been reported capable to establish an H-bond with I7, while the sulfone moiety interacts by H-bonds with S59. In addition, the presence of the OCH_3 substituent on the aliphatic chain placed at N(1), allowed intra-molecular hydrogen bonds with one of the NH_2 group decorating the dihydrotriazine core, which contributed to correctly orient the molecule within the binding cavity.

6.1.2.4 Conclusions

This novel compound series have been synthesized following the previous investigation on dihydrotriazine-based derivatives discovered as dual antiviral agents against influenza and RSV viruses, acting on the host factor DHFR, in order to

93

gain a better knowledge of the SAR relationships within the series and trying to find new agents endowed with improved activity and safety profiles[10]. Thus, the introduction of a bulkier substituent on the C(6) of the dihydrotriazine and also by mean of the nitrogen of the spiropiperidine nucleus, allowed the study of the role of different functionalized side chains to understand the chemical space for enhanced interactions within the *h*DHFR enzyme.

The novel series presents a lower antiviral activity overall, if compared to the previous series of cycloguanil-derived, who displayed nanomolar activity against both influenza B and RSV. However, among the azaspiro- derivatives two compounds emerged as dual inhibitors, endowed with a high activity and selectivity against influenza B and RSV. The two compounds were characterized by the piperidine nitrogen bearing a H-bond acceptor moiety linked to an aromatic lipophilic groups, such as the *p*-tolylcarbonyl (**4**) or (4-fluorophenyl)carbamoyl ones (**6**), combined with the 1-phenyl azaspiro dihydrotriazine.

Interestingly, compound **20** has also proved a selective and interesting activity against influenza B virus only; it's chemical structure differs from the other active compounds belonging to the novel and previous series and combines a methoxyethyl chain at N(1) with an ethylsulfonic group at spiropiperidine nitrogen. Thus, it could also represent a starting point in order to develop new optimized analogues.

6.2 Host-directed antivirals: synthesis of 2-amino-3,4-dihydrotriazino[1,2-a]benzimidazoles as new potential *h*DHFR inhibitors

6.2.1 Background

The encouraging antiviral results regarding the dihydrotriazine-based compounds, who acts as *h*DHFR inhibitors, a host cellular enzyme involved in the replication processes of different viruses, opened up the possibility to develop broad spectrum antivirals acting on host enzymes instead on specific viral components. Thus, the synthesis and evaluation of the previously described azaspiro- dihydrotriazine derivatives, led to the idea of designing and synthesizing new molecular series, specifically tailored to bind the DHFR enzyme, in order to find diverse potentially exploitable chemical scaffolds.

6.2.2 Project

Taking into account the studies on the dihydrotriazine core, during the second year of my PhD, I decided to further investigate the antiviral potential of triazine nucleus exploring different functional groups and substitutions; thus, I synthesized a set of new (2-aminotriazino)benzimidazoles, where the triazine core is condensed with differently decorated benzimidazoles. The triazino[1,2-a]benzimidazole scaffold opportunely functionalized has been previously demonstrated by Dolzhenko et al. to possess an inhibitory activity against the plasmodial DHFR[181]. Thus the 2-amino-4,4-dimethyl-3,4-dihydro-s-triazino[1,2-a]benzimidazole has been selected as prototype to develop a new series of compounds **1**-**8** to be tested for their inhibitory activity against human, plasmodial and leishmanial DHFR in order to confirm their inhibitory activity and to assess their selectivity, and then to be evaluated as potential host-directed antiviral agent (Figure 51).
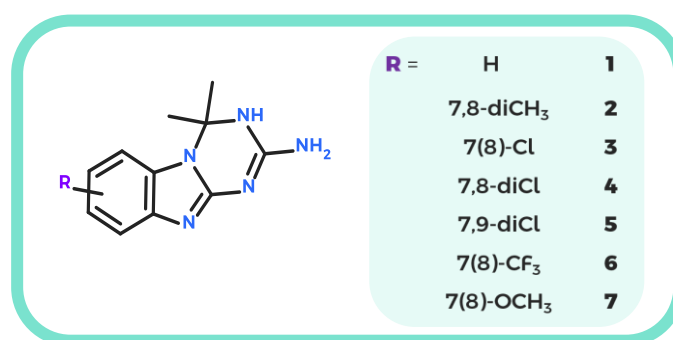
Figure 51. Structure of the investigated 2-aminotriazino[1,2-a]benzimidazoles **1**-**7**.

6.2.2.1 Chemistry

The 2-aminotriazino[1,2-a]benzimidazoles have been synthesized by cyclization of the corresponding 2-guanidinobenzimidazoles with acetone, used also as solvent, in presence of piperidine.

	R1	R2		R1	R2
I	H	H	V	5-Cl	6-Cl
II	5-Cl	H	VI	4-Cl	6-Cl
III	5-CF$_3$	H	VII	5-CH$_3$	6-CH$_3$
IV	5-OCH$_3$	H			
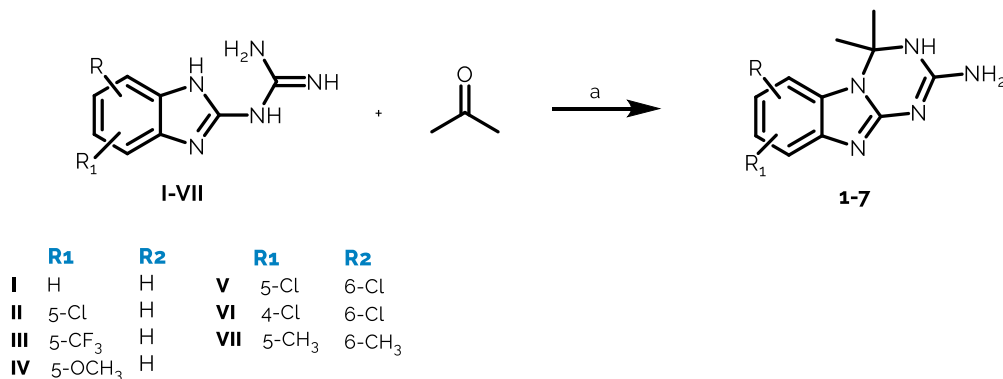
Scheme 9. Reagents and conditions: a) 0.5 eq. piperidine, reflux 7h.

Compounds **1** has been already synthesized and characterized as reported by Dolzhenko et al. In the paper mentioned above is also reported that when the cycloaddition reaction occurs between acetone and the corresponding guanidine benzimidazoles monosubstituted, it doesn't provide a regioselective product but a mixture of two isomers in different proportions[181]. Thus, also for compounds **3**, **6** and **7** the formation of the two isomers is clearly appreciable in the corresponding ^{1}H and ^{13}C NMR spectra. The assignment of the specific isomeric peaks and (if the peaks are clearly discernible, also of the corresponding isomeric proportions) in the ^{1}H NMR spectra have been determined by referring to the literature, thus the isomer carrying the substitution on C(7) of the tricyclic scaffold, presenting a lower chemical shift than the second isomer, is referred as isomer "a" and appears to be formed in minor amount compared to the C(8) substituted isomer, referred as isomer "b".

The starting 2-guanidinobenzimidazoles have been obtained starting from the corresponding 1,2-phenylendiamines with dicyandiamide (1,1 equiv.) in acid medium.
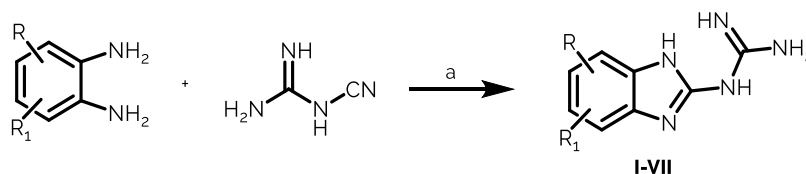
Scheme 10. Reagents and conditions: a) HCl conc. (1eq.), H$_2$O, reflux 6h.

The 4,6-dichloro-1,2-phenylendiamine, 4-trifluoromethyl-1,2-phenylendiamine and 4-methoxy-1,2-phenylendiamine, have been synthesized starting from the corresponding o-nitroanilines by reducing the nitro group with Tin(II) chloride in ethanolic solution.

R = CF$_3$, OCH$_3$, Cl
R$_1$ = H, Cl
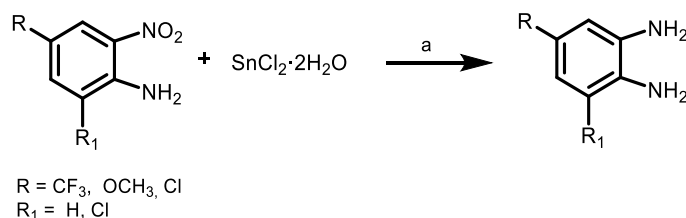
Scheme 11. Reagents and conditions: a) anhydrous EtOH, reflux 6h.

6.2.2.2 *In vitro* studies: antiviral activity and cytotoxicity assays

The entire compound series were tested in order to determine their antiviral activity in *in vitro* screening assays by the research group of Prof. L. Naesens at the University of Leuven (Belgium). The novel derivatives were screened against influenza viruses, A subtype H1N1 (A/Ned/378/05), A subtype H3N2 (A/HK/7/87) and B (B/Ned/537/05), and also versus a panel of several DNA and RNA viruses, such as (+)ssRNA viruses (YFV, CVB-4, human coronavirus 229E, FIPV, Sinbis virus), (-)ssRNA viruses (RSV, HPIV-3, VSV, Punta Toro virus), dsRNA (Reo-1 virus), and four DNA viruses (HSV-1, FHV, VV and Adenovirus type 2).

Table 6. Antiviral activity and cytotoxicity of the compounds **2**, **6** and the intermediate guanidinebenzimidazole **VII**.

Cpd	Antiviral activity: EC$_{50}$ (µM)[a]			CC$_{50}$ (µM)[b]
	A/HK/7/87 (H3N2)	**RSV**	**VV**	
2	-	-	**54.2**	>100
6	-	**6.5**	-	55.0
VII	**18.1**	-	-	39.2
Zanamivir	30.7	-	-	>100
Ribavirina	7.5	6.7	-	>100
DS-10000	-	0.01	-	>100
Brivudin	-	-	12.6	>250
Cidofovir	-		8.7	>250

[a]EC$_{50}$: 50% effective concentration producing 50% inhibition of virus-induced cytopathic effect (CPE), as determined by microscopy. [b]CC$_{50}$: 50% cytotoxic concentration, as determined by measuring the cell viability with the MTS assay. The reported values are the mean of at least 3-4 experimental determinations. The table reports only the EC$_{50}$ values of the compounds who resulted active (EC$_{50}$ < 100 µM) in the antiviral screening assays.

Table 7. Cytotoxicity values of the compounds **2**, **6** and the intermediate guanidinebenzimidazole **VII**.

Cpd	Cytotoxicity: CC$_{50}$ (µM)[a]				CC$_{50}$ (µM) mean of values
	HEL	**Hep-2**	**Vero**	**MDCK**	
2	>100	49.7	>100	12.4	>65.5
6	>100	55.0	>100	81.1	>84.0
VII	46.2	45.7	37.5	39.2	42.2

[a]CC50: 50% cytotoxic concentration in HEL, Hep-2, Vero and MDCK cells, as determined by measuring the cell viability with the MTS assay, in absence of viral infection. The reported values are the mean of at least 3-4 experimental determinations.

As reported in Table 6, only three compounds (**2**, **6** and **g**) proved to be effective by inhibiting the replication of specific viruses in tested cells.

In the two previous series of dihydrotriazine derivatives, there was a clear positive correlation between the inhibitory activity against hDHFR and the anti- and anti-RSV

potency, while the influenza A subtype H3N2 resulted insensitive to the antiviral effect. In this novel series, no compound proved to be effective against the influenza A(H1N1) and B strains, and only one compound (**VII**) exhibited an antiviral effect against IAV H3N2, surpassing the reference drug zanamivir (EC$_{50}$ = 30.7 µM) in terms of potency. In this case, the mechanism of actions could not be attributable to the *h*DHFR inhibition, since the host enzyme isn't involved in the replication process of the IAV H3N2 strain.

Only one compound (**6**, EC$_{50}$ = 6.5 µM), proved to effectively inhibit RSV replication with a potency comparable to the reference drug ribavirin (EC$_{50}$ = 6.7 µM). as discussed in the chemistry section, compound **6** has been tested as a mixture of two not separated isomers (**6a** and **6b**), bearing an electron-withdrawal trifluoromethyl group on the C(7) and C(8) positions, respectively, of the triazinobenzimidazole scaffold.

Finally, the 7,8-dimethyl- substituted derivative (**2**), proved a weak inhibitory effect on the Vaccinia virus (VV) replication, in *in vitro* antiviral assays (EC$_{50}$ = 54.2 µM).

The three active compounds (**2**, **6**, **VII**) are all endowed with a good safety profile, since they exhibited general low toxicity against four different both human and animal derived cell lines, as reported in Table 7 (42.2 < CC$_{50}$ > 84.0 µM).

6.2.2.3 *In vitro* studies: DHFR inhibition assays

The novel compounds have been evaluated by the research group of Prof. Paola Costi (UNIMORE) in enzymatic inhibition assays against the *h*DHFR, and also against two protozoan DHFRs, *Leishmania major* DHFR (*Lm*DHFR) and *Trypanosoma cruzi* DHFR (*Tc*DHFR), with the aim of exploring species-selectivity preferences.

Table 8. Inhibition constants (K_i) of compounds **1-7** on *h*DHFR and protozoan DHFR enzymes.

COMPOUND	*h*DHFR	*Lm*DHFR	*Tc*DHFR
	K_i (µM)	K_i (µM)	K_i (µM)
1	3,34	**0,74**	9,70
2	**1,68**	3,61	1,98
3	**1,64**	**0,59**	**1,12**
4	**0,69**	**1,38**	**1,17**
5	**1,56**	**0,24**	2,36
6	9.96	24.34	14.62
7	10.85	11.93	8.44
Cycloguanil[10]	0,41	-	-

All the tested compound presented generally low binding affinity with the target enzyme *h*DHFR, presenting K_i values between 0.69 µM (**4**) and 3.34 µM (**1**), for the best inhibitors among the series. Compound **1**, not presenting any substituent on the benzimidazole ring, is characterized by a low affinity for the enzyme, while the introduction of both electron-donor (**2**, **7**) or electron-withdrawal groups (**3**-**6**) improves the inhibitory profile against the target. Among this series, the most potent *h*DHFR inhibitor is represented by the 2-amino-7,8-dichloro-4,4-dimethyl-3,4-dihydro-s-triazino[1,2-a]benzimidazole (**4**), and is also featured by a favorable species-selectivity profile for human isoform, being 2-fold higher than that of protozoan DHFRs. Generally, the compounds exhibited lower K_i values, therefore corresponding higher binding affinities for the *Leishmania major* enzyme isoform, thus the anti-protozoal activity of these compound series could be investigated in future studies.

6.2.2.4 Molecular modeling

Despite the lacking of a favourable antiviral activity within these compound series, the best *h*DHFR inhibitor resulted from the enzymatic assays (**4**) in terms of both binding affinity and selectivity for the human isoform, have been selected to perform molecular docking calculations. Docking studies have been performed by Prof. E. Cichero, employing the X-ray data of the host enzyme in complex with a pyridopyrimidine-based inhibitor (**I**) (see Figure 52; pdb code = 4QHV; resolution = 1.61 Å)[180].
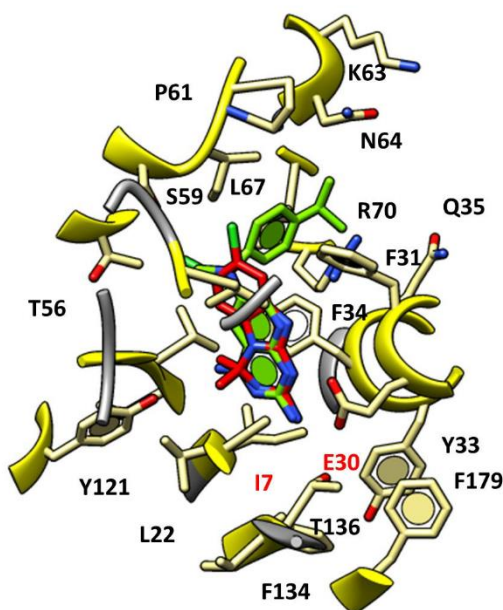
Figure 52. Docking pose of compound **4** (C atom red) on the X-ray structure of the *h*DHFR co-crystallized with the inhibitor **I** (C atom green; pdb code = 4QHV).

In the docking pose depicted the triazinobenzimidazole scaffold fully overlaps the inhibitor (**I**) pose, thus it could be worth to be objects of further structural optimization. If compared to the docking poses of the previous studied dihydrotriazine series, here the key H-bond with I7 residue is lacking, while the H-bond interaction with the carbonyl group of E30 is maintained by mean of the NH_2 group on the triazine ring. the tricyclic moiety is also involved in π-π stacking interactions within the binding site, with residues Y33 and F34.

6.2.2.5 Conclusions

Combining the knowledge of the SAR of two previous series of dihydrotriazines acting as host targeting antivirals HTAs targeting the human enzyme *h*DHFR, with the discovery of a series of plasmodial DHFR inhibitors sharing the triazino[1,2-a]benzimidazoles scaffold, prompt to the design and synthesis of this novel series of analogues as new potential antiviral agents.

The compounds have been tested against a panel of RNA and DNA viruses including Influenza A/H1N1, B, and RSV, who were susceptible to the previously studied dihydrotriazine *h*DHFR inhibitors. Additionally, since the antiviral activity data (EC_{50}) against influenza viruses and those related to *h*DHFR inhibition correlated linearly in

the previous series, also in this case enzyme inhibition assays and docking studies on the target enzyme have been performed.

However, the viral screening only occasionally showed a low susceptibility to the tested compounds, who demonstrated in general lack of antiviral activity. Only three compounds **2**, **6** and **VII** showed the capability of selectively inhibit A/H3N2 virus, RSV and VV, respectively. These three compounds proved an interesting activity and safety profiles, comparable to the ones of the reference approved drugs, although the mechanism of action had not been elucidated yet.

According to the antiviral activity results, all the compounds showed a lower binding affinity for the human isoform of the target enzyme, while the inhibitory activities against *Leishmania major* and *Trypanosoma cruzi* DHFRs of some of these derivatives make this series of compounds promising for further studies related to the treatment of pathologies caused by these protozoa.

CHAPTER 7. Discussion. Design, synthesis and biological evaluation of novel anti-influenza compounds acting on viral hemagglutinin (HA).

7.1 Background

The influenza virus hemagglutinin represents one of the antigenic determinants of the virus and is crucial for the infectivity of the virus particles since is involved in the entry, release and exit processes. The development of effective antiviral small molecules directed towards the HA protein has been hampered by its sequence diversity, since, to date, at least 18 HA subtypes of influenza A are known.

Among the small-molecule inhibitors **CL-385319** is an N-substituted piperidine compound that has been discovered as a potent inhibitor of influenza A HA-mediated fusion (Figure 53). The compound proved efficacy in inhibiting HA subtypes H1, H2, and H5 at a low micromolar level, while a 30–250-fold higher concentration is required to inhibit H3 influenza virus[12]. The antiviral activity against A/H5N1 virus have been also described by Zhu, Z. et al. for a series of amides, carboxylic acids and a benzenesulfonamide structurally related to **CL-385319**[182].

Inspired by this chemical scaffold, also the research group of Prof. S. Vazquez designed and synthesized a series of aniline analogues that were identified as inhibitors of influenza A virus subtype H1N1 (the structure of compound **9d**, the most promising compound of the series is reported in Figure 53).
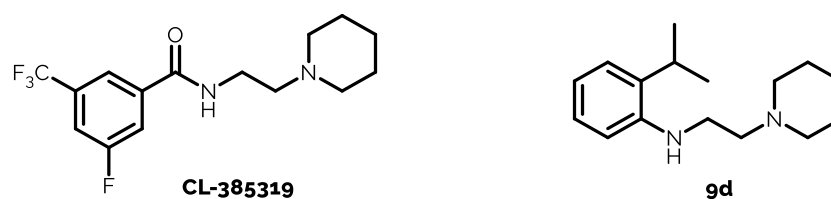
Figure 53. chemical structures of the HA inhibitor **CL-385319** and of the anilino derivative **9d**.

Along with the lead compound **9d**, several anilino analogues also displayed activity against A/H1N1 influenza with EC_{50} values in the low micromolar range. These compounds successfully inhibit the virus HA-mediated fusion by binding the HA stem and preventing its refolding at a low pH. In addition, molecular dynamics

simulations suggest that the lead compound **9d** interacts with the protein by binding a conserved region among the different IAV H1 strains referred as "TBHQ pocket" by the name of the tert-butylhydroquinone (TBHQ) an influenza fusion inhibitor for which HA co-crystallization data are available (PDB codes: 3EYK and 3EYM)[183].
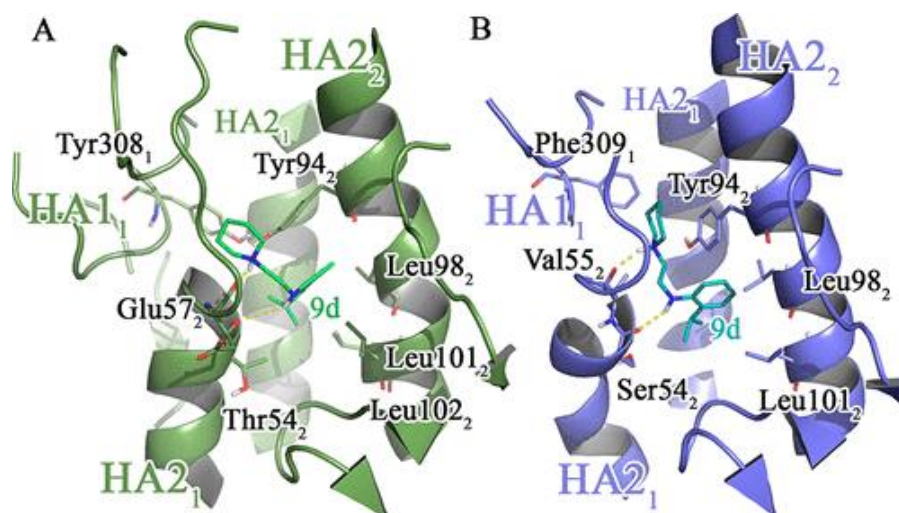
Figure 54. Protein-inhibitor complexes for compound **9d** within the HA2 binding pocket of (A) A/PR/8/34 and (B) A/Virginia/ATCC3/2009.

7.2 Project

During my PhD I spent six months abroad at the Department of Pharmacy of the University of Barcelona (UB) under the supervision of Prof. Santiago Vázquez. In the course of this period, I worked on the synthesis of two different series of anilino and sulfonamide derivatives, in order to complete the previous series of anilino analogues and to explore the effect of the bioisosteric substitution of the amide moiety of the prototype **CL-385319** with a sulfonamide group, in terms of antiviral potency.

The first small subset has been designed exploring the variation of electron-withdrawal group on the aniline ring while keeping the ethyl piperidine moiety linked to the NH group of the aromatic amine. I also synthesized some different analogues presenting a propyl linker instead of the ethylic chain and/or substituting the piperidine, with a pyrrolidine or azepane ring. Within this series, also the isosteric

substitution of the NH group with an oxygen or a sulphur atom has been considered (compounds **11** and **14**; Figure 55).
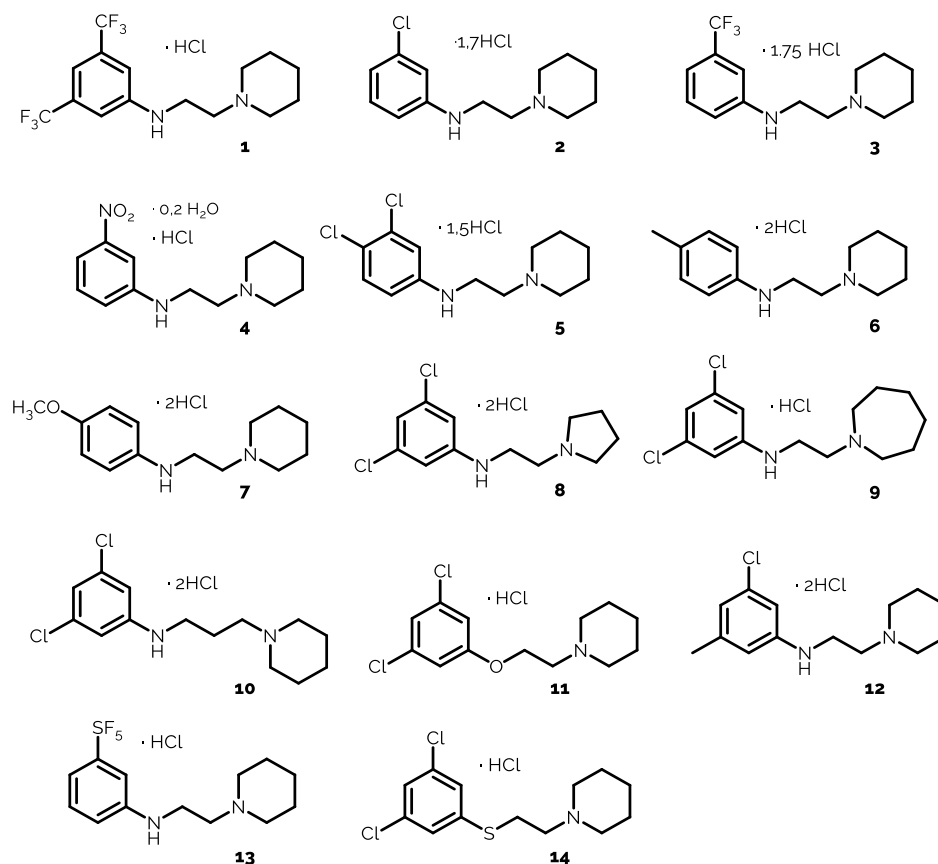
Figure 55. Structure of the anilino and of the ether and thioether derivatives **1-14**.

Taking into account the promising results in terms of anti-influenza A activity of the first set of anilino-derivatives and of the prototype **CL-385319**, the second sub-set has been designed considering the acquired knowledge of the SAR of these compounds. Thus, trying to obtain new more potent IAV fusion inhibitors I synthesized this novel series in order to investigate the effect on the antiviral activity of the replacement of the amide function of the prototype **CL-385319** with its sulfonamide bioisoster and exploring in parallel different derivatisations of the aromatic ring, while keeping unchanged the ethyl piperidine part of the molecule among the series (Figure 56,).
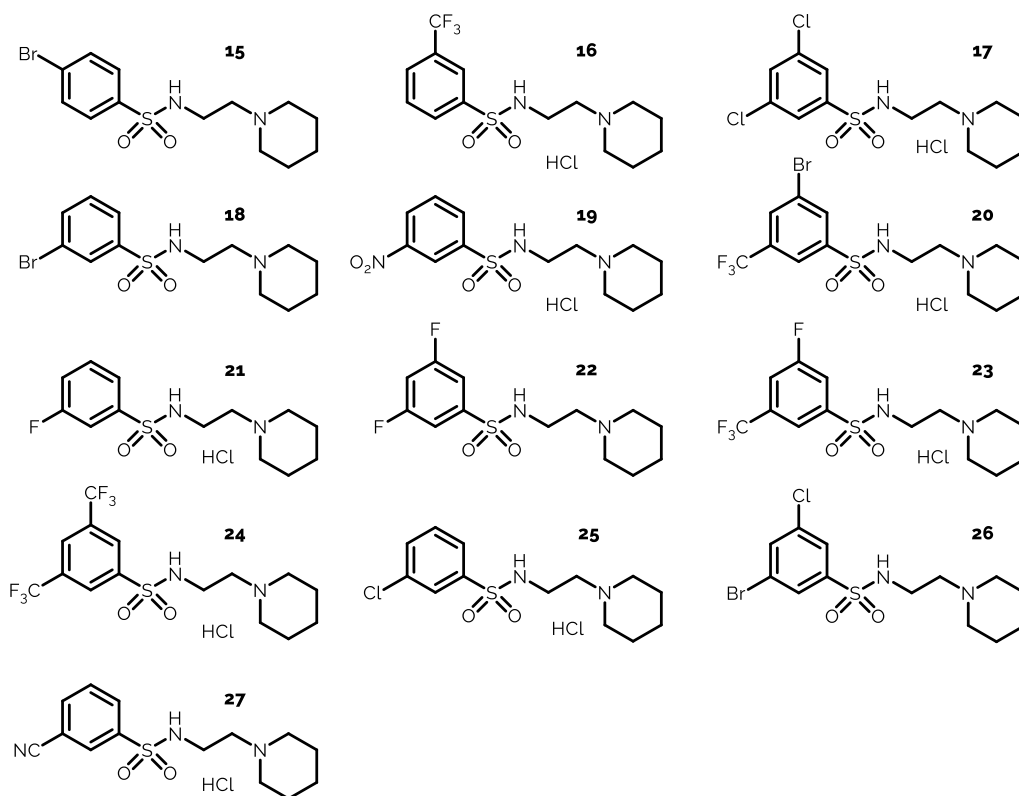
Figure 56. Structures of the second sub-set of sulfonamide derivatives **15**-**27**.

7.2.1 Chemistry

The anilino derivatives **1-10** and **12-13** were prepared by reaction of the proper anilines (2eq.) with the N-(2-chloroethyl)piperidine (for the synthesis of compounds **1-7** and **12-13**), N-(2-chloroetyl)pyrrolidine (for compound **8**), N-(2-chloroetyl)azepane (for compound **9**), and N-(3-chloropropyl)piperidine (for compound **10**) (1eq.), in the presence of potassium carbonate (2 eq.) and potassium iodide (0.5 eq.) under reflux for 23h (Scheme 12).
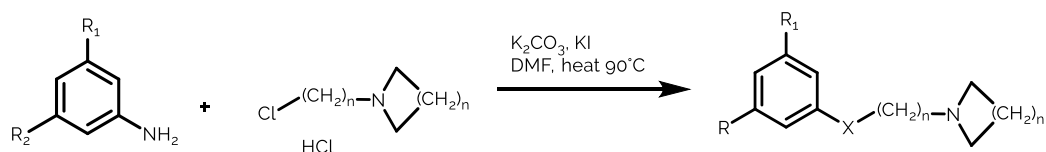
Scheme 12. General synthesis of the anilino derivatives **1-10** and **12-13**.

The ether (**11**) and thioether (**14**) derivatives have been also obtained by reaction of the 3,5-dichlorophenol and 3,5-dichlorothiophenol, respectively (1eq.) with the 1-(2-

chloroethyl)piperidine hydrochloride (1eq.) in presence of an excess of sodium hydroxide in ethanol (Scheme 13).
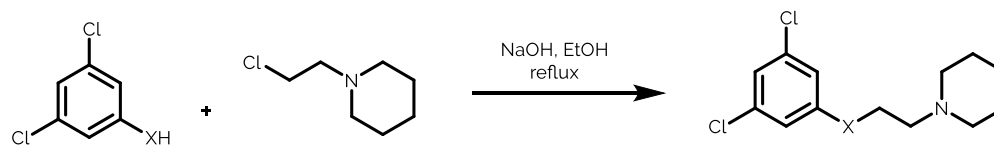
Scheme 13. Synthesis of the ether (**11**) and thioether (**14**) derivatives.

7.2.2 *In vitro* studies: antiviral activity and cytotoxicity assays

The entire compound series was tested in *in vitro* antiviral activity assays against a panel of viruses by the research group of Prof. L. Naesens at the University of Leuven (Belgium). The two sub-sets were screened against influenza viruses, A subtype H1N1 (A/Ned/378/05), A subtype H3N2 (A/HK/7/87) and B (B/Ned/537/05), and also versus a panel of several DNA and RNA viruses, such as (+)ssRNA viruses (CVB-4, human coronavirus 229E), (-)ssRNA viruses (RSV, VSV), DNA viruses (HSV-1 (G) and HSV-1 (KOS), HSV-2, VV, Adenovirus type 2). and retroviruses (HIV-1 strain IIIB and HIV-2 strain ROD).

Despite the structural similarity with the chosen active prototypes, all the tested compounds proved no antiviral activity against the three strains of influenza viruses employed in the assay, demonstrating their inability in inhibiting the influenza A fusion protein, contrarily to the previous series. The sub-set of sulfonamide derivatives **15**-**27** proved to be inactive against all the tested virus types (EC_{50} > 100µM; data not shown). Interestingly, nine anilino analogues of the first subset of compounds (**1**-**14**) demonstrated to be active against the human coronavirus 229E (HCoV 229E) with EC50 values in the range 7.8-72 µM (Table 9).

All the tested compounds were also associated with general low cytotoxicity values, suggestive of a high safety profile of these derivatives (Table 9).

Table 9. Antiviral activity against HCoV (229E) and cytotoxicity results for the anilino-derivatives **1-14**.

CPD	ANTIVIRAL ACTIVITY; EC_{50}^{a} (µM) HUMAN CORONAVIRUS (229E)		CYTOTOXICITY	
	MTS	Visual CPE score	CC_{50}^{b} (µM)	MCC^{c}
1	>100	-	>100	-
2	**43**	-	>100	-
3	**70**	-	>100	-
4	**72**	-	>100	-
5	**19**	-	41	-
6	>100	-	>100	-
7	>100	-	>100	-
8	>100	-	>100	-
9	**7.8**	**8.9**	37	100
10	**9.5**	-	34	
11	**43**	-	>100	
12	**13**	-	46	
13	**9.6**	**8.9**	>100	>100
14	>100	-	>100	
UDA^{d} (µg/mL)	1.8	2		

The antiviral and cytotoxicity assays have been performed in HEL cell cultures. [a]EC_{50} = concentration producing 50% inhibition of virus-induced cytopathic effect, as determined by visual scoring of the CPE, or by measuring the cell viability with the colorimetric formazan-based MTS assay. [b]CC50 = 50% cytotoxic concentration, as determined by measuring the cell viability with the MTS assay. [c]MCC = minimum compound concentration that causes a microscopically detectable alteration of normal cell morphology. [d]UDA = *Urtica dioica* agglutinin.

7.2.3 Conclusions

The promising antiviral activity of a series of aniline derivatives was previously discovered by Leiva, R. et al.[183]. These compounds were structurally related to **CL-385319,** a N-substituted piperidine compound that has been discovered as an inhibitor of influenza A HA-mediated fusion, capable of acting on viruses presenting diverse HA subtypes, such as H1, H2, and H5 at a low micromolar level. The anilino derivatives analogues were demonstrated to act with a similar mechanism directed toward influenza virus A/H1N1 hemagglutinin (HA), by interacting with the protein in a specific binding site, thus blocking the viral fusion process.

Taking into account the structure-activity relationships within this compound series. derived from the combination of antiviral activity assays, NMR experiments and molecular dynamics calculations on the X-ray crystallographic data of the viral H1, I designed and synthesized a series of novel structurally related analogues in order to further explore the effect of small structural variations on the same scaffold, in terms of antiviral potency. Thus, I spent six months in Prof. S. Vazquez laboratory, where I completed the synthesis of two small sets of anilino-derivatives (**1**-**14**) and of benzene sulfonamides (**15**-**27**).

The compounds have been tested by Prof. L. Naesens at the University of Leuven, to assess their cytotoxicity and antiviral activity values against a panel of several RNA and DNA viruses, including two influenza A subtypes, H1N1 and H3N2, and an influenza B virus. Despite the structural similarity with the previous studied compounds, none of the novel derivatives demonstrated to inhibit influenza A and B replication in *in vitro* tests.

However, nine of the new anilino-based compounds proved to be capable of inhibiting the human coronavirus HCoV 229E, included in the panel of the tested viruses. Along with this unexpected discovery of the anti-coronavirus activity of these derivatives, all the compounds also showed general low cytotoxicity in the cell line employed in the assays (HEL cell cultures).

Thus, these results could inspire a new line of research since some of these derivatives could be object of further studies on the base of their activity against HCoV, in order to define their molecular target and suggest a possible mechanism of action.

CHAPTER 8. Discussion. Design, synthesis and biological evaluation of novel anti-influenza compounds acting on viral hemagglutinin (HA).

8.1 Background

During the last years, the research group of Prof. M. Tonelli have developed a large variety of benzimidazole-based derivatives endowed with biological activities directed toward different targets[13,184]. In particular two series of 2-[(benzotriazol-1/2-yl)methyl)benzimidazoles (series 1)[185] and 2-benzylbenzimidazoles (series 2)[175], 1-substituted with a basic chain, have been discovered as antiviral agents, acting against different single-stranded RNA (ssRNA) viruses (Figure 57).

R= dialkylaminoalkyl, quinolizidinylalkyl
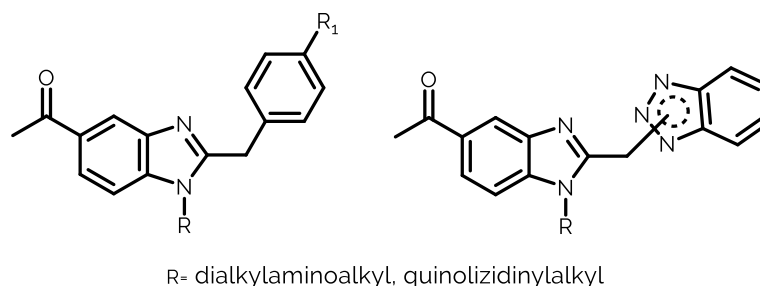
Figure 57. Chemical structures of 5-acetyl substituted 2-benzylbenzimidazoles of series 1 and 2-[(benzotriazol-1/2-yl)methyl]benzimidazoles of series 2 previously investigated as antiviral agents.

Among the tested viruses, also RSV revealed to be susceptible to these benzimidazole derivatives, with EC_{50} values derived from *in vitro* antiviral assays in the low micromolar range. The activity of series 2 was prevalent against RSV, reaching nanomolar potency for the best performing derivatives. The suggested mechanism of action of these compounds against RSV virus have been may be achieved by the inhibition of the fusion envelop glycoprotein F, thus blocking the viral fusion and entry processes, as it has been demonstrated for a set of structurally similar 1-substituted-2-[(benzotriazol-1/2-yl)methyl]benzimidazoles and other analogues[186].

Among the explored substituents at position 5 of the benzimidazole scaffold, the 5-acetyl derivatisation was also considered. The corresponding 5-acetyl benzimidazoles exhibited EC_{50} values between 1.2 and 20 µM against RSV in *in vitro* antiviral assays. Concerning the 2-benzylbenzimidazoles of series 2, the 5-acetyl substituted derivatives were completely inactive against all the virus strains studied, RSV included.

8.2 Project

Within the previously described series, the 5-acetyl substituted benzimidazoles resulted to be less effective antiviral agents; thus, starting in my second year and during my third year of PhD I worked on the synthesis of new benzimidazole analogues by probing the derivatization of the acetyl group on the position 5 of benzimidazole ring, synthesizing new (thio)semicarbazone and hydrazone derivatives, in order to evaluate the influence of this type of functionalisation in terms of antiviral activity (Figure 58-60).

1-25
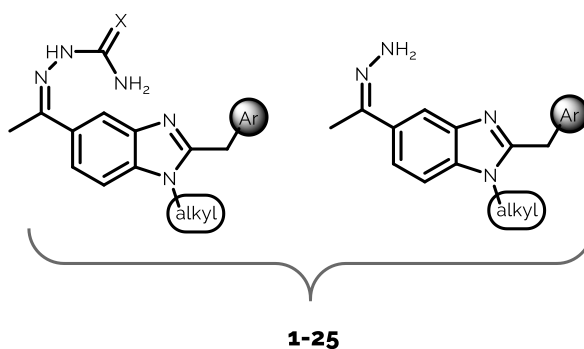
Figure 58. General structure of the novel designed hydrazone- and (thio)semicarbazone-benzimidazoles derivatives **1-25**.

1. R=(CH₂)₂N(CH₃)₂
R₁=OCH₃

2. R=(CH₂)₂N(CH₃)₂
R₁=Cl

3. R=(CH₂)₂N(CH₃)₂
R₁=OCH₂CH₃

4. R=(CH₂)₃N(CH₃)₂
R₁=Cl

5. R=(CH₂)₂N(CH₂CH₃)₂
R₁=OCH₃

6. R=(CH₂)₂N(CH₂CH₃)₂
R₁=Cl

7. R=(CH₂)₂N(CH₂CH₃)₂
R₁=OCH₂CH₃

8. R=(CH₂)₃N(CH₂CH₃)₂
R₁=H

9. R=(CH₂)₃N(CH₂CH₃)₂
R₁=OCH₃

10. R=(CH₂)₂N(CH₃)₂
R₁=OCH₃

11. R=(CH₂)₂N(CH₃)₂
R₁=Cl

12. R=(CH₂)₂N(CH₃)₂
R₁=OCH₂CH₃

13. R=(CH₂)₃N(CH₃)₂
R₁=Cl

14. R=(CH₂)₂N(CH₂CH₃)₂
R₁=OCH₃

15. R=(CH₂)₂N(CH₂CH₃)₂
R₁=Cl

16. R=(CH₂)₃N(CH₂CH₃)₂
R₁=H

17. R=(CH₂)₃N(CH₂CH₃)₂
R₁=OCH₃

18. X=S
R=(CH₂)₂N(CH₃)₂

19. X=S
R=(CH₂)₃N(CH₃)₂

20. X=O
R=(CH₂)₂N(CH₃)₂

21. X=S
R=(CH₂)₂N(CH₂CH₃)₂

22

Figure 59. Chemical structures of the (thio)semicarbazone-benzimidazoles derivatives **1-22**.

23. R=(CH₂)₂N(CH₃)₂
R₁=OCH₃

24. R=(CH₂)₂N(CH₂CH₃)₂
R₁=OCH₂CH₃

25
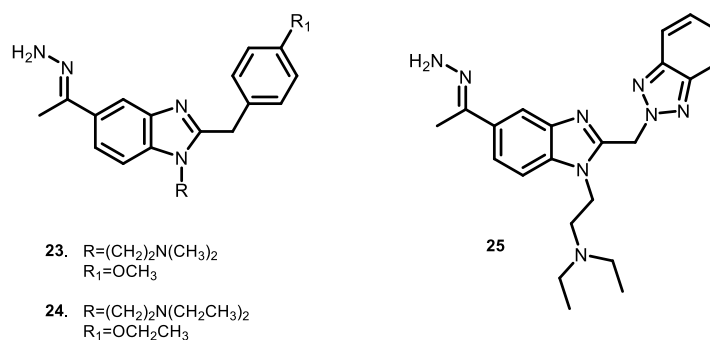
Figure 60. Chemical structures of the hydrazone-benzimidazoles derivatives **23-25**.

8.2.1 Chemistry

The new compounds have been obtained from their corresponding 5-acetyl derivatives by following the conditions showed in Schemes 14-15.
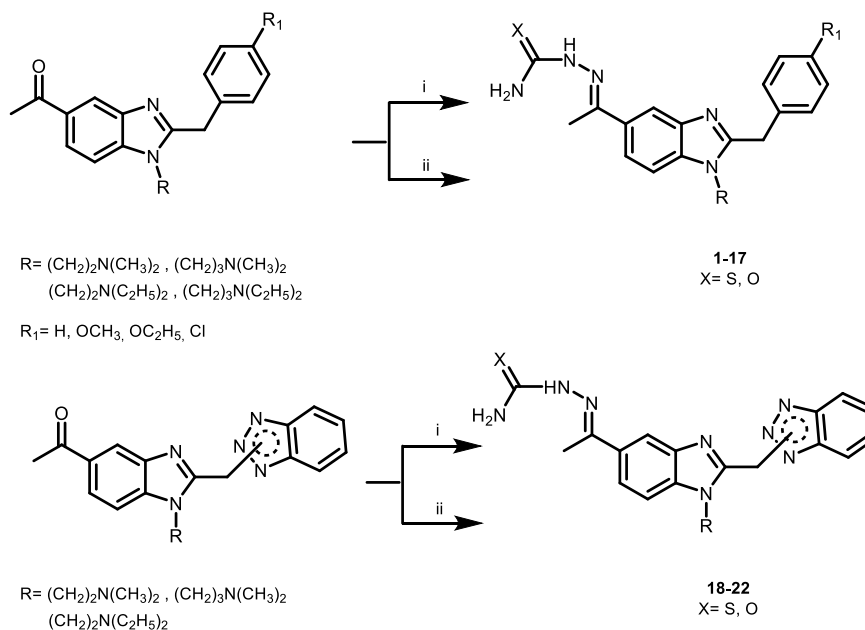
Scheme 14. Reagents and conditions: i) thiosemicarbazide in EtOH, H_2O and glacial CH_3COOH, 3h at reflux; ii) semicarbazide·HCl in EtOH and CH_3COONa 1N, 4h at reflux.

Thiosemicarbazones (**1**-**9**, **18**-**19**, **21**-**22**) have been prepared by refluxing an ethanolic aqueous solution of thiosemicarbazide and starting benzimidazole in presence of glacial acetic acid. The semicarbazone derivatives (**10**-**17**, **20**) have been obtained by reacting under reflux the starting 5-acetylderivative with the semicarbazide hydrochloride, in presence of sodium acetate, in ethanolic aqueous solution.
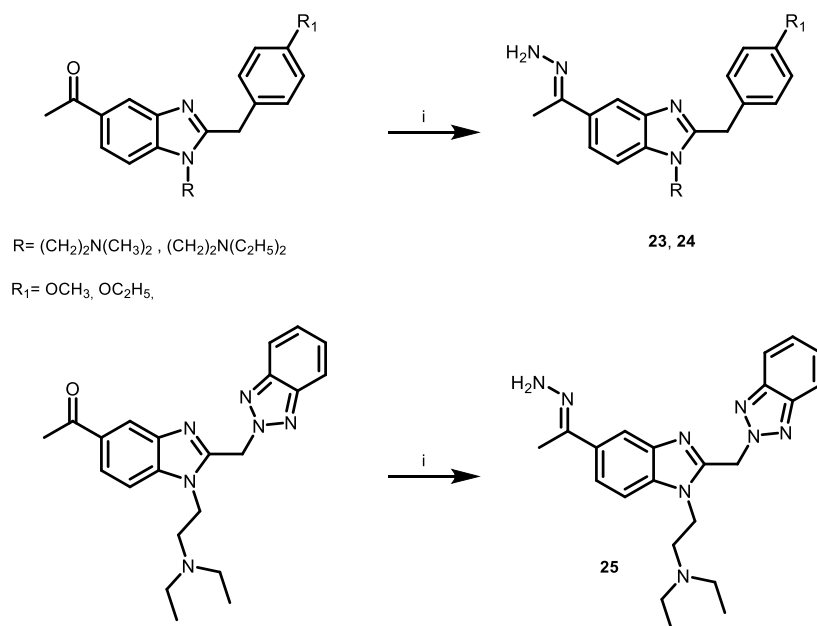
Scheme 15. Reagents and conditions: i) EtOH/H₂O, NH₂NH₂ · H₂O (1.15 equiv.), 120°C, 5h.

Hydrazone derivatives **23**-**25** have been synthesized at reflux by reacting the proper 5-acetyl benzimidazole with a slight excess of hydrazine hydrate for 5h under reflux (Scheme 15).

The starting 5-acetyl-2-benzylbenzimidazoles have been synthesized according to the literature[187] by the reaction of the proper 4-acetyl-1,2-phenylenediamine with the hydrochloride of the imminoester, previously obtained from the corresponding nitrile under Pinner conditions (Scheme 16). Also the starting 5-acetyl-2-[(benzotriazole-1/2-yl)methyl]benzimidazoles have been obtained by the condensation at 180°C of a mixture of the proper 1,2-phenylenediamine with the (benzotriazol-1/2-yl)acetic acid[188] (Scheme 17).
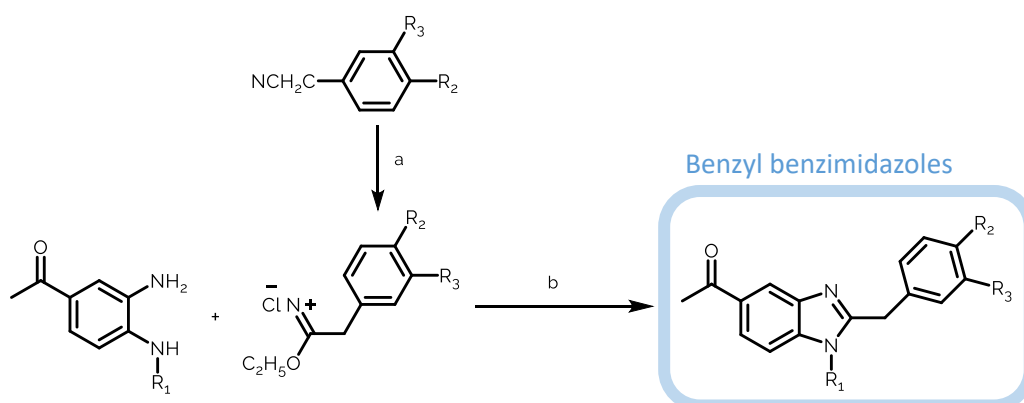
Scheme 16. Synthesis of the benzyl benzimidazole intermediates *via* imminoester (Pinner conditions). Reagents and conditions: a) EtOH abs., CHCl₃ an., HCl(g), 0°C; b) CH₃COOH glacial, 45°C, 12h.
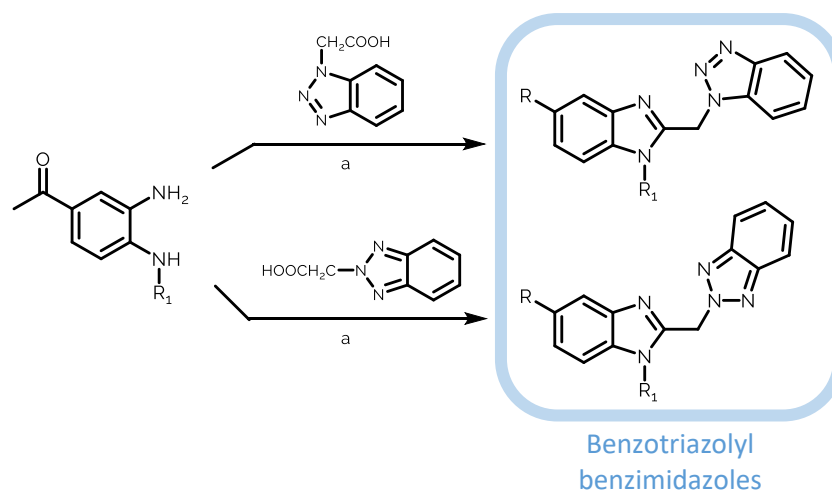
Scheme 17. Synthesis of the intermediates benzotriazol-1/2-yl benzimidazoles. Reagents and conditions: a) N_2 (g), 180°C, 2h.

The opportunely substituted 4-acetylphenylenediamines have been prepared according to literature[189], starting from the 5-acetyl-2-chloronitrobenene which was reacted with the selected primary amine by direct fusion. The derived nitroaniline derivative was then reduced to the corresponding phenylenediamine in presence of stannous chloride and hydrochloric acid (Scheme 18).
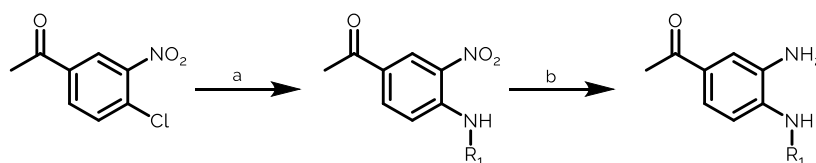
Scheme 18. Synthesis of the starting 4-acetylphenylenediamines. Reagents and conditions: a) R1-NH_2 direct fusion, 140°C, 1h; b) $SnCl_2 \cdot 2H_2O$, HCl conc., EtOH, 120°C, 6h.

Thiosemicarbazones are known to display thione-thiol tautomerism, since their hydrazidic proton (-C(=S)N*H*-N=) can shift on sulfur atom leading to its corresponding thiol form. Indeed, on the ^{1}H NMR spectra these compounds didn't exhibit the signal at 4.00 ppm, attributable to –SH proton, suggesting the thione form as the only tautomer. Within this series, the Schiff base of the thiosemicarbazone moiety demonstrated to acquire E isomerism since the hydrazinic proton (-C(=S)N*H*-N=) of these compounds always presented a chemical shift in the 9-12 ppm range[189]. In fact this signal appears around 10.18 ppm, whilst the (-C(=S)N*H*2) exhibit two different chemical shifts at ca 8.25 ppm and 7.94 ppm. This peculiar behavior of the thioamide protons ^{1}H NMR signals could be explained by the restricted free rotation brought

about by the formation of carbon-nitrogen double bond character relative to thione-thiol tautomerism[190]. In addition, it is noteworthy that the sulfur atom of thione tautomer has a greater atomic radius than oxygen atom of the corresponding semicarbazone, thus making the thioamide protons magnetically different for steric hindrance.

8.2.2 *In vitro* studies: antiviral activity and cytotoxicity assays

The novel compounds (**1**-**25**) have been evaluated in cell-based assays for antiviral activity against a broad panel of RNA and DNA viruses by Prof. Lieve Neasens, University of Leuven, Belgium.

Only few compounds showed a modest activity against IV A/H1N1, HCoV and RSV (Table 10). Interestingly, the antiviral activity is combined with a high safety profile as they exhibited no toxicity against four host cell lines used to grow the relevant virus strains here investigated (Table 11).

Table 10. Antiviral activity of compounds **6**, **8**, **16**, **17**, **22**, **24** and **25** and related reference compounds

	ANTIVIRAL ACTIVITY: EC_{50} (µM)[a]			
CPD	A/NED/378/05 (H1N1)	A/HK/7/87 (H3N2)	HCoV (229E)	RSV
6	25.3	81.3	37.8	-
8	37.6	-	55.8	-
16	46.8	-	39.1	-
17	47.1	-	41.0	-
22[b]	41.1	-	-	7.0
24	-	-	42.6	-
25	-	-	-	2.4
Zanamivir	0.6	30.7	-	-
Ribavirin	7.4	7.5	-	6.7
DS-10000 (µg/mL)	-	-	-	0.01
UDA (µg/mL)	-	-	2.2	-

[a]EC50: 50% effective concentration giving 50% protection against virus-induced reduction in cell viability, as determined by colorimetric formazan-based MTS assay. [b]The compound is also active against **CVB-4** with an EC50= 20 µM (ribavirin, EC50= 117µM; DS-10000, EC50= 8.1 µM). Values shown are the mean ± SEM of three independent experiments.

Table 11. Cytotoxicity of compounds **6**, **8**, **16**, **17**, **22**, **24** and **25** and related reference compounds.

	CYTOTOXICITY: CC_{50} (µM)[a]				MEAN CC_{50} FOR HOST CELLS
CPD	HEL	HEP-2	VERO	MDCK	
6	>100	>100	>100	>100	>100
8	>100	>100	44.4	>100	>86.1
16	>100	>100	>100	>100	>100
17	>100	47.5	42.6	>100	>72.5
22[b]	>100	100	>100	>100	>100
24	>100	>100	50.7	35.2	>71.5
25	>100	>100	>100	33.2	>83.3
Zanamivir	-	-	-	>100	-
Ribavirin	-	>250	>250	>100	-
DS-10000 (µg/mL)	-	>100	>100	-	-
UDA (µg/mL)	>100	-	-	-	-

[a]CC_{50}: 50% cytotoxic concentration, as determined by measuring the cell viability with the MTS assay. HEL= human erythroleukemia cells; Hep-2= Human epithelial type 2 cells; Vero= primate kidney epithelial cells; MDCK= Madin-Darby canine kidney cells. Values shown are the mean ± SEM of three independent experiments.

As shown in the tables above six compounds (**6**, **8**, **16**, **17**, **22** and **24**) exhibit an interesting activity against influenza viruses A/H1N1, HCoV and RSV. Length of the basic chain does not influence the antiviral activity, since both the propyl and ethyl spacers are well tolerated, on the other hand, regarding the substituent in position 2, the benzyl ring is more effective (**6**, **8**, **16**, **17** and **24**) than the bulkier (benzotriazol-1/2-yl)methyl skeleton (**22** and **25**). The nature of the substituent in para position of the benzyl ring (H, Cl, OCH_3) does not seem to play a significant role on the antiviral activity.

The most active compounds are **25** and **22** which exhibit EC_{50} values of 2.4 and 7.0 µM against RSV, respectively, and are equipotent to the reference drug ribavirin (EC_{50}= 6.7 µM). The active compounds against influenza A (H1N1) virus (**6**, **8**, **16**, **17**, **22**) have a mean EC_{50} of 39.6 µM which is 66-fold lower than that of zanamivir (EC_{50} = 0.6 µM) and 5-fold of ribavirin (EC_{50} = 7.4 µM). In addition, compounds **6**, **8**, **16**, **17** and **24** exhibited a modest activity against human coronavirus (229E).

8.2.3 Conclusions

In the past years, the research group of Prof. M. Tonelli has synthesized two different series of benzimidazole-based compounds, which have been screened for their antiviral activity against a panel of RNA and DNA viruses. Within these series several compounds have been identified as new potent antiviral agents, pointing out how this scaffold could be worthy of further investigations, while all of the 5-acetyl-substituted benzimidazoles proved to be ineffective in reducing the *in vitro* replication of all the tested virus types. Among these derivatives only some 5-acetyl-2-[(benzotriazol-1/2-yl)methyl]benzimidazoles exhibited a marginal activity against RSV, which may be related to the inhibition of the F viral glycoprotein and to the subsequent fusion process with the host cell membrane.

Thus, with the aim of finding new molecules endowed with a potent antiviral activity, in the course of my PhD, I synthesized a new series of benzimidazole analogues exploring the derivatization of the former acetyl group on the position 5 of benzimidazole ring, synthesizing new (thio)semicarbazone and hydrazone derivatives. The novel compounds have been screened against a panel of DNA and RNA viruses in order to assess their antiviral potency and cytotoxicity.

Five compounds showed a modest activity against influenza A virus H1N1, with EC_{50} values in the range of 25.3-47.1 µM. Two compounds (**22** and **25**) revealed an interesting activity against RSV with EC_{50} values of 7.0 and 2.4 µM, respectively, which are comparable to the reference drug ribavirin (EC_{50} = 6.7 µM). the interest around these compounds further raises, since they are also endowed with a high safety profile since they exhibited no toxicity against four different cell lines.

Five compounds also revealed to inhibit the human coronavirus 229E. Although the efficacy against HCoV (229E) is rather modest (mean EC_{50} = 43.3 µM) compounds **6**, **8**, **16**, **17** and **24** are, the first benzimidazole-based derivatives to be found active against this virus and that could represent a starting point to design new, more potent anti-HCoV agents.

CHAPTER 9. Conclusions

9.1 Final remarks

The aim of this thesis was to identify novel potentially active antiviral compounds designed on the basis of previously studied promising derivatives. The investigated chemical scaffolds differs in terms of structure end molecular target comprising the potent anti-BVDV acridine derivatives, the dihydrotriazine and triazino[1,2-a]benzimidazoles, the benzimidazole derivatives and the anilino and benzenesulfonamides, all designed as novel anti-influenza agents.

In many cases the activity data of the novel series of derivatives demonstrated to be comparable or, sometimes to surpass the antiviral potency of their structural prototypes or reference drugs; i.e. the acridine derivatives **2**, **6** and **14** ($EC_{50\ (BVDV)}$ = 0.8 μM, 2.9 μM and 1.2 μM respectively) surpassed the anti-BVDV potency of the prototypes **AVR15**, **AVR17**, **AVR26**, ($EC_{50\ (BVDV)}$ = 3 μM, 6 μM and 31 μM respectively)[5] and of the broad spectrum antiviral drug ribavirin ($EC_{50\ (BVDV)}$ = 8.0 μM). These promising results have been also followed by in-depth studies in order to confirm the previously proposed molecular target of this series, the viral RNA dependent RNA polymerase. Even in this case the data derived from ITC measurements, enzymatic binding assays and molecular modeling were in agreement with the formulated hypothesis, clearly proving the RdRp as the molecular target of the series and prompting to further explore the structure-activity relationships of this class of compounds designing new optimized anti-BVDV agents.

The azaspiro dihydrotriazine derivatives and the triazino[1,2-a]benzimidazoles have been designed on the basis of the previous series of structural analogues which included some potent anti-influenza B derivatives endowed with a nanomolar activity *in vitro*, combined with a good safety profile[10]. In this case the increased structural complexity and steric hindrance produced an overall loss in terms of antiviral activity, providing some pointers that could guide the design of a new series of adequately optimized derivatives.

Likewise, the two series of anilino-derivatives and benzenesulfonamides I synthesized and characterised during my stay as a PhD visiting student at the University of Barcelona, have been designed on the basis of a prototype, compound **9d**, previously published paper by Leiva, R. *et al*[183] and of the small-molecule inhibitors **CL-385319**, both described in literature as potent inhibitors of influenza A

119

HA-mediated fusion. Unfortunately, all the compounds didn't show any anti-influenza activity in *in vitro* antiviral tests, on the other hand, some benzenesulfonamide derivatives demonstrated an interesting inhibitory effect on the HCoV 229E replication, which could represent a starting point for further studies in order to optimize this activity and potentially design novel anti-CoV derivatives.

Finally, the benzimidazole derivatives were designed on the basis of previously investigated analogues which demonstrated a potent anti-RSV activity[175,186]. Thus, the novel derivatives have been synthesized and tested against a panel of several RNA and DNA viruses; among them some compounds surprisingly revealed to be dual virus inhibitors of influenza and coronavirus strains (Influenza A/Ned/378/05 (H1N1) and HCoV 229E), even if with only modest potency, while only two compounds **25** and **22** demonstrated to successfully inhibit RSV replication with the same degree of potency of ribavirin. Therefore, these novel (thio)semicarbazone- and hydrazone-based benzimidazoles may be considered worthy of further structural optimization for an improved antiviral profile against the aforementioned viral strains, secondly, as some compounds are able to target both IV and HCoV, the existence of a possible common mechanism of action is worth of future investigation.

CHAPTER 10. Experimental section.

10.1 Chemistry

Starting materials were purchased from Aldrich-Italia (Milan, Italy) and Alfa Aesar (Lancashire, UK). Melting points were determined with a Büchi 530 apparatus or with an MFB 595010M Gallenkamp and are uncorrected. Column chromatography was performed either on silica gel 60 Å (35-70 mesh), or by automatic CC (BiotageTeledyne Isco®). IR spectra were run on Perkin-Elmer Spectrum RX I spectrophotometer. Absorption values are expressed as wave-numbers (cm^{-1}); only significant absorption bands are given. ^{1}H NMR and ^{13}C NMR spectra were recorded on Varian Gemini-200 or on Varian Mercury-400, spectrometers, using DMSO-*d6*, CDCl$_3$ or CD$_3$OD as solvents. The chemical shifts (δ) in ppm were measured relative to tetramethylsilane (TMS), and coupling constants are reported in Hertz (Hz). Elemental analyses were performed on Flash 2000 CHNS (Thermo Scientific) instrument in the Microanalysis Laboratory of the Department of Pharmacy of Genoa University or in a Flash 1112 series Thermofinnigan elemental microanalyzer (A5). Analytical, preparative HPLC and Electron Spray Ionization condition (ESI) mass spectra were performed on an Agilent uHPLC (1290 Infinity) and an Agilent Prep-HPLC (1260 Infinity) both equipped with a Diode Array Detector and a Quadrupole MSD using mixture gradients of formic acid/water/acetonitrile as system solvent. Arom. = aromatic ring; Benz= benzimidazole ring; Bzt= benzotriazole ring.

10.1.1 Experimental section: synthesis of the acridine derivatives.

The intermediates **c**-**e** and **h**, **i**, **k**, required for the synthesis of the related 9-aminoacridine derivatives, were already described in literature, thus their characterization data will not be reported in this thesis.

When required, the final compounds were converted into the corresponding hydrochloride salts with 1N HCl ethanolic solution to perform elemental analysis. Results of elemental analyses indicated that the purity of all compounds was ≥95%.

10.1.1.1 General procedure for the synthesis of compounds 1-14.

A mixture of 6,9-dichloro-2-methoxyacridine (1.8 mmol), the appropriate amine (1.8 mmol) in presence of phenol (1.13 g) was heated at 90 °C for 5 h. After cooling, the

mixture was treated with 6 M NaOH till strong alkalinity and extracted with Et_2O. After removing the solvent, the residue was purified by CC (SiO_2/CH_2Cl_2 + 10%MeOH).

Compounds **2**-**8** were obtained by directly washing the reaction mixture in the order, with a boiling solution of 2N NaOH and then with water in order to remove the excess of phenol, affording a solid residue that was chromatographed on silica gel, eluting with CH_2Cl_2 + 10%MeOH.

6-Chloro-9-[2-(4'-hydroxypiperidin-1-yl)ethyl]amino-2-methoxyacridine (**1**)

Yield 42%. M.p. 208-210°C (CH_2Cl_2). ^{1}H-NMR (200 MHz, DMSO-*d6*): 8.20-7.96 (m, 2 arom. H), 7.44 (dd, *J*= 9.8 Hz, 2.2 Hz, 1 arom. H), 7.38-7.23 (m, 3 arom. H), 6.24 (br. s, NH, exchanges with D_2O), 3.99 (s, 3H, OCH_3), 3.92-3.74 (m, 1H, HO-C*H* piperidine and 2H HN*CH_2*CH_2-piperidine), 3.00-2.81 (m, 2H, piperidine), 2.68 (t, *J*= 7.0 Hz, 2H, HNCH_2*CH_2*-piperidine), 2.44-2.22 (m, 2H, piperidine), 2.13-1.85 (m, 2H, piperidine and 1H, OH, exchanges with D_2O, superimposed), 1.83-1.63 (m, 2H, piperidine). ^{13}C-NMR (50 MHz, DMSO-*d6*): 154.72, 150.15, 147.62, 133.03, 130.24, 126.56, 126.05, 123.81, 122.27, 116.83, 114.44, 99.85, 65.80, 57.14, 55.11, 50.36, 46.24, 34.04. Anal. calcd for $C_{21}H_{24}ClN_3O_2$: C 65.36, H 6.27, N 10.89; found: C 65.60, H 6.18, N 10.78.

6-Chloro-9-[[4-(2'-hydroxyethyl)piperazin-1-yl]amino]-2-methoxyacridine (**2**)

Yield 23.5%. ^{1}H-NMR (200 MHz, DMSO-*d6*): 8.31-7.24 (m, 6 arom. H), 4.44 (br s, NH, exchanges with D_2O), 3.79 (s, OCH_3), 3.51 (t, *J* = 6.0, 2H, C(2)), 3.38 (pseudo s, 4H, piperazine), 3.11-2.20 (m, 2H, C(1), 4H, piperazine and OH, exchanges with D_2O, superimposed). ^{13}C-NMR (50 MHz, DMSO-*d6*): 153.71, 151.71, 141.11, 134.30, 131.72, 120.32, 116.55, 113.11, 106.51, 59.79, 58.27, 55.08, 54.89, 53.63, 52.04. Dihydrochloride salt: m.p. 258-260°C (dec.). Anal. calcd for $C_{20}H_{23}ClN_4O_2 \cdot 2HCl \cdot 2H_2O$: C 48.45, H 5.90, N 11.30; found: C 48.14, H 5.88, N 11.67.

6-Chloro-9-[[4-(2'-chlorophenyl)piperazin-1-yl]amino]-2-methoxyacridine (**3**)

Yield 57%. M.p. 173-175°C (Et_2O/*n*-hexane). CC(SiO_2/CH_2Cl_2+10%MeOH). ^{1}H-NMR (200 MHz, DMSO-*d6*): 8.18 (d. *J* = 9.0 Hz, 1 arom. H); 7.80-7.64 (m, 2 arom. H); 7.42-6.82 (m, 7 arom. H); 3.78 (s, 3H, OCH_3); 3.37 (pseudo s, 4H, piperazine); 3.05 (pseudo s, 4H, piperazine); 2.80 (br s, NH, exchanges with D_2O). ^{13}C-NMR (50 MHz, DMSO-*d6*): 151.90, 148.32, 134.20, 129.96, 127.66, 127.26, 123.58, 120.46, 115.13, 64.52, 55.05, 54.11, 49.76.

Dihydrochloride salt: m.p. 271-272˚C. Anal. calcd for $C_{24}H_{22}Cl_2N_4O \cdot 2HCl$: C 54.77, H 4.60, N 10.65; found: C 54.83, H 4.61, N 10.60.

6-Chloro-9-{[4-(3'-chlorophenyl)piperazin-1-yl]amino}-2-methoxyacridine (4)

Yield 52.3%. CC(SiO$_2$/CH$_2$Cl$_2$+10%MeOH). ^{1}H-NMR (200 MHz, DMSO-*d6*): 8.16 (d, *J* = 8.8 Hz, 1 arom. H); 7.65 (s, 1 arom. H); 7.30-6.72 (m, 8 arom. H); 3.74 (s, 3H, OCH$_3$); 3.40 (pseudo s, 4H, piperazine); 3.07 (pseudo s, 4H, piperazine); 2.76 (br s, NH, exchanges with D$_2$O). ^{13}C-NMR (50 MHz, DMSO-*d6*): 151.58, 147.86, 134.28, 133.45, 130.04, 122.60, 117.75, 114.15, 113.21, 64.38, 54.98, 53.66, 46.56. Dihydrochloride salt: m.p. 269-270˚C. Anal. calcd for $C_{24}H_{22}Cl_2N_4O \cdot 2HCl$: C 54.77, H 4.60, N 10.65; found: C 54.66, H 4.61, N 10.75.

6-Chloro-9-{[4-(4'-chlorophenyl)piperazin-1-yl]amino}-2-methoxyacridine (5)

Yield 45%. M.p. 185.5-186.3˚C (Et$_2$O/hexane). CC(SiO$_2$/CH$_2$Cl$_2$+10%MeOH). ^{1}H-NMR (200 MHz, DMSO-*d6*): 8.14 (d. *J* = 9.6 Hz, 1 arom. H); 7.64 (s, 1 arom. H); 7.30-6.72 (m, 8 arom. H); 3.74 (s, 3H, OCH$_3$); 3.33 (pseudo s, 4H, piperazine); 3.11 (pseudo s, 4H, piperazine); 2.68 (br s, NH, exchanges with D$_2$O). ^{13}C-NMR (50 MHz, DMSO-*d6*): 149.12, 147.74, 135.31, 133.24, 128.21, 122.02, 116.38, 64.50, 54.96, 53.63, 46.96. Anal. calcd for $C_{24}H_{22}Cl_2N_4O$: C 63.58, H 4.89, N 12.36; found: C 63.69, H 4.88, N 12.28.

6-Chloro-9-{[4-(2'-methoxyphenyl)piperazin-1-yl]amino}-2-methoxyacridine (6)

Yield 65%. CC(SiO$_2$/CH$_2$Cl$_2$+10%MeOH). ^{1}H-NMR (200 MHz, DMSO-*d6*): 8.17 (d. *J* = 9.6 Hz, 1 arom. H); 7.70 (s, 1 arom. H); 7.20-6.73 (m, 8 arom. H); 3.77 (s, 6H, 2OCH$_3$); 3.38 (pseudo s, 4H, piperazine); 3.10 (pseudo s, 4H, piperazine); 2.88 (br s, NH, exchanges with D$_2$O). ^{13}C-NMR (50 MHz, DMSO-*d6*): 153.69, 151.59, 134.35, 131.73, 126.08, 120.47, 113.75, 111.63, 106.47, 64.52, 54.96, 53.92, 48.78. Dihydrochloride salt: m.p. 225-226˚C. Anal. calcd for $C_{25}H_{25}ClN_4O_2 \cdot 2HCl$: C 57.54, H 5.22, N 10.74; found: C 57.34, H 5.52, N 11.08.

6-Chloro-9-{[4-(3'-methoxyphenyl)piperazin-1-yl]amino}-2-methoxyacridine (7)

Yield 32.6%. M.p. 98-101˚C (Et$_2$O). CC(SiO$_2$/CH$_2$Cl$_2$+10%MeOH). ^{1}H-NMR (200 MHz, DMSO-*d6*): 8.17 (d. *J* = 9.2 Hz, 1 arom. H); 7.71 (s, 1 arom. H); 7.20-6.77 (m, 8 arom. H); 3.75 (s, 3H, OCH$_3$); 3.70 (s, 3H, OCH$_3$); 3.45 (br s, NH, exchanges with D$_2$O); 3.38 (pseudo s, 4H, piperazine); 3.12 (pseudo s, 4H, piperazine). ^{13}C-NMR (50 MHz, DMSO-*d6*): 153.74,

151.76, 134.38, 131.74, 126.81, 120.12, 113.87, 111.14, 106.47, 64.48, 55.05, 53.65, 48.30. Anal. calcd for $C_{25}H_{25}ClN_4O_2$: C 66.88, H 5.61, N 12.48; found: C 66.86, H 5.36, N 12.21.

6-Chloro-9-[[4-(4'-methoxyphenyl)piperazin-1-yl]amino]-2-methoxyacridine (**8**)

Yield 63.5%. M.p. 186.5-188.8°C (Et$_2$O). CC(SiO$_2$/CH$_2$Cl$_2$+10%MeOH). ^{1}H-NMR (200 MHz, DMSO-*d6*): 8.20 (d. J = 9.6 Hz, 1 arom. H); 7.71 (s, 1 arom. H); 7.30-6.91 (m, 4 arom. H); 6.52 (d, J = 7.8 Hz, 2 arom. H); 6.39 (d, J = 8.0 Hz, 2 arom. H); 3.77 (s, 3H, OCH$_3$); 3.74 (s, 3H, OCH$_3$); 3.37 (pseudo s, 4H, piperazine); 3.05 (pseudo s, 4H, piperazine and NH, exchanges with D$_2$O, superimposed). ^{13}C-NMR (50 MHz, DMSO-*d6*): 153.85, 151.71, 134.68, 129.25, 120.08, 113.91, 107.57, 103.92, 64.29, 54.99, 53.72, 47.07. Dihydrochloride salt: m.p. 243-244°C. Anal. calcd for $C_{25}H_{25}ClN_4O_2$·2HCl: C 57.54, H 5.22, N 10.74; found: C 57.33, H 5.38, N 10.91.

6-Chloro-2-methoxy-9-[(pyridin-2-yl)amino]acridine (**9**)

Yield 53%. M.p. 212-213°C. CC(Al$_2$O$_3$/CH$_2$Cl$_2$+2%DEA). ^{1}H-NMR (200 MHz, DMSO-*d6*): 9.38 (br. s, NH, exchanges with D$_2$O); 8.28-7.86 (m, 4 arom. H); 7.77-7.27 (m, 4 arom. H); 6.83 (d, J = 8.0, 2 arom. H); 3.80 (s, 3H, OCH$_3$). ^{13}C-NMR (50 MHz, DMSO-*d6*): 154.80, 147.90, 144.02, 134.90, 129.18, 125.23, 119.72, 115.02, 108.30, 101.05, 54.98. Anal. calcd for $C_{19}H_{14}ClN_3O$: C 67.96, H 4.20, N 12.51; found: C 68.21, H 4.56, N 12.49.

6-Chloro-9-[[(4'-chloro)pyridin-2-yl]amino]-2-methoxyacridine (**10**)

Yield 80%. M.p. 257-259°C (Et$_2$O). ^{1}H-NMR (200 MHz, DMSO-*d6*): 8.20-7.76 (m, 4 arom. H); 7.64-7.20 (m, 3 arom. H); 7.00-6.73 (m, 2 arom. H); 3.79 (s, 3H, OCH$_3$); 3.38 (br. s, NH, exchanges with D$_2$O). ^{13}C-NMR (50 MHz, DMSO-*d6*): 156.02, 148.88, 143.22, 133.65, 128.97, 126.56, 125.10, 121.80, 114.95, 109.11, 100.03, 55.08. Anal. calcd for $C_{19}H_{13}Cl_2N_3O$: C 61.64, H 3.54, N 11.35; found: C 61.45, H 3.65, N 10.99.

6-Chloro-9-[[(5'-chloro)pyridin-2-yl]amino]-2-methoxyacridine (**11**)

Yield 40%. M.p. 203-204°C (CH$_2$Cl$_2$). CC(SiO$_2$/CH$_2$Cl$_2$). ^{1}H-NMR (200MHz, DMSO-*d6*): 8.10-7.78 (m, 4 arom. H), 7.60-7.23 (m, 3 arom. H), 6.98-6.69 (m, 2 arom. H), 3.83 (s, 3H, OCH$_3$), 3.35 (NH, exchanges with D$_2$O). ^{13}C-NMR (50 MHz, DMSO-*d6*): 154.70, 146.04, 144.98, 133.89, 129.17, 126.76, 125.10, 119.94, 114.43, 111.24, 106.56, 99.85, 55.10. Anal. calcd for $C_{19}H_{13}Cl_2N_3O$: C 61.64, H 3.54, N 11.35; found: C 61.72, H 3.84, N 10.99.

6-Chloro-9-[[(2'-chloro)pyridin-3-yl]amino]-2-methoxyacridine hydrochloride (**12**)

Yield 38%. M.p. 286-290°C (Et$_2$O). ^{1}H-NMR (200 MHz, DMSO-*d6*): 8.36-8.24 (m, 1 arom. H); 7.96-7.34 (m, 4 arom. H); 7.30-7.20 (m, 1 arom. H); 3.66 (s, 3H, OCH$_3$ and 1H, NH, exchanges with D$_2$O). ^{13}C-NMR (50 MHz, DMSO-*d6*): 156.15, 148.76, 141.21, 137.41, 133.98, 128.84, 125.56, 123.67, 121.17, 107.93, 99.82, 54.45. Anal. calcd for C$_{19}$H$_{13}$Cl$_2$N$_3$O·HCl·H$_2$O: C 53.73, H 3.80, N 9.89; found: C 53.86, H 4.01, N 9.49.

6-Chloro-9-[[(6'-chloro)pyridin-3-yl]amino]-2-methoxyacridine (**13**)

Yield 34.94%. M.p. 158-160°C (Et$_2$O). CC(SiO$_2$/Et$_2$O). ^{1}H-NMR (200 MHz, DMSO-*d6*): 8.23-6.82 (m, 8 arom. H); 6.76 (d, *J* = 8.0, 1 arom. H); 3.70 (s, 1H, NH, exchanges with D$_2$O); 3.36 (s, 3H, OCH$_3$). ^{13}C-NMR (50 MHz, DMSO-*d6*): 156.26, 151.59, 141.53, 135.59, 133.45, 129.19, 127.53, 124.22, 121.73, 115.43, 99.65, 55.11. Anal. calcd for C$_{19}$H$_{13}$Cl$_2$N$_3$O: C 61.64, H 3.54, N 11.35; found: C 61.66, H 3.82, N 11.44.

6-Chloro-9-[[(6'-methoxy)pyridin-3-yl]amino]-2-methoxyacridine (**14**)

Yield 15%. M.p. 195-197°C (Et$_2$O). CC(CH$_2$Cl$_2$/DEA2%). ^{1}H-NMR (200MHz, DMSO-*d6*): 8.28-6.58 (m, 9 arom. H). 4.15-3.39 (m, 7H, 2OCH$_3$ and 1H, NH, exchanges with D$_2$O). ^{13}C-NMR (50 MHz, DMSO-*d6*): 158.47, 154.31, 135.55, 134.22, 130.09, 127.21, 123.15, 118.92, 110.23, 54.72, 52.68. Anal. calcd for C$_{20}$H$_{16}$ClN$_3$O$_2$: C 65.67, H 4.41, N 11.49; found: C 65.61, H 4.50, N 10.99.

10.1.1.2 General procedure for the synthesis of compounds 16-18.

A solution of 6,9-dichloro-2-methoxyacridine (3.5 mmol) and cyclic secondary amine (7.0 mmol) in DMF (5 mL) was heated at 140 °C for 3 h. The mixture was taken up with water, alkalinized with 2M NaOH and extracted with CH$_2$Cl$_2$. The solvent was evaporated and the oily residue was purified by CC. The isolated compounds were crystallized from the indicated solvents.

6-Chloro-2-methoxy-9-[4-(2'-methoxyphenyl)piperazin-1-yl]acridine (**16**)

Yield 27%. M.p. 166-168°C (CH$_2$Cl$_2$). CC(SiO$_2$/CH$_2$Cl$_2$). ^{1}H-NMR (200 MHz, DMSO-*d6*): 8.43 (d, *J* = 9.8 Hz, 1 arom. H); 8.20-7.93 (m, 2 arom. H); 7.70-7.42 (m, 3 arom. H); 7.16-6.83 (m, 4 arom. H); 3.96 (s, 3H, OCH$_3$); 3.84 (s, 3H, OCH$_3$); 3.70 (pseudo s, 4H, piperazine); 3.29 (pseudo s, 4H, piperazine). ^{13}C-NMR (50 MHz, DMSO-*d6*): 157.99,

151.80, 146.33, 138.94, 133.95, 122.13, 120.27, 118.67, 116.60, 113.75, 64.62, 54.23, 49.01, 48.84. Anal. calcd for $C_{25}H_{24}ClN_3O_2$: C 69.20, H 5.57, N 9.68; found: C 69.21, H 5.49, N 9.31.

6-Chloro-2-methoxy-9-[4-(3'-methoxyphenyl)piperazin-1-yl]acridine (**17**)

Yield 24%. M.p. 163-165°C (Et$_2$O). CC(SiO$_2$/Et$_2$O). ^{1}H-NMR (200 MHz, DMSO-*d6*): 8.38 (d. *J* = 9.8 Hz, 1 arom. H); 8.16-7.95 (m, 2 arom. H); 7.57-7.48 (m, 4 arom. H); 7.19 (t, *J* = 7.6 Hz, 1 arom. H); 6.74-6.57 (m, 2 arom. H); 6.50-6.42 (m, 1 arom. H); 3.96 (s, 3H, OCH$_3$); 3.76 (s, 3H, OCH$_3$); 3.48 (pseudo s, 4H, piperazine); 3.35 (pseudo s, 4H, piperazine). ^{13}C-NMR (50 MHz, DMSO-*d6*): 158.82, 152.53, 145.60, 138.94, 133.99, 120.11, 118.65, 116.82, 113.32, 64.47, 54.78, 54.04, 48.56. Anal. calcd for $C_{25}H_{24}ClN_3O_2$: C 69.20, H 5.57, N 9.68; found: C 69.21, H 5.49, N 9.31.

6-Chloro-2-methoxy-9-[4-(4'-metoxyphenyl)piperazin-1-yl)acridine (**18**)

Yield 45%. M.p. 172.5-174°C (Et$_2$O). CC(SiO$_2$/Et$_2$O). ^{1}H-NMR (200MHz, DMSO-*d6*): 8.42 (d. *J* = 10.0 Hz, 1 arom. H); 8.16-8.00 (m, 2 arom. H); 7.60-7.46 (m, 3 arom. H); 7.05 (d, *J* = 8.8 Hz, 2 arom. H); 6.89 (d, *J* = 8.8 Hz, 2 arom. H); 3.96 (s, 3H, OCH$_3$); 3.73 (s, 3H, OCH$_3$); 3.56 (pseudo s, 4H, piperazine); 3.35 (pseudo s, 4H, piperazine). ^{13}C-NMR (50 MHz, DMSO-*d6*): 159.35, 151.97, 146.05, 139.08, 133.85, 119.63, 115.66, 113.24, 64.52, 54.54, 53.84, 48.49. Anal. calcd for $C_{25}H_{24}ClN_3O_2$: C 69.20, H 5.57, N 9.68; found: C 69.39, H 5.72, N 9.36.

10.1.1.3 General procedure for the synthesis of intermediates a, b.

To the proper 1-phenylpiperazine hydrochloride (3.77 mmol) in H$_2$O (8 mL), 1N HCl was added dropwise until the pH reached 5-6. The solution was cooled to 0°C and a solution of NaNO$_2$ (3.77 mmol) in water (5 mL) was added over a period of 30 min, maintaining a pH of 5-6 by dropwise addition of 4N HCl. Then the reaction mixture was stirred at 70°C for 1h.

On cooling to room temperature, the solution was neutralized with 2 M NaOH. The precipitate (**a**) was collected by filtration and crystallized from dry Et$_2$O.

In the case of compound **b**, the neutral aqueous solution was extracted with CHCl$_3$. After drying (Na$_2$SO$_4$) the solvent was evaporated obtaining the title compound.

4-(2-Chlorophenyl)-1-nitroso-piperazine (**a**)

Yield 63%. M.p. 72-73°C (Et$_2$O). ^{1}H-NMR (200MHz, DMSO-*d6*): 7.46 (d, *J* = 7.8 Hz, 1 arom. H), 7.37-7.00 (m, 3 arom. H), 4.50 (pseudo s, 2H, piperazine), 4.08 (pseudo s, 2H, piperazine), 3.34 (pseudo s, 2H, piperazine), 3.09 (pseudo s, 2H, piperazine). Anal. calcd for C$_{10}$H$_{12}$ClN$_3$O: C 53.22, H 5.36, N 18.62; found: C 53.13, H 5.10, N 18.67.

4-(3-Chlorophenyl)-1-nitroso-piperazine (**b**)

Yield 83.5%. Oil. ^{1}H-NMR (200MHz, DMSO-*d6*): 7.35-7.12 (m, 1 arom. H), 7.00-6.75 (m, 3 arom. H), 4.44 (pseudo s, 2H, piperazine), 3.99 (pseudo s, 2H, piperazine), 3.46 (pseudo s, 2H, piperazine), 3.23 (pseudo s, 2H, piperazine). Anal. calcd for C$_{10}$H$_{12}$ClN$_3$O: C 53.22, H 5.36, N 18.62; found: C 53.10, H 5.18, N 18.71.

10.1.1.4 General procedure for the synthesis of intermediates f, g.

Zinc dust (5 mmol) was added over a period of 20 min to the proper nitroso derivative (1.85 mmol) previously suspended in 5 mL of 50% (v/v) aqueous AcOH. The mixture was heated at 50°C for 3h and then filtered. The solution was cooled and basified with 6N NaOH and extracted with CHCl$_3$. The organic layer was washed with H$_2$O, dried (Na$_2$SO$_4$) and then evaporated. The crude residue was purified by CC (SiO$_2$/CHCl$_3$+10%MeOH).

1-Amino-4-(2-chlorophenyl)piperazine hydrochloride (**f**)

Yield 58.8%. M.p. 197-198°C (EtOH/Et$_2$O). ^{1}H-NMR (200MHz, DMSO-*d6*): 9.64 (br s, $^+$NH$_3$, exchange with D$_2$O), 7.44 (d, *J* = 8.0 Hz, 1 arom. H), 7.39-7.00 (m, 3 arom. H), 3.13 (pseudo s, 8H, piperazine). Anal. calcd for C$_{10}$H$_{14}$ClN$_3$·HCl: C 48.40, H 6.09, N 16.93; found: C 48.07, H 5.89, N 16.90.

1-Amino-4-(3-chlorophenyl)piperazine hydrochloride (**g**)

Yield 27.5%. M.p. 229-230°C (EtOH/Et$_2$O). ^{1}H-NMR (200MHz, DMSO-*d6*): 9.56 (br s, $^+$NH$_3$, exchange with D$_2$O), 7.23 (t, *J* = 7.4 Hz, 1 arom. H), 7.12-6.79 (m, 3 arom. H), 3.74 (s, 3H, OCH$_3$), 3.41 (pseudo s, 4H, piperazine), 3.15 (pseudo s, 4H, piperazine). Anal calcd for C$_{10}$H$_{14}$ClN$_3$·HCl: C 48.40, H 6.09, N 16.93; found: C 48.20, H 6.01, N 17.02.

10.1.1.5 Synthesis of 1-amino-4-(3-methoxyphenyl)piperazine hydrochloride (j).

A mixture of 1-(3-methoxyphenyl)piperazine (3.3 mmol) in 25 mL of H_2O and NaOH pellets (1.32 g) was heated at 60° for 20 min. Maintaining the temperature at 60°C, hydroxylamine-O-sulphonic acid (5 mmol) was slowly added over 15 min. Then the mixture was stirred at 25°C for 24h. The solution was basified with 6N NaOH, and extracted with $CHCl_3$. After evaporation of the solvent, the solid residue was purified with CC (SiO_2/$CHCl_3$+10%MeOH).

1-Amino-4-(3-methoxyphenyl)piperazine hydrochloride (**j**)

Yield 40%. M.p. 175-177°C (EtOH/Et_2O). ^{1}H-NMR (200MHz, DMSO-*d6*): 9.20 (br s, $^+NH_3$, exchange with D_2O), 7.16 (t, J = 7.0 Hz, 1 arom. H), 6.71-6.54 (m, 2 arom. H), 6.47 (d, J = 8.0 Hz, 1 arom. H), 3.74 (s, 3H, OCH_3), 3.31 (pseudo s, 4H, piperazine), 3.14 (pseudo s, 4H, piperazine). Anal. calcd for $C_{11}H_{17}N_3O \cdot HCl$: C 54.21, H 7.44, N 17.24; found: C 54.30, H 7.18, N 17.19.

10.1.2 Experimental section: synthesis of the azaspiro-dihydrotriazines.

10.1.2.1 General method, three-steps synthesis

10.1.2.1.1 First step: general procedure for the synthesis of compounds 2, 8, 11, a, b.

To a solution of N-Boc Piperidone (3.4 g, 16.723 mmol), dicyandiamide (9.051 mmol) and 0.196 g of HCl conc. (5.369 mmol) in EtOH (25 mL) the proper amine (5.369 mmol) was added. The mixture was refluxed for 17 h with stirring. After evaporation, the residue was purified by reverse-phase (RP)-HPLC (water/acetonitrile).

Tert-butyl 1-(3-Chlorophenyl)-2,4-diamino-1,3,5,9-tetraazaspiro[5.5]undeca-2,4-diene-9-carboxylate (**2**)

Yield: 37%. ^{1}H NMR (300 MHz, DMSO-*d6*): 8.51 (br s, 4H, 2NH$_2$); 7.20-6.43 (m, 4H, H arom.); 3.42-3.21 (m, 4H, 2CH$_2$ in α to N of piperidine); 1.80-1.62 (m, 4H, 2CH$_2$ of piperidine); 1.30 (s, 9H, 3CH$_3$). HRMS (ESI) m/z calc. for C$_{18}$H$_{25}$ClN$_6$O$_2$ [M+H]$^+$: 393.18; found: 393.24.

Tert-butyl 2,4-diamino-1-(3-methoxyphenyl)-1,3,5,9-tetraazaspiro[5.5]undeca-2,4-diene-9-carboxylate (**8**)

Yield: 42%. ^{1}H NMR (300 MHz, DMSO-*d6*): 8.52 (br s, 4H, 2NH$_2$); 7.25-6.14 (m, 4H, H arom.); 3.83 (s, 3H, OCH$_3$); 3.55-3.32 (m, 4H, 2 CH$_2$ in α to N of piperidine); 1.82-1.60 (m, 4H, 2CH$_2$ of piperidine); 1.34 (s, 9H, 3CH$_3$). HRMS (ESI) m/z calc. for C$_{19}$H$_{28}$N$_6$O$_3$ [M+H]$^+$: 389.23; found: 389.16.

Tert-butyl 1-(3-Chlorobenzyl)-2,4-diamino-1,3,5,9-tetraazaspiro[5.5]undeca-2,4-diene-9-carboxylate (**11**)

Yield: 40%. ^{1}H NMR (300 MHz, DMSO-*d6*): 8.56 (br s, 4H, 2NH$_2$); 7.52-7.21 (m, 4H, H arom.); 4.32 (s, 2H, CH$_2$-arom.); 3.60-3.34 (m, 4H, 2CH$_2$ in α at N of piperidine); 1.82-1.52 (m, 4H, 2CH$_2$ of piperidine); 1.34 (s, 9H, 3CH$_3$). HRMS (ESI) m/z calc. for C$_{19}$H$_{27}$ClN$_6$O$_2$ [M+H]$^+$: 407.19; found: 406.99.

***Tert-butyl 2,4-Diamino-1-propyl-1,3,5,9-tetraazaspiro[5.5]undeca-2,4-diene-9-carboxylate* (a)**

Yield: 63%. ^{1}H-NMR (300 MHz, CD$_3$OD): 3.60 (t, J=6.2 Hz, 4 H), 3.45 (t, J=5.3 Hz, 2 H), 3.39 (dd, J=7.9, 14.9 Hz, 3 H), 3.29 (s, 3 H), 2.94 (t, J=5.3 Hz, 2 H), 2.50 (m, 1 H), 2.34 (t, J=6.2 Hz, 4 H), 1.61 (m, 2 H), 1.42 (s, 9 H), 1.38 (s, 4 H), 1.09 (t, J=7.0 Hz, 2 H) HRMS (ESI) m/z calc. for C$_{15}$H$_{28}$N$_6$O$_2$ [M+H]$^+$: 325.23; found: 325.30.

***Tert-butyl 2,4-Diamino-1-(2-methoxyethyl)-1,3,5,9-tetraazaspiro[5.5]undeca-2,4-diene-9-carboxylate* (b)**

Yield: 52%. ^{1}H-NMR (300 MHz, DMSO-d_6): 3.60 (t, J=6.2 Hz, 4 H), 3.45 (t, J=5.3 Hz, 2 H), 3.39 (dd, J=7.9, 14.9 Hz, 3 H), 3.29 (s, 3 H), 2.94 (t, J=5.3 Hz, 2 H), 2.50 (m, 1 H), 2.34 (t, J=6.2 Hz, 4 H), 1.61 (m, 2 H), 1.42 (s, 9 H), 1.38 (s, 4 H), 1.09 (t, J=7.0 Hz, 2 H). HRMS (ESI) m/z calc. for C$_{15}$H$_{28}$N$_6$O$_3$ [M+H]$^+$: 341.23; found: 341.00.

10.2.1.2 Second step: general procedure for the synthesis of compounds 1, 7, c, d.

A stirring solution of the azaspiro derivative (1.469 mmol) in 150 mL of CH$_2$Cl$_2$ was cooled in ice bath, and then added of 3 mL of trifluoroacetic acid obtaining a final 20% solution of TFA in CH$_2$Cl$_2$. The reaction was stirred at r.t. for 6/7h. The solvent was removed *under vacuum* affording the title compound.

***1-(3-Chlorophenyl)-2,4-diamino-1,3,5,9-tetraazaspiro[5.5]undeca-2,4-diene* (1)**

Yield: 89%. ^{1}H NMR (300 MHz, DMSO-d6): 8.63 (br s, 4H, 2NH$_2$); 7.26-6.42 (m, 4H, H arom.); 3.15-2.74 (m, 4H, 2CH$_2$ in α to N of piperidine); 1.98 (s, 1H, NH); 1.86-1.63 (m, 4H, 2CH$_2$ of piperidine); HRMS (ESI) m/z calc. for C$_{13}$H$_{17}$ClN$_6$ [M+H]$^+$: 293.12; found: 293.06.

***2,4-Diamino-1-(3-methoxyphenyl)-1,3,5,9-tetraazaspiro[5.5]undeca-2,4-diene* (7)**

Yield: 93%. ^{1}H NMR (300 MHz, DMSO-d6): 8.64 (br s, 4H, 2NH$_2$); 7.22-6.09 (m, 4H, H arom.); 4.05 (s, 3H, OCH$_3$); 2.87-2.51 (m, 4H, 2CH$_2$ in α to N of piperidine); 2.14-1.62 (m, 5H, 2CH$_2$ of piperidine and NH). HRMS (ESI) m/z calc. for C$_{14}$H$_{20}$N$_6$O [M+H]$^+$: 289.17; found: 289.20.

2,4-Diamino-1-propyl-1,3,5,9-tetraazaspiro[5.5]undeca-2,4-diene (**c**)

Yield: 80%. ^{1}H-NMR (300 MHz, DMSO-d_6): 3.43 (t, J=6.6 Hz, 4 H, 2CH$_2$ in α to N of piperidine), 2.74 (m, 2 H), 2.55 (t, J=6.6 Hz, 4 H, 2CH$_2$ of piperidine), 2.22 (s, 1H, NH), 1.55 (q, J=7.5 Hz, 2 H), 0.89 (t, J=7.5 Hz, 3H, NCH$_2$CH$_2$*CH$_3$*). HRMS (ESI) m/z calc. for C$_{10}$H$_{20}$N$_6$ [M+H]$^+$: 225.18; found: 225.15.

2,4-Diamino-1-(2-methoxyethyl)-1,3,5,9-tetraazaspiro[5.5]undeca-2,4-diene (**d**)

Yield: 79%. HRMS (ESI) m/z calc. for C$_{10}$H$_{20}$N$_6$O [M+H]$^+$: 241.17; found: 241.11.

10.1.2.1.3 Third step: general procedure for the synthesis of compounds 4, 5, 9, 13, 17.

A solution of the deprotected azaspiro compound (0.134 mmol) in 2 mL of DMF, 0.14 mL of DIPEA (0.803 mmol), 51.8 mg of EDC (0.268 mmol) and 27.9 mg of HOBT (0.201 mmol) was stirred for 15 min at r.t. Then the proper acid (0.125 mmol) was added to the mixture and the reaction was maintained at 50°C for 12h with stirring. After evaporation of the solvent, the residue was purified by reverse-phase (RP)-HPLC (water/acetonitrile).

1-(3-Chlorophenyl)-2,4-diamino-9-(p-tolylcarbonyl)-1,3,5,9-tetraazaspiro[5.5]undeca-2,4-diene (**4**)

Yield: 33%. ^{1}H NMR (300 MHz, DMSO-*d6*): 8.54 (br s, 4H, 2NH$_2$); 7.92-6.52 (m, 8H, H arom.); 3.44-3.31 (m, 4H, 2CH$_2$ in α to N of piperidine); 2.43 (s, 3H, CH$_3$-Ar); 1.86-1.53 (m, 4H, 2CH$_2$ of piperidine). HRMS (ESI) m/z calc. for C$_{21}$H$_{23}$ClN$_6$O [M+H]$^+$: 411.17; found: 411.14.

1-(3-Chlorophenyl)-2,4-diamino-9-[(naphthalen-2-yl)carbonyl]-1,3,5,9-tetraazaspiro[5.5]undeca-2,4-diene (**5**)

Yield: 42%. ^{1}H NMR (300 MHz, DMSO-*d6*): 8.63-7.48 (m, 11 H, 7H of naphthalene and 2NH$_2$); 7.34-6.45 (m, 4 H, H arom.); 3.54-3.31 (m, 4H, 2CH$_2$ in α to N of piperidine); 1.94-1.48 (m, 4H, 2CH$_2$ of piperidine); HRMS (ESI) m/z calc. for C$_{24}$H$_{23}$ClN$_6$O [M+H]$^+$: 447.17; found: 447.12.

2,4-Diamino-1-(3-methoxyphenyl)-9-(1-oxopent-1-yl)-1,3,5,9-tetraazaspiro[5.5]undeca-2,4-diene (**9**)

Yield: 47%. ^{1}H NMR (300 MHz, DMSO-*d6*): 8.57 (br s, 4H, 2NH$_2$); 7.29-6.11 (m, 4H, H arom.); 4.08 (s, 3H, OCH$_3$); 3.55-3.33 (m, 4H, 2CH$_2$ in α to N of piperidine); 2.46 (t, *J* = 7.4, 2H, CO*CH$_2$*(CH$_2$)$_4$CH$_3$); 1.84-1.32 (m, 8H, COCH$_2$*(CH$_2$)*$_4$CH$_3$ and 2CH$_2$ of piperidine); 1.10 (t, *J* = 7.2, 3H, COCH$_2$(CH$_2$)$_4$*CH$_3$*). HRMS (ESI) m/z calc. for C$_{19}$H$_{28}$N$_6$O$_2$ [M+H]$^+$: 373.23; found: 373.26.

2,4-Diamino-1-propyl-9-[(3,5-dimethylisoxazol-4-yl)carbonyl]-1,3,5,9-tetraazaspiro[5.5]undeca-2,4-diene (**13**)

Yield: 27%. ^{1}H NMR (300 MHz, DMSO-*d6*): 8.52 (br s, 4H, 2NH$_2$); 3.57-3.42 (m, 4H, 2CH$_2$ in α to N of piperidine); 2.56-2.30 (m, 8H, 2CH$_3$ of isoxazole and 2H, N*CH$_2$*CH$_2$CH$_3$); 1.86-1.42 (m, 6H, 2H of NCH$_2$*CH$_2$*CH$_3$ and 2CH$_2$ of piperidine); 1.09 (t, *J*= 6.8, 3H, NCH$_2$CH$_2$*CH$_3$*); HRMS (ESI) m/z calc. for C$_{16}$H$_{25}$N$_7$O$_2$ [M+H]$^+$: 348.21; found: 348.32.

2,4-Diamino-1-(2-methoxyethyl)-9-[(1-methyl-1H-pyrrol-2-yl)carbonyl]-1,3,5,9-tetraazaspiro[5.5]undeca-2,4-diene (**17**)

Yield: 21%. ^{1}H NMR (300 MHz, DMSO-*d6*): 8.53 (br s, 4H, 2NH$_2$); 7.87-7.51 (m, 2H of pyrrole); 6.52 (d, *J*= 8.2, 1H, pyrrole); 3.92 (s, 3H, CH$_3$ NCH$_3$); 3.64-3.22 (m, 9H, 2CH$_2$ in α to N of piperidine, O*CH$_3$* and NCH$_2$*CH$_2$*OCH$_3$); 2.63 (t, *J*= 7.2, 2H, N*CH$_2$*CH$_2$OCH$_3$); 1.70-1.52 (m, 4H, 2CH$_2$ of piperidine). HRMS (ESI) m/z calc. for C$_{16}$H$_{25}$N$_7$O$_2$ [M+H]$^+$: 348.21; found: 348.40.

10.1.2.1.4 Third step: general procedure for the synthesis of compounds 3, 10, 12, 14, 16.

The proper acyl chloride (0.134 mmol) was added at r.t. to a stirred solution of the deprotected tetraazaspiro compound (0.134 mmol) in 3 mL of dry THF and 0.13 mL of Et$_3$N (0.936 mmol). The reaction was maintained at r.t. with stirring for 12h. After evaporation of the solvent, the residue was purified by reverse-phase (RP)-HPLC (water/acetonitrile).

9-Cyclobutylcarbonyl-1-(3-chlorophenyl)-2,4-diamino-1,3,5,9-tetraazaspiro[5.5]undeca-2,4-diene (3)

Yield: 39%. ^{1}H NMR (300 MHz, DMSO-*d6*): 8.50 (br s, 4 H, 2NH$_2$); 7.17-6.44 (m, 4H, H arom.); 3.56-3.32 (m, 5H, 2CH$_2$ in α to N of piperidine and CH of cyclobutyle); 2.33-1.61 (m, 10H, 2CH$_2$ piperidine and 6H, 3CH$_2$ of cyclobutyle). HRMS (ESI) m/z calc. for C$_{18}$H$_{23}$ClN$_6$O [M+H]$^+$: 375.17; found: 375.29.

2,4-Diamino-1-(3-methoxyphenyl)-9-[(2-methyl-4-(trifluoromethyl)phenyl)carbonyl]-1,3,5,9-tetraazaspiro[5.5]undeca-2,4-diene (10)

Yield: 49%. ^{1}H NMR (300 MHz, DMSO-*d6*): 8.63 (br s, 4H, 2NH$_2$); 7.88-7.62 (m, 3H, H arom.); 7.16-6.13 (m, 4H, H arom.); 3.93 (s, 3H, OCH$_3$); 3.44-3.23 (m, 4H, 2CH$_2$ in α to N of piperidine); 2.54 (s, 3H, *CH$_3$*-arom.); 1.93-1.62 (m, 4H, 2CH$_2$ of piperidine). HRMS (ESI) m/z calc. for C$_{23}$H$_{25}$F$_3$N$_6$O$_2$ [M+H]$^+$: 475.20; found: 475.14.

9-Cyclopropylcarbonyl-2,4-diamino-1-propyl-1,3,5,9-tetraazaspiro[5.5]undeca-2,4-diene (12)

Yield: 12%. ^{1}H NMR (300 MHz, DMSO-*d6*): 8.64 (br s, 4H, 2NH$_2$); 3.44-3.22 (m, 4H, 2CH$_2$ in α to N of piperidine); 2.73 (t, *J*= 7.2, 2H, N*CH$_2$*CH$_2$CH$_3$); 1.87-0.68 (m, 14H, 2CH$_2$ of cyclopropyl, 1CH of cyclopropyl, 2H of NCH$_2$*CH$_2$*CH$_3$, 3H of NCH$_2$CH$_2$*CH$_3$* and 2CH$_2$ of piperidine). HRMS (ESI) m/z calc. for C$_{14}$H$_{24}$N$_6$O [M+H]$^+$: 293.20; found: 293.08.

Ethyl 3-(2,4-diamino-1-propyl-1,3,5,9-tetraazaspiro[5.5]undeca-2,4-diene-9-carboxamido)propanoate (14)

Yield: 27%. ^{1}H NMR (300 MHz, DMSO-*d6*): 8.60 (br s, 4H, 2NH$_2$); 4.25-3.75 (m, 4H, COO*CH$_2$*CH$_3$ and CONH*CH$_2$*CH$_2$); 3.50-3.24 (m, 4H, 2CH$_2$ in α to N of piperidine); 2.69-2.42 (m, 4H, N*CH$_2$*CH$_2$CH$_3$ and CONHCH$_2$*CH$_2$*); 1.94-1.20 (m, 9H, OCH$_2$*CH$_3$*, NCH$_2$*CH$_2$*CH$_3$ and 2CH$_2$ of piperidine); 0.96 (t, *J*= 6.0, 3H, NCH$_2$CH$_2$*CH$_3$*). HRMS (ESI) m/z calc. for C$_{16}$H$_{29}$N$_7$O$_3$ [M+H]$^+$: 368.24; found: 368.08.

9-Cyclopropylcarbonyl-2,4-diamino-1-(2-methoxyethyl)-1,3,5,9-tetraazaspiro[5.5]undeca-2,4-diene (16)

Yield: 25%. ^{1}H NMR (300 MHz, DMSO-*d6*): 8.55 (br s, 4H, 2NH$_2$); 3.75-3.34 (m, 9H, OCH$_3$, 2CH$_2$ in α to N of piperidine and CH$_2$*CH$_2$*OCH$_3$); 2.74 (t, J= 7.2, 2H, *CH$_2$*CH$_2$OCH$_3$); 1.78-0.68 (m, 9H, 2CH$_2$ of cyclopropyl, CH of cyclopropyl and 2CH$_2$ of piperidine). HRMS (ESI) m/z calc. for C$_{14}$H$_{24}$N$_6$O$_2$ [M+H]$^+$: 309.20; found: 309.06.

10.1.2.1.5 Third step: general procedure for the synthesis of compounds 15, 20, 21.

The proper sulfonyl chloride (0.134 mmol) was added at r.t to a stirred solution of the deprotected tetraazaspiro compound (0.134 mmol) in 3 mL of CH$_2$Cl$_2$ and 0.16 mL of DIPEA (0.936 mmol). The reaction was maintained for 12h at r.t. with stirring. Then after evaporation of the solvent, the residue was purified by reverse-phase (RP)-HPLC (water/acetonitrile).

2,4-Diamino-1-propyl-9-(propylsulfonyl)-1,3,5,9-tetraazaspiro[5.5]undeca-2,4-diene (15)

Yield: 37%. ^{1}H NMR (300 MHz, DMSO-*d6*): 8.58 (br s, 4H, 2NH$_2$); 3.38-2.50 (m, 8H, 2CH$_2$ in α to N of piperidine, N*CH$_2$*CH$_2$CH$_3$, S*CH$_2$*CH$_2$CH$_3$); 1.91-1.46 (m, 8H, 2CH$_2$ of piperidine, NCH$_2$*CH$_2$*CH$_3$ and SCH$_2$*CH$_2$*CH$_3$); 1.06 (s, 6H, NCH$_2$CH$_2$*CH$_3$* and SCH$_2$CH$_2$*CH$_3$*). HRMS (ESI) m/z calc. for C$_{13}$H$_{26}$N$_6$O$_2$S [M+H]$^+$: 331.19; found: 331.29.

2,4-Diamino-9-(ethylsulfonyl)-1-(2-methoxyethyl)-1,3,5,9-tetraazaspiro[5.5]undeca-2,4-diene (20)

Yield: 11%. ^{1}H NMR (300 MHz, DMSO-*d6*): 8.57 (br s, 4H, 2NH$_2$); 3.67-3.44 (m, 4H, CH$_2$*CH$_2$*OCH$_3$ and S*CH$_2$*CH$_3$.); 3.40 (s, 3H, CH$_2$CH$_2$O*CH$_3$*.); 3.18-2.70 (m, 6H, *CH$_2$*CH$_2$OCH$_3$ and 2CH$_2$ in α to N of piperidine); 1.88-1.55 (m, 4H, 2CH$_2$ of piperidine); 1.26 (t, J= 6.8, 3H, SCH$_2$*CH$_3$*). HRMS (ESI) m/z calc. for C$_{12}$H$_{24}$N$_6$O$_3$S [M+H]$^+$: 333.17; found: 333.40.

2,4-Diamino-9-(phenylsulfonyl)-1-(2-methoxyethyl)-1,3,5,9-tetraazaspiro[5.5]undeca-2,4-diene (21)

Yield: 15%. ^{1}H NMR (300 MHz, DMSO-$d6$): 8.56 (br s, 4H, 2NH$_2$); 7.80-7.56 (m, 3H, H arom.); 3.64 (t, J= 7.5, 2H, CH_2CH$_2$OCH$_3$); 3.38 (s, 3H, CH$_2$CH$_2$OCH_3); 3.18-2.60 (m, 6H, CH$_2$$CH_2OCH_3$ and 2CH$_2$ in α at N of piperidine); 1.86-1.54 (m, 4H, 2CH$_2$ of piperidine). HRMS (ESI) m/z calc. for C$_{16}$H$_{24}$N$_6$O$_3$S [M+H]+: 381.17; found: 381.25.

10.1.2.1.6 Third step: general procedure for the synthesis of compounds 6, 18, 19.

The proper isocyanate (0.134 mmol) was added to a solution of the deprotected tetraazaspiro compound (0.134 mmol) in 3 mL of CH$_2$Cl$_2$ and 0.13 mL of Et$_3$N (0.936 mmol). Then the solution was stirred at r.t. for 12h.

1-(3-Chlorophenyl)-2,4-diamino-9-[N-(4-fluorophenyl)carbamoyl]-1,3,5,9-tetraazaspiro[5.5]undeca-2,4-diene (6)

Yield: 23%. ^{1}H-NMR (300 MHz, CD$_3$OD): 7.58 (m, 3 H), 7.37 (dt, J=1.8, 7.2 Hz, 1 H), 7.27 (ddd, J=2.8, 5.3 Hz, 2 H), 7.00 (t, J=8.8 Hz, 2 H), 4.17 (dt, J=2.3, 12.1 Hz, 2 H), 3.10 (tq, J=1.9, 13.8 Hz, 2 H), 2.10 (dt, J=2.1, 13.8 Hz, 2 H), 1.75 (m, 2 H). HRMS (ESI) m/z calc. for C$_{20}$H$_{21}$ClFN$_6$O [M+H]$^+$: 430.15; found: 430.31.

2,4-Diamino-9-[(4-methylcyclohexyl)carbamoyl]-1-(2-methoxyethyl)-1,3,5,9-tetraazaspiro[5.5]undeca-2,4-diene (18)

Yield: 26%. ^{1}H NMR (300 MHz, DMSO-$d6$): 8.58 (br s, 4H, 2NH$_2$); 3.66-3.39 (m, 6H, 2CH$_2$ in α to N of piperidine and CH$_2$$CH_2OCH_3$); 3.36 (s, 3H, CH$_2CH_2OCH_3$); 2.82 (t, J= 7.5, 2H, CH_2CH$_2$OCH$_3$); 1.85-1.24 (m, 13H, 4CH$_2$ of cyclohexyl, 2CH of cyclohexyl and 2CH$_2$ of piperidine); 1.08 (d, J= 7.0, 3H, CH$_3$-cyclohexyl). HRMS (ESI) m/z calc. for C$_{18}$H$_{33}$N$_7$O$_2$ [M+H]$^+$: 380.27; found: 380.50.

2,4-Diamino-1-(2-methoxyethyl)-9[(4-methoxyphenyl)carbamoyl]-1,3,5,9-tetraazaspiro[5.5]undeca-2,4-diene (19)

Yield: 10%. ^{1}H NMR (300 MHz, DMSO-$d6$): 8.60 (br s, 4H, 2NH$_2$); 4.01 (s, 3H, OCH$_3$); 3.68-3.46 (m, 6H, 2CH$_2$ in α ad N of piperidine and CH$_2$$CH_2OCH_3$); 3.40 (s, 3H, CH$_2CH_2OCH_3$);

2.78 (t, J= 7.6, 2H, $CH_2CH_2OCH_3$); 1.84-1.57 (m, 4H, $2CH_2$ of piperidine). HRMS (ESI) m/z calc. for $C_{18}H_{27}N_7O_3$ [M+H]$^+$: 390.22; found: 390.41.

10.1.2.2 General procedure for the synthesis of compounds 22-23, one-step synthesis.

A solution of the proper aniline (5.4 mmol), HCl conc. (5.4 mmol) and 1-benzylpiperidin-3-one hydrochloride (8.1 mmol) in 25 mL of EtOH was reacted with dicyandiamide (5.67 mmol). The mixture was refluxed at 120-130°C with stirring for 7h. After cooling compounds separated directly in crystalline form from the reaction mixture, thus they were collected by filtration and washed with acetone/Et₂O an. 1:1.

8-Benzyl-2,4-diamino-1-phenyl-1,3,5,8-tetraazaspiro[5.5]undeca-2,4-diene (**22**)

Yield: 53%. M.p. 240-241°C (acetone/Et₂O an.). ^{1}H NMR (200 MHz, DMSO-$d6$): 9.69 (s, 1H, $^+$NH); 7.74-7.20 (m, 12H, 10 H arom. and 2H, NH₂, superimposed signals); 6.99 (s, 2H, NH₂); 4.06 (s, 2H, CH_2-arom.); 2.84 (s, 2H, CH_2-piperidine); 2.52 (pseudo s, 2H, CH_2-piperidine superimposed to DMSO-d6 signal); 2.38 (t, J= 7.0 Hz, CH_2-piperidine); 2.04-1.72 (m, 2H, CH_2-piperidine). Anal. Calcd for $C_{20}H_{24}N_6$ ·HCl: C 62.41; H 6.55; N 21.83. Found: C 62.41; H 6.64; N 21.83.

8-Benzyl-1-(4-chlorophenyl)-2,4-diamino-1,3,5,8-tetraazaspiro[5.5]undeca-2,4-diene (23)

Yield: 46%. M.p. 239.8-240°C (acetone/Et2O an.). 1H NMR (200 MHz, DMSO-$d6$): 9.67 (s, 1H, +NH); 7.86-7.16 (m, 11H, 9 H arom. and 2H, NH2, superimposed signals); 6.98 (s, 2H, NH2); 4.07 (s, 2H, CH2-arom.); 2.85 (s, 2H, CH2-piperidine); 2.52 (pseudo s, 2H, CH2-piperidine superimposed to DMSO-$d6$ signal); 2.40 (t, J= 6.8 Hz, CH2-piperidine); 2.00-1.76 (m, 2H, CH2-piperidine). Anal. Calcd for $C_{20}H_{23}ClN_6$ ·HCl: C 57.28; H 5.77; N 20.04. Found: C 56.99; H 5.93; N 19.84.

10.1.3 Experimental section: synthesis of the 2-aminotriazino[1,2-a]benzimidazoles.

10.1.3.1 General procedure for the synthesis of compounds 1-7

A mixture of the proper 2-guanidinobenzimidazole (5.7 mmol) and piperidine (2.9 mmol) dissolved in 5 mL of acetone was heated at 70°C for 7h. The reaction mixture was then concentrated *under vacuum* and kept cooling to r.t. overnight. The expected product precipitated as a white solid, which was filtered and recrystallized from acetone/Et_2O an.

2-Amino-4,4-dimethyl-3,4-dihydrotriazino[1,2-a]benzimidazole (**1**)

Yield: 59%. M.p. 284.8-285.6 °C. ^{1}H NMR (200 MHz, DMSO-*d6*): δ 8.23 (broad s, 1H, NH), 7.41 (d, *J* = 7Hz, 1H arom.), 7.30 (d, *J* = 7.2Hz, 1H arom.), 6.81-7.17 (m, 4H, 2H arom. superimposed to 2H NH_2), 1.84 (s, 6H, 2 C(4)-CH_3). ^{13}C NMR (50 MHz, DMSO-*d6*): 155.0, 153.2, 142.9, 130.2, 120.4, 118.8, 115.5, 109.4, 69.1, 28.2. Anal. calcd for $C_{11}H_{13}N_5$: C 61.38, H 6.09, N 32.54; found: C 61.31, H 6.12, N 32.30.

2-Amino-4,4,7,8-tetramethyl-3,4-dihydrotriazino[1,2-a]benzimidazole (**2**)

Yield: 40%. M.p. 266.5-268.5 °C. ^{1}H NMR (200 MHz, DMSO-*d6)*: δ 8.01 (broad s, 1H, NH), 7.18 (s, 1H, arom.), 7.05 (s, 1H, arom.), 6.69 (s, 2H, NH_2), 2.28 (s, 3H, C(7/8)-CH_3), 2.23 (s, 3H, C(7/8)-CH_3), 1.78 (s, 6H, 2 C(4)-CH_3). ^{13}C NMR (50 MHz, DMSO-*d6*): 154.6, 152.6, 141.5, 128.6, 127.9, 126.5, 116.3, 110.1, 68.9, 28.2, 19.5, 19.4. Anal. calcd for $C_{13}H_{17}N_5$: C 64.17, H 7.04, N 28.78; found: C 64.22, H 7.32, N 28.50.

2-Amino-7,8-dichloro-3,4-dihydrotriazino[1,2-a]benzimidazole (**3**)

Yield: 56%. M.p. 285.1-285.9 °C. ^{1}H NMR (200 MHz, DMSO-*d6)*: δ 7.76 (s, 1H, NH), 7.61 (s, 1H, arom), 7.41 (s, 1H, arom), 6.46 (s, 2H, NH_2), 1.76 (s, 6H, 2 C(4)-CH_3). ^{13}C NMR (50 MHz, DMSO-*d6*): 155.5, 155.2, 143,7, 130.0, 122.5, 120.0, 116.1, 110.1, 69.2, 27.8. Anal. calcd for $C_{11}H_{13}N_5Cl_2$: C 46.50, H 3.90, N 24.65; found: C 46.43, H 4.00, N 24.30.

2-Ammino-7(8)-cloro-3,4-diidrotriazino[1,2-a]benzimidazole (**4a,b**)

Yield: 41%, M.p. 161.2-163 °C. 4a ^{1}H NMR (200 MHz, DMSO-*d6)*: δ 7.88 (broad s, 1H, NH), 7.38 (d superimposed to 4b signal, 1H, arom.), 7.21 (pseudo s, 1H, arom.), 7.04 (d, *J* =

8Hz, J' = 2Hz, 1H, C(8)arom.), 6.56 (s, 2H, NH_2), 1.78 (s, 6H, 2 C(4) CH_3). ^{13}C NMR (50 MHz, DMSO-$d6$): 155.2, 144.7, 129.2, 124.7, 120.3, 118.0, 114.9, 110.1, 69.1, 28.0. 4b ^{1}H NMR (200 MHz, DMSO-$d6$): δ 7.88 (broad s, 1H, NH), 7.42 (d superimposed to 5a signal, 1H, arom.), 7.25 (pseudo s, 1H, arom.), 6.93 (dd, J = 8.5Hz, J' = 2Hz, 1H, C(7) arom.), 6.60 (s, 2H, NH_2), 1.78 (s, 6H, 2 C(4) CH_3). ^{13}C NMR (50 MHz, DMSO-$d6$): 154.7, 142.2, 131.0, 124.7, 122.7, 118.0, 116.4, 109.0, 69.1, 28.0. The ^{1}H and ^{13}C NMR signals have been attributed to the two different isomers on the base of the literature data[181]. Anal. calcd for $C_{11}H_{12}N_5Cl$: C 52.91, H 4.84, N 28.05; found: C 52.89, H 5.16, N 28.09.

2-Amino-7(8)-methoxy-3,4-dihydrotriazino[1,2-a]benzimidazole (5a,b)

Yield: 12%. M.p. 264-266 ˚C. ^{1}H NMR (200 MHz, DMSO-$d6$): δ 7.83 (broad s, 1H, NH), 7.24 (d, J=6Hz, 1H arom.), 6.83 (s, 1H arom), 6.24-6.73 (m, 3H, 1H arom. superimposed to 2H NH_2), 3.73 (s, 3H, OCH_3), 1.75 (s, 6H, 2 C(4) CH_3). ^{13}C NMR (50 MHz, DMSO-$d6$) 154.7, 154.4, 144.3, 124.7, 116.0, 109.3, 106.1, 100.3, 68.9, 55.0, 28.1. The signals of the isomer **5a** are only in part distinguishable in the ^{1}H NMR spectrum since they are partially superimposed to the **5b**, which appeared to be formed in major quantity. Anal. calcd for $C_{12}H_{14}N_5O$: C 58.76, H 6.16, N 28.55; found: C 59.03, H 6.22, N 28.93.

2-Amino-7(8)-trifluoromethyl-3,4-dihydrotriazino[1,2-a]benzimidazole (6a,b)

Yield: 20%, M.p. 259-261˚C. ^{1}H NMR (200 MHz, DMSO-$d6$): δ 7.89 (broad s, 1H, NH), 7.53 (s, 1H, arom.), 7.36 (d, J=5.8Hz, 1H, arom.), 7.23 (d, J=7.4Hz, 1H, arom.), 6.55 (s, 2H, NH_2), 1.80 (s, 6H, 2 C(4) CH_3). ^{13}C NMR (50 MHz, DMSO-$d6$): 155.2, 143.3, 132.9, 130.0, 115.5, 115.2, 112.0, 109.4, 105.8, 69.3, 28.0. The signals of the isomer **6a** are only in part distinguishable in the ^{1}H NMR spectrum since they are partially superimposed to the **6b**, which appeared to be formed in major quantity. Anal. calcd for $C_{12}H_{12}F_3N_5$: C 50.88, H 4.74, N 24.72; found: C 50.82, H 4.53, N 24.75.

2-Amino-7,9-dichloro-3,4-dihydrotriazino[1,2-a]benzimidazole (7)

Yield: 89%, M.p. 283.2-283.7 ˚C. ^{1}H NMR (200 MHz, DMSO-$d6$): δ 7.70 (s, 1H, NH), 7.43 (s, 1H, arom.), 7.13 s, 1H, arom.), 6.44 (s, 2H, NH_2), 1.76 (s, 6H, 2 C(4) CH_3). [13]C (50 MHz, DMSO-$d6$): 155.2, 154.0, 139.6, 131.7, 122.4, 119.8, 119.6, 108.0, 69.4, 27.8. Anal. calcd for $C_{11}H_{11}N_5Cl_2$: C 46.50, H 3.90, N 24,65; found: C 46.68, H 3.71, N 24,71.

10.1.3.2 General procedure for the synthesis of intermediates I-VII

The properly substituted 1,2-phenylendiamine (1,4 mmol) and dicyandiamide (1,4 mmol) were dissolved in 5 mL of H_2O and 0.23 mL (1,4 mmol) of HCl conc. were slowly added to the obtained solution. The mixture was heated to reflux for 6h under magnetic stirring. After cooling to r.t, the solution was alkalinized with 6M NaOH inducing the precipitation of an amorphous solid, which was either recrystallized from Et_2O (**I**) or purified by CC (SiO_2/Et_2O+10% MeOH) (**II-VII**), to afford the final product.

2-Guanidinebenzimidazole (**I**)

Yield: 59%. M.p. 237-240°C (m.p. reported in literature 243-244 °C)[181].

5(6)-Chloro-2-guanidinebenzimidazole (**II**)

Yield: 40%. M.p. 208-211 °C (m.p. reported in literature 207 °C)[181]. Anal. calcd for $C_8H_8ClN_5 \cdot 2HCl$: C 34.01, H 3.57, N 24.79; found: C 34.06, H 3.45, N 24.88.

5(6)-Methoxy-2-guanidinebenzimidazole (**III**)

Yield: 36%. M.p. 201.7-202.7 °C. Anal. calcd for $C_9H_{11}N_5O$: C 52.67, H 5.40, N 34.13; found: C 52.63, H 5.45, N 34.43.

5(6)-Trifluoromethyl-2-guanidinebenzimidazole (**IV**)

Yield 38%. M.p. 200-203 °C. Anal. calcd for $C_9H_9ClF_3N_5 \cdot HCl$: C 38.65, H 3.24, N 25.04; found: C 38.41, H 3.21, N 25.01.

5,6-Dichloro-2-guanidinebenzimidazole (**V**)

Yield: 70%. M.p. 236-240 °C (m.p. reported in literature 244°C)[181]. Anal. calcd for $C_8H_7Cl_2N_5 \cdot HCl$: C 34.25, H 2.87, N 24.96; found: C 34.31, H 3.10, N 24.54.

5,7-Dichloro-2-guanidinebenzimidazole (**VI**)

Yield: 40%. M.p. 244-245.5 °C. Anal. calcd for $C_8H_7Cl_2N_5$: C 39.37, H 2.89, N 28.69; found: C 39.44, H 3.02, N 28.38.

5,6-Dimethyl-2-guanidinebenzimidazole (**VII**)

Yield: 65%. M.p. 167.2-170 °C (m.p. reported in literature 191°C)[181]. Anal. calcd for $C_{10}H_7N_5Cl_2$: C 59.10, H 6.45, N 34.46; found: C 59.16, H 6.74, N 34.73.

10.1.4 Experimental section: synthesis of the anilino-based derivatives.

10.1.4.1 General procedure for the synthesis of compounds 1-10 and 12-13.

In a two-neck flask, to a solution of the proper aniline (2eq.) and dry DMF at r.t., the chloroalkyl derivative hydrochloride (1eq), K_2CO_3 (2eq.) and KI (0.1eq.) were sequentially added; dry DMF was further added and the suspension was stirred and heated at 90°C during 23h: at 90°C the suspension became a solution. After cooling down to room temperature, DCM was added in the flask and the organic layer was then washed three times with water in a separating funnel, dried over anhydrous Na_2SO_4 and filtered, then concentrated *in vacuo* to obtain the crude mixtures as yellow/brown oils.

The crude products were purified by automatic CC (Teledyne Isco) using column: Silica 40g (Flow Rate: 40 ml/min), and gradient elution with Solvent A: hexane and increasing percentage of Solvent B: ethyl acetate yielding the expected products as yellow/transparent oils. The final products were dissolved in EtOAc and converted into the corresponding di- or monohydrochloride salts adding (2eq) of HCl 1N (in ether), kept precipitating overnight then collected by filtration obtaining the desired compounds as beige/white solids.

N-[2-(Piperidin-1-yl)ethyl]-3,5-bis(trifluoromethyl)aniline hydrochloride (**1**)

Yield: 32%. m.p. 170-171°C. IR: ν 3278, 2952, 2733, 2632, 2529, 1697, 1621, 1566, 1473, 1381, 1274, 1168, 1112, 996, 970, 948, 888, 855, 730, 701, 681 cm^{-1}. ^{1}H NMR (400 MHz, CD$_3$OD): δ 7.16 (m, 3H, arom.), 3.64 (t, *J* = 6,4Hz, 2H, -CH$_2$—NH-Ar), 3.60 (dm, 2H, C*H*$_2$ piperidine), 3.35 (t, *J* = 6.4 Hz, 2H, —C*H*$_2$-N-piperidine), 3.03 (td, *J* = 12.4 Hz, *J'* = 2.8 Hz, 2H, C*H*$_2$ piperidine), 1.96 (m, 2H, C*H*$_2$ piperidine), 1.76-1.90 (m, 3H, C*H*$_2$ piperidine), 1.55 (m, 1H, C*H*$_2$ piperidine).

3-Chloro-N-[2-(piperidin-1-yl)ethyl]aniline dihydrochloride (**2**)

Yield: 60%. m.p. 154-156°C. IR: ν 3258, 2930, 2641, 2548, 1593, 1522, 1474, 1426, 1186, 1104, 1080, 1042, 971, 841, 782, 688, 675 cm^{-1}. ^{1}H NMR (400 MHz, DMSO-*d$_6$*): δ 10.85 (s, 1H, NH). 7.08 (t, *J* = 8Hz, 1H, H-arom. superimposed to NH$^+$ signal, H(6)), 7.00-7.20 (broad s, 2H$^+$, NH$^+$), 6.67 (t, *J* = 2Hz, 1H, H-arom., H(2)), 6.60 (m, 2H, H arom., H(4,5)), 3.47 (t, *J* = 6.5 Hz, 2H, -C*H*$_2$—NH-Ar), 3.38-3.44 (dm, 2H, C*H*$_2$ piperidine), 3.10-3.18 (m, 2H, —

CH_2-N-piperidine), 2.81-2.94 (m, 2H, CH_2 piperidine), 1.62-1.92 (m, 5H, CH_2 piperidine), 1.27-1.42 (m, 1H, CH_2 piperidine). ^{13}C NMR (100.5 MHz, DMSO-d_6): 149.5, 134.2, 130.9, 116.5, 112.1, 111.7, 54.7, 52.5 (2C), 37.7, 22.7 (2C), 21.8. Anal calcd. for C$_{13}$H$_{19}$ClN$_2$ · 1.7HCl: C 51.92, H 6.94, N 9.31; found: C 52.02, H 6.94, N 9.19.

N-[2-(Piperidin-1-yl)ethyl]-3-(trifluoromethyl)aniline dihydrochloride (**3**)

Yield: 64%. m.p. 153-154˚C. IR: ν 3053, 2963, 2660, 2560, 2269, 1481, 1457, 1425, 1325, 1169, 1122, 1037, 1001, 961, 916, 860, 803, 738, 696, 659, 636 cm^{-1}. ^{1}H NMR (400 MHz, DMSO-d_6): δ 10.88 (s, 1H, NH), 7.29 (t, *J* = 8Hz, 1H, H-arom.), 6.96-7.22 (broad s, 2H$^+$, NH$^+$), 6.88 (m, 3H, H-arom.), 3.52 (t, *J* = 6.4Hz, 2H, N-CH_2 linker), 3.43 (d, *J* = 12Hz, 2H, CH_2 piperidine), 3.16 (m, 2H, N-CH_2 linker), 2.89 (m, 2H, CH_2 piperidine), 1.62-1.92 (complex signal, 5H, CH_2 piperidine), 1.35 (qt, *J* = 12.5 Hz, *J′* = 4 Hz 1H, CH_2 piperidine). ^{13}C NMR (100.5 MHz, DMSO-d_6): 148.7, 130.4, 126.3, 123.5, 116.2, 112.2, 108.7, 54.7, 52.5 (2C), 37.6, 22.7 (2C), 21.8. Anal calcd. for C$_{14}$H$_{19}$F$_3$N$_2$ · 1.75 HCl: C 50.03, H 6.22, N 8.33; found: C 49.77, H 6.45, N 8.09.

N-[2-(Piperidin-1-yl)ethyl]-3-nitroaniline hydrochloride (**4**)

Yield: 54%. m.p. 183-185˚C. IR: ν 3241, 2930, 2608, 2511, 1623, 1546, 1520, 1455, 1347, 1272, 1200, 1079, 978, 849, 797, 737, 673 cm^{-1}. ^{1}H NMR (400 MHz, DMSO-d_6): δ 10.81 (s, 1H, NH), 7.31-7.40 (complex signal, 3H, H-arom.), 7.08 (ddd, *J* = 7.6 Hz, *J′* = 2.4 Hz, *J′′* = 1.6 Hz, 1H, H-arom.), 5.50 (broad s, 2H$^+$, NH$^+$), 3.55 (t, *J* = 6.4 Hz, 2H, N-CH_2 linker), 3.45 (d, *J* = 12 Hz, 2H, CH_2 piperidine), 3.18 (q, *J* = 6.4 Hz, 2H, N-CH_2 linker), 2.90 (m, 2H, CH_2 piperidine), 1.63-1.91 (complex signal, 5H, CH_2 piperidine), 1.35 (qt, *J* = 12.8 Hz, *J′* = 4 Hz, 1H, CH_2 piperidine). ^{13}C NMR (100.5 MHz, DMSO-d_6): 149.4, 149.3, 130.5, 119.0, 111.0, 106.0, 54.6, 52.5 (2C), 37.6, 22.7 (2C), 21.8. Anal calcd. for C$_{13}$H$_{19}$N$_3$O$_2$ · HCl · 0.2 H$_2$O: C 53.96, H 7.11, N 14.52; found: C 53.82, H 6.86, N 14.74.

3,4-Dichloro-N-[2-(piperidin-1-yl)ethyl]aniline hydrochloride (**5**)

Yield: 60%. m.p. 219-220˚C. IR: ν 3324, 2947, 2647, 2626, 2523, 2125, 1589, 1552, 1474, 1433, 1394, 1385, 1358, 1199, 1131, 1113, 1090, 1034, 1014, 972, 879, 859, 838, 805, 707, 644, 602 cm^{-1}. ^{1}H NMR (400 MHz, DMSO-d_6): δ 10.80 (s, 1H, NH), 7.25 (d, *J* = 8.8 Hz, 1H, H-arom.), 6.83 (d, *J* = 2,4 Hz, 1H arom.), 6.63 (dd, *J* = 8.8 Hz, *J′* = 2.8 Hz, 1H, H-arom.), 5.44 (broad s, 2H$^+$, NH$^+$),3.26-3.55 (complex signal, 4H, 2H N-CH_2 linker and 2H CH_2 piperidine), 3.13 (q, *J* = 6 Hz, 2H, N-CH_2 linker), 2.88 (m, 2H, CH_2 piperidine), 1.60-1.95

(complex signal, 5H, CH_2 piperidine), 1.34 (m, CH_2 piperidine). ^{13}C NMR (100.5 MHz, DMSO-d_6): 148.4, 131.8, 131.0, 117.5, 113.4 (2C), 54.6, 52.5 (2C), 37.6, 22.8 (2C), 21.8. Anal calcd. for C$_{13}$H$_{19}$ClN$_2$ · 1.5HCl: C 47.62, H 5.99, N 8.54; found: C 47.26, H 5.99, N 8.45.

4-Methyl-N-[2-(piperidin-1-yl)ethyl]aniline dihydrochloride (6)

Yield: 69%. m.p. 177-179°C. IR: ν 639, 706, 747, 769, 814, 870, 956, 971, 1005, 1026, 1106, 1196, 1226, 1293, 1323, 1391, 1458, 1471, 1514, 2370, 2481, 2610, 2943 cm^{-1}. ^{1}H NMR (400 MHz, DMSO-d_6): δ 10.87 (s, 1H, NH), 7.18 (s, 4H, H-arom.), 6.64 (broad s, 2H$^+$, NH$^+$),3.65 (t, J = 6.8 Hz, 2H, N-CH_2 linker), 3.26-3.45 (pseudo s, 2H, CH_2 piperidine), 3.35 (t, J = 6.8 Hz, 2H, N-CH_2 linker), 2.93 (pseudo s, 2H, CH_2 piperidine), 2.25 (s, 3H, p-CH_3), 1.59-1.90 (complex signal, 5H, CH_2 piperidine), 1.37 (pseudo s, CH_2 piperidine). ^{13}C NMR (100.5 MHz, DMSO-d_6): δ 138.2, 130.4, (3C), 119.5 (2C), 53.2, 52.9 (2C), 42.3, 22.8 (2C), 21.6, 20.8. Anal calcd. for C$_{13}$H$_{19}$ClN$_2$ · 2HCl: C 57.73, H 8.31, N 9.62; found: C 57.80, H 8.37, N 9.64.

4-Methoxy-N-[2-(piperidin-1-yl)ethyl]aniline dihydrochloride (7)

Yield: 65%. m.p. 151.5-153.3°C. IR: ν 635, 702, 723, 819, 838, 926, 970, 989, 1032, 1083, 1103, 1179, 1223, 1251, 1275, 1306, 1332, 1456, 1510, 1561, 1602, 2468, 2604, 2941, 2996 cm^{-1}. ^{1}H NMR (400 MHz, DMSO-d_6): δ 10.88 (s, 1H, NH), 7.41 (d, J = 8.8 Hz, 2H, CH-arom.), 7.02 (dt, J = 8.8 Hz, J' = 3.6 Hz, 2H, CH-arom.), 3.74 (s, 3H, O-CH_3), 3.70 (t, J = 6.8 Hz, 2H, N-CH_2 linker), 3,47 (pseudo s, 2H, CH_2 piperidine), 3.41 (t, J = 6.8 Hz, 2H, N-CH_2 linker, superimposed CH_2 piperidine signal), 2.96 (pseudo s, 2H, CH_2 piperidine), 1.23-1.91 (complex signal, 6H, CH_2 piperidine). ^{13}C NMR (100.5 MHz, DMSO-d_6): δ 158.3, 122.8, 115.4 (4C), 56.0, 53.0 (2C), 52.7 (2C) 43.9, 22.8 (2C), 21.6. Anal calcd. for C$_{14}$H$_{22}$N$_2$O · 2HCl · 0.5H$_2$O: C 53.17, H 7.97, N 8.86; found: C 53.06, H 7.78, N 8.72.

3,5-Dichloro-N-[2-(pyrrolidin-1-yl)ethyl]aniline dihydrochloride (8)

Yield: 13% m.p. 147-150°C. IR: ν 671, 806, 849, 937, 983, 1093, 1119, 1136, 1285, 1311, 1433, 1454, 1480, 1527, 1589, 2488, 2593, 2954, 3060, 3264 cm^{-1}. ^{1}H NMR (400 MHz, DMSO-d_6): δ 10.98 (s, 1H, NH), 6.64 (s, 3H, CH-arom.), 4.31 (broad s, 2H+, NH+), 3.54 (m, 2H, N-CH_2 pyrrolidine), 3.45 (t, J = 6 Hz, 2H, N-CH_2 linker), 3.24 (q, J = 11.6 Hz, J' = 6 Hz, 2H, N-CH_2 linker), 2.97 (m, 2H, CH_2 pyrrolidine), 1.74-2.03 (complex signal, 4H, CH_2 pyrrolidine). ^{13}C NMR (100.5 MHz, DMSO-d_6): δ 150.6, 135.0 (2C), 115.5, 110.8 (2C), 53.4, 52.6, 39.0, 23.0 (2C). Anal calcd. for C$_{12}$H$_{16}$Cl$_2$N$_2$ · 2HCl · 3.5 H$_2$O: C 36.47, H 6.38, N 7.09; found: C 36.25, H 6.13, N 6.75.

N-[2-(Azepan-1-yl)ethyl]-3,5-dichloroaniline hydrochloride (9)

Yield: 76%. m.p. 177-179°C. IR: ν 674, 802, 827, 841, 867, 881, 926, 991, 1002, 1043, 1082, 1091, 1116, 1139, 1324, 1389, 1431, 1454, 1478, 1531, 1593, 2424, 2522, 2600, 2618, 2700, 2942, 3058, 3271 cm^{-1}. ^{1}H NMR (400 MHz, DMSO-d_6): δ 10.85 (s, 1H, NH), 6.65 (d, J = 1.6 Hz, 1H, CH-arom.), 6.63 (t, J = 1.6 Hz, 1H, CH-arom.), 6.46 (broad s, 2H$^+$, NH$^+$), 3.48 (t, J = 6 Hz, 2H, N-CH_2 linker), 3.36 (m, 2H, N-CH_2 azepine), 3.19 (q, J = 12 Hz, J' = 6.4 Hz, 2H, N-CH_2 linker), 3.10 (m, 2H, CH_2 azepine), 1.71-1.94 (complex signal, 4H, CH_2 azepine), 1.64 (m, 2H, CH$_2$ azepine), 1.54 (m, 2H, CH$_2$ azepine). ^{13}C NMR (100.5 MHz, DMSO-d_6): δ 150.6, 134.9 (2C), 115.4, 110.8 (2C), 55.0, 54.1 (2C), 37.8, 26.4 (2C), 23.2. Anal calcd. for C$_{14}$H$_{20}$Cl$_2$N$_2$ · HCl: C 51.95, H 6.54, N 8.65; found: C 51.76, H 6.50, N 8.53.

3,5-Dichloro-N-[2-(piperidin-1-yl)propyl]aniline dihydrochloride (10)

Yield: 12%. m.p. 180-182°C. IR: ν 626, 675, 757, 805, 860, 947, 958, 1003, 1021, 1102, 1117, 1195, 1211, 1295, 1433, 1469, 1516, 1591, 2409, 2558, 2645, 2943, 3287 cm^{-1}. ^{1}H NMR (400 MHz, DMSO-d_6): δ 10.60 (s, 1H, NH), 6.58 (pseudo s, 3H, CH arom.), 5.87 (broad s, 2H$^+$, NH$^+$), 3.34 (d, J = 12.4 Hz, 2H, N-CH_2 piperidine), 2.99-3.10 (complex signal, 4H, N-CH_2 linker), 2.80 (m, 2H, CH$_2$ piperidine), 1.94 (m, 2H, CH_2 linker), 1.60-1.87 (complex signal, 5H, CH_2 piperidine), 1.34 (m, 1H, CH$_2$ piperidine). ^{13}C NMR (100.5 MHz, DMSO-d_6): δ 151.1, 134.8 (2C), 114.8, 110.6 (2C), 54.3, 52.4 (2C), 40.2, 23.0, 22.6 (2C), 21.8. Anal calcd. for C$_{14}$H$_{20}$Cl$_2$N$_2$ · 2HCl · 0.5H$_2$O: C 45.55, H 6.28, N 7.59; found: C 45.37, H 6.27, N 7.35.

3-Chloro-5-methyl-N-[2-(piperidin-1-yl)ethyl]aniline dihydrochloride (12)

Yield: 68%. m.p. 183-185°C. IR: ν 606, 678, 687, 845, 857, 880, 904, 959, 971, 996, 1042, 1061, 1092, 1120, 1198, 1387, 1398, 1427, 1439, 1465, 1481, 1586, 1622, 1699, 2129, 2541, 2631, 2646 cm^{-1}. ^{1}H NMR (400 MHz, DMSO-d_6): δ 10.86 (s, 1H, NH), 8.03 (broad s, 2H$^+$, NH$^+$), 6.50 (t, J = 2 Hz, 1H, CH arom., H(4)), 6.44 (d, J = 2.2 Hz, 2H, CH arom., H(2,6)), 3.45 (t, J = 6.4 Hz, 2H, N-CH_2 linker, superimposed), 3.41 (d, J = 12.8 Hz, 2H, CH$_2$ piperidine, superimposed), 3.13 (m, 2H, CH_2 linker), 2.88 (m, 2H, CH$_2$ piperidine), 2.16 (s, 3H, arom-CH$_3$), 1.61-1.92 (complex signal, 5H, CH_2 piperidine), 1.34 (dt, J = 12.8 Hz, J' = 3.6 Hz, 1H, CH$_2$ piperidine). ^{13}C NMR (100.5 MHz, DMSO-d_6): δ 149.1, 140.7, 133.9, 117.6, 112.4, 109.7, 54.7, 52.5 (2C), 37.8, 22.7 (2C), 21.8, 21.4. Anal calcd. for C$_{14}$H$_{21}$ClN$_2$ · 2HCl: C 51.63, H 7.12, N 8.60; found: C 51.57, H 7.09, N 8.36.

3-(pentafluoro-^{6}-sulfaneyl)-N-(2-(piperidin-1-yl)ethyl)aniline hydrochloride (13)

Yield: 17%. m.p. 183-185˚C. IR: ν 644, 684, 777, 806, 827, 845, 906, 949, 963, 1010, 1272, 1309, 1339, 1346, 1456, 1480, 1535, 1610, 1671, 2541, 2636, 2936, 2957, 3270 cm^{-1}. ^{1}H NMR (400 MHz, DMSO-d_6): δ 10.68 (s, 1H, NH), 7.30 (t, J = 8 Hz, 1H, CH arom., H(5)), 7.04 (t, J = 2 Hz, 1H, CH arom., H(2)), 7.00 (dd, J = 8 Hz, J' = 2 Hz, 1H, CH arom., H(6)), 6.90 (m, 1H, CH arom., H(4)), 6.68 (broad s, 2H$^+$, NH$^+$), 3.51 (m, 2H, N-CH_2 linker), 3.44 (m, 2H, CH$_2$ piperidine), 3.15 (m, 2H, CH_2 linker), 2.88 (m, 2H, CH$_2$ piperidine), 1.60-1.93 (complex signal, 5H, CH_2 piperidine), 1.35 (m, 1H, CH$_2$ piperidine). ^{13}C NMR (100.5 MHz, DMSO-d_6): δ 148.9, 134.4, 130.2, 115.5, 113.3, 109.7, 54.7, 52.5 (2C), 37.6, 22.7 (2C), 21.8. Anal calcd. for $C_{13}H_{19}F_5N_2S \cdot HCl$: C 42.57, H 5.50, N 7.64; found: 42.86, 5.51, 7.30.

10.1.4.2 General procedure for the synthesis of compounds 11 and 14

Sodium hydroxide (20 mmol, 2eq) was refluxed in ethanol (150 mL) for 30 minutes. To the resulting solution (10 mmol, 1eq), the required phenol or thiophenol was added and the resulting mixture further refluxed for 1h. Then a solution of 1-(2-chloroethyl)piperidine hydrochloride (10 mmol, 1eq) in 35 mL of EtOH was added to the basic solution and the reaction mixture was refluxed for further 3h. The reaction mixture was cooled down and poured into 125 mL of cold water then extracted four times with DCM. The organic layer was then washed four times with water, dried over anhydrous Na$_2$SO$_4$, filtered and concentrated *in vacuo*, obtaining the crude product as a transparent oil. The crude product was purified by automatic CC (Teledyne Isco®) using column: Silica 40g (Flow Rate: 40 ml/min), and gradient elution with Solvent A: hexane and increasing percentage of Solvent B: ethyl acetate. The fractions containing the expected product were concentrated *in vacuo* to obtain the final product as a transparent oil. The oils were dissolved in EtOAc then converted into the corresponding hydrochloride salts adding (1eq) of HCl 1N (ether).

1-[2-(3,5-Dichlorophenoxy)ethyl]piperidine hydrochloride (11)

Yield 82%. m.p. 196.3-198˚C. IR: ν 633, 675, 799, 829, 857, 883, 911, 957, 978, 1015, 1038, 1073, 1108, 1221, 1260, 1301, 1380, 1424, 1445, 1477, 1572, 1757, 2506, 2585, 2617, 2927, 2949, 2992, 3051, 3293 cm^{-1}. ^{1}H NMR (400 MHz, DMSO-d_6): δ 11.02 (s, 1H, NH), 7.18 (t, J = 1.8 Hz, 1H, CH arom., H(4)), 7.11 (d, J = 1.8 Hz, 2H, CH arom., H(2,6)), 4.48 (t, J = 5.1 Hz, 2H, O-CH_2 linker), 3.36-3.49 (complex signal, 4H, 2H N-CH_2 linker and 2H CH_2 piperidine), 2.95 (m, 2H, CH$_2$ piperidine), 1.61-1.91 (complex signal, 5H, CH_2 piperidine),

1.35 (m, 1H, CH_2 piperidine). ^{13}C NMR (100.5 MHz, DMSO-d_6): δ 159.4, 135.1 (2C), 121.4, 114.6 (2C), 63.6, 54.7, 52.9 (2C), 22.7 (2C), 21.6. Anal calcd. for C$_{13}$H$_{17}$Cl$_2$NO · HCl: C 50.26, H 5.84, N 4.51; found: C 50.29, H 5.61, N 4.36.

1-[2-[(3,5-Dichlorophenyl)thio]ethyl]piperidine hydrochloride (14)

Yield: 90%. m.p. 201-202°C. IR: ν 661, 720, 783, 802, 848, 862, 888, 906, 966, 988, 1002, 1109, 1152, 1196, 1208, 1293, 1321, 1378, 1401, 1424, 1442, 1473, 1559, 1570, 2224, 2245, 2499, 2604, 2662, 2949, 3045, 3207 cm^{-1}. ^{1}H NMR (400 MHz, DMSO-d_6): δ 11.11 (s, 1H$^+$, NH$^+$), 7.48 (d, J = 1.8 Hz, 2H, CH arom.), 7.42 (t, J = 1.8 Hz, 1H, CH arom.), 3.54 (m, 2H, S-CH_2 linker), 3.46 (d, J = 11.6 Hz, 2H, N-CH_2 piperidine), 3.17 (m, 2H, N-CH_2 linker), 2.85 (m, 2H, CH$_2$ piperidine), 1.63-1.85 (complex signal, 5H, CH_2 piperidine), 1.34 (m, 1H, CH$_2$ piperidine). ^{13}C NMR (100.5 MHz, DMSO-d_6): δ 139.6, 135.1 (2C), 126.1, 125.9 (2C), 54.5, 52.2 (2C), 25.3 (2C), 22.8, 21.8. Anal calcd. for C$_{13}$H$_{17}$Cl$_2$NS · HCl: C 47.79, H 5.55, N 4.29; C 47.95, H 5.29, N 4.14.

10.1.5 Experimental section: synthesis of the benzenesulfonamides.

10.1.5.1 General method for the synthesis of compounds 15-27.

In a 100 mL two-necks round bottom flask, 0,20 mL of the key amine were dissolved in 10 anhydrous DCM; 0.20 mL of Et_3N were added then the solution was cooled down to 0°C in an ice bath. A solution of the opportune benzene sulfonyl chloride in 5 mL anhydrous DCM was slowly added, then the ice bath was removed and the mixture was left stirring at room temperature for 5h.

The crude mixture was purified by flash chromatography (silica/DCM:0-2%MeOH) or (silica/hexane:0-50%EtOAc) in the case of compounds **15** and **16**, affording the final compounds as light-yellow transparent oils. Compounds **15**, **18**, **22**, **26**, were crystallised from ether/hexane while compounds **16**, **17**, **19**-**21**, **23**-**25**, **27** and a small portion of compound 18, were converted into the corresponding monohydrochloride salts with 1.5 eq. of HCl 1N in MeOH.

4-Bromo-N-(2-(piperidin-1-yl)ethyl)benzenesulfonamide (**15**)[191].

Yield: 60%. m.p. 94-95°C. IR: ν 3278, 2936, 2858, 2726, 1575, 1466, 1410, 1389, 1342, 1318, 1277, 1251, 1207, 1156, 1127, 1090, 1065, 1010, 964, 869, 835, 820, 758, 736, 704, 612 cm^{-1}. ^{1}H NMR (400 MHz, CDCl$_3$): δ 7.74 (d, J = 8.7 Hz, 2H, H(3,5)arom.), 7.66 (d, J = 8.8 Hz, 2H, H(2,6)arom.), 2.97 (t, J = 5.8 Hz, 2H, SO$_2$NH—C$\underline{H_2}$), 2.35 (t, J = 5.8 Hz, 2H, —CH$_2$C$\underline{H_2}$—N piperidine), 2.20 (pseudo s, 4H, N-C$\underline{H_2}$ piperidine), 1.48 (t, J = 4.8 Hz, 4H, C$\underline{H_2}$— piperidine), 1.41 (pseudo s, 2H, C$\underline{H_2}$— piperidine). ^{13}C NMR (100.5 MHz, CDCl$_3$): δ 138.77, 132.28 (2C), 128.65 (2C), 127.43, 56.06, 53.86 (2C), 39.27, 25.87 (2C), 24.17. Anal. calcd. for C$_{13}$H$_{19}$BrN$_2$O$_2$S · 0.1 H$_2$O · 0.1 C$_6$H$_{14}$: C, 45.67; H, 5.80; N, 7.83; found: 45.67; H, 5.76; N, 7.87.

3-(Trifluoromethyl)-N-(2-(piperidin-1-yl)ethyl)benzenesulfonamide hydrochloride (**16**)[182].

Yield: 42%. m.p. 174-176°C. IR: ν 3046, 2947, 2856, 2621, 2537, 1610, 1440, 1325, 1310, 1159, 1124, 1104, 1069, 1042, 1009, 967, 906, 863, 820, 803, 777, 728, 690, 652, 606 cm^{-1}. ^{1}H NMR as free base (400 MHz, CDCl$_3$): δ 8.16 – 8.12 (m, 1H, H(2)arom.), 8.07 (ddq, J = 7.8, 1.7, 0.5 Hz, 1H, H(6)arom.), 7.84 (m, 1H, H(4)arom.), 7.68 (tt, J = 7.9, 0.6 Hz, 1H,

H(5)arom.), 2.99 (t, J = 5.8 Hz, 2H, SO$_2$NH—C$\underline{H_2}$), 2.40-2.30 (m, 2H, ,—CH$_2$C$\underline{H_2}$—N piperidine), 2.19 (pseudo s, 4H, N-C$\underline{H_2}$ piperidine), 1.48 (p, J = 5.5 Hz, 4H, C$\underline{H_2}$— piperidine), 1.44-1.35 (m, 2H, C$\underline{H_2}$— piperidine). Anal. calcd. for C$_{13}$H$_{19}$BrN$_2$O$_2$S: C, 45.10; H, 5.41; N, 7.51; found: 45.37; H, 5.68; N, 7.47.

3,5-Dichloro-N-(2-(piperidin-1-yl)ethyl)benzenesulfonamide (17)

Yield: 85%. m.p. (hydrochloride) 188-189°C. IR (hydrochloride): ν 3038, 2956, 2861, 2645, 2554, 1765, 1570, 1445, 1415, 1387, 1339, 1329, 1294, 1248, 1199, 1160, 1139, 1096, 999, 958, 946, 872, 863, 841, 799, 766, 668 cm^{-1}. ^{1}H NMR (400 MHz, CDCl$_3$): δ 7.75 (d, J = 1.9 Hz, 2H, H(2,6)arom.), 7.55 (t, J = 1.9 Hz, 1H, H(4)arom.), 3.00 (t, J = 5.6 Hz, 2H, SO$_2$NH—C$\underline{H_2}$), 2.37 (t, J = 5.8 Hz, 2H, —CH$_2$C$\underline{H_2}$—N piperidine), 2.22 (pseudo s, 4H, N-C$\underline{H_2}$ piperidine), 1.51 (p, J = 5.5 Hz, 4H, C$\underline{H_2}$—piperidine), 1.42 (d, J = 5.2 Hz, 2H, C$\underline{H_2}$—piperidine). ^{13}C NMR (100.5 MHz, CDCl$_3$): δ 142.75, 136.01 (2C), 132.48, 125.48 (2C), 55.92, 53.90 (2C), 39.31, 25.89 (2C), 24.18. Anal. calcd for C$_{13}$H$_{19}$Cl$_3$N$_2$O$_2$S: C 41.78, H 5.12, N 7.50; found: C 42.02, H 5.27, N 7.43.

3-Bromo-N-(2-(piperidin-1-yl)ethyl)benzenesulfonamide (18)

Yield: 94%. m.p. 47-48.5°C. IR (hydrochloride): ν 3040, 2956, 2865, 2646, 2553, 1770, 1758, 1570, 1446, 1414, 1386, 1340, 1329, 1293, 1248, 1167, 1139, 1096, 998, 958, 884, 863, 841, 797, 675, 657 cm^{-1}. ^{1}H NMR (400 MHz, CDCl$_3$): δ 8.02 (t, J = 1.8 Hz, 1H, H(2)arom.), 7.81 (ddd, J = 7.8, 1.7, 1.0 Hz, 1H, H(6)arom.), 7.70 (ddd, J = 8.0, 1.9, 1.0 Hz, 1H, H(4)arom.), 7.40 (t, J = 7.9 Hz, 1H, H(5)arom.), 3.00 (t, J =5.7 Hz, 2H, SO$_2$NH—C$\underline{H_2}$), 2.37 (t, J = 5.7 Hz, 2H, ,—CH$_2$C$\underline{H_2}$—N piperidine), 2.23 (pseudo s, 4H, N-C$\underline{H_2}$ piperidine), 1.51 (p, J = 5.5 Hz, 4H, C$\underline{H_2}$—piperidine), 1.46 – 1.35 (m, 2H, C$\underline{H_2}$—piperidine). ^{13}C NMR (100.5 MHz, CDCl$_3$): δ 141.58, 135.55, 130.52, 129.97, 125.61, 123.04, 56.03, 53.89 (2C), 39.25, 25.79 (2C), 24.10. Anal. calcd for C$_{13}$H$_{19}$BrN$_2$O$_2$S · HCl: C 40.69, H 5.25, N 7.30; found: C 40.70, H 5.21, N 6.74. The melting point, ^{1}H and ^{13}C spectra have been obtained from the free base.

3-Nitro-N-(2-(piperidin-1-yl)ethyl)benzenesulfonamide (19)

Yield: 86%. m.p. (hydrochloride) 167-168°C. IR (hydrochloride): ν 3083, 2947, 2723, 2692, 2649, 1608, 1532, 1421, 1400, 1351, 1172, 1123, 1069, 1011, 988, 957, 907, 880, 808, 764, 734, 698, 670 cm^{-1}. ^{1}H NMR (400 MHz, CDCl$_3$): δ 8.72 (t, J = 2.0 Hz, 1H, H(2)arom.), 8.44 (ddd, J = 8.0, 2.2, 1.2 Hz, 1H, H(4)arom.), 8.22 (ddd, J = 7.8, 1.7, 1.1 Hz, 1H, H(6)arom.), 7.76 (t, J = 8.0 Hz, 1H, H(5)arom.), 3.90 (broad s, 2H, NH and NH$^+$), 3.04 (t, J = 5.8 Hz, 2H,

SO$_2$NH—C$\underline{H_2}$), 2.39 (t, J = 5.7 Hz, 2H, ,—CH$_2$C$\underline{H_2}$—N piperidine), 2.23 (pseudo s, 4H, N—C$\underline{H_2}$ piperidine), 1.49 (p, J = 5.5 Hz, 4H, —C$\underline{H_2}$ piperidine), 1.45 – 1.35 (m, 2H, —C$\underline{H_2}$ piperidine). ^{13}C NMR (100.5 MHz, CDCl$_3$): δ 148.30, 142.22, 132.59, 130.44, 126.98, 122.25, 56.18, 53.93 (2C), 39.37, 25.78 (2C), 24.11. Anal. calcd for C$_{13}$H$_{19}$N$_3$O$_4$S · HCl: C 44.63, H 5.76, N 12.01; found: C 44.84, H 5.96, N 11.87.

3-Bromo-N-(2-(piperidin-1-yl)ethyl)-5-(trifluoromethyl)benzensulfonamide (**20**)

Yield: 53%. m.p. (hydrochloride) 204-205˚C. IR (hydrochloride): ν 3044, 2943, 2617, 2529, 1429, 1333, 1306, 1187, 1160, 1136, 1098, 1010, 955, 933, 889, 836, 782, 688, 636 cm^{-1}. ^{1}H NMR (400 MHz, CDCl$_3$): δ 8.22-8.18 (m, 1H, H(6)arom.), 8.12 – 8.02 (m, 1H, H(2)arom.), 7.97 – 7.92 (m, 1H, H(4)arom.), 3.02 (t, J = 5.8 Hz, 2H, SO$_2$NH—C$\underline{H_2}$), 2.39 (t, J = 5.8 Hz, 2H, ,—CH$_2$C$\underline{H_2}$—N piperidine), 2.24 (pseudo s, 4H, N—C$\underline{H_2}$ piperidine), 1.51 (p, J = 5.5 Hz, 4H, —C$\underline{H_2}$ piperidine), 1.46 – 1.35 (m, 2H, —C$\underline{H_2}$ piperidine). ^{13}C NMR (100.5 MHz, CDCl$_3$): δ 142.95, 133.28, 132.24, 123.64, 122.66, 120.95, 55.98, 53.92 (2C), 42.66, 39.28, 25.78 (2C), 24.10. Anal. calcd for C$_{14}$H$_{18}$BrF$_3$N$_2$O$_2$S · HCl: C 37.22, H 4.24, N 6.20; found: C 37.56, H 4.57, N 6.14.

3-Fluoro-N-(2-(piperidin-1-yl)ethyl)benzenesulfonamide (**21**)

Yield: 86%. m.p. (hydrochloride) 185-186˚C. IR (hydrochloride): ν 3059, 2955, 2854, 2648, 1590, 1471, 1419, 1328, 1304, 1271, 1225, 1153, 1122, 1085, 1073, 1010, 987, 956, 906, 888, 874, 819, 786, 754, 713, 677 cm^{-1}. ^{1}H NMR (400 MHz, CDCl$_3$): δ 7.67 (ddd, J = 7.8, 1.7, 1.0 Hz, 1H, H(2)arom.), 7.58 (dddd, J = 8.2, 1.8, 0.4 Hz, 1H, H(6)arom.), 7.51 (tdd, J = 8.2, 5.2, 0.4 Hz, 1H, H(3)arom.), 7.28 (tdd, J =8.4, 2.8, 1.0 Hz, 1H, H(4)arom.), 2.99 (t, J = 5.8 Hz, 2H, SO$_2$NH—C$\underline{H_2}$), 2.35 (t, J = 5.8 Hz, 2H, ,—CH$_2$C$\underline{H_2}$—N piperidine), 2.19 (pseudo s, 4H, N—C$\underline{H_2}$ piperidine), 1.48 (p, J = 5.5 Hz, 4H, —C$\underline{H_2}$ piperidine), 1.43 – 1.36 (m, 2H, —C$\underline{H_2}$ piperidine). ^{13}C NMR (100.5 MHz, CDCl$_3$): δ 162.47, 141.83, 130.82, 122.82, 119.60, 114.47, 56.05, 53.85 (2C), 39.32, 25.84 (2C), 24.16. Anal. calcd for C$_{13}$H$_{19}$FN$_2$O$_2$S · HCl: C 48.37, H 6.24, N 8.68; found: C 48.73, H 6.59, N 8.56.

3,5-Difluoro-N-(2-(piperidin-1-yl)ethyl)benzenesulfonamide (**22**)

Yield: 90%. m.p. 61-62˚C. IR: ν 3307, 3091, 2940, 2847, 2632, 1604, 1439, 1416, 1328, 1294, 1155, 1124, 1087, 1039, 987, 964, 873, 861, 812, 757, 673, 620 cm^{-1}. ^{1}H NMR (400 MHz, CDCl$_3$): δ 7.43 – 7.40 (m, 2H, H(2,6)arom.), 7.03 (tt, J = 8.5, 2.3 Hz, 1H, H(4)arom.), 3.05 – 3.01 (t, J = 5.8 Hz, 2H, SO$_2$NH—C$\underline{H_2}$CH$_2$—), 2.44 – 2.39 ((t, J = 5.8 Hz, 2H,—CH$_2$C$\underline{H_2}$—N

piperidine), 2.27 (pseudo s, 4H, N—C$\underline{H_2}$ piperidine), 1.53 (p, J = 5.6 Hz, 4H, —C$\underline{H_2}$ piperidine), 1.43 (m, 2H, —C$\underline{H_2}$ piperidine). ^{13}C NMR (100.5 MHz, CDCl$_3$): δ 164.08, 161.54, 143.23, 110.59 (2C), 108.08, 56.14, 53.94 (2C), 39.21, 25.68 (2C), 24.04. Anal. calcd for C$_{13}$H$_{18}$F$_2$N$_2$O$_2$S: C 51.30, H 5.96, N 9.20; found: C 51.31, H 6.13, N 9.06.

3-Fluoro-N-(2-(piperidin-1-yl)ethyl)-5-(trifluoromethyl)benzenesulfonamide (23)

Yield: 91%. m.p. (hydrochloride) 164-165°C. IR (hydrochloride): ν 3018, 2950, 2859, 2641, 2552, 1599, 1442, 1332, 1217, 1183, 1156, 1096, 1079, 995, 959, 934, 883, 868, 842, 696, 672, 640, 604 cm^{-1}. ^{1}H NMR (400 MHz, CDCl$_3$): δ 7.94 (pseudo s, 1H, H(6)arom.), 7.79 (dt, J = 7.6, 1.6 Hz, 1H, H(2)arom.), 7.54 (d, J = 8 Hz, 1H, H(4)arom.), 3.02 (t, J = 5.8 Hz, 2H, SO$_2$NH—C$\underline{H_2}$), 2.38 (t, J = 5.6 Hz, 2H, ,—CH$_2$C$\underline{H_2}$—N piperidine), 2.23 (pseudo s, 4H, N—C$\underline{H_2}$ piperidine), 1.50 (p, J = 5.5 Hz, 4H, —C$\underline{H_2}$ piperidine), 1.45 – 1.39 (m, 2H, —C$\underline{H_2}$ piperidine). ^{13}C NMR (100.5 MHz, CDCl$_3$): δ 163.54, 161.01, 143.57, 119.78, 117.96, 116.90, 56.00, 53.89 (2C), 39.31, 25.78 (2C), 24.12. Anal. calcd for C$_{14}$H$_{18}$F$_4$N$_2$O$_2$S · HCl: C 54.38, H 3.95, N 4.23; found: C 54.56, H 4.13, N 4.13.

N-(2-(Piperidin-1-yl)ethyl)-3,5-bis(trifluoromethyl)benzenesulfonamide (24)

Yield: 93%. m.p. (hydrochloride) 203-205°C. IR (hydrochloride): ν 3030, 2948, 2639, 2619, 2537, 1627, 1417, 1359, 1335, 1320, 1275, 1200, 1179, 1160, 1127, 1097, 1010, 995, 956, 934, 905, 838, 771, 728, 697, 678, 624 cm^{-1}. ^{1}H NMR (400 MHz, CDCl$_3$): δ 8.82 – 8.29 (m, 2H, H(2,6)arom), 8.07 (pseudo s, 1H, H(4)arom.), 3.04 (t, J = 5.8 Hz, 2H, SO$_2$NH—C$\underline{H_2}$), 2.47 (t, J = 5.8 Hz, 2H, ,—CH$_2$C$\underline{H_2}$—N piperidine), 2.24 (pseudo s, 4H, N—C$\underline{H_2}$ piperidine), 1.50 (p, J = 5.5 Hz, 4H, —C$\underline{H_2}$ piperidine), 1.45 – 1.38 (m, 2H, —C$\underline{H_2}$ piperidine). ^{13}C NMR (100.5 MHz, CDCl$_3$): δ 142.93, 132.93 (2C), 127.33 (2C), 126.05, 123.82, 121.10, 55.99, 53.89 (2C), 39.29, 25.74 (2C), 24.09. Anal. calcd for C$_{15}$H$_{18}$F$_6$N$_2$O$_2$S · HCl · 0.1 C$_6$H$_{14}$: C 41.69, H 4.57, N 6.23; found: C 41.31, H 4.90, N 6.25.

3-Chloro-N-(2-(piperidin-1-yl)ethyl)benzenesulfonamide (25)

Yield: 88%. m.p. (hydrochloride) 175-176°C. IR (hydrochloride): ν 3066, 2952, 2861, 2649, 2580, 2539, 1579, 1456, 1415, 1343, 1320, 1293, 1243, 1203, 1168, 1154, 1123, 1074, 1010, 986, 958, 893, 828, 787, 700, 677, 669 cm^{-1}. ^{1}H NMR (400 MHz, CDCl$_3$): δ 7.87 (td, J = 1.8, 0.4 Hz, 1H, H(2)arom.), 7.77 (ddd, J = 7.7, 1.7, 1.1 Hz, 1H, H(6)arom.), 7.55 (ddd, J = 8.0, 2.0, 1.1 Hz, 1H, H(4)arom.), 7.49 – 7.43 (td, J = 8.0, 0.4 Hz, 1H, H(5)arom.), 3.00 (t, J = 5.8 Hz, 2H, SO$_2$NH—C$\underline{H_2}$), 2.38 (t, J = 5.8 Hz, 2H, —CH$_2$C$\underline{H_2}$—N piperidine), 2.23 (pseudo

s, 4H, N—C$\underline{H}_2$ piperidine), 1.51 (p, J = 5.5 Hz, 4H, —C$\underline{H}_2$ piperidine), 1.44 – 1.33 (m, 2H, —C$\underline{H}_2$ piperidine). ^{13}C NMR (100.5 MHz, CDCl$_3$): δ 141.46, 135.26, 132.65, 130.32, 127.17, 125.18, 56.08, 53.90 (2C), 39.25, 25.74 (2C), 24.08. Anal. calcd for C$_{13}$H$_{19}$ClN$_2$O$_2$S · HCl: C 46.02, H 5.94, N 8.26; found: C 46.27, H 5.89, N 8.13.

3-Bromo-5-chloro-N-(2-(piperidin-1-yl)ethyl)benzenesulfonamide (**26**)

Yield: 78%. m.p. 74-75˚C. IR: ν 3090, 3035, 2928, 2851, 2805, 1562, 1494, 1445, 1411, 1333, 1295, 1271, 1210, 1152, 1126, 1095, 1066, 1042, 1028, 989, 879, 858, 782, 759, 664 cm^{-1}. ^{1}H NMR (400 MHz, CDCl$_3$): δ 7.90 (t, J = 1.6 Hz, 1H, H(2)arom.), 7.79 (t, J = 1.6 Hz, 1H, H(6)arom.), 7.70 (t, J = 1.8 Hz, 1H, H(4)arom.), 3.00 (t, J = 5.8 Hz, 2H, SO$_2$NH—C$\underline{H}_2$), 2.37 (t, J = 5.8 Hz, 2H, —CH$_2$C$\underline{H}_2$—N piperidine), 2.23 (pseudo s, 4H, N—C$\underline{H}_2$ piperidine), 1.52 (p, J = 5.5 Hz, 4H, —C$\underline{H}_2$ piperidine), 1.45 – 1.17 (m, 2H, —C$\underline{H}_2$ piperidine). ^{13}C NMR (100.5 MHz, CDCl$_3$): δ 142.88, 136.10, 135.25, 128.26, 125.92, 123.44, 55.95, 53.92 (2C), 39.31, 25.88 (2C), 24.17. Anal. calcd for C$_{13}$H$_{18}$BrClN$_2$O$_2$S: C 40.91, H 4.75, N 7.34; found: C 41.29, H 4.79, N 7.21.

3-Cyano-N-(2-(piperidin-1-yl)ethyl)benzenesulfonamide (**27**)

Yield: 52%. m.p. (hydrochloride) 176-177˚C. IR (hydrochloride): ν 3040, 2967, 2946, 2828, 2681, 2648, 2587, 2234, 1476, 1456, 1450, 1433, 1337, 1207, 1156, 1098, 1030, 967, 912, 855, 800, 760, 685 cm^{-1}. ^{1}H NMR (400 MHz, CDCl$_3$): δ δ 8.18 (t, J = 1.5 Hz, 1H, H(2)arom.), 8.13 (dd, J = 7.9, 1.5 Hz, 1H, H(6)arom.), 7.86 (dt, J = 7.8, 1.4 Hz, 1H, H(4)arom.), 7.68 (t, J = 7.9 Hz, 1H, H(5)arom.), 3.06 (t, J = 5.9 Hz, 2H, SO$_2$NH—C$\underline{H}_2$), 2.48 (t, J = 5.8 Hz, 2H, —CH$_2$C$\underline{H}_2$—N piperidine), 2.34 (pseudo s, 4H, N—C$\underline{H}_2$ piperidine), 1.57 (p, J = 5.6 Hz, 4H, —C$\underline{H}_2$ piperidine), 1.49-1.41 (m, 2H, —C$\underline{H}_2$ piperidine). ^{13}C NMR (100.5 MHz, CDCl$_3$): δ 141.69, 135.65, 131.04, 131.64, 130.17, 117.16, 113.62, 56.37, 54.01 (2C), 39.16, 25.42 (2C), 23.83. Anal. calcd for C$_{14}$H$_{19}$N$_3$O$_2$S · HCl: C 50.98, H 6.11, N 12.74; found: C 51.05, H 6.24, N 12.54.

10.1.6 Experimental section: synthesis of the (thio)semicarbazone and hydrazone derivatives.

10.1.6.1 General procedure for the preparation of thiosemicarbazones 1-9, 18, 19, 21, 22.

To a solution of the proper 5-acetyl benzimidazole (0.80 mmol) in ethanol (2 mL), a solution of thiosemicarbazide (0.85 mmol) in water (2.8 ml) and glacial acetic acid (0.22 ml) was added. The mixture was refluxed for 3h under stirring. The reaction mixture was then evaporated under vacuum, yielding an oily residue that was treated with warm water to get rid of the remaining thiosemicarbazide. The crude was purified by CC (SiO_2, CH_2Cl_2+5% DEA), affording the final product as white solid.

2-(1-{1-[2-(N,N-Dimethylamino)ethyl]-2-(4-methoxybenzyl)-1H-benzo[d]imidazol-5-yl}ethylidene)hydrazine-1-carbothioamide (**1**)

Yield: 36%; m.p. 183-184°C. ^{1}H NMR (200 MHz, DMSO-*d6)*: 10.18 (s, 1H, NH), 8.24 (s, 1H, N*H₂*), 8.16 (s, 1H, H(4)benz.), 8.00-7.83 (m, 1H, H(7)benz.), 7.98 (s superimposed, 1H, N*H₂*), 7.44 (d, *J* = 8.6 Hz, 1H, H(6)benz.), 7.24 (d, *J* = 8.6 Hz, 2H, H(3',5')arom.), 6.90 (d, *J* = 8.6 Hz, 2H, H(2',6')arom.), 4.32-4.08 (m, 4H, C*H₂*-Ar and C*H₂*CH₂-N(CH₃)₂), 3.74 (s, 3H, -OC*H₃*), 2.38 (pseudo s, 5H, 3H C*H₃*C=N- and 2H, CH₂C*H₂*-N(CH₃)₂), 2.13 (s, 6H, N(C*H₃*)₂). ^{13}C-NMR (50 MHz, DMSO-*d6)*: 178.13, 157.63, 154.48, 148.55, 141.98, 135.97, 131.00 (2C), 129.38 (2C), 128.22, 120.46, 116.96, 113.57 (2C), 109.37, 54.67, 45.00 (2C), 41.09, 31.88, 13.99. Anal. calcd. for $C_{22}H_{28}N_6OS$: % C 62.24, H 6.65, N 19.79, S 7.55; found: % C 62.44, H 6.67, N 19.80, S 7.16.

2-{1-[2-(4-Chlorobenzyl)-1-[2-(N,N-dimethylamino)ethyl]-1H-benzo[d]imidazol-5-yl]ethylidene]hydrazine-1-carbothioamide (**2**)

Yield: 42%; m.p. 199-200.5°C. ^{1}H NMR (200 MHz, DMSO-*d₆)*: 10.18 (s, 1H, NH), 8.24 (s, 1H, N*H₂*), 8.12 (s, 1H, H(4)benz.), 7.97 (s superimposed, 1H, N*H₂*), 7.93 (d superimposed, *J* = 9.2 Hz, 1H, H(7)benz.), 7.58-7.22 (m, 5H, H(6)benz. and H(2',3',5',6')arom.), 4.34 (s superimposed, 2H, C*H₂*-Ar), 4.40-4.18 (m superimposed, 2H, C*H₂*CH₂-N(CH₃)₂), 2.37 (pseudo s, 5H, 3H C*H₃*C=N- and 2H, CH₂C*H₂*-N(CH₃)₂), 2.13 (s, 6H, N(C*H₃*)₂). ^{13}C-NMR (50 MHz, DMSO-*d₆)*: 178.12, 153.82, 148.54, 142.00, 135.72, 135.61, 131.08, 130.87, 130.42 (2C), 128.01 (2C), 120.91, 117.77, 109.82, 57.71, 45.06 (2C), 41.39, 32.01, 14.00. Anal. calcd.

for $C_{21}H_{25}ClN_6S$: % C 58.80, H 5.87, N 19.59, S 7.47; found: % C 58.68, H 5.57, N 19.82, S 7.11.

2-(1-{1-[2-(N,N-Dimethylamino)ethyl]-2-(4-ethoxybenzyl)-1H-benzo[d]imidazol-5-yl}ethylidene)hydrazine-1-carbothioamide (3)

Yield: 47%; m.p. 177-180˚C. ^{1}H NMR (200 MHz, DMSO-d_6): 10.18 (s, 1H, NH), 8.23 (s, 1H, N$\underline{H}_2$), 8.11 (s, 1H, H(4)benz.), 7.96 (s superimposed, 1H, N$\underline{H}_2$), 7.92 (d superimposed, J = 8.6 Hz, 1H, H(7)benz.), 7.45 (d, J = 8.6 Hz, 1H, H(6)benz.), 7.19 (d, J = 7.6 Hz, 2H, H(3′,5′)arom.), 6.87 (d, J = 8.0 Hz, 2H, H(2′,6′)arom.), 4.24 (pseudo s, 4H, C$\underline{H}_2$-Ar and C$\underline{H}_2$CH$_2$-N(CH$_3$)$_2$), 3.98 (d, J = 6.2 Hz, 2H, OC$\underline{H}_2$CH$_3$), 2.37 (pseudo s, 5H, 3H C$\underline{H}_3$C=N- and 2H, CH$_2$C$\underline{H}_2$-N(CH$_3$)$_2$), 2.12 (s, 6H, N(C$\underline{H}_3$)$_2$), 1.41-1.18 (m, 3H, OCH$_2$C$\underline{H}_3$). ^{13}C-NMR (50 MHz, DMSO-d_6): 178.20, 156.87, 154.44, 148.58, 141.84, 135.79, 130.99 (2C), 129.36 (2C), 128.15, 120.42, 117.02, 114.04 (2C), 109.31, 62.54, 57.46, 45.03 (2C), 41.21, 31.91, 14.25, 14.00. Anal. calcd. for $C_{23}H_{30}N_6OS$: % C 62.99, H 6.09, N 19.16, S 7.30; found: % C 63.12, H 6.48, N 19.16, S 7.07.

2-{1-[2-(4-Chlorobenzyl)-1-[3-(N,N-dimethylamino)propyl]-1H-benzo[d]imidazol-5-yl]ethylidene}hydrazine-1-carbothioamide (4)

Yield: 45%; m.p. 110-111˚C. ^{1}H NMR (200 MHz, DMSO-d_6): 10.18 (s, 1H, NH), 8.26 (s, 1H, N$\underline{H}_2$), 8.13 (s, 1H, H(4)benz.), 7.97 (s superimposed, 1H, N$\underline{H}_2$), 8.10-7.87 (m superimposed, 1H, H(7)benz.), 7.47 (d superimposed, J = 8.6 Hz, 1H, H(6)benz.), 7.37 (pseudo s superimposed, 4H, H(2′,3′,5′,6′)arom.), 4.35 (s superimposed, 2H, C$\underline{H}_2$-Ar), 4.20 (pseudo s superimposed, 2H, C$\underline{H}_2$CH$_2$CH$_2$-N(CH$_3$)$_2$), 2.37 (pseudo s, 3H, C$\underline{H}_3$C=N-), 2.07 (pseudo s, 8H, N(C$\underline{H}_3$)$_2$ and CH$_2$CH$_2$C$\underline{H}_2$-N(CH$_3$)$_2$), 1.69 (pseudo s, 2H, CH$_2$C$\underline{H}_2$CH$_2$-N(CH$_3$)$_2$). ^{13}C-NMR (50 MHz, DMSO-d_6): 178.22, 153.66, 148.54, 141.88, 135.64 (2C), 131.08, 130.90, 130.32 (2C), 128.06 (2C), 120.54, 117.11, 109.33, 55.17, 44.58 (2C), 40.74, 31.80, 26.59, 14.00. Anal. calcd. for $C_{22}H_{27}ClN_6S$: % C 59,65, H 6.14, N 18.97, S 7.24; found: % C 59.51, H 6.18, N 19.24, S 7.18.

2-(1-{1-[2-(N,N-Diethylamino)ethyl]-2-(4-methoxybenzyl)-1H-benzo[d]imidazol-5-yl}ethylidene)hydrazine-1-carbothioamide (5)

Yield: 35%; m.p. 165-168˚C. ^{1}H NMR (200 MHz, DMSO-d_6): 10.16 (s, 1H, NH), 8.25 (s, 1H, N$\underline{H}_2$), 8.10 (s, 1H, H(4)benz.), 7.94 (s superimposed, 1H, N$\underline{H}_2$), 8.15-7.85 (m superimposed, 1H, H(7)benz.), 7.43 (d superimposed, J = 8.6 Hz, 1H, H(6)benz.), 7.20 (d,

J = 8.2 Hz, 2H, H(3′,5′)arom.), 6.89 (d, J = 7.8 Hz, 2H, H(2′,6′)arom.), 4.26 (s superimposed, 2H, C$\underline{H_2}$-Ar), 4.17 (pseudo s superimposed, 2H, C$\underline{H_2}$CH$_2$-N(CH$_2$CH$_3$)$_2$), 3.72 (s, 3H, OC$\underline{H_3}$), 2.58-2.24 (m superimposed to DMSO, 6H, 2H CH$_2$C$\underline{H_2}$-N(CH$_2$CH$_3$)$_2$ and 4H CH$_2$CH$_2$-N(C$\underline{H_2}$CH$_3$)$_2$), 2.36 (s superimposed, 3H, C$\underline{H_3}$C=N-), 0.78 (t, J = 6.6 Hz, 6H, N-(CH$_2$C$\underline{H_3}$)$_2$). ^{13}C-NMR (50 MHz, DMSO-d_6): 178.17, 157.61, 154.61, 148.61, 141.81, 135.75, 131.08, 130.87, 129.33 (2C), 128.31, 120.32, 117.01, 113.56 (2C), 109.31, 54.66, 51.33, 46.42 (2C), 41.03, 31.99, 13.95, 11.31 (2C). Anal. calcd. for C$_{24}$H$_{32}$N$_6$OS: % C 63.69, H 7.13, N 18.57, S 7.08; found: % C 63.51, H 6.77, N 18.84, S 7.16.

2-{1-[2-(4-Chlorobenzyl)-1-[2-(N,N-diethylamino)ethyl]-1H-benzo[d]imidazol-5-yl]ethylidene}hydrazine-1-carbothioamide (**6**)

Yield: 37%; m.p. 190-192˚C. ^{1}H NMR (200 MHz, DMSO-d_6): 10.18 (s, 1H, NH), 8.25 (s, 1H, N$\underline{H_2}$), 8.11 (s, 1H, H(4)benz.), 7.96 (s superimposed, 1H, N$\underline{H_2}$), 8.10-7.85 (m superimposed, 1H, H(7)benz.), 7.48-7.21 (m, 5H, H(6)benz. and H(2′,3′,5′,6′)arom.), 4.35 (s, 2H, C$\underline{H_2}$-Ar), 4.20 (pseudo s, 2H, C$\underline{H_2}$CH$_2$-N(CH$_2$CH$_3$)$_2$), 2.60-2.19 (m superimposed to DMSO, 6H, 2H CH$_2$C$\underline{H_2}$-N(CH$_2$CH$_3$)$_2$ and 4H CH$_2$CH$_2$-N(C$\underline{H_2}$CH$_3$)$_2$), 2.36 (s superimposed, 3H, C$\underline{H_3}$C=N-), 0.76 (t, J = 6.6 Hz, 6H, N(CH$_2$C$\underline{H_3}$)$_2$). ^{13}C-NMR (50 MHz, DMSO-d_6): 178.13, 153.94, 148.59, 141.92, 135.64 (2C), 131.12 (2C), 130.38 (2C), 128.03 (2C), 120.29, 117.09, 109.52, 51.93, 46.43 (2C), 41.08, 32.03, 14.01, 11.31 (2C). Anal. calcd. for C$_{23}$H$_{29}$ClN$_6$S: % C 60.44, H 6.40, N 18.39, S 7.01; found: % C 60.57, H 6.45, N 18.52, S 7.10.

2-(1-{1-[2-(N,N-Diethylamino)ethyl]-2-(4-ethoxybenzyl)-1H-benzo[d]imidazol-5-yl}ethylidene)hydrazine-1-carbothioamide (**7**)

Yield: 47%; m.p. 189-192.5˚C. ^{1}H NMR (200 MHz, DMSO-d_6): 10.18 (s, 1H, NH), 8.24 (s, 1H, N$\underline{H_2}$), 8.10 (s, 1H, H(4)benz.), 7.94 (s superimposed, 1H, N$\underline{H_2}$), 8.05-7.85 (m superimposed, 1H, H(7)benz.), 7.42 (d, J = 8.6 Hz, 1H, H(6)benz.), 7.19 (d, J = 8.4 Hz, 2H, H(3′,5′)arom.), 6.87 (d, J = 8.4 Hz, 2H, H(2′,6′)arom.), 4.27 (s superimposed, 2H, C$\underline{H_2}$-Ar), 4.18 (pseudo s superimposed, 2H, C$\underline{H_2}$CH$_2$-N(CH$_2$CH$_3$)$_2$), 3.98 (q, J = 7 Hz, 2H, OC$\underline{H_2}$CH$_3$), 2.60-2.23 (m superimposed to DMSO, 6H, 2H CH$_2$C$\underline{H_2}$-N(CH$_2$CH$_3$)$_2$ and 4H CH$_2$CH$_2$-N(C$\underline{H_2}$CH$_3$)$_2$), 2.37 (s superimposed, 3H, C$\underline{H_3}$C=N-), 1.30 (t, J = 6.8 Hz, 3H, OCH$_2$C$\underline{H_3}$), 0.78 (t, J = 6.6 Hz, 6H, N(CH$_2$C$\underline{H_3}$)$_2$). ^{13}C-NMR (50 MHz, DMSO-d_6): 178.20, 156.87, 154.60, 148.60, 141.85, 135.75, 130.89, 129.32 (2C), 128.19, 120.32, 117.03, 114.06 (2C), 109.31,

62.55, 51.46, 46.41 (2C), 41.06, 32.01, 14.25, 13.97, 11.32 (2C). Anal. calcd. for $C_{25}H_{34}N_6OS$: % C 64.35, H 7.34, N 18.01, S 6.87; found: % C 64.30, H 7.51, N 18.10, S 6.77.

2-(1-[2-Benzyl-1-[3-(N,N-diethylamino)propyl]-1H-benzo[d]imidazol-5-yl]ethylidene)hydrazine-1-carbothioamide (8)

Yield: 38%; m.p. 168-169°C. ^{1}H NMR (200 MHz, DMSO-d_6): 10.19 (s, 1H, NH), 8.27 (s, 1H, N$\underline{H}_2$), 8.14 (s, 1H, H(4)benz.), 7.97 (s superimposed, 1H, N$\underline{H}_2$), 8.03-7.87 (m superimposed, 1H, H(7)benz.), 7.47 (d, J = 8.2 Hz, 1H, H(6)benz.), 7.31 (s, 5H, H(2',3',4',5',6')arom.), 4.34 (s, 2H, C$\underline{H}_2$-Ar), 4.19 (pseudo s, 2H, C$\underline{H}_2$CH$_2$CH$_2$-N(CH$_2$CH$_3$)$_2$), 2.37 (s, 3H, C$\underline{H}_3$C=N-), 2.45-2.19 (m, 9H, 4H N(C$\underline{H}_2$CH$_3$)$_2$, 2H CH$_2$CH$_2$C$\underline{H}_2$-N(CH$_2$CH$_3$)$_2$ and 3H C$\underline{H}_3$C=N-), 1.63 (pseudo s, 2H, CH$_2$C$\underline{H}_2$CH$_2$-N(CH$_2$CH$_3$)$_2$), 0.90 (pseudo s, 6H, N(CH$_2$C$\underline{H}_3$)$_2$). ^{13}C-NMR (50 MHz, DMSO-d_6): 178.20, 153.90, 148.58, 141.93, 136.59, 135.60, 131.02, 128.25 (2C), 128.16 (2C), 126.23, 120.45, 117.11, 109.31, 48.66, 45.56 (2C), 41.03, 32.65, 26.16, 14.01, 11.05 (2C). Anal. calcd. for $C_{24}H_{32}N_6S$: % C 66.02, H 7.39, N 19.25, S 7.34; found % C 65.84, H 7.53, N 19.37, S 7.58.

2-(1-[1-[3-(N,N-Diethylamino)propyl]-2-(4-methoxybenzyl)-1H-benzo[d]imidazol-5-yl]ethylidene)hydrazine-1-carbothioamide (9)

Yield: 38%; m.p. 180.7-182.9°C. ^{1}H NMR (200 MHz, DMSO-d_6): 10.18 (s, 1H, NH), 8.24 (s, 1H, N$\underline{H}_2$), 8.12 (s, 1H, H(4)benz.), 7.95 (s superimposed, 1H, N$\underline{H}_2$), 8.03-7.85 (m superimposed, 1H, H(7)benz.), 7.45 (d, J = 8.6 Hz, 1H, H(6)benz.), 7.21 (d, J = 8.4 Hz, 2H, H(3',5')arom.), 6.88 (d, J = 8.2 Hz, 2H, H(2',6')arom.), 4.26 (s superimposed, 2H, C$\underline{H}_2$-Ar), 4.16 (pseudo s superimposed, 2H, C$\underline{H}_2$CH$_2$CH$_2$-N(CH$_2$CH$_3$)$_2$), 3.71 (s, 3H, OC$\underline{H}_3$), 2.37 (s, 3H, C$\underline{H}_3$C=N-), 2.42-2.17 (m, 6H, 4H N(C$\underline{H}_2$CH$_3$)$_2$ and 2H CH$_2$CH$_2$C$\underline{H}_2$-N(CH$_2$CH$_3$)$_2$), 1.61 (pseudo s, 2H, CH$_2$C$\underline{H}_2$CH$_2$-N(CH$_2$CH$_3$)$_2$), 0.89 (t, J = 6.8 Hz, 6H, N(CH$_2$C$\underline{H}_3$)$_2$). ^{13}C-NMR (50 MHz, DMSO-d_6): 178.20, 157.62, 154.23, 148.60, 141.92, 135.63, 130.97, 129.23 (2C), 128.34, 120.40, 117.07, 113.55 (2C), 109.26, 54.62, 48.75, 45.56 (2C), 41.04, 31.84, 26.23, 14.00, 11.16 (2C). Anal. calcd. for $C_{25}H_{34}N_6OS$: % C 64.35, H 7.34, N 18.01, S 6.87; found % C 64.19, H 7.74, N 17.96, S 6.85.

2-(1-[2-[(2H-Benzo[d][1,2,3]triazol-2-yl)methyl]-1-[2-(N,N-dimethylamino)ethyl]-1H-benzo[d]imidazol-5-yl]ethylidene)hydrazine-1-carbothioamide (18)

Yield: 46%; m.p. 214-217°C. ^{1}H NMR (200 MHz, DMSO-d_6): 10.19 (s, 1H, NH), 8.26 (s, 1H, N$\underline{H}_2$), 8.14 (s, 1H, H(4)benz.), 8.07-7.85 (m, 4H, 1H H(7)benz., 1H N$\underline{H}_2$ and 2H H(4',7')bzt.),

7.55 (d, J = 8.6 Hz, 1H, H(6)benz.), 7.52-7.39 (m, 2H, H(5′,6′)bzt.), 6.44 (s, 2H, C$\underline{H}_2$-Ar), 4.44 (pseudo s, 2H, C$\underline{H}_2$CH$_2$-N(CH$_3$)$_2$), 2.43-2.29 (m superimposed, 2H, CH$_2$C$\underline{H}_2$-N(CH$_3$)$_2$), 2.36 (s, 3H, C$\underline{H}_3$C=N-), 2.14 (s, 6H, N(C$\underline{H}_3$)$_2$). ^{13}C-NMR (50 MHz, DMSO-d_6): 178.24, 148.60, 148.23, 143.58 (2C), 141.49, 135.68, 131.65, 126.43 (2C), 121.45, 117.74, 117.54 (2C), 109.91, 57.79, 52.31, 45.08 (2C), 41.84, 13.96. Anal. calcd. for C$_{21}$H$_{25}$N$_9$S: % C 57.91, H 5.79, N 28.94, S 7.36; found % C 57.90, H 5.90, N 28.64, S 7.22.

2-(1-[2-[(2H-Benzo[d][1,2,3]triazol-2-yl)methyl]-1-[3-(N,N-dimethylamino)propyl]-1H-benzo[d]imidazol-5-yl]ethylidene)hydrazine-1-carbothioamide (**19**)

Yield: 31%; m.p. 212-214°C. ^{1}H NMR (200 MHz, DMSO-d_6): 10.19 (s, 1H, NH), 8.26 (s, 1H, -N$\underline{H}_2$), 8.14 (s, 1H, H(4)benz.), 8.06-7.80 (m, 4H, 1H H(7)benz., 1H N$\underline{H}_2$ and 2H H(4′,7′)bzt.), 7.68-7.50 (m, 1H, H(6)benz.), 7.47 (pseudo s superimposed, 2H, H(5′,6′)bzt.), 6.47 (s, 2H, C$\underline{H}_2$-Ar), 4.39 (pseudo s, 2H, C$\underline{H}_2$CH$_2$CH$_2$-N(CH$_3$)$_2$), 2.36 (s, 3H, C$\underline{H}_3$C=N-), 2.21-1.90 (m superimposed, 2H, CH$_2$CH$_2$C$\underline{H}_2$-N(CH$_3$)$_2$), 2.05 (s superimposed, 6H, N(C$\underline{H}_3$)$_2$), 1.73 (pseudo s, 2H, CH$_2$C$\underline{H}_2$CH$_2$-N(CH$_3$)$_2$). ^{13}C-NMR (50 MHz, DMSO-d_6): 178.25, 148.38, 148.25, 143.56 (2C), 141.61, 135.48, 131.66, 126.40 (2C), 121.47, 117.77, 117.53 (2C), 109.94, 54.86, 52.01, 44.41 (2C), 41.11, 26.30, 13.96. Anal. calcd. for C$_{22}$H$_{27}$N$_9$S: % C 58.77, H 6.05, N 28.04, S 7.13; found % C 58.88, H 5.96, N 27.78, S 7.33.

2-(1-[2-[(2H-Benzo[d][1,2,3]triazol-2-yl)methyl]-1-[3-(N,N-diethylamino)propyl]-1H-benzo[d]imidazol-5-yl]ethylidene)hydrazine-1-carbothioamide (**21**)

Yield: 78%; m.p. 214-216°C. ^{1}H NMR (200 MHz, DMSO-d_6): 10.18 (s, 1H, NH), 8.27 (s, 1H, N$\underline{H}_2$), 8.13 (s, 1H, H(4)benz.), 8.09-7.86 (m, 4H, 1H H(7)benz., 1H N$\underline{H}_2$ and 2H H(4′,7′)bzt.), 7.55 (d, J = 8.8 Hz, 1H, H(6)benz.), 7.53-7.39 (m, 2H, H(5′,6′)bzt.), 6.47 (s, 2H, C$\underline{H}_2$-Ar), 4.40 (pseudo s, 2H, C$\underline{H}_2$CH$_2$-N(CH$_2$CH$_3$)$_2$), 2.67-2.25 (m superimposed to DMSO, 6H, 2H CH$_2$C$\underline{H}_2$-N(CH$_2$CH$_3$)$_2$ and 4H N(C$\underline{H}_2$CH$_3$)$_2$), 2.36 (s, 3H, C$\underline{H}_3$C=N-), 0.77 (t, J = 6.8 Hz, 6H, N(CH$_2$C$\underline{H}_3$)$_2$). ^{13}C-NMR (50 MHz, DMSO-d_6): 178.25, 148.82, 148.25, 143.59 (2C), 141.52, 135.58, 131.54, 126.40 (2C), 121.34, 117.74, 117.54 (2C), 109.88, 52.43, 51.68, 46.55 (2C), 42.29, 13.91, 11.26 (2C). Anal. calcd. for C$_{23}$H$_{29}$N$_9$S: % C 59.59, H 6.31, N 27.19, S 6.92; found % C 59.61, H 6.54, N 27.06, S 7.15.

2-(1-{2-[(2H-Benzo[d][1,2,3]triazol-1-yl)methyl]-1-[3-(N,N-dimethylamino)propyl]-1H-benzo[d]imidazol-5-yl}ethylidene)hydrazine-1-carbothioamide (**22**)

Yield: 34%; m.p. 201-203˚C. ^{1}H NMR (200 MHz, DMSO-d_6): 10.17 (s, 1H, NH), 8.23 (s, 1H, N$\underline{H}_2$), 8.12 (s superimposed, 1H, H(4)benz.), 8.18-8.05 (m, 1H, H(7')bzt.), (s, 1H, N$\underline{H}_2$), 8.02-7.93 (m, 2H, 1H H(4')bzt. and 1H N$\underline{H}_2$), 7.89 (d, J = 8.6 Hz, 1H H(7)benz.), 7.63-7.50 (m, 2H, H(5',6')bzt.), 7.45 (d, J = 8.4 Hz, 1H, H(6)benz.), 6.45 (s, 2H, C$\underline{H}_2$-Ar), 4.42 (pseudo s, 2H, C$\underline{H}_2$CH$_2$CH$_2$-N(CH$_3$)$_2$), 2.33 (s, 3H, C$\underline{H}_3$C=N-), 2.35-1.90 (m superimposed, 2H, CH$_2$CH$_2$C$\underline{H}_2$-N(CH$_3$)$_2$), 2.13 (s, 6H, N(C$\underline{H}_3$)$_2$), 1.79 (pseudo s, 2H, CH$_2$C$\underline{H}_2$CH$_2$-N(CH$_3$)$_2$). ^{13}C-NMR (50 MHz, DMSO-d_6): 178.21, 148.98, 148.25, 144.91, 141.50, 135.61, 132.87, 131.58, 127.23, 123.80, 121.39, 118.85, 117.62, 110.61, 109.89, 54.86, 44.43 (2C), 44.03, 41.02, 26.27, 13.90. Anal. calcd. for C$_{22}$H$_{27}$N$_9$S: % C 58.77, H 6.05, N 28.04, S 7.13; found % C 58.92, H 6.18, N 28.06, S 6.84.

10.1.6.2 General procedure for the preparation of semicarbazones 10-17, 20.

To a solution of the proper 5-acetyl benzimidazole (0.80 mmol) in ethanol (2 mL), a solution of semicarbazide hydrochloride (2.4 mmol) previously dissolved in 8 mL of a 1N solution of sodium acetate was added. The mixture was refluxed for 4h under stirring. After evaporation of the solvent, the oily residue was treated with warm water to get rid of the remaining semicarbazide. The crude was purified by CC (SiO$_2$, CH$_2$Cl$_2$+5% DEA), obtaining the title compound as white solid.

2-(1-{1-[2-(N,N-Dimethylamino)ethyl]-2-(4-methoxybenzyl)-1H-benzo[d]imidazol-5-yl)ethylidene)hydrazine-1-carboxamide (**10**)

Yield: 69%; m.p. 203-205˚C. ^{1}H NMR (200 MHz, DMSO-d_6): 9.28 (s, 1H, NH), 7.98 (s, 1H, H(4)benz.), 7.83 (d, J = 8.8 Hz, 1H, H(7)benz.), 7.43 (d, J = 8.6 Hz, 1H, H(6)benz.), 7.21 (d, J = 8.6 Hz, 2H, H(3',5')arom.), 6.89 (d, J = 8.6 Hz, 2H, H(2',6')arom.), 6.50 (broad s, 2H, N$\underline{H}_2$), 4.24 (s superimposed, 2H, C$\underline{H}_2$-Ar), 4.39-4.17 (m, 2H, C$\underline{H}_2$CH$_2$-N(CH$_3$)$_2$), 3.72 (s, 3H, OC$\underline{H}_3$), 2.41-2.20 (m superimposed, 2H, CH$_2$C$\underline{H}_2$-N(CH$_3$)$_2$), 2.25 (s superimposed, 3H, C$\underline{H}_3$C=N-), 2.12 (s superimposed, 6H, N(C$\underline{H}_3$)$_2$). ^{13}C-NMR (50 MHz, DMSO-d_6): 157.63, 157.09, 154.20, 144.64, 141.86, 135.23, 131.78, 129.37 (2C), 128.34, 119.88, 116.18, 113.56 (2C), 109.25, 57.45, 54.67, 45.04 (2C), 41.12, 31.91, 13.38. Anal. calcd. for C$_{22}$H$_{28}$N$_6$O$_2$: % C 64.68, H 6.91, N 20.57; found % C 64.70, H 6.67, N 20.35.

2-{1-[2-(4-Chlorobenzyl)-1-[2-(N,N-dimethylamino)ethyl]-1H-benzo[d]imidazol-5-yl)ethylidene)hydrazine-1-carboxamide (11)

Yield: 59%; m.p. 217-220 ˚C. ^{1}H NMR (200 MHz, DMSO-d_6): 9.29 (s, 1H, NH), 7.99 (s, 1H, H(4)benz.), 7.83 (d, J = 8.2 Hz, 1H, H(7)benz.), 7.48-7.24 (m, 5H, H(7)benz. and H(2',3',5',6')arom.), 6.52 (broad s, 2H, NH_2), 4.33 (s superimposed, 2H, CH_2-Ar), 4.41-4.17 (m superimposed, 2H, CH_2CH$_2$-N(CH$_3$)$_2$), 3.72 (s, 3H, OCH_3), 2.42-2.30 (m, 2H, CH$_2$CH_2-N(CH$_3$)$_2$), 2.26 (s, 3H, CH_3C=N-), 2.13 (s, 6H, N(CH_3)$_2$). ^{13}C-NMR (50 MHz, DMSO-d_6): 157.11, 153.57, 144.64, 141.83, 135.66, 135.16, 131.88, 130.87, 130.39 (2C), 128.03 (2C), 120.01, 116.23, 109.34, 57.57, 45.05 (2C), 41.18, 31.92, 13.37. Anal. calcd. for C$_{21}$H$_{25}$ClN$_6$O: % C 61.08, H 6.10, N 20.35; found % C 61.08, H 5.95, N 20.65.

2-(1-{1-[2-(N,N-Dimethylamino)ethyl]-2-(4-ethoxybenzyl)-1H-benzo[d]imidazol-5-yl)ethylidene)hydrazine-1-carboxamide (12)

Yield: 38%; m.p. 210-213˚C. ^{1}H NMR (200 MHz, DMSO-d_6): 9.28 (s, 1H, NH), 7.99 (s, 1H, H(4)benz.), 7.83 (d, J = 8.6 Hz, 1H, H(7)benz.), 7.43 (d, J = 8.6 Hz, 1H, H(6)benz.), 7.19 (d, J = 7.4 Hz, 2H, H(3',5')arom.), 6.87 (d, J = 7.6 Hz, 2H, H(2',6')arom.), 6.50 (broad s, 2H, NH_2), 4.24 (pseudo s, 4H, CH_2-Ar and CH_2CH$_2$-N(CH$_3$)$_2$), 3.98 (q, J = 6.8 Hz, 2H, OCH_2CH$_3$), 2.41-2.18 (m superimposed, 2H, CH$_2$CH_2-N(CH$_3$)$_2$), 2.25 (s superimposed, 3H, CH_3C=N-), 2.12 (s, 6H, N(CH_3)$_2$), 1.30 (t, J = 6.8 Hz, 3H, OCH$_2$CH_3). ^{13}C-NMR (50 MHz, DMSO-d_6): 157.09, 156.87, 154.20, 144.64, 141.87, 135.23, 131.79, 129.34 (2C), 128.21, 119.88, 116.19, 114.06 (2C), 109.25, 62.56, 57.44, 45.03 (2C), 41.13, 31.92, 14.25, 13.38. Anal. calcd. for C$_{23}$H$_{30}$N$_6$O$_2$: % C 65.38, H 7.16, N 19.89; found % C 65.56, H 7.48, N 19.70.

2-{1-[2-(4-Chlorobenzyl)-1-[3-(N,N-dimethylamino)propyl]-1H-benzo[d]imidazol-5-yl)ethylidene)hydrazine-1-carboxamide (13)

Yield: 67%; m.p. 211-212.5 ˚C. ^{1}H NMR (200 MHz, DMSO-d_6): 9.29 (s, 1H, NH), 8.00 (s, 1H, H(4)benz.), 7.83 (d, J = 8.2 Hz, 1H, H(7)benz.), 7.47-7.20 (m, 5H, H(6)benz. and H(2',3',5',6')arom.), 6.51 (broad s, 2H, NH_2), 4.34 (s, 2H, CH_2-Ar), 4.26-4.13 (m, 2H, CH_2CH$_2$CH$_2$-N(CH$_3$)$_2$), 2.26 (s, 3H, CH_3C=N-), 2.20-1.98 (m, 8H, 2H CH$_2$CH$_2$CH_2-N(CH$_3$)$_2$ and 6H N(CH_3)$_2$), 1.81-1.58 (m, 2H, CH$_2$CH_2CH$_2$-N(CH$_3$)$_2$. ^{13}C-NMR (50 MHz, DMSO-d_6): 157.08, 153.40, 144.58, 141.90, 135.69, 135.07, 131.87, 130.89, 130.29 (2C), 128.06 (2C), 119.98, 116.27, 109.28, 55.17, 44.58 (2C), 40.71, 31.80, 26.59, 13.37. Anal. calcd. for C$_{22}$H$_{27}$ClN$_6$O: % C 61.89, H 6.37, N 19.68; found % C 62.09, H 6.63, N 19.89.

2-(1-{1-[2-(N,N-Diethylamino)ethyl]-2-(4-methoxybenzyl)-1H-benzo[d]imidazol-5-yl}ethylidene)hydrazine-1-carboxamide (14)

Yield: 72%; m.p. 207-209 ˚C. ^{1}H NMR (200 MHz, DMSO-d_6): 9.26 (s, 1H, NH), 7.98 (s, 1H, H(4)benz.), 7.84 (d, J = 8.6 Hz, 1H, H(7)benz.), 7.41 (d, J = 8.6 Hz, 1H, H(6)benz.), 7.20 (d, J = 8.8 Hz, 2H, H(3',5')arom.), 6.89 (d, J = 8.8 Hz, 2H, H(2',6')arom.), 6.49 (broad s, 2H, N$\underline{H_2}$), 4.27 (s, 2H, C$\underline{H_2}$-Ar), 4.22-4.09 (m, 2H, C$\underline{H_2}$CH$_2$-N(CH$_2$CH$_3$)$_2$), 3.72 (s, 3H, OC$\underline{H_3}$), 2.50-2.36 (m superimposed to DMSO, 6H, 2H CH$_2$C$\underline{H_2}$-N(CH$_2$CH$_3$)$_2$ and 4H CH$_2$CH$_2$-N(C$\underline{H_2}$CH$_3$)$_2$), 2.26 (s, 3H, C$\underline{H_3}$C=N-), 0.78 (t, J = 7.0 Hz, 6H, N(CH$_2$C$\underline{H_3}$)$_2$). ^{13}C-NMR (50 MHz, DMSO-d_6): 157.63, 157.09, 154.36, 144.67, 141.88, 135.20, 131.68, 129.30 (2C), 128.40, 119.76, 116.19, 113.57 (2C), 109.21, 54.66, 51.39, 46.45 (2C), 41.13, 32.02, 13.34, 11.39 (2C). Anal. calcd. for C$_{24}$H$_{32}$N$_6$O$_2$: % C 66.03, H 7.39, N 19.25; found % C 65.98, H 7.42, N 19.56.

2-{1-[2-(4-Chlorobenzyl)-1-[2-(N,N-diethylamino)ethyl]-1H-benzo[d]imidazol-5-yl}ethylidene)hydrazine-1-carboxamide (15)

Yield: 56%; m.p. 196.5-198.5˚C. ^{1}H NMR (200 MHz, DMSO-d_6): 9.27 (s, 1H, NH), 7.97 (s, 1H, H(4)benz.), 7.85 (d, J = 8.6 Hz, 1H, H(7)benz.), 7.51-7.24 (m, 5H, H(6)benz. and H(2',3',5',6')arom.), 6.50 (broad s, 1H, N$\underline{H_2}$), 4.34 (s, 2H, C$\underline{H_2}$-Ar), 4.19 (pseudo s, 2H, C$\underline{H_2}$CH$_2$-N(CH$_2$CH$_3$)$_2$), 2.58-2.33 (m superimposed to DMSO, 6H, 2H CH$_2$C$\underline{H_2}$-N(CH$_2$CH$_3$)$_2$ and 4H CH$_2$CH$_2$-N(C$\underline{H_2}$CH$_3$)$_2$), 2.25 (s superimposed, 3H, C$\underline{H_3}$C=N-), 0.76 (t, J = 6.4 Hz, 6H, N(CH$_2$C$\underline{H_3}$)$_2$). ^{13}C-NMR (50 MHz, DMSO-d_6): 157.09, 153.73, 144.62, 141.81, 135.68, 135.12, 131.74, 130.87, 130.34 (2C), 128.03 (2C), 119.88, 116.23, 109.32, 51.41, 46.43 (2C), 42.10, 32.04, 13.32, 11.23 (2C). Anal. calcd. for C$_{23}$H$_{29}$ClN$_6$O: % C 62.65, H 6.63, N 19.06; found: % C 62.58, H 6.50, N 19.26.

2-(1-{1-[3-(N,N-Diethylamino)propyl]-2-benzyl-1H-benzo[d]imidazol-5-yl}ethylidene)hydrazine-1-carboxamide (16)

Yield: 32%; m.p. 185-189˚C. ^{1}H NMR (200 MHz, DMSO-d_6): 9.28 (s, 1H, NH), 8.01 (s, 1H, H(4)benz.), 7.82 (d, J = 8.6 Hz, 1H, H(7)benz.), 7.45 (d, J = 8.6 Hz, 1H, H(6)benz.), 7.30 (pseudo s, 5H, H(2',3',5',6')arom.), 6.50 (broad s, 1H, N$\underline{H_2}$), 4.33 (s, 2H, C$\underline{H_2}$-Ar), 4.17 (pseudo s, 2H, C$\underline{H_2}$CH$_2$CH$_2$-N(CH$_2$CH$_3$)$_2$), 2.47-2.27 (m superimposed, 6H, 2H CH$_2$CH$_2$C$\underline{H_2}$-N(CH$_2$CH$_3$)$_2$ and 4H CH$_2$CH$_2$-N(C$\underline{H_2}$CH$_3$)$_2$), 2.26 (s superimposed, 3H, C$\underline{H_3}$C=N-), 1.62 (pseudo s, 2H, CH$_2$C$\underline{H_2}$CH$_2$-N(CH$_2$CH$_3$)$_2$), 0.90 (pseudo s, 6H, N(CH$_2$C$\underline{H_3}$)$_2$). ^{13}C-NMR (50 MHz, DMSO-d_6): 157.07, 153.64, 144.62, 141.95, 136.65, 135.04, 131.80, 128.22 (2C), 128.15 (2C), 126.20, 119.89, 116.26, 109.25, 48.69, 45.56 (2C), 41.10,

32.65, 26.17, 13.36, 11.06 (2C). Anal. calcd. for $C_{24}H_{32}N_6O$: % C 68.54, H 7.67, N 19.98; found: % C 68.35, H 7.84, N 20.30.

2-(1-{1-[3-(N,N-Diethylamino)propyl]-2-(4-methoxybenzyl)-1H-benzo[d]imidazol-5-yl)ethylidene)hydrazine-1-carboxamide (17)

Yield: 32%; m.p. 190-192 ˚C. ^{1}H NMR (200 MHz, DMSO-d_6): 9.28 (s, 1H, NH), 7.99 (s, 1H, H(4)benz.), 7.83 (d, J = 8.6 Hz, 1H, H(7)benz.), 7.44 (d, J = 8.6 Hz, 1H, H(6)benz.), 7.21 (d, J = 7.0 Hz, 2H, H(3′,5′)arom.), 6.88 (d, J = 7.2 Hz, 2H, H(2′,6′)arom.), 6.51 (broad s, 2H, N$\underline{H_2}$), 4.25 (s, 2H, C$\underline{H_2}$-Ar), 4.22-4.07 (m superimposed, 2H, C$\underline{H_2}$CH₂CH₂-N(CH₂CH₃)₂), 3.71 (s, 3H, OC$\underline{H_3}$), 2.46-2.20 (m superimposed, 6H, 2H CH₂CH₂C$\underline{H_2}$-N(CH₂CH₃)₂ and 4H N(C$\underline{H_2}$CH₃)₂), 2.26 (s, 3H, C$\underline{H_3}$C=N-), 1.60 (pseudo s, 2H, CH₂C$\underline{H_2}$CH₂-N(CH₂CH₃)₂), 0.89 (pseudo s, 6H, N(CH₂C$\underline{H_3}$)₂). ^{13}C-NMR (50 MHz, DMSO-d_6): 157.61, 157.07, 153.98, 144.62, 141.95, 135.07, 131.75, 129.22 (2C), 128.40, 119.84, 116.23, 113.55 (2C), 109.20, 54.61, 48.76, 45.56 (2C), 41.29, 31.85, 26.24, 13.37, 11.15 (2C). Anal. calcd. for $C_{25}H_{34}N_6O_2$: % C 66.64, H 7.61, N 18.65; found % C 66.38, H 7.56, N 18.31.

2-(1-{2-[(2H-Benzo[d][1,2,3]triazol-2-yl)methyl]-1-[2-(N,N-dimethylamino)ethyl]-1H-benzo[d]imidazol-5-yl)ethylidene)hydrazine-1- carboxamide (20)

Yield: 48%; m.p. 209-212˚C. ^{1}H NMR (200 MHz, DMSO-d_6): 9.31 (s, 1H, NH), 8.03 (s, 1H, H(4)benz.), 8.00-7.85 (m, 3H, 1H H(7)benz., and 2H H(4′,7′)bzt.), 7.59-7.41 (m, 3H, 1H H(6)benz. and 2H H(5′,6′)bzt.), 6.53 (broad s, 2H, N$\underline{H_2}$), 6.43 (s, 2H, C$\underline{H_2}$-Ar), 4.53-4.34 (m, 2H, C$\underline{H_2}$CH₂-N(CH₃)₂), 2.46-2.34 (m, 2H, CH₂C$\underline{H_2}$-N(CH₃)₂), 2.24 (s, 3H, C$\underline{H_3}$C=N-), 2.14 (s, 6H, N(C$\underline{H_3}$)₂). ^{13}C-NMR (50 MHz, DMSO-d_6): 157.03, 148.32, 144.29, 143.57 (2C), 141.52, 135.14, 132.42, 126.42 (2C), 120.95, 117.74, 117.54 (2C), 116.85, 109.85, 57.77, 52.30, 45.08 (2C), 41.56, 13.31. Anal. calcd. for $C_{21}H_{25}N_9O$: % C 60.13, H 6.01, N 30.05; found % C 60.39, H 6.35, N 30.80.

10.1.6.3 General procedure for the preparation of hydrazones 23-25.

A solution of $NH_2NH_2 \cdot H_2O$ (2.5 mmol) in 3 mL of water was refluxed for 5h with a solution of the proper 5-acetyl benzimidazole (0.50 mmol) in 2.5 mL of ethanol with stirring. At room temperature, 5 mL of water were added and the solution was kept at 0-5˚C overnight. The expected product directly separated from the solution as an amorphous solid that was filtered and crystallized from anhydrous Et_2O.

1-[2-(N,N-Dimethylamino)ethyl]-2-(4-methoxybenzyl)-5-(1-hydrazineylideneethyl)-1H-benzo[d]imidazole (23)

Yield: 53%; m.p. 175.5-176.5°C. ^{1}H NMR (200 MHz, DMSO-d_6): 8.11 (s, 1H, H(4)benz.), 7.92 (pseudo s, 1H, H(7)benz.), 7.55 (pseudo s, 1H, H(6)benz.), 7.22 (pseudo s, 2H, H(3′,5′)arom.), 6.91 (pseudo s, 2H, H(2′,6′)arom.), 6.27 (broad s, 2H, NH$_2$), 4.39-4.10 (m, 4H, C$\underline{H}_2$-Ar and C$\underline{H}_2$CH$_2$-N(CH$_3$)$_2$), 3.73 (s, 3H, OC$\underline{H}_3$), 2.61-2.28 (m superimposed to DMSO, 5H, 2H CH$_2$C$\underline{H}_2$-N(CH$_3$)$_2$ and 3H C$\underline{H}_3$C=N-), 2.14 (s, 6H, N(C$\underline{H}_3$)$_2$). ^{13}C-NMR (50 MHz, DMSO-d_6): 158.17, 157.66, 154.57, 141.84, 136.09, 131.58, 129.36 (2C), 128.28, 120.17, 116.89, 113.60 (2C), 109.53, 57.42, 54.67, 45.05 (2C), 41.13, 31.93, 14.53. Anal. calcd. for C$_{21}$H$_{27}$N$_5$O: % C 69.01, H 7.45, N 19.16; found % C 69.20, H 7.35, N 19.16.

1-[2-(N,N-diethylamino)ethyl]-2-(4-ethoxybenzyl)-5-(1-hydrazineylideneethyl)-1H-benzo[d]imidazole (24)

Yield: 44%; m.p. 80-82°C. ^{1}H NMR (200 MHz, DMSO-d_6): 8.11 (s, 1H, H(4)benz.), 7.87 (d, J = 8.6 Hz, 1H, H(7)benz.), 7.47 (d, J = 8.6 Hz, 1H, H(6)benz.), 7.21 (pseudo s, 2H, H(3′,5′)arom.), 6.89 (pseudo s, 2H, H(2′,6′)arom.), 6.32 (broad s, 2H, NH$_2$), 4.41-4.13 (m, 4H, 2H C$\underline{H}_2$-Ar and 2H C$\underline{H}_2$CH$_2$-N(CH$_2$CH$_3$)$_2$), 3.97 (pseudo s, 2H, OC$\underline{H}_2$CH$_3$), 2.58-2.27 (m superimposed to DMSO, 6H, 2H CH$_2$C$\underline{H}_2$-N(CH$_2$CH$_3$)$_2$ and 4H N(C$\underline{H}_2$CH$_3$)$_2$), 2.29 (s superimposed, 3H, C$\underline{H}_3$C=N-), 1.31 (t, J = 6.8 Hz, 3H, OC$\underline{H}_2$CH$_3$), 0.78 (t, J = 6.8 Hz, 6H, N(CH$_2$C$\underline{H}_3$)$_2$). ^{13}C-NMR (50 MHz, DMSO-d_6): 158.18, 157.64, 154.24, 141.87, 135.89, 131.67, 129.23 (2C), 128.34, 120.04, 116.89, 113.78 (2C), 109.57, 62.67, 57.43, 45.09 (2C), 41.12, 31.91, 14.44, 13.98, 11.23 (2C). Anal. calcd. for C$_{24}$H$_{33}$N$_5$O: % C 70.73, H 8.16, N 17.18; found % C 70.67, H 8.47, N 17.43.

2-[(Benzotriazol-2-yl)methyl]-1-[2-(N,N-diethylamino)ethyl]-5-(1-hydrazineylideneethyl)-1H-benzo[d]imidazole (25)

Yield: 35%; m.p. 128-130°C. ^{1}H NMR (200 MHz, DMSO-d_6): 8.01-7.87 (m, 2H, H(4′,7′)bzt.), 7.76 (s, 1H, H(4)benz.), 7.70 (d, J = 8.8 Hz, 1H, H(7)benz.), 7.60-7.38 (m, 3H, 1H H(6)benz. and 2H H(5′,6′)bzt.), 6.43 (s, 2H, C$\underline{H}_2$-Ar), 6.26 (broad s, 2H, NH$_2$), 4.43-4.21 (m, 2H, C$\underline{H}_2$CH$_2$-N(CH$_2$CH$_3$)$_2$), 2.64-2.48 (m superimposed to DMSO, 2H, CH$_2$C$\underline{H}_2$-N(CH$_2$CH$_3$)$_2$), 2.42 (q, J = 6.8 Hz, 4H, N(C$\underline{H}_2$CH$_3$)$_2$), 2.08 (s, 3H, C$\underline{H}_3$C=N-), 1.31 (t, J = 6.8 Hz, 3H, OC$\underline{H}_2$CH$_3$), 0.76 (t, J = 6.8 Hz, 6H, N(CH$_2$C$\underline{H}_3$)$_2$). ^{13}C-NMR (50 MHz, DMSO-d_6): 158.04, 148.86, 147.97, 143.57, 141.42, 135.84, 134.07, 132.11, 126.49 (2C), 121.15, 117.51 (2C), 110.16, 52.31, 51.61, 46.49 (2C), 42.59, 14.52, 11.15 (2C). Anal. calcd. for C$_{22}$H$_{28}$N$_8$: % C 65.32, H 6.98, N 27.70; found % C 65.57, H 6.69, N 27.58.

10.2 Biological tests and computational methods

Experimental details are reported in the manuscripts, as follows:

(a) for the acridine derivatives see reference[6], describing *in vitro* cell-based assays, enzymatic inhibition, isothermal titration calorimetry, site-directed mutagenesis assays and computational experiments

(b) for the azaspiro dihydrotriazines see reference[11], describing *in vitro* cell-based assays, enzymatic inhibition and computational experiments

(c) for the triazino[1,2-a]benzimidazoles (unpublished results) the experimental section may be referred to citation[11]

(d) for the anilino derivatives and the benzenesulfonamides (unpublished results) the experimental section may be referred to citation[183]

(e) for the (thio)semicarbazone and hydrazone benzimidazoles (unpublished results, submitted manuscript to *Molecules* on February 17th, 2020) the experimental section may be referred to citation[11]

Bibliography

(1)   Ryu, W.-S. *Molecular Virology of Human Pathogenic Viruses*; 2017. https://doi.org/10.1016/B978-0-12-800838-6.00002-3.

(2)   Tonelli, M.; Cichero, E. Fight Against H1N1 Influenza A Virus: Recent Insights Towards the Development of Druggable Compounds. *Curr. Med. Chem.* **2016**, *23* (18), 1802–1817. https://doi.org/10.2174/0929867323666160210124930.

(3)   Houe, H. Economic Impact of BVDV Infection in Dairies. *Biologicals* **2003**, *31* (2), 137–143. https://doi.org/10.1016/S1045-1056(03)00030-7.

(4)   The Lancet Gastroenterology & Hepatology. Drug Pricing: Still a Barrier to Elimination of HCV. *Lancet Gastroenterol. Hepatol.* **2018**, *3* (12), 813. https://doi.org/10.1016/S2468-1253(18)30354-6.

(5)   Tonelli, M.; Vettoretti, G.; Tasso, B.; Novelli, F.; Boido, V.; Sparatore, F.; Busonera, B.; Ouhtit, A.; Farci, P.; Blois, S.; et al. Acridine Derivatives as Anti-BVDV Agents. *Antiviral Res.* **2011**, *91* (2), 133–141. https://doi.org/10.1016/j.antiviral.2011.05.005.

(6)   Loddo, R.; Francesconi, V.; Laurini, E.; Boccardo, S.; Aulic, S.; Fermeglia, M.; Pricl, S.; Tonelli, M. 9-Aminoacridine-Based Agents Impair the Bovine Viral Diarrhea Virus (BVDV) Replication Targeting the RNA-Dependent RNA Polymerase (RdRp). *Bioorg. Med. Chem.* **2018**, *26* (4), 855–868. https://doi.org/10.1016/j.bmc.2018.01.001.

(7)   Hodinka, R. L. Respiratory RNA Viruses. *Microbiol. Spectr.* **2016**, *4* (4), 233–271. https://doi.org/10.1128/microbiolspec.dmih2-0028-2016.

(8)   Barr, R.; Green, C. A.; Sande, C. J.; Drysdale, S. B. Respiratory Syncytial Virus: Diagnosis, Prevention and Management. *Ther. Adv. Infect. Dis.* **2019**, *6*, 204993611986579. https://doi.org/10.1177/2049936119865798.

(9)   Behzadi, M. A.; Leyva-Grado, V. H. Overview of Current Therapeutics and Novel Candidates against Influenza, Respiratory Syncytial Virus, and Middle East Respiratory Syndrome Coronavirus Infections. *Front. Microbiol.* **2019**, *10*, 1327. https://doi.org/10.3389/fmicb.2019.01327.

(10)   Tonelli, M.; Naesens, L.; Gazzarrini, S.; Santucci, M.; Cichero, E.; Tasso, B.; Moroni, A.; Costi, M. P.; Loddo, R. Host Dihydrofolate Reductase (DHFR)-Directed Cycloguanil Analogues Endowed with Activity against Influenza Virus and Respiratory Syncytial Virus. *Eur. J. Med. Chem.* **2017**, *135*, 467–478. https://doi.org/10.1016/j.ejmech.2017.04.070.

(11)   Francesconi, V.; Giovannini, L.; Santucci, M.; Cichero, E.; Costi, M. P.; Naesens, L.; Giordanetto, F.; Tonelli, M. Synthesis, Biological Evaluation and Molecular Modeling of Novel Azaspiro Dihydrotriazines as Influenza Virus Inhibitors Targeting the Host Factor Dihydrofolate Reductase (DHFR). *Eur. J. Med. Chem.* **2018**, *155*, 229–243. https://doi.org/10.1016/j.ejmech.2018.05.059.

(12) Liu, S.; Li, R.; Zhang, R.; Chan, C. C. S.; Xi, B.; Zhu, Z.; Yang, J.; Poon, V. K. M.; Zhou, J.; Chen, M.; et al. CL-385319 Inhibits H5N1 Avian Influenza A Virus Infection by Blocking Viral Entry. *Eur. J. Pharmacol.* **2011**, *660* (2–3), 460–467. https://doi.org/10.1016/j.ejphar.2011.04.013.

(13) Tonelli, M.; Tasso, B.; Mina, L.; Paglietti, G.; Boido, V.; Sparatore, F. Primary Anti-Proliferative Activity Evaluation of 1-(Quinolizidin-1'-Yl) Methyl- and 1-(ω-Tert-Amino)Alkyl-Substituted 2-Phenyl-, 2-Benzyl- and 2-[(Benzotriazol-1/2-Yl)Methyl]Benzimidazoles on Human Cancer Cell Lines. *Mol. Divers.* **2013**, *17* (3), 409–419. https://doi.org/10.1007/s11030-013-9440-3.

(14) Krupovic, M.; Dolja, V. V.; Koonin, E. V. Origin of Viruses: Primordial Replicators Recruiting Capsids from Hosts. *Nat. Rev. Microbiol.* **2019**, *17* (7), 449–458. https://doi.org/10.1038/s41579-019-0205-6.

(15) Baltimore, D. Expression of Animal Virus Genomes. *Bacteriol. Rev.* **1971**, *35* (3), 235–241.

(16) Lefkowitz, E. J.; Dempsey, D. M.; Hendrickson, R. C.; Orton, R. J.; Siddell, S. G.; Smith, D. B. Virus Taxonomy: The Database of the International Committee on Taxonomy of Viruses (ICTV). *Nucleic Acids Res.* **2018**, *46* (D1), D708–D717. https://doi.org/10.1093/nar/gkx932.

(17) Lefkowitz, E. . Taxonomy and Classification of Viruses. In *Manual of Clinical Microbiology*; 2015; pp 1393–1404.

(18) Bochkov, Y. A.; Gern, J. E. Rhinoviruses and Their Receptors: Implications for Allergic Disease. *Curr. Allergy Asthma Rep.* **2016**, *16* (4), 30. https://doi.org/10.1007/s11882-016-0608-7.

(19) Leopold, P. L.; Pfister, K. K. Viral Strategies for Intracellular Trafficking: Motors and Microtubules. *Traffic* **2006**, *7* (5), 516–523. https://doi.org/10.1111/j.1600-0854.2006.00408.x.

(20) Cohen, S.; Au, S.; Panté, N. How Viruses Access the Nucleus. *Biochim. Biophys. Acta - Mol. Cell Res.* **2011**, *1813* (9), 1634–1645. https://doi.org/10.1016/j.bbamcr.2010.12.009.

(21) Jiang, P.; Liu, Y.; Ma, H.-C.; Paul, A. V; Wimmer, E. Picornavirus Morphogenesis. *Microbiol. Mol. Biol. Rev.* **2014**, *78* (3), 418–437. https://doi.org/10.1128/mmbr.00012-14.

(22) Sun, S.; Rao, V. B.; Rossmann, M. G. Genome Packaging in Viruses. *Curr. Opin. Struct. Biol.* **2010**, *20* (1), 114–120. https://doi.org/10.1016/j.sbi.2009.12.006.

(23) Bruss, V. Envelopment of the Hepatitis B Virus Nucleocapsid. *Virus Res.* **2004**, *106* (2), 199–209. https://doi.org/10.1016/j.virusres.2004.08.016.

(24) San Martín, C. Virus Maturation. *Adv. Exp. Med. Biol.* **2019**, *1140*, 129–158. https://doi.org/10.1007/978-3-030-14741-9_7.

(25) Simmonds, P.; Becher, P.; Bukh, J.; Gould, E. A.; Meyers, G.; Monath, T.; Muerhoff, S.; Pletnev, A.; Rico-Hesse, R.; Smith, D. B.; et al. ICTV Virus Taxonomy Profile: Flaviviridae. *J. Gen. Virol.* **2017**, *98* (1), 2–3. https://doi.org/10.1099/jgv.0.000672.

(26) Becher, P.; Ramirez, R. A.; Orlich, M.; Rosales, S. C.; König, M.; Schweizer, M.; Stalder, H.; Schirrmeier, H.; Thiel, H. J. Genetic and Antigenic Characterization of Novel Pestivirus Genotypes: Implications for Classification. *Virology* **2003**, *311* (1), 96–104. https://doi.org/10.1016/S0042-6822(03)00192-2.

(27) Blome, S.; Beer, M.; Wernike, K. New Leaves in the Growing Tree of Pestiviruses. In *Advances in Virus Research*; Academic Press Inc., 2017; Vol. 99, pp 139–160. https://doi.org/10.1016/bs.aivir.2017.07.003.

(28) Pan, S.; Mou, C.; Chen, Z. An Emerging Novel Virus: Atypical Porcine Pestivirus (APPV). *Rev. Med. Virol.* **2019**, *29* (1), 1–8. https://doi.org/10.1002/rmv.2018.

(29) Ridpath, J. F.; Bolin, S. R. Differentiation of Types 1a, 1b and 2 Bovine Viral Diarrhoea Virus (BVDV) by PCR. *Mol. Cell. Probes* **1998**, *12* (2), 101–106. https://doi.org/10.1006/mcpr.1998.0158.

(30) Ridpath, J. F. BVDV Genotypes and Biotypes: Practical Implications for Diagnosis and Control. *Biologicals* **2003**, *31* (2), 127–131. https://doi.org/10.1016/S1045-1056(03)00028-9.

(31) Reichel, M. P.; Hill, F. I.; Voges, H. Does Control of Bovine Viral Diarrhoea Infection Make Economic Sense? *N. Z. Vet. J.* **2008**, *56* (2), 60–66. https://doi.org/10.1080/00480169.2008.36809.

(32) Yeşilbağ, K.; Alpay, G.; Becher, P. Variability and Global Distribution of Subgenotypes of Bovine Viral Diarrhea Virus. *Viruses* **2017**, *9* (6), 128. https://doi.org/10.3390/v9060128.

(33) Seong, G.; Oem, J. K.; Choi, K. S. Pathogenetic Differences after Experimental Infection of Calves with Korean Non-Cytopathic BVDV-1 and BVDV-2 Isolates. *Vet. Immunol. Immunopathol.* **2013**, *156* (1–2), 147–152. https://doi.org/10.1016/j.vetimm.2013.09.010.

(34) Lanyon, S. R.; Hill, F. I.; Reichel, M. P.; Brownlie, J. Bovine Viral Diarrhoea: Pathogenesis and Diagnosis. *Vet. J.* **2014**, *199* (2), 201–209. https://doi.org/10.1016/j.tvjl.2013.07.024.

(35) Flores, E. F.; Ridpath, J. F.; Weiblen, R.; Vogel, F. S. F.; Gil, L. H. V. G. Phylogenetic Analysis of Brazilian Bovine Viral Diarrhea Virus Type 2 (BVDV-2) Isolates: Evidence for a Subgenotype within BVDV-2. *Virus Res.* **2002**, *87* (1), 51–60. https://doi.org/10.1016/s0168-1702(02)00080-1.

(36) Vilcek, S.; Durkovic, B.; Kolesarova, M.; Paton, D. J. Genetic Diversity of BVDV: Consequences for Classification and Molecular Epidemiology. *Prev. Vet. Med.* **2005**, *72* (1–2), 31–35. https://doi.org/10.1016/j.prevetmed.2005.08.004.

(37) Buckwold, V. E.; Beer, B. E.; Donis, R. O. Bovine Viral Diarrhea Virus as a Surrogate Model of Hepatitis C Virus for the Evaluation of Antiviral Agents. *Antiviral Res.* **2003**, *60* (1), 1–15. https://doi.org/10.1016/S0166-3542(03)00174-8.

(38) Yu, H.; Isken, O.; Grassmann, C. W.; Behrens, S.-E. A Stem-Loop Motif Formed by the Immediate 5' Terminus of the Bovine Viral Diarrhea Virus Genome Modulates Translation as Well as Replication of the Viral RNA. *J. Virol.* **2000**, *74* (13), 5825–5835.

https://doi.org/10.1128/jvi.74.13.5825-5835.2000.

(39)   Neill, J. D. Molecular Biology of Bovine Viral Diarrhea Virus. *Biologicals* **2013**, *41* (1), 2–7. https://doi.org/10.1016/j.biologicals.2012.07.002.

(40)   Mätzener, P.; Magkouras, I.; Rümenapf, T.; Peterhans, E.; Schweizer, M. The Viral RNase Erns Prevents IFN Type-I Triggering by Pestiviral Single- and Double-Stranded RNAs. *Virus Res.* **2009**, *140* (1–2), 15–23. https://doi.org/10.1016/j.virusres.2008.10.015.

(41)   Callens, N.; Brügger, B.; Bonnafous, P.; Drobecq, H.; Gerl, M. J.; Krey, T.; Roman-Sosa, G.; Rümenapf, T.; Lambert, O.; Dubuisson, J.; et al. Morphology and Molecular Composition of Purified Bovine Viral Diarrhea Virus Envelope. *PLoS Pathog.* **2016**, *12* (3), e1005476. https://doi.org/10.1371/journal.ppat.1005476.

(42)   Hilton, L.; Moganeradj, K.; Zhang, G.; Chen, Y.-H.; Randall, R. E.; McCauley, J. W.; Goodbourn, S. The NPro Product of Bovine Viral Diarrhea Virus Inhibits DNA Binding by Interferon Regulatory Factor 3 and Targets It for Proteasomal Degradation. *J. Virol.* **2006**, *80* (23), 11723–11732. https://doi.org/10.1128/jvi.01145-06.

(43)   Lackner, T.; Muller, A.; Pankraz, A.; Becher, P.; Thiel, H.-J.; Gorbalenya, A. E.; Tautz, N. Temporal Modulation of an Autoprotease Is Crucial for Replication and Pathogenicity of an RNA Virus. *J. Virol.* **2004**, *78* (19), 10765–10775. https://doi.org/10.1128/jvi.78.19.10765-10775.2004.

(44)   Gu, B.; Liu, C.; Lin-Goerke, J.; Maley, D. R.; Gutshall, L. L.; Feltenberger, C. A.; Del Vecchio, A. M. The RNA Helicase and Nucleotide Triphosphatase Activities of the Bovine Viral Diarrhea Virus NS3 Protein Are Essential for Viral Replication. *J. Virol.* **2000**, *74* (4), 1794–1800. https://doi.org/10.1128/jvi.74.4.1794-1800.2000.

(45)   Zhong, W.; Gutshall, L. L.; Del Vecchio, A. M. Identification and Characterization of an RNA-Dependent RNA Polymerase Activity within the Nonstructural Protein 5B Region of Bovine Viral Diarrhea Virus. *J. Virol.* **1998**, *72* (11), 9365–9369.

(46)   Choi, K. H.; Groarke, J. M.; Young, D. C.; Kuhn, R. J.; Smith, J. L.; Pevear, D. C.; Rossmann, M. G. The Structure of the RNA-Dependent RNA Polymerase from Bovine Viral Diarrhea Virus Establishes the Role of GTP in de Novo Initiation. *Proc. Natl. Acad. Sci. U. S. A.* **2004**, *101* (13), 4425–4430. https://doi.org/10.1073/pnas.0400660101.

(47)   Choi, K. H.; Gallei, A.; Becher, P.; Rossmann, M. G. The Structure of Bovine Viral Diarrhea Virus RNA-Dependent RNA Polymerase and Its Amino-Terminal Domain. *Structure* **2006**, *14* (7), 1107–1113. https://doi.org/10.1016/j.str.2006.05.020.

(48)   Brodersen, B. W. Bovine Viral Diarrhea Virus Infections: Manifestations of Infection and Recent Advances in Understanding Pathogenesis and Control. *Vet. Pathol.* **2014**, *51* (2), 453–464. https://doi.org/10.1177/0300985813520250.

(49)   Newcomer, B. W.; Chamorro, M. F.; Walz, P. H. Vaccination of Cattle against Bovine Viral Diarrhea Virus. *Vet. Microbiol.* **2017**, *206*, 78–83. https://doi.org/10.1016/j.vetmic.2017.04.003.

(50)   Fulton, R. W.; Ridpath, J. F.; Confer, A. W.; Saliki, J. T.; Burge, L. J.; Payton, M. E. Bovine Viral Diarrhoea Virus Antigenic Diversity: Impact on Disease and Vaccination Programmes. *Biologicals* **2003**, *31* (2), 89–95. https://doi.org/10.1016/S1045-1056(03)00021-6.

(51)   Newcomer, B. W.; Givens, M. D. Approved and Experimental Countermeasures against Pestiviral Diseases: Bovine Viral Diarrhea, Classical Swine Fever and Border Disease. *Antiviral Res.* **2013**, *100* (1), 133–150. https://doi.org/10.1016/j.antiviral.2013.07.015.

(52)   Manfredini, S.; Angusti, A.; Veronese, A. C.; Durini, E.; Vertuani, S.; Nalin, F.; Solaroli, N.; Pricl, S.; Ferrone, M.; Mura, M.; et al. Hindered Nucleoside Analogs as Antiflaviviridae Agents. *Pure Appl. Chem.* **2004**, *76* (5), 1007–1015. https://doi.org/10.1351/pac200476051007.

(53)   Baginski, S. G.; Pevear, D. C.; Seipel, M.; Sun, S. C. C.; Benetatos, C. A.; Chunduru, S. K.; Rice, C. M.; Collett, M. S. Mechanism of Action of a Pestivirus Antiviral Compound. *Proc. Natl. Acad. Sci.* **2000**, *97* (14), 7981–7986. https://doi.org/10.1073/PNAS.140220397.

(54)   Paeshuyse, J.; Leyssen, P.; Mabery, E.; Boddeker, N.; Vrancken, R.; Froeyen, M.; Ansari, I. H.; Dutartre, H.; Rozenski, J.; Gil, L. H. V. G.; et al. A Novel, Highly Selective Inhibitor of Pestivirus Replication That Targets the Viral RNA-Dependent RNA Polymerase. *J. Virol.* **2006**, *80* (1), 149–160. https://doi.org/10.1128/jvi.80.1.149-160.2006.

(55)   Puerstinger, G.; Paeshuyse, J.; Herdewijn, P.; Rozenski, J.; De Clercq, E.; Neyts, J. Substituted 5-Benzyl-2-Phenyl-5H-Imidazo[4,5-c]Pyridines: A New Class of Pestivirus Inhibitors. *Bioorganic Med. Chem. Lett.* **2006**, *16* (20), 5345–5349. https://doi.org/10.1016/j.bmcl.2006.07.081.

(56)   Puerstinger, G.; Paeshuyse, J.; Heinrich, S.; Mohr, J.; Schraffl, N.; De Clercq, E.; Neyts, J. Antiviral 2,5-Disubstituted Imidazo[4,5-c]Pyridines: Further Optimization of Anti-Hepatitis C Virus Activity. *Bioorganic Med. Chem. Lett.* **2007**, *17* (18), 5111–5114. https://doi.org/10.1016/j.bmcl.2007.07.015.

(57)   Paeshuyse, J.; Chezal, J.-M.; Froeyen, M.; Leyssen, P.; Dutartre, H.; Vrancken, R.; Canard, B.; Letellier, C.; Li, T.; Mittendorfer, H.; et al. The Imidazopyrrolopyridine Analogue AG110 Is a Novel, Highly Selective Inhibitor of Pestiviruses That Targets the Viral RNA-Dependent RNA Polymerase at a Hot Spot for Inhibition of Viral Replication. *J. Virol.* **2007**, *81* (20), 11046–11053. https://doi.org/10.1128/JVI.00388-07.

(58)   Chezal, J. M.; Paeshuyse, J.; Gaumet, V.; Canitrot, D.; Maisonial, A.; Lartigue, C.; Gueiffier, A.; Moreau, E.; Teulade, J. C.; Chavignon, O.; et al. Synthesis and Antiviral Activity of an Imidazo[1,2-a]Pyrrolo[2,3-c]Pyridine Series against the Bovine Viral Diarrhea Virus. *Eur. J. Med. Chem.* **2010**, *45* (5), 2044–2047. https://doi.org/10.1016/j.ejmech.2010.01.023.

(59)   Paeshuyse, J.; Letellier, C.; Froeyen, M.; Dutartre, H.; Vrancken, R.; Canard, B.; De Clercq, E.; Gueiffier, A.; Teulade, J. C.; Herdewijn, P.; et al. A Pyrazolotriazolopyrimidinamine Inhibitor of Bovine Viral Diarrhea Virus Replication That Targets the Viral RNA-

Dependent RNA Polymerase. *Antiviral Res.* **2009**, *82* (3), 141–147. https://doi.org/10.1016/j.antiviral.2009.02.192.

(60)   Sako, K.; Aoyama, H.; Sato, S.; Hashimoto, Y.; Baba, M. γ-Carboline Derivatives with Anti-Bovine Viral Diarrhea Virus (BVDV) Activity. *Bioorganic Med. Chem.* **2008**, *16* (7), 3780–3790. https://doi.org/10.1016/j.bmc.2008.01.052.

(61)   Carta, A.; Briguglio, I.; Piras, S.; Corona, P.; Boatto, G.; Nieddu, M.; Giunchedi, P.; Marongiu, M. E.; Giliberti, G.; Iuliano, F.; et al. Quinoline Tricyclic Derivatives. Design, Synthesis and Evaluation of the Antiviral Activity of Three New Classes of RNA-Dependent RNA Polymerase Inhibitors. *Bioorganic Med. Chem.* **2011**, *19* (23), 7070–7084. https://doi.org/10.1016/j.bmc.2011.10.009.

(62)   Tabarrini, O.; Manfroni, G.; Fravolini, A.; Cecchetti, V.; Sabatini, S.; De Clercq, E.; Rozenski, J.; Canard, B.; Dutartre, H.; Paeshuyse, J.; et al. Synthesis and Anti-BVDV Activity of Acridones as New Potential Antiviral Agents. *J. Med. Chem.* **2006**, *49* (8), 2621–2627. https://doi.org/10.1021/jm051250z.

(63)   Asthana, S.; Shukla, S.; Vargiu, A. V; Ceccarelli, M.; Ruggerone, P.; Paglietti, G.; Marongiu, M. E.; Blois, S.; Giliberti, G.; La Colla, P. Different Molecular Mechanisms of Inhibition of Bovine Viral Diarrhea Virus and Hepatitis C Virus RNA-Dependent RNA Polymerases by a Novel Benzimidazole. *Biochemistry* **2013**, *52* (21), 3752–3764. https://doi.org/10.1021/bi400107h.

(64)   Desideri, N.; Fioravanti, R.; Monaco, L. P.; Atzori, E. M.; Carta, A.; Delogu, I.; Collu, G.; Loddo, R. Design, Synthesis, Antiviral Evaluation, and Sar Studies of New 1-(Phenylsulfonyl)-1H-Pyrazol-4-Yl-Methylaniline Derivatives. *Front. Chem.* **2019**, *7* (APR), 214. https://doi.org/10.3389/fchem.2019.00214.

(65)   Peek, S. F.; Bonds, M. D.; Gangemi, D. G.; Thomas, C. B.; Schultz, R. D. Evaluation of Cytotoxicity and Antiviral Activity of Recombinant Interferon Alfa-2a and Recombinant Human Interferon Alfa-B/D Hybrid against Bovine Viral Diarrhea Virus, Infectious Bovine Rhinotracheitis Virus, and Vesicular Stomatitis Virus in Vitro. *Am. J. Vet. Res.* **2004**, *65* (6), 871–874. https://doi.org/10.2460/ajvr.2004.65.871.

(66)   Lambkin-Williams, R.; Noulin, N.; Mann, A.; Catchpole, A.; Gilbert, A. S. The Human Viral Challenge Model: Accelerating the Evaluation of Respiratory Antivirals, Vaccines and Novel Diagnostics. *Respir. Res.* **2018**, *19* (1), 123. https://doi.org/10.1186/s12931-018-0784-1.

(67)   Berry, M.; Gamieldien, J.; Fielding, B. C. Identification of New Respiratory Viruses in the New Millennium. *Viruses* **2015**, *7* (3), 996–1019. https://doi.org/10.3390/v7030996.

(68)   Brough, H. A.; Nataraja, R. Upper Respiratory Tract Infection (URTI). In *Rapid Paediatrics and Child Health*; John Wiley & Sons, Ltd, 2018; pp 222–227. https://doi.org/10.1002/9781119548447.ch20.

(69)   Benson, V.; Marano, M. A. Current Estimates from the National Health Interview Survey,
168

1995. *Vital Health Stat. 10.* **1998**, No. 199, 1–428.

(70)   Marom, T.; Alvarez-Fernandez, P. E.; Jennings, K.; Patel, J. A.; McCormick, D. P.; Chonmaitree, T. Acute Bacterial Sinusitis Complicating Viral Upper Respiratory Tract Infection in Young Children. *Pediatr. Infect. Dis. J.* **2014**, *33* (8), 803–808. https://doi.org/10.1097/INF.0000000000000278.

(71)   Troeger, C.; Blacker, B.; Khalil, I. A.; Rao, P. C.; Cao, J.; Zimsen, S. R. M.; Albertson, S. B.; Deshpande, A.; Farag, T.; Abebe, Z.; et al. Estimates of the Global, Regional, and National Morbidity, Mortality, and Aetiologies of Lower Respiratory Infections in 195 Countries, 1990–2016: A Systematic Analysis for the Global Burden of Disease Study 2016. *Lancet Infect. Dis.* **2018**, *18* (11), 1191–1210. https://doi.org/10.1016/S1473-3099(18)30310-4.

(72)   Walter, J. M.; Wunderink, R. G. Severe Respiratory Viral Infections: New Evidence and Changing Paradigms. *Infect. Dis. Clin. North Am.* **2017**, *31* (3), 455–474. https://doi.org/10.1016/j.idc.2017.05.004.

(73)   Christiansen, K. Treatment of Common Lower Respiratory Tract Infections. *Aust. Prescr.* **1996**, *16* (2), 48–51. https://doi.org/10.18773/austprescr.1996.052.

(74)   Murdoch, D. R.; C Howie, S. R. The Global Burden of Lower Respiratory Infections: Making Progress, but We Need to Do Better. *Lancet Infect. Dis.* **2018**, *18*, 1162–1163. https://doi.org/10.1016/S1473-3099(18)30407-9.

(75)   Afonso, C. L.; Amarasinghe, G. K.; Bányai, K.; Bào, Y.; Basler, C. F.; Bavari, S.; Bejerman, N.; Blasdell, K. R.; Briand, F. X.; Briese, T.; et al. Taxonomy of the Order Mononegavirales: Update 2016. *Arch. Virol.* **2016**, *161* (8), 2351–2360. https://doi.org/10.1007/s00705-016-2880-1.

(76)   Lamb, R. A.; Parks, G. D. Paramyxoviridae : The Viruses and Their Replication. In *Fields Virology*; Lippincott, Williams, and Wilkins, 2007; Vol. 5, pp 1449–1496.

(77)   Boncristiani, H. F.; Criado, M. F.; Arruda, E. Respiratory Viruses. In *Encyclopedia of Microbiology*; Elsevier, 2009; pp 500–518. https://doi.org/10.1016/B978-012373944-5.00314-X.

(78)   Nam, H. H.; Ison, M. G. Respiratory Syncytial Virus Infection in Adults. *BMJ* **2019**, *62*, l5021. https://doi.org/10.1136/bmj.l5021.

(79)   Taleb, S. A.; Al Thani, A. A.; Al Ansari, K.; Yassine, H. M. Human Respiratory Syncytial Virus: Pathogenesis, Immune Responses, and Current Vaccine Approaches. *Eur. J. Clin. Microbiol. Infect. Dis.* **2018**, *37* (10), 1817–1827. https://doi.org/10.1007/s10096-018-3289-4.

(80)   McLellan, J. S.; Ray, W. C.; Peeples, M. E. Structure and Function of Respiratory Syncytial Virus Surface Glycoproteins. *Curr. Top. Microbiol. Immunol.* **2013**, *372*, 83–104. https://doi.org/10.1007/978-3-642-38919-1-4.

(81)   Collins, P. L.; Fearns, R.; Graham, B. S. Respiratory Syncytial Virus: Virology, Reverse Genetics, and Pathogenesis of Disease. In *Current Topics in Microbiology and*

Immunology; 2013; pp 3–38. https://doi.org/10.1007/978-3-642-38919-1_1.

(82)   Kiss, G.; Holl, J. M.; Williams, G. M.; Alonas, E.; Vanover, D.; Lifland, A. W.; Gudheti, M.; Guerrero-Ferreira, R. C.; Nair, V.; Yi, H.; et al. Structural Analysis of Respiratory Syncytial Virus Reveals the Position of M2-1 between the Matrix Protein and the Ribonucleoprotein Complex. *J. Virol.* **2014**, *88* (13), 7602–7617. https://doi.org/10.1128/jvi.00256-14.

(83)   Boyoglu-Barnum, S.; Chirkova, T.; Anderson, L. J. Biology of Infection and Disease Pathogenesis to Guide RSV Vaccine Development. *Front. Immunol.* **2019**, *10* (July), 1–10. https://doi.org/10.3389/fimmu.2019.01675.

(84)   Heylen, E.; Neyts, J.; Jochmans, D. Drug Candidates and Model Systems in Respiratory Syncytial Virus Antiviral Drug Discovery. *Biochem. Pharmacol.* **2017**, *127*, 1–12. https://doi.org/10.1016/j.bcp.2016.09.014.

(85)   Shahriari, S.; Gordon, J.; Ghildyal, R. Host Cytoskeleton in Respiratory Syncytial Virus Assembly and Budding. *Virol. J.* **2016**, *13* (1), 161–172. https://doi.org/10.1186/s12985-016-0618-z.

(86)   Jorquera, P. A.; Tripp, R. A. Respiratory Syncytial Virus: Prospects for New and Emerging Therapeutics. *Expert Rev. Respir. Med.* **2017**, *11* (8), 609–615. https://doi.org/10.1080/17476348.2017.1338567.

(87)   Tripp, R. A.; Power, U. F.; Openshaw, P. J. M.; Kauvar, L. M. Respiratory Syncytial Virus: Targeting the G Protein Provides a New Approach for an Old Problem. *J. Virol.* **2017**, *92* (3), e01302-17. https://doi.org/10.1128/jvi.01302-17.

(88)   Kim, Y.-I.; Pareek, R.; Murphy, R.; Harrison, L.; Farrell, E.; Cook, R.; DeVincenzo, J. The Antiviral Effects of RSV Fusion Inhibitor, MDT-637, on Clinical Isolates, vs Its Achievable Concentrations in the Human Respiratory Tract and Comparison to Ribavirin. *Influenza Other Respi. Viruses* **2017**, *11* (6), 525–530. https://doi.org/10.1111/irv.12503.

(89)   Roymans, D.; Alnajjar, S. S.; Battles, M. B.; Sitthicharoenchai, P.; Furmanova-Hollenstein, P.; Rigaux, P.; Van Den Berg, J.; Kwanten, L.; Van Ginderen, M.; Verheyen, N.; et al. Therapeutic Efficacy of a Respiratory Syncytial Virus Fusion Inhibitor. *Nat. Commun.* **2017**, *8* (1), 167. https://doi.org/10.1038/s41467-017-00170-x.

(90)   Huntjens, D. R. H.; Ouwerkerk-Mahadevan, S.; Brochot, A.; Rusch, S.; Stevens, M.; Verloes, R. Population Pharmacokinetic Modeling of JNJ-53718678, a Novel Fusion Inhibitor for the Treatment of Respiratory Syncytial Virus: Results from a Phase I, Double-Blind, Randomized, Placebo-Controlled First-in-Human Study in Healthy Adult Subjects. *Clin. Pharmacokinet.* **2017**, *56* (11), 1331–1342. https://doi.org/10.1007/s40262-017-0522-8.

(91)   Israel, S.; Rusch, S.; DeVincenzo, J.; Boyers, A.; Fok-Seang, J.; Huntjens, D.; Lounis, N.; Mariën, K.; Stevens, M.; Verloes, R. Effect of Oral JNJ-53718678 (JNJ-678) on Disease Severity in Healthy Adult Volunteers Experimentally Inoculated With Live Respiratory

Syncytial Virus (RSV): A Placebo-Controlled Challenge Study. *Open Forum Infect. Dis.* **2016**, *3* (suppl_1), 650. https://doi.org/10.1093/ofid/ofw172.513.

(92)   Sun, Z.; Pan, Y.; Jiang, S.; Lu, L. Respiratory Syncytial Virus Entry Inhibitors Targeting the F Protein. *Viruses*. January 16, 2013, pp 211–225. https://doi.org/10.3390/v5010211.

(93)   Bonfanti, J. F.; Doublet, F.; Fortin, J.; Lacrampe, J.; Guillemont, J.; Muller, P.; Queguiner, L.; Arnoult, E.; Gevers, T.; Janssens, P.; et al. Selection of a Respiratory Syncytial Virus Fusion Inhibitor Clinical Candidate, Part 1: Improving the Pharmacokinetic Profile Using the Structure-Property Relationship. *J. Med. Chem.* **2007**, *50* (19), 4572–4584. https://doi.org/10.1021/jm070143x.

(94)   González-Parra, G.; Dobrovolny, H. M. Modeling of Fusion Inhibitor Treatment of RSV in African Green Monkeys. *J. Theor. Biol.* **2018**, *456*, 62–73. https://doi.org/10.1016/j.jtbi.2018.07.029.

(95)   Toovey, S.; Wu, J.; Wang, V.; Elliot, S. Safety And Pharmacokinetics In Healthy Volunteers Of The Anti-RSV Antiviral AK0529. In *1st International Meeting on Respiratory Pathogens, Singapore*; 2015.

(96)   Das, K.; Arnold, E. Negative-Strand RNA Virus L Proteins: One Machine, Many Activities. *Cell* **2015**, *162* (2), 239–241. https://doi.org/10.1016/j.cell.2015.06.063.

(97)   De Vincenzo, J. P.; McClure, M. W.; Symons, J. A.; Fathi, H.; Westland, C.; Chanda, S.; Lambkin-Williams, R.; Smith, P.; Zhang, Q.; Beigelman, L.; et al. Activity of Oral ALS-008176 in a Respiratory Syncytial Virus Challenge Study. *N. Engl. J. Med.* **2015**, *373* (21), 2048–2058. https://doi.org/10.1056/NEJMoa1413275.

(98)   Liuzzi, M.; Mason, S. W.; Cartier, M.; Lawetz, C.; McCollum, R. S.; Dansereau, N.; Bolger, G.; Lapeyre, N.; Gaudette, Y.; Lagace, L.; et al. Inhibitors of Respiratory Syncytial Virus Replication Target Cotranscriptional MRNA Guanylylation by Viral RNA-Dependent RNA Polymerase. *J. Virol.* **2005**, *79* (20), 13105–13115. https://doi.org/10.1128/jvi.79.20.13105-13115.2005.

(99)   Fordyce, E. A. F.; Brookes, D. W.; Lise-Ciana, C.; Coates, M. S.; Hunt, S. F.; Ito, K.; King-Underwood, J.; Onions, S. T.; Parra, G. F.; Rapeport, G.; et al. Discovery of Novel Benzothienoazepine Derivatives as Potent Inhibitors of Respiratory Syncytial Virus. *Bioorganic Med. Chem. Lett.* **2017**, *27* (10), 2201–2206. https://doi.org/10.1016/j.bmcl.2017.03.053.

(100) Xiong, H.; Foulk, M.; Aschenbrenner, L.; Fan, J.; Tiong-Yip, C. L.; Johnson, K. D.; Moustakas, D.; Fleming, P. R.; Brown, D. G.; Zhang, M.; et al. Discovery of a Potent Respiratory Syncytial Virus RNA Polymerase Inhibitor. *Bioorganic Med. Chem. Lett.* **2013**, *23* (24), 6789–6793. https://doi.org/10.1016/j.bmcl.2013.10.018.

(101) Gottlieb, J.; Zamora, M. R.; Hodges, T.; Musk, A. W.; Sommerwerk, U.; Dilling, D.; Arcasoy, S.; DeVincenzo, J.; Karsten, V.; Shah, S.; et al. ALN-RSV01 for Prevention of Bronchiolitis Obliterans Syndrome after Respiratory Syncytial Virus Infection in Lung Transplant

Recipients. *J. Hear. Lung Transplant.* **2016**, *35* (2), 213–221. https://doi.org/10.1016/j.healun.2015.08.012.

(102) Ouizougun-Oubari, M.; Pereira, N.; Tarus, B.; Galloux, M.; Lassoued, S.; Fix, J.; Tortorici, M. A.; Hoos, S.; Baron, B.; England, P.; et al. A Druggable Pocket at the Nucleocapsid/Phosphoprotein Interaction Site of Human Respiratory Syncytial Virus. *J. Virol.* **2015**, *89* (21), 11129–11143. https://doi.org/10.1128/jvi.01612-15.

(103) Sizun, C.; Duquerroy, S.; Eleouet, J.-F.; Rey, F.; Slama Schwok, A.; Desmaele, D.; Couvreur, P.; Tarus, B. N1-Benzyl Substituted Pyrazoles as Antiviral Agents Directed against Respiratory Synctical Virus (RSV). EP3017812A1, 2016.

(104) Li, Y.; To, J.; Verdia-Baguena, C.; Dossena, S.; Surya, W.; Huang, M.; Paulmichl, M.; Liu, D. X.; Aguilella, V. M.; Torres, J. Inhibition of the Human Respiratory Syncytial Virus Small Hydrophobic Protein and Structural Variations in a Bicelle Environment. *J. Virol.* **2014**, *88* (20), 11899–11914. https://doi.org/10.1128/jvi.00839-14.

(105) Bailly, B.; Richard, C.-A.; Sharma, G.; Wang, L.; Johansen, L.; Cao, J.; Pendharkar, V.; Sharma, D.-C.; Galloux, M.; Wang, Y.; et al. Targeting Human Respiratory Syncytial Virus Transcription Anti-Termination Factor M2-1 to Inhibit in Vivo Viral Replication. *Sci. Rep.* **2016**, *6* (1), 25806. https://doi.org/10.1038/srep25806.

(106) Fuller, H. L.; Del Mar, C. Immunoglobulin Treatment for Respiratory Syncytial Virus Infection. In *Cochrane Database of Systematic Reviews*; Fuller, H. L., Ed.; John Wiley & Sons, Ltd: Chichester, UK, 2006. https://doi.org/10.1002/14651858.CD004883.pub2.

(107) Sanders, S. L.; Agwan, S.; Hassan, M.; van Driel, M. L.; Del Mar, C. B. Immunoglobulin Treatment for Hospitalised Infants and Young Children with Respiratory Syncytial Virus Infection. *Cochrane database Syst. Rev.* **2019**, *8*, CD009417. https://doi.org/10.1002/14651858.CD009417.pub2.

(108) Whimbey, E.; Champlin, R. E.; Englund, J. A.; Mirza, N. Q.; Piedra, P. A.; Goodrich, J. M.; Przepiorka, D.; Luna, M. A.; Morice, R. C.; Neumann, J. L. Combination Therapy with Aerosolized Ribavirin and Intravenous Immunoglobulin for Respiratory Syncytial Virus Disease in Adult Bone Marrow Transplant Recipients. *Bone Marrow Transplant.* **1995**, *16* (3), 393–399.

(109) Wasserman, R. L.; Greener, B. N.; Mond, J. RI-002, an Intravenous Immunoglobulin Containing High Titer Neutralizing Antibody to RSV and Other Respiratory Viruses for Use in Primary Immunodeficiency Disease and Other Immune Compromised Populations. *Expert Rev. Clin. Immunol.* **2017**, *13* (12), 1107–1119. https://doi.org/10.1080/1744666X.2017.1389647.

(110) Luna, M. S.; Manzoni, P.; Paes, B.; Baraldi, E.; Cossey, V.; Kugelman, A.; Chawla, R.; Dotta, A.; Rodríguez Fernández, R.; Resch, B.; et al. Expert Consensus on Palivizumab Use for Respiratory Syncytial Virus in Developed Countries. *Paediatr. Respir. Rev.* **2020**, *33*, 35–44. https://doi.org/10.1016/j.prrv.2018.12.001.

(111) Simões, E. A. F.; Bont, L.; Manzoni, P.; Fauroux, B.; Paes, B.; Figueras-Aloy, J.; Checchia, P. A.; Carbonell-Estrany, X. Past, Present and Future Approaches to the Prevention and Treatment of Respiratory Syncytial Virus Infection in Children. *Infect. Dis. Ther.* **2018**, *7* (1), 87–120. https://doi.org/10.1007/s40121-018-0188-z.

(112) Palomo, C.; Mas, V.; Detalle, L.; Depla, E.; Cano, O.; Vázquez, M.; Stortelers, C.; Melero, J. A. Trivalency of a Nanobody Specific for the Human Respiratory Syncytial Virus Fusion Glycoprotein Drastically Enhances Virus Neutralization and Impacts Escape Mutant Selection. *Antimicrob. Agents Chemother.* **2016**, *60* (11), 6498–6509. https://doi.org/10.1128/AAC.00842-16.

(113) Power, U. F.; Stortelers, C.; Allosery, K.; Melero, J. A. J. A.; Detalle, L.; Stohr, T.; Palomo, C.; Piedra, P. A.; Gilbert, B. E.; Mas, V.; et al. Generation and Characterization of ALX-0171 , a Potent Novel Therapeutic Nanobody for the Treatment of Respiratory Syncytial Virus Infection. *Antimicrob. Agents Chemother.* **2016**, *60* (1), 6–13. https://doi.org/10.1128/AAC.01802-15.Address.

(114) Zhao, M.; Zheng, Z.-Z.; Chen, M.; Modjarrad, K.; Zhang, W.; Zhan, L.-T.; Cao, J.-L.; Sun, Y.-P.; McLellan, J. S.; Graham, B. S.; et al. Discovery of a Prefusion Respiratory Syncytial Virus F-Specific Monoclonal Antibody That Provides Greater In Vivo Protection than the Murine Precursor of Palivizumab. *J. Virol.* **2017**, *91* (15), e00176-17. https://doi.org/10.1128/JVI.00176-17.

(115) Gilman, M. S. A.; Moin, S. M.; Mas, V.; Chen, M.; Patel, N. K.; Kramer, K.; Zhu, Q.; Kabeche, S. C.; Kumar, A.; Palomo, C.; et al. Characterization of a Prefusion-Specific Antibody That Recognizes a Quaternary, Cleavage-Dependent Epitope on the RSV Fusion Glycoprotein. *PLOS Pathog.* **2015**, *11* (7), e1005035. https://doi.org/10.1371/journal.ppat.1005035.

(116) Mousa, J. J.; Kose, N.; Matta, P.; Gilchuk, P.; Crowe, J. E. A Novel Pre-Fusion Conformation-Specific Neutralizing Epitope on the Respiratory Syncytial Virus Fusion Protein. *Nat. Microbiol.* **2017**, *2*, 16271. https://doi.org/10.1038/nmicrobiol.2016.271.

(117) Domachowske, J. B.; Khan, A. A.; Esser, M. T.; Jensen, K.; Takas, T.; Villafana, T.; Dubovsky, F.; Griffin, M. P. Safety, Tolerability and Pharmacokinetics of MEDI8897, an Extended Half-Life Single-Dose Respiratory Syncytial Virus Prefusion F-Targeting Monoclonal Antibody Administered as a Single Dose to Healthy Preterm Infants. *Pediatr. Infect. Dis. J.* **2018**, *37* (9), 886–892. https://doi.org/10.1097/INF.0000000000001916.

(118) Boyoglu-Barnum, S.; Todd, S. O.; Chirkova, T.; Barnum, T. R.; Gaston, K. A.; Haynes, L. M.; Tripp, R. A.; Moore, M. L.; Anderson, L. J. An Anti-G Protein Monoclonal Antibody Treats RSV Disease More Effectively than an Anti-F Monoclonal Antibody in BALB/c Mice. *Virology* **2015**, *483*, 117–125. https://doi.org/10.1016/j.virol.2015.02.035.

(119) Caidi, H.; Miao, C.; Thornburg, N. J.; Tripp, R. A.; Anderson, L. J.; Haynes, L. M. Anti-Respiratory Syncytial Virus (RSV) G Monoclonal Antibodies Reduce Lung Inflammation

and Viral Lung Titers When Delivered Therapeutically in a BALB/c Mouse Model. *Antiviral Res.* **2018**, *154*, 149–157. https://doi.org/10.1016/j.antiviral.2018.04.014.

(120) Kim, H. W.; Canchola, J. G.; Brandt, C. D.; Pyles, G.; Chanock, R. M.; Jensen, K.; Parrott, R. H. Respiratory Syncytial Virus Disease in Infants despite Prior Administration of Antigenic Inactivated Vaccine. *Am. J. Epidemiol.* **1969**, *89* (4), 422–434. https://doi.org/10.1093/oxfordjournals.aje.a120955.

(121) Broadbent, L.; Groves, H.; Shields, M. D.; Power, U. F. Respiratory Syncytial Virus, an Ongoing Medical Dilemma: An Expert Commentary on Respiratory Syncytial Virus Prophylactic and Therapeutic Pharmaceuticals Currently in Clinical Trials. *Influenza Other Respi. Viruses* **2015**, *9* (4), 169–178. https://doi.org/10.1111/irv.12313.

(122) Blanco, J. C. G.; Boukhvalova, M. S.; Morrison, T. G.; Vogel, S. N. A Multifaceted Approach to RSV Vaccination. *Human Vaccines and Immunotherapeutics*. 2018, pp 1734–1745. https://doi.org/10.1080/21645515.2018.1472183.

(123) Noor, A.; Krilov, L. R. Respiratory Syncytial Virus Vaccine: Where Are We Now and What Comes Next? *Expert Opin. Biol. Ther.* **2018**, *18* (12), 1247–1256. https://doi.org/10.1080/14712598.2018.1544239.

(124) Buchholz, U. J.; Cunningham, C. K.; Muresan, P.; Gnanashanmugam, D.; Sato, P.; Siberry, G. K.; Rexroad, V.; Valentine, M.; Perlowski, C.; Schappell, E.; et al. Live Respiratory Syncytial Virus (RSV) Vaccine Candidate Containing Stabilized Temperature-Sensitivity Mutations Is Highly Attenuated in RSV-Seronegative Infants and Children. *J. Infect. Dis.* **2018**, *217* (9), 1338–1346. https://doi.org/10.1093/infdis/jiy066.

(125) O'Konek, J. J.; Makidon, P. E.; Landers, J. J.; Cao, Z.; Malinczak, C. A.; Pannu, J.; Sun, J.; Bitko, V.; Ciotti, S.; Hamouda, T.; et al. Intranasal Nanoemulsion-Based Inactivated Respiratory Syncytial Virus Vaccines Protect against Viral Challenge in Cotton Rats. *Hum. Vaccines Immunother.* **2015**, *11* (12), 2904–2912. https://doi.org/10.1080/21645515.2015.1075680.

(126) Beugeling, M.; De Zee, J.; Woerdenbag, H. J.; Frijlink, H. W.; Wilschut, J. C.; Hinrichs, W. L. J. Respiratory Syncytial Virus Subunit Vaccines Based on the Viral Envelope Glycoproteins Intended for Pregnant Women and the Elderly. *Expert Rev. Vaccines* **2019**, *18* (9), 935–950. https://doi.org/10.1080/14760584.2019.1657013.

(127) Langley, J. M.; Aggarwal, N.; Toma, A.; Halperin, S. A.; McNeil, S. A.; Fissette, L.; Dewé, W.; Leyssen, M.; Toussaint, J. F.; Dieussaert, I. A Randomized, Controlled, Observer-Blinded Phase 1 Study of the Safety and Immunogenicity of a Respiratory Syncytial Virus Vaccine With or Without Alum Adjuvant. *J. Infect. Dis.* **2017**, *215* (1), 24–33. https://doi.org/10.1093/infdis/jiw453.

(128) Widjojoatmodjo, M. N.; Bogaert, L.; Meek, B.; Zahn, R.; Vellinga, J.; Custers, J.; Serroyen, J.; Radošević, K.; Schuitemaker, H. Recombinant Low-Seroprevalent Adenoviral Vectors Ad26 and Ad35 Expressing the Respiratory Syncytial Virus (RSV) Fusion Protein

Induce Protective Immunity against RSV Infection in Cotton Rats. *Vaccine* **2015**, *33* (41), 5406–5414. https://doi.org/10.1016/j.vaccine.2015.08.056.

(129) Kuchipudi, S. V.; Nissly, R. H. Novel Flu Viruses in Bats and Cattle: "Pushing the Envelope" of Influenza Infection. *Vet. Sci.* **2018**, *5* (3), 1–10. https://doi.org/10.3390/vetsci5030071.

(130) Zambon, M. Orthomyxoviruses: Influenza. In *Medical Microbiology: Eighteenth Edition*; Elsevier Inc., 2012; pp 497–509. https://doi.org/10.1016/B978-0-7020-4089-4.00064-0.

(131) Petrova, V. N.; Russell, C. A. The Evolution of Seasonal Influenza Viruses. *Nat. Rev. Microbiol.* **2018**, *16* (1), 47–60. https://doi.org/10.1038/nrmicro.2017.118.

(132) Foni, E.; Chiapponi, C.; Baioni, L.; Zanni, I.; Merenda, M.; Rosignoli, C.; Kyriakis, C. S.; Luini, M. V.; Mandola, M. L.; Bolzoni, L.; et al. Influenza D in Italy: Towards a Better Understanding of an Emerging Viral Infection in Swine. *Sci. Rep.* **2017**, *7* (1), 11660. https://doi.org/10.1038/s41598-017-12012-3.

(133) Shao, W.; Li, X.; Goraya, M.; Wang, S.; Chen, J.-L. Evolution of Influenza A Virus by Mutation and Re-Assortment. *Int. J. Mol. Sci.* **2017**, *18* (8), 1650. https://doi.org/10.3390/ijms18081650.

(134) Gounder, A. P.; Boon, A. C. M. Influenza Pathogenesis: The Effect of Host Factors on Severity of Disease. *J. Immunol.* **2019**, *202* (2), 341–350. https://doi.org/10.4049/jimmunol.1801010.

(135) Bouvier, N. M.; Palese, P. The Biology of Influenza Viruses. *Vaccine* **2008**, *26* (SUPPL. 4), D49–D53. https://doi.org/10.1016/j.vaccine.2008.07.039.

(136) Biere, B.; Bauer, B.; Schweiger, B. Differentiation of Influenza b Virus Lineages Yamagata and Victoria by Real-Time PCR. *J. Clin. Microbiol.* **2010**, *48* (4), 1425–1427. https://doi.org/10.1128/JCM.02116-09.

(137) Hatta, M.; Goto, H.; Kawaoka, Y. Influenza B Virus Requires BM2 Protein for Replication. *J. Virol.* **2004**, *78* (11), 5576–5583. https://doi.org/10.1128/jvi.78.11.5576-5583.2004.

(138) Kollerova, E.; Betáková, T. Influenza Viruses and Their Ion Channels. *Acta Virol.* **2006**, *50* (1), 7–16.

(139) Collin, E. A.; Sheng, Z.; Lang, Y.; Ma, W.; Hause, B. M.; Li, F. Cocirculation of Two Distinct Genetic and Antigenic Lineages of Proposed Influenza D Virus in Cattle. *J. Virol.* **2015**, *89* (2), 1036–1042. https://doi.org/10.1128/jvi.02718-14.

(140) Muraki, Y.; Hongo, S. The Molecular Virology and Reverse Genetics of Influenza C Virus. *Jpn. J. Infect. Dis.* **2010**, *63* (3), 157–165.

(141) Liu, R.; Sheng, Z.; Lin, T.; Sreenivasan, C.; Gao, R.; Thomas, M.; Druce, J.; Hause, B. M.; Kaushik, R. S.; Li, F.; et al. Genetic and Antigenic Characteristics of a Human Influenza C Virus Clinical Isolate. *J. Med. Virol.* **2020**, *92* (2), 161–166. https://doi.org/10.1002/jmv.25589.

(142) Kim, H.; Webster, R. G.; Webby, R. J. Influenza Virus: Dealing with a Drifting and Shifting Pathogen. *Viral Immunol.* **2018**, *31* (2), 174–183. https://doi.org/10.1089/vim.2017.0141.

(143) Clements, J. E.; Gdovin, S. L. Antigenic Variation. In *Encyclopedia of Immunology*; Elsevier, 1998; pp 199–201. https://doi.org/10.1006/rwei.1999.0054.

(144) Dawood, F. S.; Bresee, J. Influenza Viruses. In *Principles and Practice of Pediatric Infectious Diseases*; 2018; pp 1181-1190.e5. https://doi.org/10.1016/B978-0-323-40181-4.00229-2.

(145) Zambon, M. C. Epidemiology and Pathogenesis of Influenza. *J. Antimicrob. Chemother.* **1999**, *44* (TOPIC B), 3–9. https://doi.org/10.1093/jac/44.suppl_2.3.

(146) Cho, K. J.; Lee, J. H.; Hong, K. W.; Kim, S. H.; Park, Y.; Lee, J. Y.; Kang, S.; Kim, S.; Yang, J. H.; Kim, E. K.; et al. Insight into Structural Diversity of Influenza Virus Haemagglutinin. *J. Gen. Virol.* **2013**, *94* (PART8), 1712–1722. https://doi.org/10.1099/vir.0.051136-0.

(147) Harrison, S. C. Viral Membrane Fusion. *Nat. Struct. Mol. Biol.* **2008**, *15* (7), 690–698. https://doi.org/10.1038/nsmb.1456.

(148) Wang, M.; Veit, M. Hemagglutinin-Esterase-Fusion (HEF) Protein of Influenza C Virus. *Protein Cell* **2016**, *7* (1), 28–45. https://doi.org/10.1007/s13238-015-0193-x.

(149) Betáková, T.; Kollerová, E. PH Modulating Activity of Ion Channels of Influenza A, B, and C Viruses. *Acta Virol.* **2006**, *50* (3), 187–193.

(150) Chen, B. J.; Leser, G. P.; Jackson, D.; Lamb, R. A. The Influenza Virus M2 Protein Cytoplasmic Tail Interacts with the M1 Protein and Influences Virus Assembly at the Site of Virus Budding. *J. Virol.* **2008**, *82* (20), 10059–10070. https://doi.org/10.1128/jvi.01184-08.

(151) Pielak, R. M.; Chou, J. J. Influenza M2 Proton Channels. *Biochim. Biophys. Acta - Biomembr.* **2011**, *1808* (2), 522–529. https://doi.org/10.1016/j.bbamem.2010.04.015.

(152) Schnell, J. R.; Chou, J. J. Structure and Mechanism of the M2 Proton Channel of Influenza A Virus. *Nature* **2008**, *451* (7178), 591–595. https://doi.org/10.1038/nature06531.

(153) To, J.; Torres, J. Viroporins in the Influenza Virus. *Cells* **2019**, *8* (7), 654. https://doi.org/10.3390/cells8070654.

(154) Furukawa, T.; Muraki, Y.; Noda, T.; Takashita, E.; Sho, R.; Sugawara, K.; Matsuzaki, Y.; Shimotai, Y.; Hongo, S. Role of the CM2 Protein in the Influenza C Virus Replication Cycle. *J. Virol.* **2011**, *85* (3), 1322–1329. https://doi.org/10.1128/jvi.01367-10.

(155) Boulo, S.; Akarsu, H.; Ruigrok, R. W. H.; Baudin, F. Nuclear Traffic of Influenza Virus Proteins and Ribonucleoprotein Complexes. *Virus Res.* **2007**, *124* (1–2), 12–21. https://doi.org/10.1016/j.virusres.2006.09.013.

(156) Samji, T. Influenza A: Understanding the Viral Life Cycle. *Yale J. Biol. Med.* **2009**, *82* (4), 153–159.

(157) Dou, D.; Revol, R.; Östbye, H.; Wang, H.; Daniels, R. Influenza A Virus Cell Entry, Replication, Virion Assembly and Movement. *Front. Immunol.* **2018**, *9* (JUL).

https://doi.org/10.3389/fimmu.2018.01581.

(158) Te Velthuis, A. J. W.; Fodor, E. Influenza Virus RNA Polymerase: Insights into the Mechanisms of Viral RNA Synthesis. *Nat. Rev. Microbiol.* **2016**, *14* (8), 479–493. https://doi.org/10.1038/nrmicro.2016.87.

(159) Nayak, D. P.; Balogun, R. A.; Yamada, H.; Zhou, Z. H.; Barman, S. Influenza Virus Morphogenesis and Budding. *Virus Res.* **2009**, *143* (2), 147–161. https://doi.org/10.1016/j.virusres.2009.05.010.

(160) McAuley, J. L.; Gilbertson, B. P.; Trifkovic, S.; Brown, L. E.; McKimm-Breschkin, J. L. Influenza Virus Neuraminidase Structure and Functions. *Front. Microbiol.* **2019**, *10* (JAN), 39. https://doi.org/10.3389/fmicb.2019.00039.

(161) Cohen, M.; Zhang, X.-Q.; Senaati, H. P.; Chen, H.-W.; Varki, N. M.; Schooley, R. T.; Gagneux, P. Influenza A Penetrates Host Mucus by Cleaving Sialic Acids with Neuraminidase. *Virol. J.* **2013**, *10* (1), 321. https://doi.org/10.1186/1743-422X-10-321.

(162) Paules, C.; Subbarao, K. Influenza. *Lancet* **2017**, *390* (10095), 697–708. https://doi.org/10.1016/S0140-6736(17)30129-0.

(163) Tripathi, S.; Batra, J.; Lal, S. K. Interplay between Influenza A Virus and Host Factors: Targets for Antiviral Intervention. *Arch. Virol.* **2015**, *160* (8), 1877–1891. https://doi.org/10.1007/s00705-015-2452-9.

(164) Yeh, S. H. Influenza. In *Netter's Infectious Diseases*; Elsevier, 2012; pp 34–38. https://doi.org/10.1016/B978-1-4377-0126-5.00008-2.

(165) Shie, J.-J.; Fang, J.-M. Development of Effective Anti-Influenza Drugs: Congeners and Conjugates – a Review. *J. Biomed. Sci.* **2019**, *26* (1), 84. https://doi.org/10.1186/s12929-019-0567-0.

(166) Principi, N.; Camilloni, B.; Alunno, A.; Polinori, I.; Argentiero, A.; Esposito, S. Drugs for Influenza Treatment: Is There Significant News? *Front. Med.* **2019**, *6*, 109. https://doi.org/10.3389/fmed.2019.00109.

(167) Furuta, Y.; Komeno, T.; Nakamura, T. Favipiravir (T-705), a Broad Spectrum Inhibitor of Viral RNA Polymerase. *Proc. Japan Acad. Ser. B* **2017**, *93* (7), 449–463. https://doi.org/10.2183/pjab.93.027.

(168) Wu, N. C.; Wilson, I. A. Structural Insights into the Design of Novel Anti-Influenza Therapies. *Nat. Struct. Mol. Biol.* **2018**, *25* (2), 115–121. https://doi.org/10.1038/s41594-018-0025-9.

(169) Friesen, R. H. E.; Koudstaal, W.; Koldijk, M. H.; Weverling, G. J.; Brakenhoff, J. P. J.; Lenting, P. J.; Stittelaar, K. J.; Osterhaus, A. D. M. E.; Kompier, R.; Goudsmit, J. New Class of Monoclonal Antibodies against Severe Influenza: Prophylactic and Therapeutic Efficacy in Ferrets. *PLoS One* **2010**, *5* (2), e9106. https://doi.org/10.1371/journal.pone.0009106.

(170) Koszalka, P.; Tilmanis, D.; Hurt, A. C. Influenza Antivirals Currently in Late-Phase Clinical

Trial. *Influenza Other Respi. Viruses* **2017**, *11* (3), 240–246. https://doi.org/10.1111/irv.12446.

(171) Vanderlinden, E.; Naesens, L. Emerging Antiviral Strategies to Interfere with Influenza Virus Entry. *Med. Res. Rev.* **2014**, *34* (2), 301–339. https://doi.org/10.1002/med.21289.

(172) Tonelli, M.; Boido, V.; Canu, C.; Sparatore, A.; Sparatore, F.; Paneni, M. S.; Fermeglia, M.; Pricl, S.; La Colla, P.; Casula, L.; et al. Antimicrobial and Cytotoxic Arylazoenamines. Part III: Antiviral Activity of Selected Classes of Arylazoenamines. *Bioorganic Med. Chem.* **2008**, *16* (18), 8447–8465. https://doi.org/10.1016/j.bmc.2008.08.028.

(173) Giliberti, G.; Ibba, C.; Marongiu, E.; Loddo, R.; Tonelli, M.; Boido, V.; Laurini, E.; Posocco, P.; Fermeglia, M.; Pricl, S. Synergistic Experimental/Computational Studies on Arylazoenamine Derivatives That Target the Bovine Viral Diarrhea Virus RNA-Dependent RNA Polymerase. *Bioorganic Med. Chem.* **2010**, *18* (16), 6055–6068. https://doi.org/10.1016/j.bmc.2010.06.065.

(174) Tonelli, M.; Vazzana, I.; Tasso, B.; Boido, V.; Sparatore, F.; Fermeglia, M.; Paneni, M. S.; Posocco, P.; Pricl, S.; Colla, P. La; et al. Antiviral and Cytotoxic Activities of Aminoarylazo Compounds and Aryltriazene Derivatives. *Bioorganic Med. Chem.* **2009**, *17* (13), 4425–4440. https://doi.org/10.1016/j.bmc.2009.05.020.

(175) Tonelli, M.; Simone, M.; Tasso, B.; Novelli, F.; Boido, V.; Sparatore, F.; Paglietti, G.; Pricl, S.; Giliberti, G.; Blois, S.; et al. Antiviral Activity of Benzimidazole Derivatives. II. Antiviral Activity of 2-Phenylbenzimidazole Derivatives. *Bioorganic Med. Chem.* **2010**, *18* (8), 2937–2953. https://doi.org/10.1016/j.bmc.2010.02.037.

(176) Tonelli, M.; Boido, V.; Colla, P. La; Loddo, R.; Posocco, P.; Paneni, M. S.; Fermeglia, M.; Pricl, S. Pharmacophore Modeling, Resistant Mutant Isolation, Docking, and MM-PBSA Analysis: Combined Experimental/Computer-Assisted Approaches to Identify New Inhibitors of the Bovine Viral Diarrhea Virus (BVDV). *Bioorganic Med. Chem.* **2010**, *18* (6), 2304–2316. https://doi.org/10.1016/j.bmc.2010.01.058.

(177) Malina, A.; Khan, S.; Carlson, C. B.; Svitkin, Y.; Harvey, I.; Sonenberg, N.; Beal, P. A.; Pelletier, J. Inhibitory Properties of Nucleic Acid-Binding Ligands on Protein Synthesis. *FEBS Lett.* **2005**, *579* (1), 79–89. https://doi.org/10.1016/j.febslet.2004.06.103.

(178) Luan, X.; Gao, C.; Zhang, N.; Chen, Y.; Sun, Q.; Tan, C.; Liu, H.; Jin, Y.; Jiang, Y. Exploration of Acridine Scaffold as a Potentially Interesting Scaffold for Discovering Novel Multi-Target VEGFR-2 and Src Kinase Inhibitors. *Bioorganic Med. Chem.* **2011**, *19* (11), 3312–3319. https://doi.org/10.1016/j.bmc.2011.04.053.

(179) Santi, D. V; Marlowe, C. K. Phenyltriazine Inhibitors of Pneumocystis Carinii Dihydrofolate Reductase for Treatment of Pneumonia. WO9108668, December 7, 1991.

(180) Cody, V.; Pace, J.; Namjoshi, O. A.; Gangjee, A. Structure-Activity Correlations for Three Pyrido[2,3-d]Pyrimidine Antifolates Binding to Human and Pneumocystis Carinii Dihydrofolate Reductase. *Acta Crystallogr. Sect. FStructural Biol. Commun.* **2015**, *71*,

799–803. https://doi.org/10.1107/S2053230X15008468.

(181) Dolzhenko, A. V.; Chui, W. K. Synthesis of 2-Amino-s-Triazino[1,2-a]Benzimidazoles as Potential Antifolates from 2-Guanidino- and 2-Guanidino-5-Methylbenzimidazoles. *J. Heterocycl. Chem.* **2006**, *43* (1), 95–100. https://doi.org/10.1002/jhet.5570430115.

(182) Zhu, Z.; Li, R.; Xiao, G.; Chen, Z.; Yang, J.; Zhu, Q.; Liu, S. Design, Synthesis and Structure-Activity Relationship of Novel Inhibitors against H5N1 Hemagglutinin-Mediated Membrane Fusion. *Eur. J. Med. Chem.* **2012**, *57*, 211–216. https://doi.org/10.1016/j.ejmech.2012.08.041.

(183) Leiva, R.; Barniol-Xicota, M.; Codony, S.; Ginex, T.; Vanderlinden, E.; Montes, M.; Caffrey, M.; Luque, F. J.; Naesens, L.; Vázquez, S. Aniline-Based Inhibitors of Influenza H1N1 Virus Acting on Hemagglutinin-Mediated Fusion. *J. Med. Chem.* **2018**, *61* (1), 98–118. https://doi.org/10.1021/acs.jmedchem.7b00908.

(184) Tonelli, M.; Cichero, E.; Mahmoud, A. M.; Rabbito, A.; Tasso, B.; Fossa, P.; Ligresti, A. Exploring the Effectiveness of Novel Benzimidazoles as CB2 Ligands: Synthesis, Biological Evaluation, Molecular Docking Studies and ADMET Prediction†. *Medchemcomm* **2018**, *9* (12), 2045–2054. https://doi.org/10.1039/C8MD00461G.

(185) Tonelli, M.; Paglietti, G.; Boido, V.; Sparatore, F.; Marongiu, F.; Marongiu, E.; La Colla, P.; Loddo, R. Antiviral Activity of Benzimidazole Derivatives. I. Antiviral Activity of 1-Substituted-2-[(Benzotriazol-1/2-Yl)Methyl]Benzimidazoles). *Chem. Biodivers.* **2008**, *5* (11), 2386–2401. https://doi.org/10.1002/cbdv.200890203.

(186) Tonelli, M.; Novelli, F.; Tasso, B.; Vazzana, I.; Sparatore, A.; Boido, V.; Sparatore, F.; La Colla, P.; Sanna, G.; Giliberti, G.; et al. Antiviral Activity of Benzimidazole Derivatives. III. Novel Anti-CVB-5, Anti-RSV and Anti-Sb-1 Agents. *Bioorganic Med. Chem.* **2014**, *22* (17), 4893–4909. https://doi.org/10.1016/j.bmc.2014.06.043.

(187) G. Paglietti, F. Sparatore. Dialchilamminoalchilbenzimidazoli d'interesse Farmacologico. *Farm. Sci.* **1972**, *27*, 333–342.

(188) G. Paglietti, V. Boido, F. S. Dialchilamminoalchilbenzimidazoli d'interesse Farmacologico. *Farm. Sci.* **1975**, *30*, 504–511.

(189) Carroll, F. I.; Handy, R. W.; Kepler, J. A.; Gratz, J. A. The Synthesis of Some 1-(Β-diethylaminoethyl)-2-(P-ethoxybenzyl)-5-substituted Benzimidazoles. *J. Heterocycl. Chem.* **1967**, *4* (2), 262–267. https://doi.org/10.1002/jhet.5570040217.

(190) Venkatachalam, T. K.; Pierens, G. K.; Reutens, D. C. Synthesis, NMR Structural Characterization and Molecular Modeling of Substituted Thiosemicarbazones and Semicarbazones Using DFT Calculations to Prove the Syn/Anti Isomer Formation. *Magn. Reson. Chem.* **2014**, *52* (3), 98–105. https://doi.org/10.1002/mrc.4041.

(191) John, C. S.; Lim, B. B.; Vilner, B. J.; Geyer, B. C.; Bowen, W. D. Substituted Halogenated Arylsulfonamides: A New Class of σ Receptor Binding Tumor Imaging Agents. *J. Med. Chem.* **1998**, *41* (14), 2445–2450. https://doi.org/10.1021/jm9800447.

List of Publications

Reference 6: Loddo, R.; Francesconi, V.; Laurini, E.; Boccardo, S.; Aulic, S.; Fermeglia, M.; Pricl, S.; Tonelli, M. 9-Aminoacridine-Based Agents Impair the Bovine Viral Diarrhea Virus (BVDV) Replication Targeting the RNA-Dependent RNA Polymerase (RdRp). *Bioorg. Med. Chem.* **2018**, *26* (4), 855–868. https://doi.org/10.1016/j.bmc.2018.01.001.

Reference 11: Francesconi, V.; Giovannini, L.; Santucci, M.; Cichero, E.; Costi, M. P.; Naesens, L.; Giordanetto, F.; Tonelli, M. Synthesis, Biological Evaluation and Molecular Modeling of Novel Azaspiro Dihydrotriazines as Influenza Virus Inhibitors Targeting the Host Factor Dihydrofolate Reductase (DHFR). *Eur. J. Med. Chem.* **2018**, *155*, 229–243. https://doi.org/10.1016/j.ejmech.2018.05.059.

Submitted article, currently under review: Francesconi, V.; Cichero, E.; Schenone, S.; Naesens, L.; Tonelli, M. Synthesis and biological evaluation of novel (thio)semicarbazone-based benzimidazoles as antiviral agents against human respiratory viruses. *Molecules* **2020**, submitted on February 17th. Manuscript ID: molecules-735728.